2018-08-21

FUS and Excitotoxicity Cross Paths in ALS: New Insights into Cellular Stress and Disease

Maeve Tischbein
University of Massachusetts Medical School

FUS AND EXCITOTOXICITY CROSS PATHS IN ALS: NEW INSIGHTS INTO CELLULAR STRESS AND DISEASE

A Dissertation Presented

By

MAEVE TISCHBEIN

Submitted to the Faculty of the

University of Massachusetts Graduate School of Biomedical Sciences, Worcester

in partial fulfillment of the requirements for the degree of

DOCTOR OF PHILOSOPHY

AUGUST 21, 2018

CELL BIOLOGY

For Kent.

ACKNOWLEDGMENTS

Of the many people I would like to thank, I would first like to acknowledge my thesis advisor, Dr. Daryl Bosco. I so am grateful to have had the opportunity and freedom to develop a project from scratch in your lab. From conception to funding to writing to presenting to publishing, this experience was invaluable. Thank you for being as excited as I was when a discovery was made and for providing guidance when nothing worked. Thank you for providing a sheltered space in which I had the chance to emotionally wrestle and reconcile the many winding highs and lows of research. I still have personal and scientific growing to do as well as insecurities to overcome, but I know that I am well on my way having had your help.

I would also like to thank my lab family, both old and new. Having always been the older sister in 'real life', I can't tell you how much I enjoyed my time as the baby of the lab. I began so naïve, shiny and new and I thank the members of the Bosco lab for taking me under your collective wing. Catherine Douthwright, Melissa Rotunno, Reddy Sama, Laura Kaushansky, Sivakumar Boopathy, Desiree Baron and Kristin Boggio, you all set the best of examples for me and I've done my best to remember and emulate them. I also want to thank the new lab members, who I saw grow and evolve during my time in the Bosco lab. During the second half of my graduate training was when the bloom fell off the GSBS rose and I thank Yen-Chen Lin, Salome Funes, Meenakshi Sundaram Kumar, Katherine Gall, Eric Schmidt, Jeanne McKeon and Heather Yonutas for all their help camaraderie as I found new blossoms to enjoy.

For their mentoring and guidance, I would like to thank my thesis research advisory committee, Drs. Jeff Nickerson, Jeanne Lawrence, Kenny Futai, Robert as well as Dr. Brian Waigner. Jeff, you were a wonderful chair and I have recommended you many times over to others. I greatly appreciate the insight and advice each member has given me both inside and outside of official thesis meetings. I would also like to acknowledge and thank the Landers's lab, especially Drs. Claudia Fallini and Anthony Giampetruzzi for their help and insight. Further thanks to all the wonderful scientists and staff members of the Neurology department. Your kindness always brightened my day. With complete sincerity, I would also like to acknowledge all the mice that died so that I could complete my project. I hope my work has value and that these animals did not die unnecessarily.

I would like to thank my family. My parents, Anne and Peter, and my sister, Alexis. Thank you for weathering this rollercoaster ride, your love and support means so much. Last, but definitely not least, I would like to thank and thank and thank my husband, Kent. You have seen me and my feelings about science change like a crazy kaleidoscope. Despite the yearly, weekly and sometimes even hourly, changing in my imaginings and aspirations you've always loved and supported every version. Thank you Kent. Thank you everyone.

ABSTRACT

Amyotrophic lateral sclerosis (ALS) is an incurable and fatal neurodegenerative disease characterized by motor neuron loss. Although pathological mutations exist in >15 genes, the mechanism(s) underlying ALS are unknown. *FUS* is one such gene and encodes the nuclear RNA-binding protein (RBP), fused in sarcoma (FUS), which actively shuttles between the nucleus and cytoplasm. Intriguingly, nearly half of the ALS mutations identified in FUS cause this protein to mislocalize, suggesting that FUS localization is relevant to disease.

Here, we found that excitotoxicity, a neuronal stress caused by aberrant glutamate signaling, induces the rapid redistribution of FUS and additional disease-linked RBPs from the nucleus to the cytoplasm. As excitotoxicity is pathologically associated with ALS, it was notable that the nuclear egress of FUS was particularly robust. Further, ALS-FUS variants that predominantly localize to the nucleus also undergo redistribution. Thus, we sought to understand the purpose underlying FUS translocation and the potential relevance of this response to disease. As calcium dysregulation is strongly associated with neurodegenerative disorders, we examined the contribution of calcium to FUS egress. In addition to global changes to nucleocytoplasmic transport following excitotoxic insult, we found that FUS translocation caused by excitotoxicity is calcium mediated. Moreover, we found that dendritic expression of Gria2, a transcript encoding an AMPA receptor subunit responsible for regulating calcium permeability, is FUS-dependent under conditions of stress. Together, these

observations support the premise that FUS has a normal function during excitotoxic stress and that glutamatergic signaling may be dysregulated in FUS-mediated ALS.

TABLE OF CONTENTS

LIST OF TABLES

LIST OF FIGURES

Chapter I

Chapter II

Appendix III

LIST OF THIRD PARTY COPYRIGHTED MATERIAL

The following material was reproduced from published work with no permission required:

Figure Number	**Publisher**
Appendix III	National Academy of Sciences

LIST OF ABBREVIATIONS

AA	amino acids
ALS	amyotrophic lateral sclerosis
AMPA	α-amino-3-hydroxy-5-methyl-4-isoxazolepropionic acid
ANK-G	ankyrin-G
AraC	β-D-arabinofuranoside hydrochloride
ATP	adenosine triphosphate
BCA	bicinchoninic acid
C:N	cytoplasmic:nuclear
C9orf72	Chromosome 9 Open Reading Frame 72
CAZ	cabeza
CHOP	C/EBP homologous protein
CHX	cycloheximide
CNS	central nervous system
CRM1	chromosome region maintenance 1
DIV	day *in vitro*
DMEM	Dulbecco's minimal essential medium
DMSO	dimethyl sulfoxide
DPBS	Dulbecco's phosphate-buffered salt solution
EB	embryoid body
EDTA	ethylene diamine tetraacetic acid
eEF2	eukaryotic elongation factor 2
EGTA	ethylene glycol tetraacetic acid
EIF2α	eukaryotic translation initiation factor 2 alpha
EIF4G	eukaryotic translation initiation factor 4G
ER	endoplasmic reticulum
EWS	Ewing sarcoma
FALS	familial amyotrophic lateral sclerosis
FBS	fetal bovine serum
FISH	Fluorescence *in situ* hybridization
FMRP	fragile X mental retardation protein
FTD	frontotemporal dementia
FTLD	frontotemporal lobar degeneration
FUS	fused in sarcoma
G3BP1	ras GTPase-activating protein-binding protein 1
$GABA_A$	type-A γ-aminobutyric acid
GAPDH	glyceraldehyde 3-phosphate dehydrogenase
GDP	guanosine diphosphate
GFAP	glial fibrillary acidic protein
GFP	green fluorescent protein
Glu^{excito}	10μM Glutamate
GluR2	glutamate receptor 2
GLY	glycine-rich region
GTP	guanosine triphosphate

HBSS	Hank's balanced salt solution
HGPS	Hutchinson-Gilford progeria syndrome
hnRNP C1/C2	heterogeneous nuclear ribonucleoproteins C1/C2
hnRNPA1	heterogeneous nuclear ribonucleoprotein A1
HOS	hyperosmotic stress
IP	immunoprecipitation
iPSC	induced pluripotent stem cell
KCl	potassium chloride
KIF5α	kinesin family member 5 alpha
LC-MS/MS	liquid chromatography-tandem mass spectrometry
LDH	lactate dehydrogenase
LLPS	liquid-liquid phase separation
LTP	long term potentiation
MAP2	microtubule-associated protein 2
mGluR5	metabotropic glutamate receptor 5
$NaAsO_2$	sodium arsenite
NES	nuclear export sequences
NLS	nuclear localization sequence
NMDA	N-methyl-D-aspartate
P/S	penicillin and streptomycin
PABP-1	poly(A)-binding protein 1
PCM	primary neuron cultured media
PFA	4% paraformaldehyde
PFN1	profilin-1
PI	propidium iodide
PTM	posttranslational modifications
QGSY	glutamine-glycine-serine-tyrosine rich region
RAN	Ras-related nuclear protein
RBPs	RNA binding proteins
RGG	arginine-glycine-glycine
rpm	rotation per minute
RRM	RNA recognition motif
SALS	sporadic amyotrophic lateral sclerosis
SARFH	sarcoma-associated RNA-binding fly homolog
SDS-PAGE	sodium dodecyl sulfate–polyacrylamide gel electrophoresis
SEM	standard error of the mean
SMI-32	neurofilament H non-phosphorylated
SOD1	superoxide dismutase 1
TAF15	TATA-Box Binding Protein Associated Factor 15
TDP-43	TAR DNA-binding protein 43
TLS	translocated in liposarcoma
UTR	untranslated region
XPO1	exportin-1
ZF	zinc-binding domain

PREFACE

Parts of this dissertation will appear in:

Tischbein, M., Baron, D.M., Lin, Y.C., Gall, K., Landers, J.E., Fallini, C., and D.A. Bosco. FUS/TLS undergoes calcium-mediated nuclear egress during excitotoxic stress and is required for Gria2 mRNA processing. (2018)

Parts of this dissertation have appeared in:

Boopathy, S., Silvas, T.V., Tischbein, M., Jansen, S., Shandilya, S.M., Zitzewitz, J.A., Landers, J.E., Goode B.L., Schiffer, C.A. and D.A. Bosco**.** Structural basis for mutation-induced destabilization of profilin 1 in ALS*. PNAS.* 2015. 112 (26), 7984-7989.

CHAPTER I: INTRODUCTION

Central Nervous System (CNS) and Neuron Biology

The central nervous system (CNS) is composed of the brain and spinal cord and functions to transmit sensory information throughout the body. Within the CNS there are two primary cell types: neurons and glia (**Fig. I-1**). glia (**Fig. I-1B;** purple) While glia function broadly to maintain the CNS environment and support neuron function, neurons are responsible for the flow of information within a neuronal network. Due to the need to differentially receive and transmit information, neurons undergo polarization, resulting in the formation of axons and dendrites (Yogev & Shen 2017) (**Fig. I-1C**). Each are functionally distinct compartments that differ in their membrane, protein and cytoskeletal composition (Yogev & Shen 2017). Information is received in dendrites while axons electrically propagate and chemically transmit integrated signals. Depending on the function of a given neuron, dendritic and axonal morphology can vary widely. While the *in vivo* environment does heavily influence neuron structure, cell polarity is observed in dissociated neuron cultures, demonstrating that polarization is an intrinsic neuronal feature (Yogev & Shen 2017).

Neuronal communication is achieved though the release of neurotransmitters (acetylcholine, amino acids, biogenic amines and/or peptides) from presynaptic axon terminals that bind and activate postsynaptic dendritic receptors (**Fig. I-1D**). Such transmission results in the influx of ions and subsequent depolarization of the resting membrane potential (-70mV), thereby

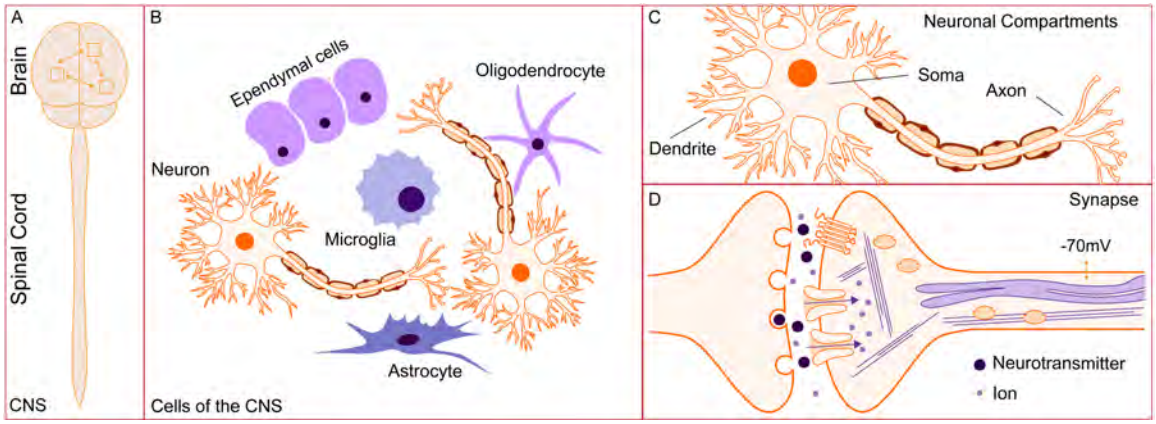

Figure I-1. Overview of the CNS. (**A**) The CNS is composed of the brain and spinal cord and serves to transmit sensory information. (**B**) Neurons (orange) and glia (purple) are the primary cell types found within the CNS. (**C**) Neurons are highly polarized, resulting in the formation of specialized compartments called dendrites or axons that are connected to the neuronal cell body, or soma. (**D**) Neurons transmit chemical information though the release of neurotransmitters at specialized junctions called synapses. Receptors that bind neurotransmitters modulate intracellular ion concentrations in response to activity, thus altering the electrochemical gradient that spans the cellular membrane (referred to as membrane potential; resting membrane potential is -70mV).

promoting or inhibiting the overall formation of an action potential initiated at the axon hillock (achieved at +40mV). The frequency and strength of signaling can induce change in the number and composition of synapses, thereby iteratively tuning the neuronal response to stimuli (Koleske 2013). This physical alteration to stimuli is referred to as plasticity and relies heavily on cytoskeletal dynamics, translation machinery as well as Golgi, endoplasmic reticulum (ER) and mitochondrial organelles for the rapid and local production of proteins, lipid and energy (Koleske 2013). Although individual synapses may fluctuate, the intricate and physical network of neurons within the CNS endures over a lifetime, in part due to the post-mitotic nature of neuronal cells (Bezprozvanny & Hiesinger 2013).

Neuronal Stress and Neurodegenerative Disease

Neuronal Vulnerabilities to Altered Homeostasis, Stress and Disease

The previously described neuronal properties are critical to overall cell function and thus, must be carefully maintained. As with any cell, physiological processes are maintained through homeostasis, a mechanism by which essential cellular variables are regulated through measurable processes (Chovatiya & Medzhitov 2014; Kotas & Medzhitov 2015). The resting membrane potential of a neuron is one such example and maintenance of this variable relies on the controlled gene, mRNA and protein expression as well as activity and turnover of protein ion channels and pumps (Davis 2013). In addition to processes that dynamically regulate cellular variables (e.g. through feedback loops), physical

compartmentalization also contributes to homeostatic regulation. In neurons there are notable differences in the localization and expression of transcripts (Cajigas et al. 2012, Zappulo et al. 2017) that allows for the subcellular specialization and regulation of cellular processes. Not necessarily unique to neurons, the nuclear envelope also serves as a barrier that dampens transcriptional 'noise' (mRNA expression), thereby maintaining order within the larger cellular environment (Stoeger et al. 2016). As described, biological systems employ multiple levels of regulation that allow for the dynamic "buffering" of a given variable as well as existence of compensatory mechanisms, should one fail (Kotas & Medzhitov 2015). Thus, the overall status of a variable results from the net effect of these nested and layered homeostatic processes.

Unlike maintaining a system at a constant level (known as homostasis), homeostasis refers to the ability of a system to operate within a limited range of variability, thus allowing for cells and cellular processes to adapt to change (Kotas & Medzhitov 2015). For instance, neuronal communication may be tuned through synaptic plasticity, the process of which is regulated by intrinsic neuronal excitability as well as neurotransmitter receptor expression and presynaptic neurotransmitter release (Davis 2013). Despite this functional understanding however, the expression of genes required to 'sense' and maintain synaptic connections varies widely between individual cells and thus, complicates our research and understanding of the specific players that regulate synaptic homeostasis (Davis 2013, Schulz et al. 2007). While the ability for self-modification

and regulation can be beneficial, such highly adaptive processes are also vulnerable to dysregulation (Kotas & Medzhitov 2015).

Environmental stress is one means by which homeostatic processes may be pushed outside of their normal operating range, allowing for dysregulation to occur. More specifically, environmental stress represents those forces perceived by the cell as capable of causing damage to biological macromolecules (e.g. membrane lipids, proteins, and/or DNA). Despite the myriad of ways in which a cell can be stressed, cell stress-response pathways are commonly organized around primary forms of cellular damage (e.g. ER stress, oxidative stress etc.) and function to minimize cellular harm (Chovatiya & Medzhitov 2014). As such, inherent neuron morphology and biology can create particular vulnerabilities to stress. Given the high energy demands of neurons met through oxidative metabolism, neurons are predisposed to oxidative stress (Gandhi & Abramov 2012) and the dysregulation of protein quality control. Neuronal size and complex structure also increases the susceptibility of these cells to damage; synapses in particular are considered among most vulnerable neuronal structures (Mattson & Magnus 2006). Unlike other cell types in which a spatial existence is essential to function, once neurons degenerate or die, they are infrequently replaced and can cause added network vulnerability (Bezprozvanny & Hiesinger 2013).

Apart from events encountered by a cell, homeostatic dysregulation and stress may also result from spontaneous or inherited mutations that trigger the failure essential variables or processes. For instance, as a result of aging as well

as post-mitotic nature, neurons accumulate genomic aberrations (McConnell et al. 2013) as well as DNA damage (Lu et al., Madabhushi et al. 2014). Albeit limited in the number of samples, a study by McConnell and colleagues (2013) indicates that neurons exhibit increased genomic variation relative to dividing cell types due to the accumulation of mutations and alterations over time (McConnell et al. 2013). While certain mutations may be capable of directly triggering cell stress, others may not until compounded by secondary factors (e.g. accumulation of DNA, structural or other damage) and is known as the two/multiple-hit hypothesis (Dormann & Haass 2011, Dormann et al. 2010). Regardless of activation mechanism (i.e. environmental event or mutation), cell stress pathways function to temporarily mitigate any real or perceived damage. In parallel, stress also triggers an interconnected shift in homeostasis through the expression of adaptive genes, in an attempt to adjust the cellular equilibrium to reflect the new environmental state (Kültz 2005). If such processes are disrupted and homeostasis is lost or cannot be maintained or restored, such a situation may lead to cell death (Kotas & Medzhitov 2015).

Neurodegenerative Disease

In 2018, the Global Burden of Disease Project reported that in terms of years lost due to death or illness from a disease, neurological disorders have the largest effect on the global population (Feigin et al. 2017). In step with prolonged human longevity and vulnerabilities of neurons, age-linked neurodegenerative

diseases are an important component of this group. Although other cell types may be affected, neurodegeneration typically refers to disorders resulting in the loss of neuronal structure and/or function. In disease, neurodegeneration is typically observed within specific neuronal subtypes and/or populations (Bertram & Tanzi 2005, Palop et al. 2006), although spreading may occur as the disease progresses. For example, Alzheimer's primarily affects the hippocampus, amyotrophic lateral sclerosis (ALS) the motor cortex and spinal cord and frontotemporal dementia (FTD) the frontal and temporal cortices (Mattson & Magnus 2006). As a result, the observed clinical manifestations have traditionally driven the differential classification of these disorders (Armstrong 2012, Bertram & Tanzi 2005).

In light of such observations, it might be assumed that the corresponding molecular pathology for each disease is equally distinct. Indeed, select components found within protein deposits (a hallmark of neurodegeneration) do appear to correlate with different diseases (Ross & Poirier 2004). Interestingly however, there is growing evidence that multiple molecular phenotypes are shared amongst varying diseases as well as 'non-diseased' aged persons (80+ years) (Elobeid et al. 2016, Wyss-Coray 2016). For example, a study conducted by Elobeid and colleagues (2016) found that protein hallmarks of neurodegeneration including hyperphosphorylated-tau, β-amyloid and hyperphosphorylated TAR DNA-binding protein 43 (TDP-43) were observed in 98, 47 and 36% of cognitively unimpaired brains, respectively (Elobeid et al. 2016). In addition to protein deposits, abnormal accumulations of carbohydrates and lipids, DNA damage and

inflammation can also be observed in both diseased and 'normal' aged brains (Wyss-Coray 2016). Thus, while the presence of molecular pathology may correlate with specific diseases, the mechanisms underlying their presence must be carefully considered. Regardless, while it is currently unclear if such macromolecular deposits are protective, harmful or causative in relation to disease, their presence implies that the cellular mechanisms normally mitigating their accumulation are impaired.

Given the heterogeneity of molecular phenotypes, what drives the development of neurodegenerative disease? While a portion of disease may be explained through genetic inheritance, many cases occur sporadically (i.e. with no familial history); for example only 10% of ALS cases are familial (Brown & Al-Chalabi 2017). Environmental factors (e.g. lifestyle, diet, toxins) (Wyss-Coray 2016) and sleep patterns (Musiek & Holtzman 2016) may also contribute to neurodegeneration. It has similarly been hypothesized that for proteins associated with multiple diseases, disease-specific pathology may result from select forms of environmental stress that cause the degeneration of a select brain regions (Saxena & Caroni 2011).

Amyotrophic lateral sclerosis (ALS)

Clinical Presentation

ALS is the most common adult motor neuron disorder and is characterized by both upper and lower motor neuron death. ALS is currently fatal and incurable. The

overall prevalence of this disease is estimated at 5/100,000 individuals (Mehta et al. 2018). However in comparing age groups <49 and >50 years, prevalence increases from 0.5-3.8/100,00 cases to 7.9-20/100,00 (Mehta et al. 2018). For this reason, ALS is considered a late-onset disorder.

Clinically, ALS patients present with progressive muscle weakening and wasting, followed by muscle cramps, fasciculations, paralysis and ultimately respiratory failure (Mehta et al. 2018). Following the appearance of symptoms, the median survival of ALS patients is 30 months (Salameh et al. 2015). The onset of ALS is typically mild and painless, initiating from a focal point of origin that spreads outwards as the disease progresses. For the majority of patients, onset occurs in the limbs and manifests as a clumsy hand or foot drop (Salameh et al. 2015). However, approximately one third of cases exhibit bulbar onset and present with a difficulty in swallowing or speech (Salameh et al. 2015). While ALS primarily affects motor function, mild cognitive impairment occurs for ~40% of patients and FTD within 5-14% (Salameh et al. 2015).

Currently, a diagnosis of ALS relies heavily on a patient's clinical presentation of symptoms. Further diagnostic support can be provided by the analysis of blood and cerebrospinal fluid, electrophysiology studies as well as magnetic resonance or neuroimaging; however many of these tests serve to exclude other possible diagnoses rather than to positively identify ALS (Salameh et al. 2015). Due to the subtle onset of symptoms, current lack of disease-specific biomarkers and potential development of atypical features, patient diagnoses are

often delayed and run the risk of an initial misdiagnosis and/or improper treatment prior to the final diagnosis (Kiernan et al. 2011, Salameh et al. 2015).

ALS Genetics and Molecular Pathology

The vast majority of patients with ALS develop the disease sporadically (SALS), although familial inheritance (FALS) represents approximately 10% of all cases (Brown & Al-Chalabi 2017). The first pathogenic mutations were identified within the *SOD1* gene in 1993 (Rosen et al. 1993) and were found to account for 20% and 2% of FALS and SALS cases, respectively (Taylor et al. 2016). Over next ~25 years, mutations in additional genes including *FUS* (Kwiatkowski et al. 2009, Vance et al. 2009), *TARDBP* (Kabashi et al. 2008, Sreedharan et al. 2008), *OPTN* (Maruyama et al. 2010) and *VCP*, (Johnson et al. 2014) were identified. However, the combined contribution of these genes ALS accounted for about that of superoxide dismutase 1 (SOD1) alone (Taylor et al. 2016). In 2011 however, an expanded hexanucleotide repeat within *C9ORF72* (DeJesus-Hernandez et al. 2011, Renton et al. 2011) was found not only to cause ALS, but to account for 25-40% and 6-10% of FALS and SALS, respectively (Renton et al. 2014, Taylor et al. 2016). Although additional genes have been found since then (Brown & Al-Chalabi 2017), the identification of mutations in (Chromosome 9 Open Reading Frame 72) C9orf72 represents a landmark discovery within the ALS field. Unlike most ALS genes or mutations, C9orf72 pathogenicity arises from an intronic gene repeat expansion. Further, mutations in C9orf72 as well as TDP43 and FUS have

genetically linked ALS and FTD (Couratier et al. 2017), two diseases previously considered separate disorders but are now recognized as related and potentially existing on a spectrum. While genetics clearly plays an important role in ALS pathogenesis, epidemiological studies also indicate that environmental factors (e.g. heavy metals, lifestyle, socioeconomic factors and trauma) (Riancho et al. 2018) and head injury (Chen et al. 2007) may contribute to disease development, however their involvement is not yet definitive.

Intriguingly, despite the diverse set of causing or contributing factors, both FALS and SALS share clinical manifestations that suggest the existence of common underlying pathways and/or mechanisms. ALS results in the atrophy of muscle, spinal cord and to a lesser extent, brain tissue. There is also neuronal loss and decreased axonal myelination (Saberi et al. 2015). Notably, degeneration across motor neuron types is not equal; ocular motor neurons are spared altogether in ALS as well as other forms of motor neuron disease (Nijssen et al. 2017). Neuroinflammation as a result of glial proliferation and activation in patient spinal cord tissue represents another key pathological feature (Saberi et al. 2015) and is supported by models demonstrating a non-autonomous role of glia in mediating neuronal degeneration in ALS (Di Giorgio et al. 2007, Nagai et al. 2007). Intracellularly, ALS phenotypes include nuclear fragmentation and condensation, vacuolization (Saberi et al. 2015) as well as mitochondrial and Golgi fragmentation (Rowland & Shneider 2001). Protein inclusions and/or skein-like aggregates are widely observed in the cytoplasm and (to a lesser extent) the nuclei of neurons

and glia in end-stage CNS tissue (Blokhuis et al. 2013, Peters et al. 2015, Rowland & Shneider 2001). In contrast to other neurodegenerative diseases, ALS cytoplasmic inclusions are often devoid of other common neurodegenerative disease associated proteins (e.g. tau and alpha synuclein) (Saberi et al. 2015).

Current Mechanisms of ALS

Although there is some degree of overlap between groups, the vast majority of ALS-causing genes fall broadly into three functional categories: protein degradation, RNA processing and cytoskeletal dynamics (Brown & Al-Chalabi 2017) (**Fig. I-2**). Thus, in evaluating possible ALS pathomechanisms, the implications of these pathways are closely considered. Relevant to the theme of protein homeostasis, ubiquitin-, p62- and TDP-43-postive protein aggregates are commonly observed in end stage, patient tissue (Saberi et al. 2015). Ubiquitin and p62 are both linked to the Ubiquitin-proteasome system and autophagic protein degradation processes and thus, their common presence in pathological aggregates suggest that ALS-mutations may induce such pathology, but how? Given that many ALS-linked genes are involved in protein homeostasis (**Fig. I-2**), their malfunction could contribute to disease. Furthermore, one recent study found proteins FUS, TDP-43 and SOD1 are supersaturated in spinal motor neurons and, as suggested by the authors, may be predisposed or prone to aggregation (Ciryam et al. 2017). This idea is intriguing as specifically these proteins are known to form

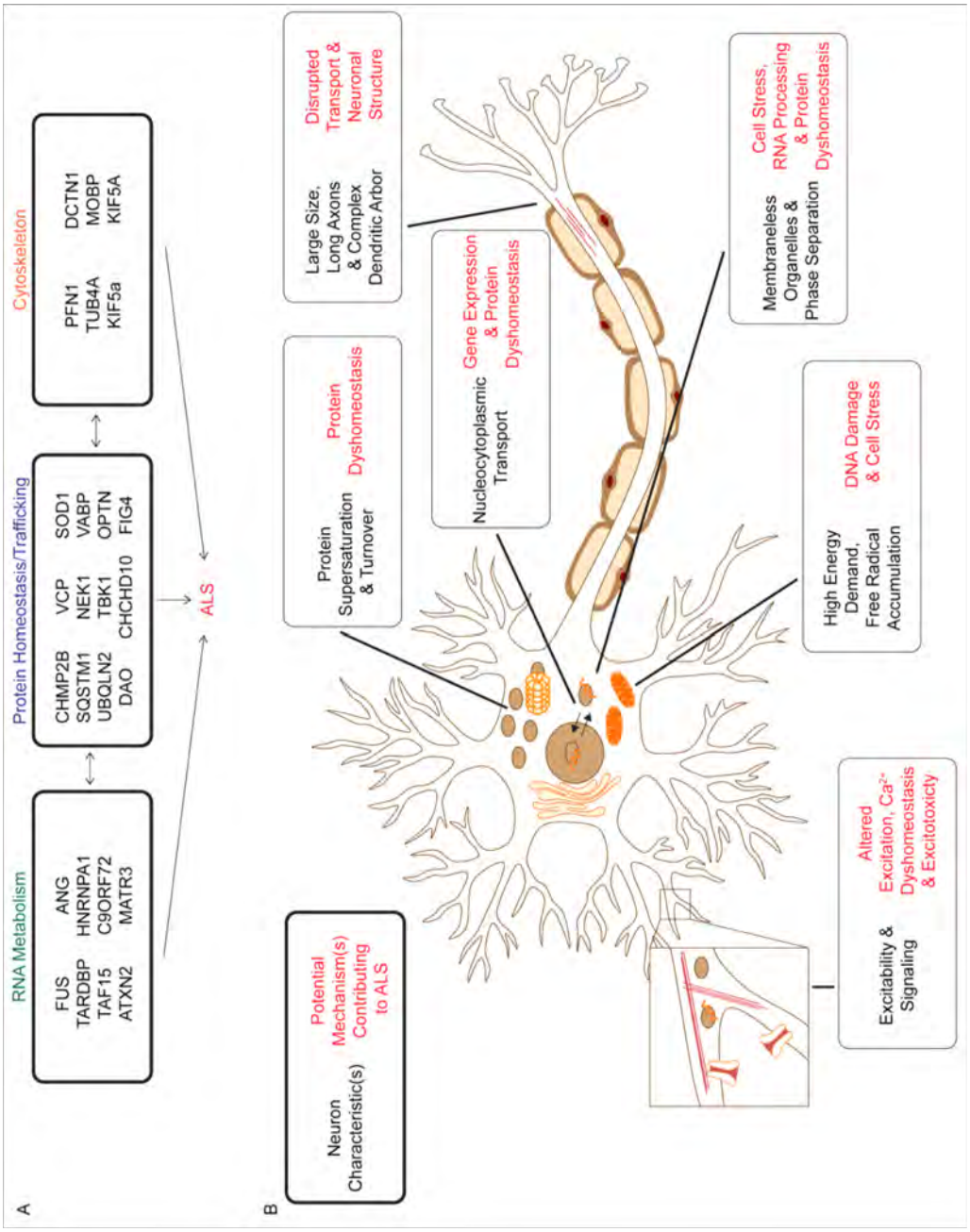

Figure I-2. Proposed ALS mechanisms. (A) Major genes associated with ALS can be grouped in the functional categories of RNA metabolism, protein homeostasis/trafficking and cytoskeleton (Brown & Al-Chalabi 2017, Eykens et al. 2015). (B) Genetic and model studies have uncovered evidence for cellular characteristics that may potentially contribute to disease.

aggregates in patients possessing mutations in these proteins themselves (e.g. patients with FUS mutations exhibit FUS-positive aggregates). Moreover, as previously mentioned, wildtype TDP-43, is a common aggregate component in both FALS and SALS. Interestingly, while SOD1-postive aggregates are not observed outside of SOD1-medaited ALS, there are reports (although contradictory to other studies) of FUS-positive aggregates in non-FUS familial and sporadic ALS cases (Blokhuis et al. 2013, Deng et al. 2010, Keller et al. 2012).

In addition to supersaturation, multiple ALS-linked proteins also possess the ability to undergo liquid-liquid phase separation (LLPS). Phase separation involves the reversible, bio-physical concentration and condensation of proteins from a mixed and dispersed state (St George-Hyslop et al. 2018). In regards to ALS, recent studies have demonstrated the ability of ALS-causing mutations to impair phase separation and/or cause aggregation *in vitro* (Conicella et al. 2016, Murakami et al. 2015, Patel et al. 2015), thus suggesting a possible mechanism by which aggregation occurs in disease. Currently, ALS-linked proteins shown to phase separate *in vitro* include: FUS (Patel et al. 2015), TDP-43 (Conicella et al. 2016), Ubiquilin 2 (Dao et al. 2018) and heterogeneous nuclear ribonucleoprotein A1 (hnRNPA1) (Molliex et al. 2015).

Although an active area of current research, it this though that the ability of ‘client’ proteins to undergo LLPS form a scaffold capable of sequestering associated ‘cargo’ thereby promoting the formation of membraneless organelles (stress granules, nucleoli etc.) (St George-Hyslop et al. 2018, Uversky 2016).

Profilin-1 (PFN1) (Posey et al. 2018) as well as the RNA or dipeptides produced from the *C9ORF72* repeat expansion (Fay et al. 2017, Lee et al. 2016) have been observed to alter aspects of phase separation biology. Notably, FUS, TDP43 and hnRNPA1 are strongly associated with stress granules, transient and membraneless mRNA-protein complexes thought to form via phase separation (St George-Hyslop et al. 2018, Uversky 2016) in response to stress (Kedersha & Anderson 2007). This connection has promoted the hypothesis that stress granules may promote or be linked to the formation of pathological aggregates (Molliex et al. 2015). Beyond stress granules, the inability for such LLPS to occur is also implicated in the aging process (Alberti & Hyman 2016). Although an active area of current research, the contribution of LLPS biology to disease pathogenesis is intriguing, but currently unclear.

Disruptions in the exchange of materials (e.g. mRNA, protein) between the nucleus and cytoplasm has recently emerged as yet another potential disease mechanism (Kim & Taylor 2017) and is strongly linked to the theme of RNA processing (**Fig. I-2**). In reprise of LLPS, the altered ability of proteins to phase separate might contribute to impaired nucleocytoplasmic transport (Guo et al. 2018, Yoshizawa et al. 2018). Furthermore, RNA-binding proteins including FUS (Kwiatkowski et al. 2009, Vance et al. 2009) and TDP43 as well as nuclear transport factors (Chou et al. 2018, Keller et al. 2012, Kinoshita et al. 2009, Zhang et al. 2015) are mislocalized to the cytosol in patient tissue. In light of such observations, it has been hypothesized that pathological alterations in

nucleocytoplasmic partitioning could alter RNA localization, as observed in models of C9orf72 (Freibaum et al. 2015), and thereby promote disease. Mutations cytoskeletal genes (**Fig. I-2**) may also have relevance to altered RNA processing and disease. The transport of mRNA to distal neuronal processes relies upon microtubule and actin dynamics (Hirokawa 2006, Koleske 2013) and, if disrupted, may impair neuronal function. In terms of structure alone, disruptions in cytoskeletal dynamics are especially relevant to motor neurons, whose axons are especially long and vulnerable to damage and aging (Mattson & Magnus 2006).

The extrapolation of ALS gene mutations to disease mechanism has revealed several processes that may contribute to ALS. However, how such implicated cellular processes induce the ALS pathology is essential in understanding their relevance, let alone contribution, to disease. Of significance to this work, phenotypes observed in patient and animal disease models include alterations in neuron excitability and neurotransmission. Motor neurons intrinsically express low levels of inhibitory type-A γ-aminobutyric acid ($GABA_A$) receptors and calcium buffering proteins to allow for rapid calcium transients (Nijssen et al. 2017, Saxena et al. 2013). However, such intrinsic biology can predispose motor neurons to hyperexcitability, an increased propensity for excitation in regards to a given stimulus. To this end, hyperexcitability has been observed in cases of familial and sporadic ALS as well as pre-symptomatic SOD1 carriers (Bae et al. 2013, Geevasinga et al. 2015, Vucic et al. 2008) and is correlated with patient survival (Kanai et al. 2012). The contribution of altered excitability to disease is widely

supported by observations in animal (Saba et al. 2015, Sharma et al. 2016, van Zundert et al. 2012) as well as induced pluripotent stem cell (iPSC)-derived motor neurons (Wainger et al. 2014). Although hyperexcitability is widely observed, there are also reports of hypoexcitability in ALS-models, giving rise to the notions of potential neuronal progression from hyper to hypoexcitability (de Lourdes Martínez-Silva et al. 2018, Devlin et al. 2015). Together, altered patterns of neuron excitability are widely observed in ALS patients and disease models.

Motor neurons are excited by glutamate and increased levels of this neurotransmitter are observed in patient cerebrospinal fluid (Fiszman et al. 2010, Spreux-Varoquaux et al. 2002). Further, altered processing of α-amino-3-hydroxy-5-methyl-4-isoxazolepropionic acid (AMPA) receptor subunits that control sodium and calcium influx have been observed at both the transcript and protein level in patient tissue and disease models (Hideyama et al. 2012, Kawahara et al. 2004, Selvaraj et al. 2018, Van Damme et al. 2007). Further, ALS-causing mutations have been identified in *DAO*, a gene encoding an enzyme involved in the degradation of the N-methyl-D-aspartate (NMDA) co-agonist, D-serine (Mitchell et al. 2010). Together, these observations suggest a contribution of glutamate receptors to disease. Prolonged or aberrant glutamate signaling, known as excitotoxicity, can lead to a state of cellular dysfunction through the influx of calcium ions and ultimate neuron death (Van Den Bosch et al. 2006). Downstream cellular effects of excitotoxicity include oxidative damage, mitochondrial dysfunction and protein misfolding, all of which are associated with ALS (Dong et

al. 2009, Szydlowska & Tymianski 2010, Van Den Bosch et al. 2006). Additionally, excitotoxicity has relevance in an emerging model of non-cell autonomous motor neuron death in ALS (Kia et al. 2018, Van Damme et al. 2007). In these models, astrocytes secrete molecule(s) that selectively alter AMPA-mediated signaling in a manner that is toxic to motor neurons (Kia et al. 2018, Van Damme et al. 2007). Whether such perturbations are the cause of or result from neuronal compensatory mechanisms, excitotoxicity represents one possible mechanism for motor neuron death in ALS.

Through further exploration a more complete understanding of disease mechanisms will hopefully lead to improved therapeutic treatments. Currently there are two FDA approved treatments for ALS: Riluzole and Edaravone. Riluzole was approved in 1995 and increases the longevity of ALS patients by 2-3 months (Bensimon et al. 1994, Miller et al. 2012). Although the exact mechanism is unknown, Riluzole is thought to reduce glutamate signaling and exert anti-excitotoxic properties (Cheah et al. 2010). Edaravone reduces free radicals and thereby could reduce the effects of oxidative stress (Writing Group et al. 2017). Although both drugs provide only modest relief, their effects implicate the relevance of their associated pathways (e.g. glutamate signaling and oxidative stress) to disease. Current directions for therapeutic development currently include stem cell therapies, aimed to support and modulate the nervous system environment during disease (Ciervo et al. 2017), as well as nucleic acid-based therapies (e.g. siRNA, antisense oligonucleotides) to modulate the expression of

disease-linked transcripts (Mathis & Le Masson 2018). Together, these efforts may soon offer a means for improved and prolonged patient survival.

Fused in sarcoma (FUS)

FUS Structure

Fused in sarcoma (FUS, also known as translocated in liposarcoma, hnRNP P2 and hPOMp75) is a 526-amino acid (**Fig. I-3**), RNA/DNA binding protein that is primarily localized to the cell nucleus. First discovered as part of a C/EBP homologous protein (CHOP)-fusion protein in myxoid liposarcoma (Crozat et al. 1993), FUS has since been shown to bind RNA, undergo nucleocytoplasmic shuttling (Zinszner et al. 1997). Moreover, FUS is an established hnRNP protein (Calvio et al. 1995) as well as member of the FET protein family (Tan & Manley 2009). Other members of this family include Ewing sarcoma (EWS), TATA-Box Binding Protein Associated Factor 15 (TAF15) and the fly homolog of FUS, cabeza/ sarcoma-associated RNA-binding fly homolog (CAZ/SARFH), all of which are united by their conserved structural domains and involvement in mRNA processing (Tan & Manley 2009).

The N-terminus of FUS is comprised of a low-complexity, prion-like domain composed of a glutamine-glycine-serine-tyrosine rich region (QGSY) and glycine-rich region (GLY) that was initially shown to promote aberrant transcription when

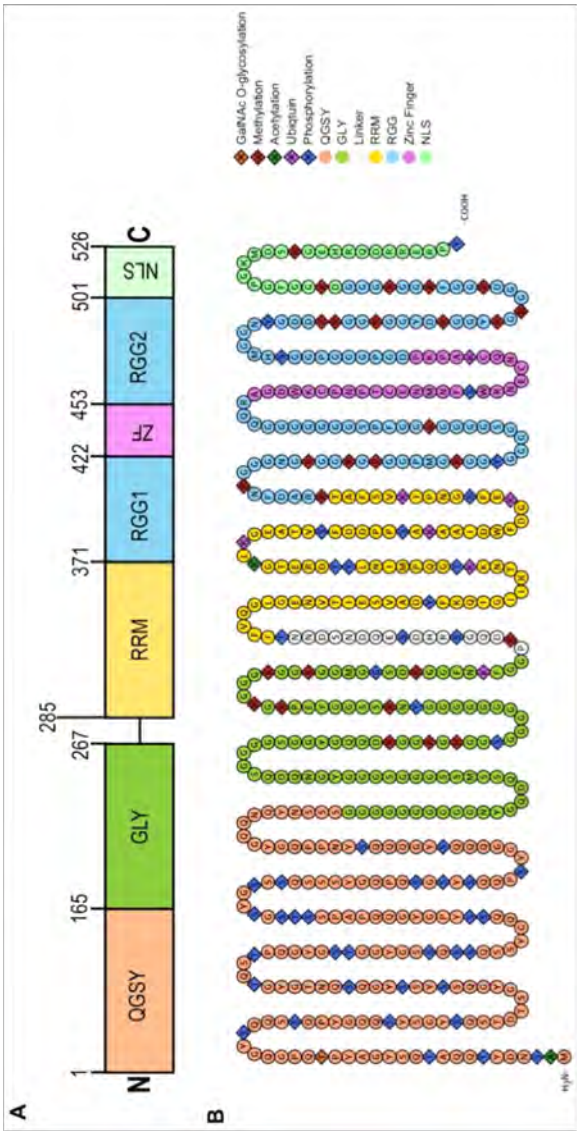

Figure I-3. FUS structure and posttranslational modifications. (A) FUS is a multi-domain protein involved in RNA/DNA binding activities (Sama et al. 2014). The N-terminus of FUS contains a glutamine-glycine-serine-tyrosine rich region (QGSY) and glycine-rich region (GLY). Following GLY is a short linker, RNA recognition motif (RRM) and two domains rich in arginine-glycine-glycine (RGG) rich repeats separated by a zinc-binding domain (ZF), all domains of which are involved in nucleic acid binding. The C-terminus of FUS is comprised of a non-classical nuclear localization sequence (NLS) that contributes to the nuclear localization of FUS. **(B)** FUS is heavily modified by post translational modifications, primarily phosphorylation and methylation (Rhoads et al. 2018b). Although not shown, T19 is also reported to be phosphorylated, K357 acetylated and K365 methylated (Rhoads et al. 2018b).

fused with CHOP in myxoid Liposarcoma (Crozat et al. 1993). FUS binds RNA cooperatively via the C-terminal domain and self-associates via the QGSY domain (Kato et al. 2012, Kwon et al. 2013, Schwartz et al. 2013, Yang et al. 2014). This ability to self-assemble is implicated in driving the association of FUS and (C-terminal repeat domain) C-terminal repeat domain of RNA Polymerase II, influencing C-terminal repeat domain phosphorylation and thus, transcription (Burke et al. 2015, Kwon et al. 2013, Schwartz et al. 2012, 2014). This QGSY domain has recently gained renewed attention for facilitating FUS LLPS, an observation that has further contributed to mechanistic understanding of how FUS might participate in various cellular functions. For instance, regulation of FUS LLPS appears linked to the phosphorylation and methylation of the FUS QGSY and arginine-glycine-glycine-rich repeats (RGG) regions, respectively (Han et al. 2012, Hofweber et al. 2018, Qamar et al. 2018) (**Fig. I-3**). As the N-terminal domain is highly subject to phosphorylation and self-association, it has been further attributed to the exclusion of FUS from LLPS phase-separated nucleoli (Deng, Holler, et al. 2014; Kino et al. 2011) and thus appears important in the subcellular distribution of this protein. Further *in vitro* research has also shown that such modifications alter the association of FUS with nuclear import proteins and RNA interactions that are currently believed to 'solubilize' FUS (i.e. lower self-association) in the cytoplasm and nucleus (Guo et al. 2018, Hofweber et al. 2018, Maharana et al. 2018, Yoshizawa et al. 2018).

Proximal to the N-terminal domain of FUS is a flexible linker followed by an RNA recognition motif (RRM) and two arginine-glycine-glycine (RGG) rich repeat regions that flank a zinc finger domain (**Fig. I-3**). Together these domains are important for DNA/RNA binding interactions (Bentmann et al. 2012, Iko et al. 2004, Liu et al. 2013). The RRM also contains a predicted nuclear export sequence (NES). However there is conflicting evidence as to if this NES is functional (Kino et al. 2015). Recent reports suggest that FUS may instead diffuse from the nucleus to the cytoplasm instead of being actively transported (Ederle et al. 2018). At the extreme C-terminus of FUS is a non-classical PY-NLS (Lee et al. 2006). The methylation status of residues flanking the NLS are known to influence the association of this protein with Transportin-1 (also known as Karyopherin β2) for active nuclear import (Dormann et al. 2012). Further, it is reported that the FUS NLS is subject to phosphorylation that can influence FUS compartmentalization (Darovic et al. 2015). Together, the FUS protein is comprised of modular domains that give rise to the functional versatility of this protein. Further, the high subjectivity of FUS to posttranslational modifications (**Fig. I-3**) allows for this protein to serve as an effector of signaling cascades in response to stimuli (Rhoads et al. 2018b, Svetoni et al. 2017).

FUS Function

FUS expression is near ubiquitous (Andersson et al. 2008) and FUS knockout mouse models show either perinatal death or sterility as well as

chromosomal instability, thus demonstrating the importance of this protein to survival (Hicks et al. 2000, Kuroda et al. 2000, Zahirovic & Sendscheid 2016). As previously mentioned, FUS is involved transcriptional processes and binds the promoter regions of >1000 genes, resulting in their altered expression upon FUS deletion (Tan et al. 2012). Further, FUS is involved in DNA damage repair and associates with telomeres (Sama et al. 2014), consistent with the genomic instability observed in certain murine models lacking FUS (Hicks et al. 2000).

The cellular roles of FUS extend beyond an association with DNA to also include interactions with various classes of RNA. Despite various efforts, no clear or consistent RNA-binding consensus sequence and/or FUS secondary structure has been identified (Sama et al. 2014). Although FUS appears to bind nucleotide sequences non-specifically (Wang et al. 2015), the association of FUS with RNA is influenced by nucleotide length (Wang et al. 2015; Lagier-Tourenne et al. 2012). FUS exhibits a strong preference for binding introns and, when normalized for transcript length, the 3' untranslated region (UTR) (Ishigaki et al. 2012, Lagier-Tourenne et al. 2012). The strong association of FUS with introns indicates the involvement of FUS in pre-mRNA splicing. Indeed, FUS associates with spliceosome components (Reber et al. 2016) and FUS knockdown or knockout results in widespread changes in splicing in addition to gene expression (Ishigaki et al. 2012, Lagier-Tourenne et al. 2012, Nakaya et al. 2013, Rogelj et al. 2012).

As a nucleocytoplasmic shuttling protein, FUS also participates in cytoplasmic RNA processing activities (Zinszner et al. 1997). FUS has been

implicated in mRNA transport as well as translation (Mili et al. 2008). Although extensive research has focused on the relationship of FUS and mRNA, there is new evidence that FUS is involved in the processing of microRNA (Zhang et al. 2018b). Specific to neurons, there is evidence that FUS localizes to neuronal dendrites (Fujii et al. 2005) as well as presynaptic axonal terminals (Schoen et al. 2015). Although there may be other mechanisms of FUS transport, kinesin family member 5 alpha (KIF5α) has been shown to transport FUS within RNA granules to dendrites (Kanai et al. 2004). Within dendrites, there are reports that FUS protein particles appear stationary until metabotropic glutamate receptor 5 (mGluR5) activation triggers the movement of FUS into spines (Fujii et al. 2005, Sephton et al. 2014). Moreover, myosin-Va has been shown to transport FUS and Nd1-L, a transcript encoding an actin-stabilizing protein, from the dendritic shaft into spines, presumably for translation (Fujii & Takumi 2005, Yoshimura et al. 2006). Reports further demonstrate that the association of FUS with actin motors myosin-Va and-VI are calcium-dependent (Takarada et al. 2009, Yoshimura et al. 2006). Thus, it is possible that FUS may be released in dendritic spines as part of a functional response to calcium.

Apart from Nd1-L, FUS has been shown to synaptically regulate SynGAPα2 mRNA to promote spine maturation, stabilization and function (Yokoi et al. 2017) as well as bind and stabilize Gria1 (Udagawa et al. 2015), a transcript encoding an AMPA receptor subunit. Furthermore, FUS knock out models show a decrease in spine number and altered neurite branching (Fujii et al. 2005). Together, these

data demonstrate the relevance of FUS to dendritic development. Furthermore, they indicate that the FUS function within neurons is critical to normal neuron development and function.

FUS and the Cellular Stress Response

As observed for other RNA-binding proteins (Dewey et al. 2011, van Oordt et al. 2000), FUS can translocate from the nucleus to the cytoplasm in response to cellular stress. However, FUS does not undergo cellular redistribution in response to all types of stress. For example, endogenous FUS does not translocate in response to heat shock, ER or oxidative stress (Sama et al. 2013). While there is one report showing a response of green fluorescent protein (GFP)-FUS to heat shock (Patel et al. 2015), this has not been observed for the endogenous protein (Sama et al. 2013). To date, the only environmental stressors shown to induce endogenous FUS translocation is sorbitol-induced, hyperosmotic stress (HOS) (Sama et al. 2013) and excitotoxity, the latter being the focus of this thesis. Thus, it appears there is selectivity with respect to the redistribution of FUS in response to environmental stress. HOS results from an increase in extracellular osmolytes, causing a rapid efflux of water from the cell to correct the osmotic imbalance (Burg et al. 2007). Further, HOS reduces global protein translation, selectively upregulates expression of stress-response genes (including heat shock proteins) (Burg et al. 2007) and induces macromolecular crowding (Bounedjah et al. 2012). Although not an environmental stress *per se*, in response to transcriptional, (but

not translational) inhibitors, FUS egress is also observed along with hnRNPA1 and heterogeneous nuclear ribonucleoproteins C1/C2 (hnRNP C1/C2) (Zinszner et al. 1994). Intriguingly, unlike HOS where FUS associates with stress granules (Sama et al. 2013), cytoplasmic FUS following transcriptional inhibition appears diffuse. Similarly, reports of DNA damage (Deng et al. 2014b) and fibroblast growth factor receptor 1 stimulation (Klint et al. 2004) also cause FUS egress, although the response of FUS to DNA damage is conflicting (Rhoads et al. 2018a).

Although the response of FUS to stress and stimuli appear selective, the purpose and mechanism for the redistribution of FUS is currently unclear. The responses of FUS to HOS is reversible and HeLa cells exhibit a decreased viability following hyperosmotic stress and FUS knockdown (Sama et al. 2013). These data imply a functional response of FUS to HOS stress. Further, RNA-binding proteins including hnRNPA1 (van Oordt et al. 2000) and TDP-43 (Dewey et al. 2011) as well as components of nuclear transport (e.g. RAN and importin β) likewise undergo a subcellular redistribution following HOS (Kelley & Paschal 2007). Thus, suggesting nuclear FUS egress is part of the global cellular response to HOS. Given the noted stress-linked changes in protein and gene expression, one possibility is that FUS might be involved cytoplasmic mRNA processing at this time. In immortalized cells, FUS is found within stress granules (Sama et al. 2013) following HOS treatment. The association of ALS-mutant FUS with stress granules (Baron et al. 2013) and the redistribution of FUS following transcriptional inhibition (Zinszner et al. 1994) is linked to the nucleotide-binding, C-terminal domains of

FUS. Thus, RNA binding may functionally contribute in the response of FUS to stress.

FUS and Disease

FUS mutations and disease-linked pathology are primarly neuropathological or cancerous in nature (**Table I-1**). Although investigated, no FUS mutations have been identified in Parkinson's or Alzheimer's to date (Svetoni et al. 2016; Lagier-Tourenne et al. 2010). Further, while FTD-causing mutations in FUS are rare, their presence has helped conceptualize of the existence of the ALS/FTD spectrum (Ling et al. 2013). However, unlike ALS, where a large number of FUS mutations (**Fig. I-4**) can induce cytoplasmic FUS pathology, cytoplasmic inclusions of wildtype FUS are observed in approximately 10% of FTD cases (Ling et al. 2013-b). The mislocalization of other FET members (TAF15 and EWS) as well as the import protein Transportin-1 are also observed in FUS-positive FTLD inclusions (FTD pathology is defined as frontotemporal lobar degeneration, FTLD) (Neumann et al. 2011). Based on such presentation in FTD, instances of FTLD with FUS pathology are classified as a disease subtype and referred to as FTLD-FUS.

Within the context of ALS, FUS mutations account for ~5% of FALS and are rarely observed *de novo* in SALS (Renton et al. 2014). Essentially all ALS-FUS mutations are present within the exonic regions of FUS (**Fig. I-4**), although at least one known mutation lies in the 3'UTR (Sabatelli et al. 2013). More specifically, FUS

Table I-1. FUS mutations and pathology linked to human disease. Mutations in FUS and FUS pathology are associated with multiple disorders.

Disease	Classification	Mutations
amyotrophic lateral sclerosis (ALS) (Kwiatkowski et al. 2009, Vance et al. 2009)	Motor Neuron Disease (affects both upper and lower motor neurons)	Yes; 5% of familial ALS; <1% sporadic. (**Fig. I-4**)
Frontotemporal dementia (FTD) (Neumann et al. 2009a) (Van Langenhove et al. 2010)	Dementia (degeneration of the frontal and temporal lobes)	Yes; rare <1%.
Polyglutamine diseases (Sca I, II, III and dentatorubral-pallidoluysian atrophy) (Doi et al. 2010)	Repeat expansion neurodegenerative diseases	No. However FUS-positive aggregates have been observed in patient samples
Essential Tremor (Merner et al. 2012, Schmouth et al. 2014)	Neurological movement disorder	Yes, although pathogenicity is unclear/controversial
Myxoid Liposarcoma (Crozat et al. 1993)	Form of cancer occurring in fat cells	Yes; chromosomal translocation. Resultant fusion protein with CHOP accounts for >90% of Myxoid Liposarcoma cases (Antonescu et al. 2000)
Acute Myeloid Leukemia (Ichikawa et al. 1994)	Cancer of the blood and bone marrow	Formation of a fusion protein between FUS and the transcription factor, ERG
Angiomatoid Fibrous Histiocytoma (Raddaoui et al. 2002, Waters et al. 2000)	Soft tissue neoplasm	Formation of a fusion protein between FUS and ATF1
Low-grade Fibromyxoid sarcoma (Storlazzi 2003)	Soft tissue sarcoma that typically occurs in the legs, trunk and abdomen	Formation of a fusion protein between FUS and BBF2H7
Ewing's tumors (Shing et al. 2003)	Pediatric bone and soft tissue tumor	Formation of a fusion protein between FUS and the transcription factor, ERG

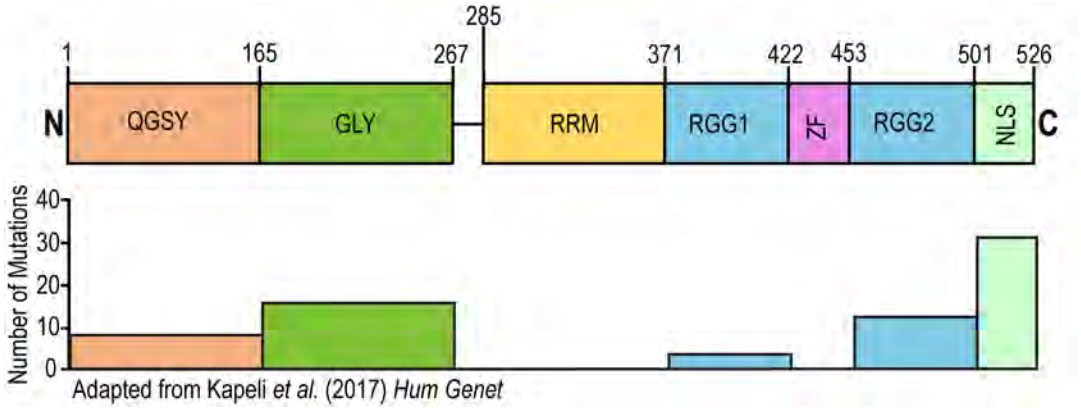

Figure I-4. Distribution of ALS-FUS mutations in the FUS protein sequence. ALS-causing mutations are found throughout FUS, however, the NLS contains the highest number of individual mutations (Kapeli et al. 2017). FUS domains: glutamine-glycine-serine-tyrosine rich region (QGSY), glycine-rich (GLY), RNA recognition motif (RRM) arginine-glycine-glycine- rich (RGG), zinc-binding domain (ZF) and nuclear localization sequence (NLS).

mutations are typically found within the N or C termini, the NLS being considered a ‘hot spot’ in terms of mutation number and frequency of occurrence (Deng et al. 2014a, Lattante et al. 2013). Intriguingly, ALS mutations are rarely observed in the RRM, RGG1 and zinc finger binding domains (**Fig. I-4**). *In vitro* studies have shown that multiple mutations proximal to the NLS induce FUS mislocalization to the cytoplasm, albeit to varying degrees (Bosco et al. 2010, Dormann et al. 2010). Further, there is a noted inverse correlation between the increased cytoplasmic localization of FUS and decreased age of disease onset (Dormann et al. 2010), suggesting that FUS mislocalization contributes to disease. In patient tissue, FUS is present in cytoplasmic inclusions that also include Ubiquitin, p62 and stress granule proteins including poly(A)-binding protein 1 (PABP-1) and eukaryotic translation initiation factor 4G (EIF4G) (Dormann & Haass 2013). While it is generally thought that FUS-positive inclusions do not overlap and contain TDP-43 or SOD1, several contradictory reports do show their co-existence in aggregates (Blokhuis et al. 2013, Deng et al. 2010, Keller et al. 2012).

FUS Gain of Function vs. Loss of Function in ALS

Despite the identification of mutations in FUS, the exact mechanism of FUS in ALS is unclear. With the exception of H517Q, the only recessive ALS-FUS mutation(Kwiatkowski et al. 2009), the autosomal dominant inheritance of FUS mutations raises the possibility that FUS may operate through a gain of function mechanism. Multiple models have addressed this question (Lanson & Pandey

2012) and, although overexpression of wildtype FUS expression produces disease-linked phenotypes (Mitchell et al. 2013), FUS overexpression is not observed in disease and the presence of endogenous FUS often served as confounder in these studies. As FUS mouse and fly knockout models frequently cause lethality (Hicks et al. 2000, Wang et al. 2011, Zahirovic & Sendscheid 2016), efforts to determine if ALS phenotypes resulted from gain and/or loss of function was stymied until two reports of FUS knockout and knockin mouse models in 2016. One study found that knockin murine models expressing the pathogenic mutations R521C and P525L (the latter a severely localized variant of mutant FUS) caused motor neuron loss and denervation as well as altered neuromuscular synapse function (Sharma et al. 2016). Interestingly, upon generation of conditional FUS knockout models, it was observed that such mice did not develop motor neuron loss. Moreover, no change to denervation was observed in mutant-FUS phenotypes when assessed in a FUS knockout background (Sharma et al. 2016). Similarly, a second group reported a knockin model of delta-NLS FUS, which results in the cytoplasmic localization of wildtype FUS (Zahirovic & Sendscheid 2016). When compared to a knockout FUS model, motor neuron loss was specifically observed in the delta-NLS mice (Zahirovic & Sendscheid 2016). The delta-NLS model also indicated the presence of nuclear FUS loss-of-function changes in splicing patterns when compared to FUS knockout mice (Zahirovic & Sendscheid 2016). Given the relevance motor neuron degeneration to ALS, these

findings support the notion that cytoplasmic FUS contributes to disease in a gain-of-function manner.

If cytoplasmic FUS is linked to disease and there is evidence for a gain of function mechanism, what might FUS be doing in the cytoplasm? ALS-mutant FUS has been shown to incorporate into stress granules, presumably translationally repressed RNA-protein complexes, caused by oxidative stress and to alter rates of stress granule assembly and disassembly (Baron et al. 2013, Bosco et al. 2010). The association of FUS and stress granules has also been observed in models of iPSC-derived neurons (Lenzi et al. 2015, Lim et al. 2016). Further, expression of mutant FUS in *Xenopus* retinal ganglion neurons reduced levels of protein translation (Murakami et al. 2015) and conditional expression of FUS knock-in mutations increase eukaryotic initiation factor 2 alpha (EIF2α) phosphorylation (Zahirovic & Sendscheid 2016). Together these data suggest cytoplasmic FUS is capable of directly or indirectly affecting RNA regulation and translation. While the exact mechanism by which FUS contributes to disease is an area of active research, the development of increasingly sophisticated and disease-relevant models increases the possibility of increased mechanistic insight.

Summary

Neurons are highly specialized cells that allow for the transfer of information in the body. As with any cell, essential physiological processes are maintained through homeostasis, yet such processes are often subject to dysregulation during stress

and disease. ALS is a neurodegenerative disease that results in motor neuron degeneration and ~5% of familial cases result from mutations in the RNA/DNA binding protein, FUS. Strikingly, near half of the ALS mutations identified result in cytoplasmic mislocalization of this protein. Moreover, the degree of mislocalization inversely correlates with age of disease onset. Supported by findings from cellular and animal disease models, these data indicate a role for cytoplasmic FUS in the progression of FUS-mediated ALS, although the exact mechanism is unknown.

FUS is one of multiple RBPs that shuttles between the nucleus and cytoplasm and accumulates in the cytoplasm following cellular stimuli and stress. Specifically, FUS egress has been observed in response to HOS stress and excitotoxicity, the discovery of the latter described herein. Excitotoxicity is a neuronal stress caused by prolonged glutamate signaling and is associated with ALS. While the redistribution of multiple disease linked RBPs was observed following excitotoxic stress, the nuclear egress of FUS was particularly robust. Moreover, predominately nuclear ALS-FUS variants were found to similarly exhibit excitotoxic egress, thus representing a possible mechanism by which FUS accumulates in the cytoplasm during disease. Apart from the distribution of RBPs, excitotoxity alters nuclear transport and induces translational repression, all of which are features consistent with cell stress. Together, these findings support the growing relevance of cell stress to the pathomechanism(s) of ALS.

Investigation into the specific response of FUS revealed the FUS egress as calcium dependent. Moreover, in response to stress, FUS was found to regulate

the dendritic expression of Gria2, a transcript encoding the calcium-regulating subunit of the AMPA glutamate receptor. Together, this work demonstrates a novel role of FUS in calcium and glutamate signaling pathways. As glutamate-mediated, calcium entry in motor neurons occurs primarily through AMPA receptors, these observations further support the premise that FUS has a normal function during excitotoxic stress and that glutamatergic signaling may be dysregulated in FUS-mediated ALS.

PREFACE TO CHAPTER II:

Parts of this chapter will appear in:

Tischbein, M., Baron, D.M., Lin, Y.C., Gall, K., Landers, J.E., Fallini, C., and D.A. Bosco. FUS/TLS undergoes calcium-mediated nuclear egress during excitotoxic stress and is required for Gria2 mRNA processing. (2018)

The work and analysis presented in this chapter was performed by Maeve Tischbein with the following exceptions:

Murine primary motor neuron experiments were performed and analyzed by Dr. Claudia Fallini. NLS-tdTomato-NES construct preparation and KPT-330 optimization were performed by Yen-Chen Lin. Puromycin experiments without FUS knockdown and fluorescence *in situ* hybridization studies were performed and analyzed by Dr. Desiree Baron. Human induced pluripotent stem cell (iPSC)-derived motor neurons were differentiated and cultured by Yen-Chen Lin and Dr. Jeanne McKeon. Assistance with Western blotting, cloning, lentiviral production as well as primary cortical neuron harvesting and culture by Katherine Gall. Mass spectrometry samples were run by Dr. John Leszyk (Mass Spectrometry Facility, UMMS).

CHAPTER II: INVESTIGATING THE RESPONSE OF FUS TO EXCITOTOXIC INSULT

Introduction

Glutamate is the major excitatory neurotransmitter in the central nervous system. Upon release from pre-synaptic terminals, relatively low levels of glutamate activate metabotropic glutamate receptors as well as the ionotropic receptors: α-amino-3-hydroxy-5-methyl-4-isoxazolepropionic acid (AMPA), N-methyl-D-aspartate and kainite, for normal neurotransmission. However, excessive glutamate exposure overstimulates neurons. This causes a massive influx of calcium, which triggers an excitotoxic cascade involving oxidative damage as well as mitochondrial and ER dysfunction (Van Den Bosch et al. 2006). Excitotoxicity has been implicated in neuronal death and degeneration for various neurological conditions, including the fatal neurodegenerative disease amyotrophic lateral sclerosis (ALS) (Fogarty 2018, Starr & Sattler 2018, Van Den Bosch et al. 2006). Pathological evidence for excitotoxity includes elevated levels of glutamate in patient cerebrospinal fluid (Fiszman et al. 2010, Spreux-Varoquaux et al. 2002) as well as aberrant processing of the AMPA subunit that controls calcium influx at both the transcript (Gria2) and protein (Glutamate Receptor 2; GluR2) level in patient tissue and disease models(Hideyama et al. 2012, Kawahara et al. 2004, Van Damme et al. 2007). Further, ALS-causing mutations are present in D-amino acid oxidase, an enzyme that regulates the degradation of the N-methyl-D-aspartate co-agonist, D-serine (Mitchell et al. 2010). Riluzole, the first FDA

approved treatment for ALS, is thought to reduce glutamate signaling through anti-excitotoxic effects (Cheah et al. 2010). Despite this wealth of knowledge and profound disease relevance, the biological mechanisms underlying the cellular response to excitotoxicity have not been fully elucidated.

RNA-binding proteins (RBPs) have emerged as relevant factors in neurodegenerative disease pathogenesis, particularly in the context of ALS and the related disorder, frontotemporal dementia (FTD) (Brown & Al-Chalabi 2017). RBPs belong to a unique class of biomolecules that undergo nucleocytoplasmic shuttling in response to various stimuli, including stress. For instance, the disease-linked RBPs fused in sarcoma/translocated in liposarcoma (FUS/TLS or FUS), TAR DNA-binding protein 43 (TPD-43) and heterogeneous nuclear ribonucleoprotein A1 (hnRNPA1) all exhibit nuclear egress during hyperosmotic stress (Dewey et al. 2011, Sama et al. 2013, van Oordt et al. 2000). The purpose of this translocation is unclear, and may represent a functional response to cellular stress (Sama et al. 2013, 2014). In support of this notion, cell viability under hyperosmotic stress is compromised when FUS expression is reduced (Sama et al. 2013). However, cell stress also represents a non-genetic factor that likely contributes to neurodegenerative disease pathogenesis (Sama et al. 2014). Indeed, chronic stress may contribute to the pathological cytoplasmic accumulation of TDP-43 and FUS, prevalent features of ALS and FTD (Deng et al. 2010, Keller et al. 2012, Kwiatkowski et al. 2009, Neumann et al. 2009a, Vance et al. 2009). For example, TDP-43 partitions into the insoluble fraction of cultured

cells following oxidative stress or heat shock (Boyd et al. 2014, Xu et al. 2012) and disease-linked RBPs have been found to aggregate *in vivo* following cerebral ischemia (Kahl et al. 2018). Intriguingly, the effects of stress on RBP translocation appear selective. While ER stress, oxidative stress and heat shock induce the cytoplasmic accumulation of TDP-43 and other RBPs (Colombrita et al. 2009, McDonald et al. 2011), these stressors fail to elicit a response of FUS (Bosco et al. 2010, Sama et al. 2013). Given the physiological relevance of excitotoxicity to neurodegenerative disease, an important but unanswered question is whether excitotoxic stress elicits a functional and/or pathological response from disease-associated RBPs.

Here, we demonstrate that excitotoxic levels of glutamate induce the nuclear egress of several ALS- and FTD-linked RBPs, including FUS, TDP-43 and hnRNPA1 into the cytoplasm of neurons. The nucleocytoplasmic equilibrium of FUS was especially sensitive to excitotoxic stress, as FUS was found to rapidly and robustly accumulate within soma and dendrites of cortical and motor neurons under stress. Further, a glutamate-induced increase in dendritic Gria2 was dependent on FUS, consistent with a role for FUS in glutamatergic signaling during the cellular response to excitotoxic stress. Our results also revealed potentially adverse consequences of excitotoxicity, including the translocation of ALS-linked FUS variants and early signs of nucleocytoplasmic transport dysregulation. This study therefore demonstrates that excitotoxicity can trigger neurodegenerative

disease-associated pathologies including cytoplasmic RBP accumulation and nucleocytoplasmic transport decline.

Results

Developing a Cellular Model of Excitotoxicity

To investigate a potential relationship between excitotoxicity and neurodegenerative disease-linked RBPs, I first established a tractable, *in vitro* model of excitotoxicity. Day *in vitro* (DIV) 14-16 primary cortical neurons were bath treated with 10μM glutamate, an excitotoxic (Schubert & Piasecki 2001) and physiological amount of the neurotransmitter (Fiszman et al. 2010), for 10 minutes followed by a 30-minute washout period (**Fig. II-1A**). Unless indicated, 'neuron' hereon refers to primary cortical neurons and Glu^{excito} to 10μM glutamate. Neurons and dendrites were identified using the marker, microtubule-associated protein 2 (MAP2). Following treatment with Glu^{excito}, cytoskeletal arrangements were observed using this marker; MAP2 staining was increased in neuronal soma as well as highlighted dendritic fragmentation (**Fig. II-1B**). That neuron morphology is altered at 30 minutes (**Fig. II-1A**) is potentially indicative of a stressed cell state (Chen et al. 2011, Murphy et al. 2008), consistent with excitotoxity.

Given the toxicity of Glu^{excito} on neurons (Schubert & Piasecki 2001), cell death at 30 minutes was assessed using the Lactate Dehydrogenase (LDH) cytotoxicity assay. This assay detects the activity of cytoplasmic LDH released into the media from dead or dying cells. In contrast to cells treated with lysis buffer,

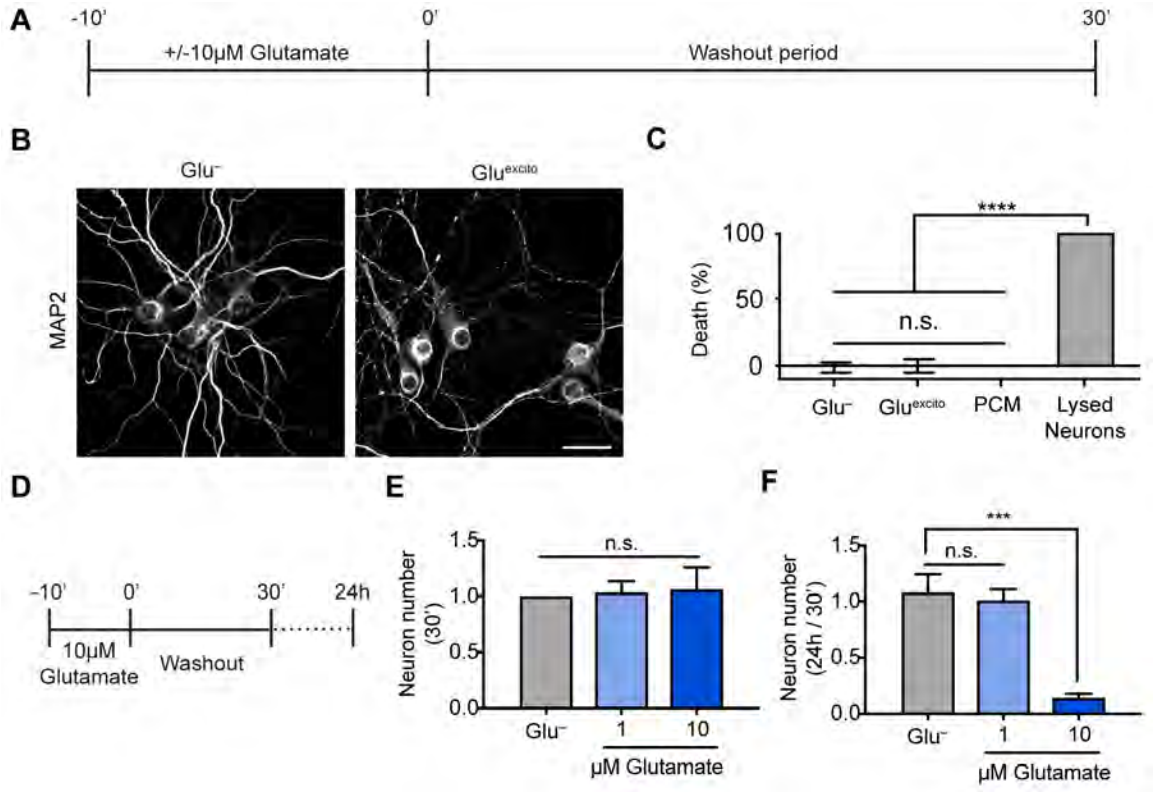

Figure II-1. Glutamate induces excitotoxicity in primary cortical neurons. (A) Day *in vitro* (DIV) 14-16 primary cortical neurons were bath treated with 10μM glutamate (Glu^{excito}) for 10 minutes, after which the glutamate-containing media was washed out and replaced with cultured neuronal media for an additional 30 minutes. **(B)** Following excitotoxic insult, cytoskeletal rearrangements were detected by confocal analysis of immunofluorescence staining with the neuronal marker, MAP2. Scale bar = 10μm. **(C)** Cytotoxicity induced by Glu^{excito} was assessed after the wash-out period with the LDH assay. In contrast to the positive control (neurons treated with lysis buffer; lysed neurons), membrane permeabilization was not detected for neurons exposed to Glu^{excito}. Neurons cultured in the absence of Glu^{excito} (Glu^{-}) served as a negative control. Wells containing only primary conditioned media (PCM) served as a background control. Results reflect three biological replicates analyzed with a one-way ANOVA and Tukey's post-hoc test (****$p<0.0001$, n.s. = non-significant). **(D,E)** Quantification of MAP2-postive neurons shows no change in relative neuron number at 30'. **(F)** However, quantification at 24h relative to 30' shows a significant reduction in neuron number relative to Glu^{-} following treatment with 10 but not 1μM glutamate (One-way ANOVA and Tukey's post-hoc test, ***$p<0.001$, n.s. = non-significant, n = 3 biological replicates). Error bars = SEM.

there was no cell death for neuron cultures treated with Glu^{excito} (**Fig. II-1C**). Similarly, there was no difference in neuron number following exposure to excitotoxic stimuli at 30 minutes (**Fig. II-1D,E**). However, Glu^{excito}-treated neurons do undergo eventual cell death (**Fig. II-1D,F**), as expected (Schubert & Piasecki 2001). This effect was not observed for 1μM glutamate, a sub-toxic concentration of glutamate (**Fig. II-1D-F**). Together these data provide evidence for the inducement of excitotoxicity in cortical neurons by Glu^{excito} (**Fig. II-1**). The response of neurons to glutamate is further characterized and supported herein.

Response of RNA Binding Proteins to Excitotoxicity

Upon establishing a model of excitotoxicity, we next examined whether the cytoplasmic:nuclear (C:N) equilibrium of RBPs were affected by excitotoxic stress. We examined a panel of RBPs including FUS, TDP-43, hnRNPA1 and TAF15, all of which have been linked to ALS (Brown & Al-Chalabi 2017). In addition, FUS, TDP-43 and TAF15 are associated with the related disorder, FTD (Ito et al. 2017). Immunofluorescence microscopy was used to assess the effect of Glu^{excito} on the C:N ratio of the endogenous RBPs (**Fig. II-2A-H**). Strikingly, the C:N of FUS was significantly increased ~15 fold from 0.04 ± 0.05 to 0.6 ± 0.3 in response to Glu^{excito} (**Fig. II-2A,E**). This increase is likely due to a rapid egress of FUS from the nucleus into the cytoplasm as opposed to changes in FUS expression levels, as a western analysis revealed similar levels of FUS protein in the presence and absence of stress (**Fig. II-2I,J**). Glu^{excito} likewise induced a significant increase in the C:N ratio

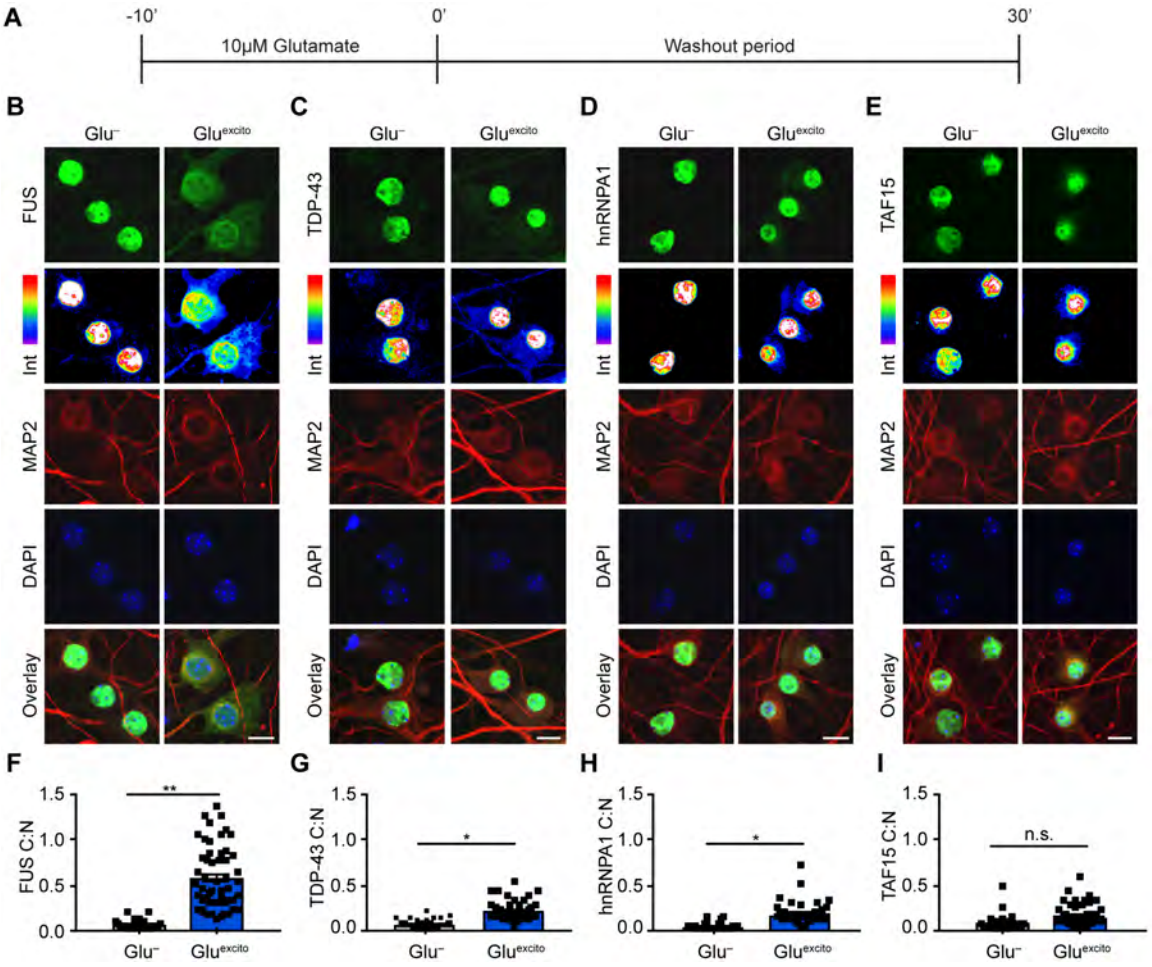

Figure II-2. Nuclear RBPs translocate to the cytoplasm following excitotoxic stress. (A) DIV 14-16 primary cortical neurons were bath treated with 10μM glutamate (Glu^{excito}) for 10 minutes, after which the glutamate-containing media was 'washed out' and replaced with cultured neuronal media for an additional 30 minutes. **(B-E)** Immunofluorescence and confocal microscopy revealed the subcellular localization of FUS, TDP-43, hnRNPA1 and TAF15 (green) with or without Glu^{excito}. A 16-color intensity map (Int) of endogenous RBP staining (green) further demonstrates RBP localization. Neurons and dendrites were identified with anti-MAP2 staining (red), and nuclei with DAPI (blue). Scale bars = 10μm. **(F-I)** A significant egress in the cytoplasmic to nuclear ratio (C:N) of FUS (F), TDP-43 (G) and hnRNPA1 (H), but not TAF15 (I) was observed following Glu^{excito} treatment (Student's T-test; $^{**}p<0.01$, $^{*}p<0.05$, n.s. = non-significant; n = 3-4 biological replicates). Experimental means were calculated from the average C:N ratio across the individual biological replicates. Black squares represent the C:N ratio of individual cells. Error bars correspond to SEM.

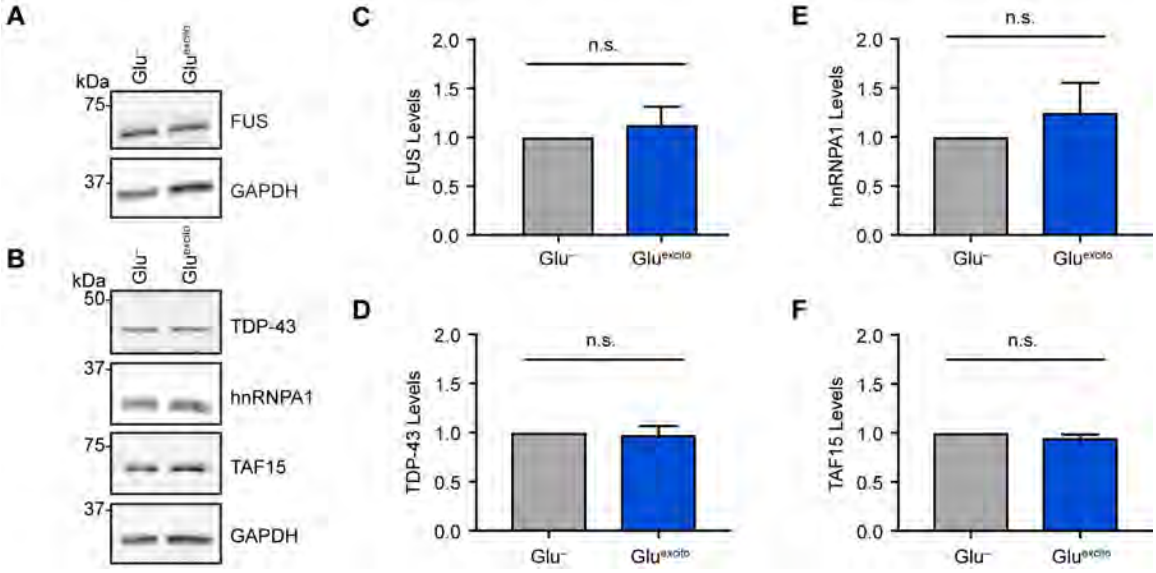

Figure II-2 continued. (I) Western analysis of cortical neurons demonstrates that FUS, TAF15, hnRNPA1 and TDP-43 protein levels do not change in response to Glu^{excito}. **(J-M)** Observations from (I) were confirmed by densitometry. For quantification, RBP levels were first normalized to the loading standard, GAPDH, and then to the control condition, Glu^{-} (Student's t-test, n.s. = non-significant, n=3 biological replicates). Error bars represent SEM.

of TDP-43 (**Fig. II-2B,F**) and hnRNPA1 (**Fig. II-2C,G**), also without accompanying changes in total proteins levels (**Fig. II-2I,K,L**). Conversely, this stress did not significantly alter the C:N ratio (**Fig. II-2D,H**) or total protein levels (**Fig. II-2I,M**) of TAF15.

In light of the robust response of FUS to Glu^{excito}, we focused our attention on the properties of FUS translocation in more detail. First, the translocation of endogenous FUS to Glu^{excito} was assessed using a panel of different anti-FUS antibodies, all of which confirmed FUS translocation under excitotoxic stress (**Fig. II-3A,B**). Moreover, FUS egress was not observed in astrocytes (a non-neuronal cell type present in the CNS; **Fig. I-1**), which suggests that glutamate-induced FUS translocation is specific to neurons (**Fig. II-3C**). We then examined the relationship between FUS redistribution and glutamate concentration. With 10μM glutamate, the vast majority (91.3±11.5%) of neurons exhibited FUS translocation (**Fig. II-3D,E**) whereas with ≤1μM, egress was observed for <5% of neurons and reveals a dependence of FUS translocation on glutamate concentration (**Fig. II-3E**). Within the time course of our experiment (**Fig. II-1A**) a significant accumulation of endogenous FUS was also detected throughout MAP2-positive dendrites (**Fig. II-3F,G**). Increased FUS staining was also detected in ankyrin-G-positive axon initial segments following excitotoxic insult (**Fig II-3H**, not quantified). Together these data demonstrate the rapid redistribution of FUS throughout the cell in response to Glu^{excito}.

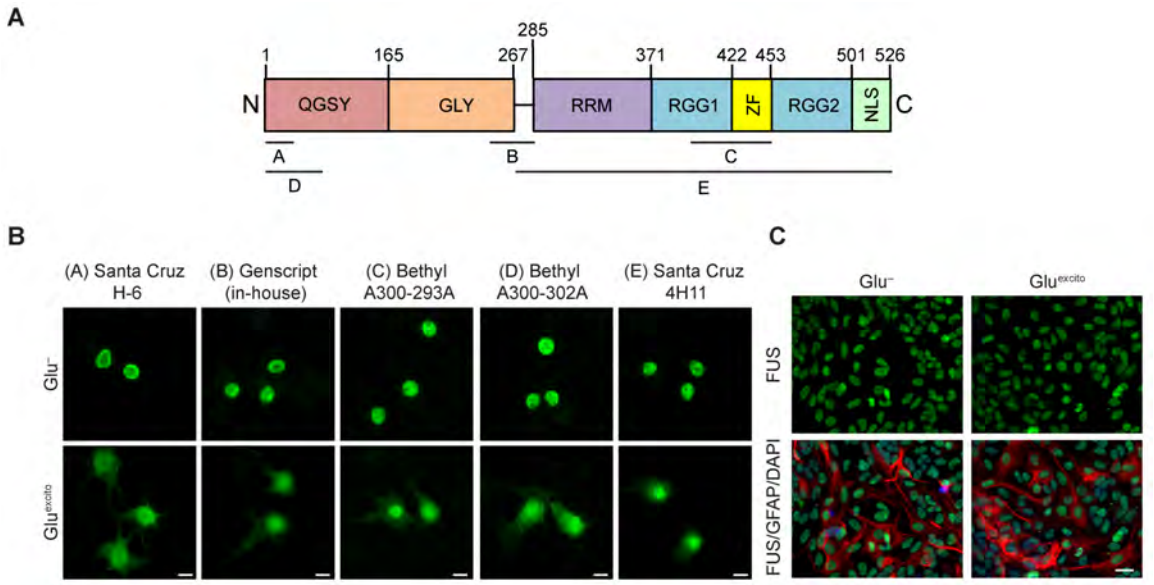

Figure II-3. Endogenous FUS exhibits a rapid and robust response to excitotoxicity. (A) Anti-FUS antibody epitopes mapped to the domain structure of human FUS (QGSY = glycine-serine-tyrosine rich region, GLY = glycine-rich region, RRM = RNA recognition motif, RGG = arginine-glycine-glycine-rich region, ZF = zinc-finger domain and NLS = nuclear localization sequence). **(B)** Immunofluorescence staining of endogenous FUS (green) using antibodies with epitopes described in (A) consistently demonstrates FUS translocation following treatment with Glu^{excito}. **(C)** FUS translocation (green) was not observed in glial fibrillary acidic protein (GFAP)-positive astrocytes (red), n=3 biological replicates. Nuclei stained with DAPI (blue). Scale bars = 20μm.

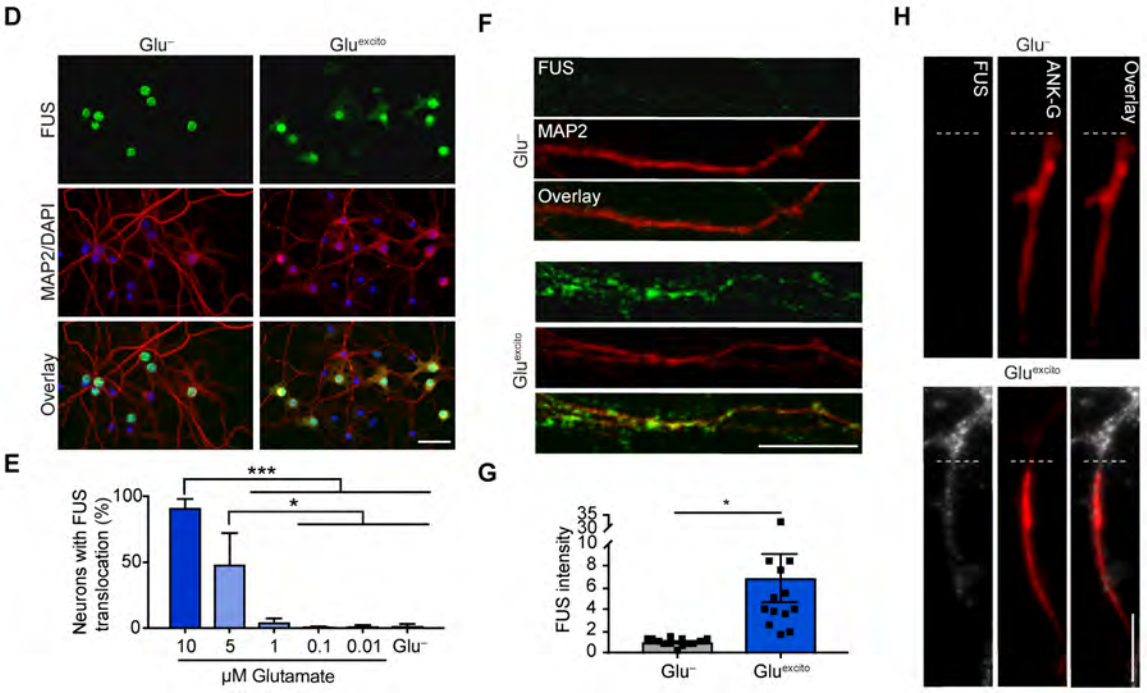

Figure II-3 continued. (D,E) Excitotoxic FUS was detected by anti-FUS (green) in >90% MAP2-postive PCNs (red). Nuclei stained with DAPI (blue). Scale bar = 40µm. Quantification of (D) revealed a dependence of FUS translocation on glutamate dose in MAP2-positive neurons (One-way ANOVA and Tukey's post-hoc test; ***p<0.001, *p<0.05; n=3 biological replicates). Error bars represent SEM. **(F)** Increased dendritic FUS staining (green) was observed by confocal microscopy following excitotoxic stress. Dendrites were indicated by MAP2 (red). Scale bar = 10µm. **(G)** Quantification of (E). Black squares represent the relative intensity of dendritic FUS staining per cell. Means represent the average of four biological replicates normalized to the control (Glu^{-}) (Student's T-test; * = p<0.05). Error bars represent SEM. **(H)** Excitotoxic insult increased FUS staining intensity (white) within initial axon segments as detected using the maker, ankyrin-G (ANK-G, red; n=2 biological replicates). White lines denote the start of the axon initial segment. Scale bar = 10µm.

Excitotoxic Stress Disrupts Nucleocytoplasmic Transport

To understand the redistribution of RBPs to excitotoxity, I investigated the mechanism(s) underlying endogenous FUS egress in response to Glu^{excito}. I began by assessing general nuclear envelope integrity. Immunofluorescence of anti-Lamin A/C staining revealed an intact nuclear envelope in neurons exposed to Glu^{excito} (**Fig. II-4A**). Although the nuclear lamina appeared thickened and the size of nuclei smaller in stressed neurons, no gross disruptions to the nuclear membrane were observed (**Fig. II-4A**). Further, nucleocytoplasmic partitioning also appears intact as the localization of nuclear TAF15 (**Fig. II-2D,H**) and cytoplasmic fragile X mental retardation protein (FMRP; **Fig. II-4B**) were respectively maintained under conditions of Glu^{excito}. As neurons are viable (**Fig. II-1C-F**) and apparent nuclear envelope integrity preserved at 30 minutes (**Fig. II-4A**,**B**), these data suggest that excitotoxic FUS egress could be a biologically relevant response that warrants further investigation.

We next examined the contribution of nucleocytoplasmic transport factors to FUS egress. FUS contains two predicted chromosome region maintenance 1 (CRM1)-dependent nuclear export sequences (NES) within the RNA-recognition motif (RRM) (Ederle et al. 2018). CRM1, also known as exportin-1 (XPOI), is a major nuclear protein export factor, although whether this receptor controls nuclear export of FUS is controversial (Ederle et al. 2018, Kino et al. 2011). To determine if Glu^{excito}–induced FUS egress is CRM1-dependent, we pre-treated neurons with the CRM-1 inhibitor, KPT-330, 48 hours prior to exposure to Glu^{excito} (Grima et al.

2017). The CRM-1 dependent NLS-tdTomato-NES shuttling reporter was used as a positive control (Hatch et al. 2013). As expected, NLS-tdTomato-NES was observed in both the nucleus and cytoplasm under basal conditions, whereas the localization of NLS-tdTomato-NES was significantly restricted to the nucleus in the presence of KPT-330 (**Fig. II-4C,D**). In contrast, KPT-330 had no effect on the nuclear egress of FUS in response to Glu^{excito} (**Fig. II-4C,E**). Surprisingly, KPT-330 also failed to fully restrict NLS-tdTomato-NES to the nucleus under conditions of Glu^{excito} (**Fig. II-4C,D**). Although there was a significant decrease in the percentage of cells with cytoplasmic NLS-tdTomato-NES in the presence of both KPT-330 and Glu^{excito} (60.1±8.0%) compared to Glu^{excito} alone (98.3±2.6, p=<0.0001), these results demonstrate that inhibition of CRM1-mediated export is compromised following excitotoxic insult (**Fig. II-4D**). KPT exerted a partial effect over the localization of our shuttling reporter (**Fig. II-4D**), indicating there might be a modest rescue of nucleocytoplasmic transport and possible downstream effects of excitotoxicity, such as cell death. To test if KPT-330 could improve neuron survival, I applied propidium iodide (PI), a chromatin stain that is impermeant to live cells, and monitored cell viability following treatment with Glu^{excito}. The addition of KPT to neurons did not improve cell survival following acute excitotoxic treatment (**Fig. II-4G**). Of note, this assay further confirmed that excitotoxic stress has no effect on neuron survival at 30 minutes (**Fig II-4G**) relative to unstressed cells and is consistent with previous results (**Fig II-1C-F**).

To gain further insight into this nuclear transport phenomenon, we assessed the localization of endogenous CRM1 by immunofluorescence. While CRM1 predominately localized to the nucleus under basal conditions, we observed a striking and significant increase in cytoplasmic CRM1 following Glu^{excito} treatment (**Fig. II-4H,I**). This finding prompted us to examine another critical nucleocytoplasmic transport factor, Ras-related nuclear protein (Ran). Ran is a GTPase that shuttles between the nucleus and cytoplasm and facilitates both nuclear import and export (Kim & Taylor 2017). Indeed, Glu^{excito} also induced a significant change in Ran localization from the nucleus to the cytoplasm (**Fig. 4J,K**). The dramatic redistribution of critical transport factors under Glu^{excito} implies a dysregulation of nucleocytoplasmic transport under stress and may explain the attenuated effects of KPT-330 on CRM1 export and survival under excitotoxic conditions. That KPT-330 had no effect on FUS localization (**Fig. 4C**) suggests that the nuclear egress of FUS caused by excitotoxic stress occurs through a CRM1-independent pathway.

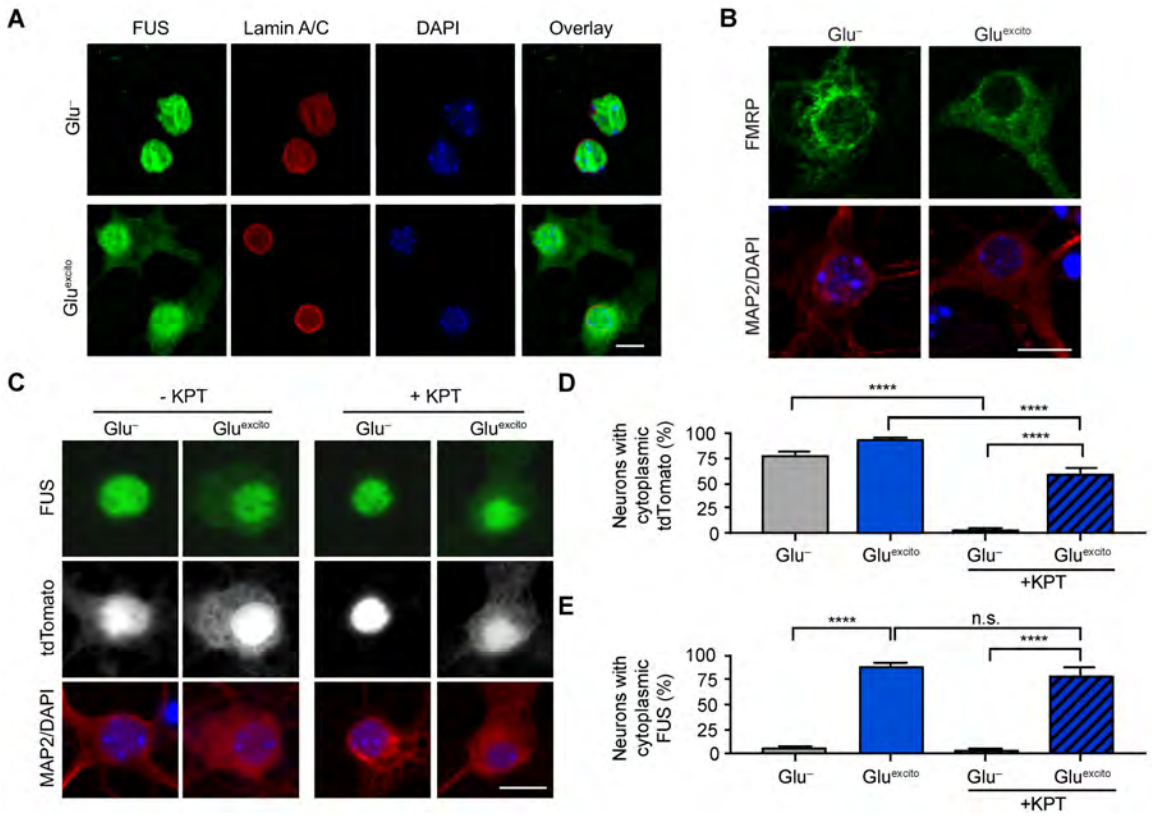

Figure II-4. Nucleocytoplasmic transport is disrupted by Glu^{excito}. (A) Immunofluorescence staining and confocal microscopy of Lamin A/C (red), revealed a thickened yet morphologically intact nuclear envelope in neurons exhibiting FUS translocation (green) after Glu^{excito} exposure at 30' (n=3 biological replicates). Scale bar = 25μm. **(B)** Confocal analysis demonstrates that the cytoplasmic localization of FMRP (green) is retained following excitotoxic insult in neurons (red; n=2 biological replicates). **(C-E)** Neurons expressing the shuttling reporter, NLS-tdTomato-NES, were treated with or without 500 nM of the CRM1 inhibitor, KPT-330 (KPT), prior to Glu^{excito} exposure. The percentage of MAP2-positive neurons (C; red) expressing cytoplasmic NLS-tdTomato-NES (C; white) or FUS (C; green) was quantified for three biological experiments (D and E, respectively). KPT effectively prevents NLS-tdTomato-NES from localizing to the cytoplasm in the absence of stress (Glu^{-}; two-way ANOVA and Tukey's post-hoc test; ****p<0.0001), as expected. Conversely, KPT fails to restrict NLS-tdTomato-NES and FUS localization to the nucleus upon excitotoxic insult (in D and E, compare Glu^{-} to Glu^{excito} in the presence of KPT, two-way ANOVA and Tukey's post-hoc test; ****p<0.0001, n.s. = non-significant). Error bars represent SEM.

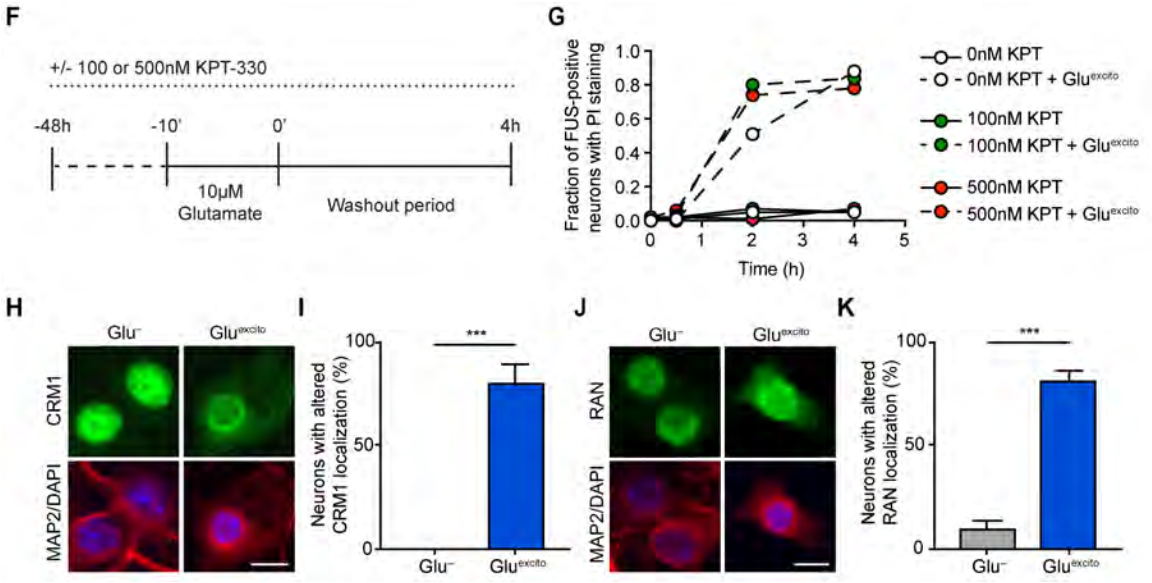

Figure II-4 continued. (F,G) Neuron cultures treated with 500nM KPT were assessed for viability by propidium iodide staining (PI) at 0', 30', 2h and 4 hours (h) following excitotoxic insult. The fraction of FUS-positive cells exhibiting PI staining indicates that KPT does not improve neuron survival (no statistical analysis; n=1 biological replicate). **(H-K)** The localization of nuclear transport factors CRM1 **(H, I)** and RAN **(J, K)** were significantly altered under conditions of Glu^{excito} in MAP2-positive neurons (red). **(H)** CRM1 and **(J)** RAN (green) were depleted from the nucleus (DAPI; blue) and exhibited a perinuclear accumulation. The percentage of neurons with CRM1 or RAN mislocalization were quantified in I and K, respectively (Student's T-test; ****p<0.0001, **p<0.01; n = 3 biological replicates). Error bars represent SEM. Scale bars for all images = 10μm.

Excitotoxicity Induces Translation Repression Independent of FUS and EIF2α-Phosphorylation

Translational repression and stress granule formation are common cellular responses to stress (Holcik & Sonenberg 2005, Kedersha et al. 2013). Given that expression of endogenous FUS is required for cellular homeostasis under basal and stress conditions, and that cytoplasmic forms of FUS have been linked to both translational regulation (Murakami et al. 2015, Yasuda et al. 2013) and stress granule formation (Bosco et al. 2010, Dormann et al. 2010, Gal et al. 2011, Sama et al. 2013), we investigated whether FUS egress during Glu^{excito} affected one or both of these processes. Protein translation was assessed by pulse labeling neurons with puromycin, a small molecule that incorporates into elongating peptides (Schmidt et al. 2009) (**Fig. II-5A)**. Immunofluorescence detection of puromycin revealed a near-perfect correlation between neurons exhibiting FUS translocation and translational repression; all neurons with translocated FUS were puromycin-negative, and vice versa (**Fig. II-5B**). This correlation strengthens the notion that neurons with translocated FUS are under a stressed state (Sama et al. 2013). Further, the degree of translational repression induced by Glu^{excito} was comparable to treatment with the translational inhibitor cycloheximide (**Fig. II-5A**), as assessed by both immunofluorescence (**Fig. II-5B**) and western blot **(Fig. II-5C,D)** analyses. We note that translational inhibition with cycloheximide is not sufficient to cause FUS translocation (**Fig. II-5B**) (Zinszner et al. 1994). Surprisingly, Glu^{excito}-induced translational repression occurred independently of

eukaryotic translation initiation factor 2 alpha (EIF2α)-phosphorylation, a key event that initiates translational repression as part of the integrated stress response pathway, which is generally induced by various types of cellular stress including sodium arsenite (**Fig. II-5E,F**) (Holcik & Sonenberg 2005). Glu^{excito} was also dissimilar to sodium arsenite-induced stress in that Ras GTPase-activating protein-binding protein 1 (G3BP1)-positive stress granules formed in response to arsenite stress, whereas these granules failed to assemble in response to Glu^{excito} (**Fig. II-5G**).

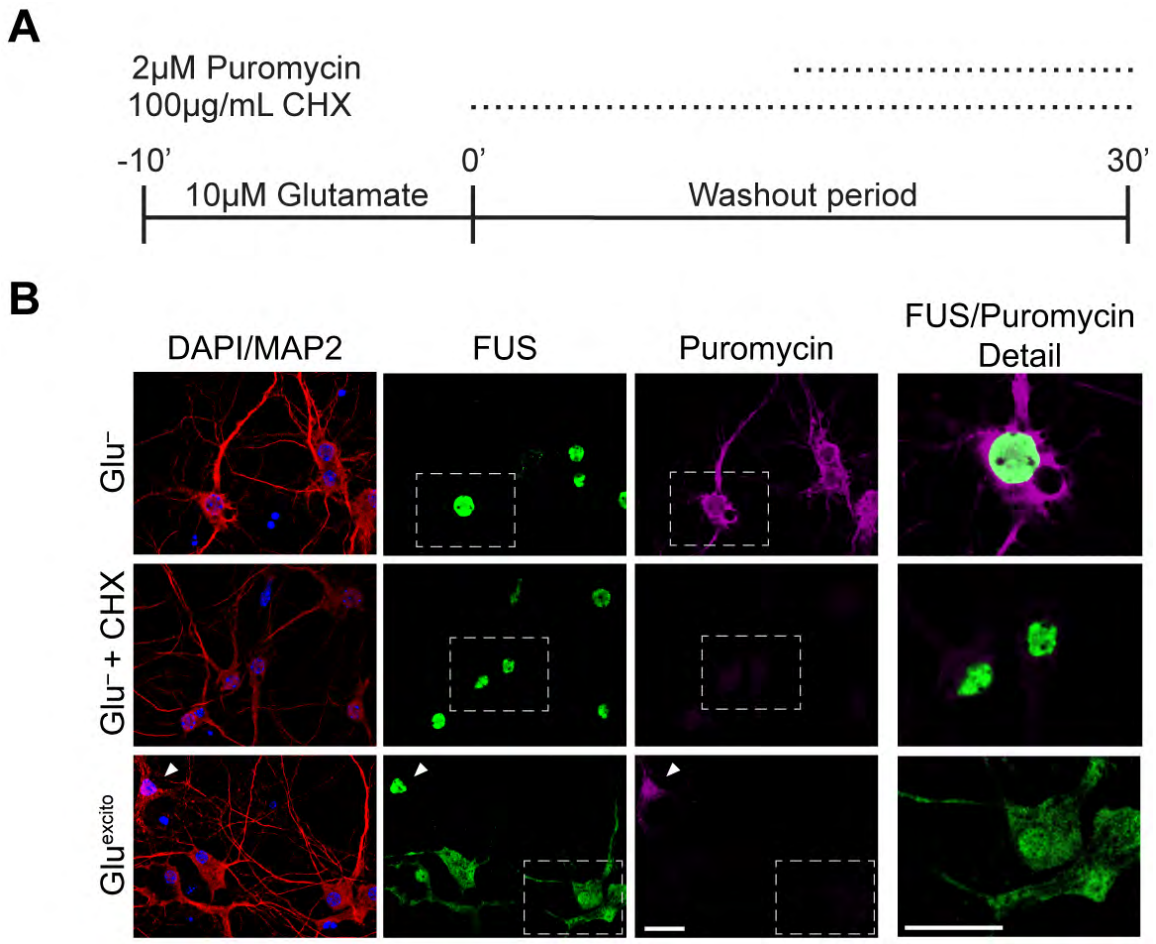

Figure II-5. Translational repression in neurons exposed to Glu^{excito} occurs independent EIF2α-phosphorylation. (A) Cellular translation in neurons was monitored by pulse-treatment and incorporation of the small molecule, puromycin, into nascent peptides during excitotoxic and/or cycloheximide treatment (CHX; inhibitor of protein translation). **(B)** The localization of FUS (green) and incorporated puromycin (magenta) in MAP2-postive neurons (red) was assessed by immunofluorescence. Relative to Glu^{-}, protein translation was reduced upon application of CHX or Glu^{excito}, however CHX did not induce FUS egress from nuclei (DAPI; blue). White arrowhead marks a neuron with predominately nuclear FUS expression and high puromycin staining under Glu^{excito}, whereas most neurons under this condition have cytoplasmic FUS expression and reduced puromycin staining. White boxes denote higher magnification details (*right)* to highlight neurons with representative levels of translation, as observed by anti-puromycin staining. Scale bars = 10μm.

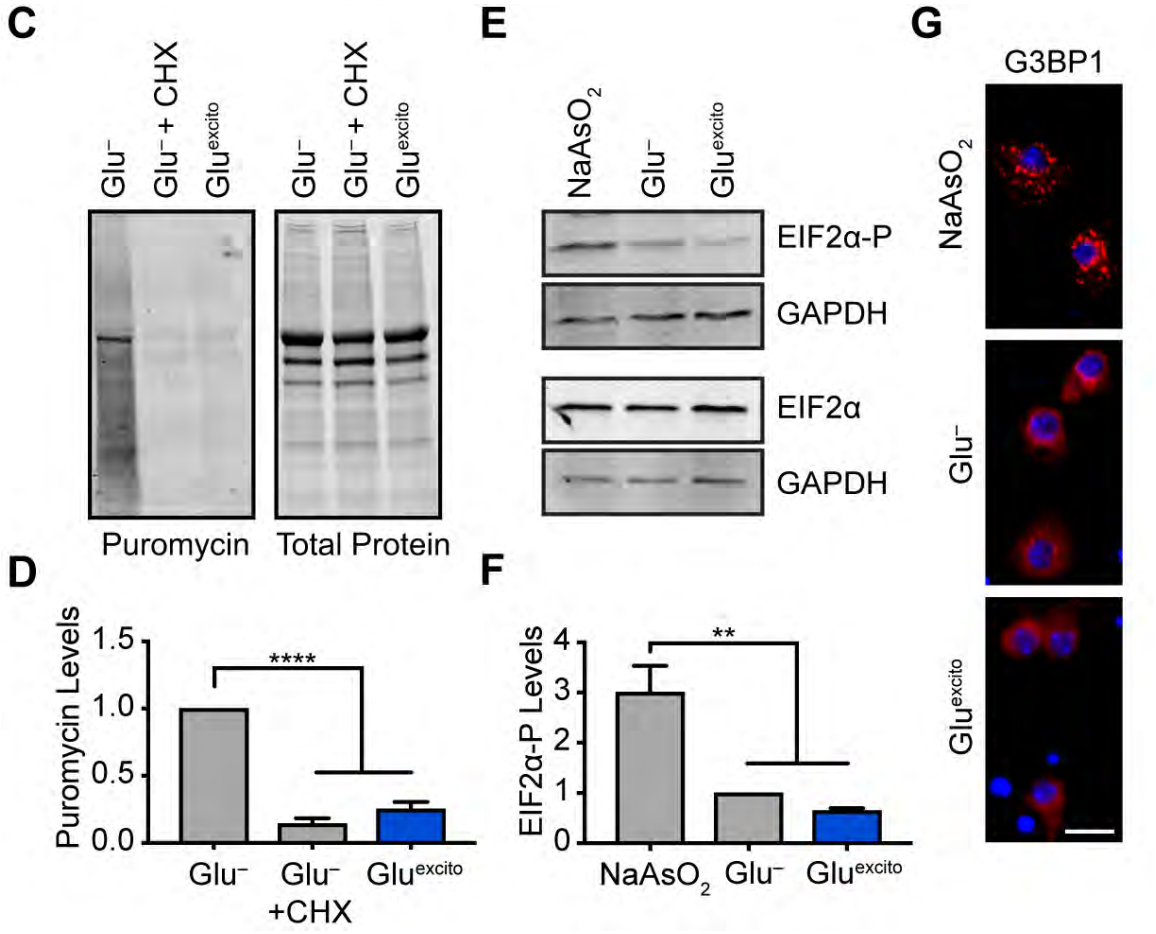

Figure II-5 continued. (C, D) Western and densitometry analysis of puromycin incorporation confirms a significant reduction in translation following CHX or Glu^{excito} treatment relative to Glu^{-} (One-Way ANOVA and Tukey's post-hoc test, ****p<0.0001, n = 3 biological replicates). Puromycin signal was normalized to total protein levels. **(E,F)** Western and densitometry analysis demonstrate a significant increase in EIF2α phosphorylation (EIF2α-P) following sodium arsenite treatment ($NaAsO_2$) relative to Glu^{-} but no significant change was observed for Glu^{excito}. Levels of EIF2α-P were normalized to total EIF2α protein and the loading control, glyceraldehyde 3-phosphate dehydrogenase (GAPDH; one-way ANOVA and Tukey's post-hoc test, **p<0.01, n = 3 biological replicates). Scale bars = 10μm. Error bars represent SEM. **(G)** Immunofluorescence staining of the stress granule marker, G3BP1 (red), shows neurons treated sodium arsenite ($NaAsO_2$) form stress granules, unlike Glu^{excito} or Glu^{-} conditions where G3BP1 signal remains diffuse (n=3 biological replicates). Scale bar = 20μm.

Given the strong correlation between FUS egress and translational repression (**Fig. II-5A** and (Murakami et al. 2015, Yasuda et al. 2013), I examined if FUS contributes to the attenuation of global translation. Lentivirus expressing shRNA against mouse FUS (shFUS1, shFUS2) as well as GFP reporter were expressed in PCNs to reduce FUS levels (**Fig. II-6A-C**). A scrambled control (shSC) shRNA was used as a negative control (**Fig. II-6A-C**). Puromycin levels either in the presence or absence of Glu^{excito} were unaffected by knockdown of endogenous FUS relative to shSC (**Fig. II-6D-G**). Thus, while FUS translocation strongly correlates with EIF2α-independent translational repression, FUS expression is not required for translational repression.

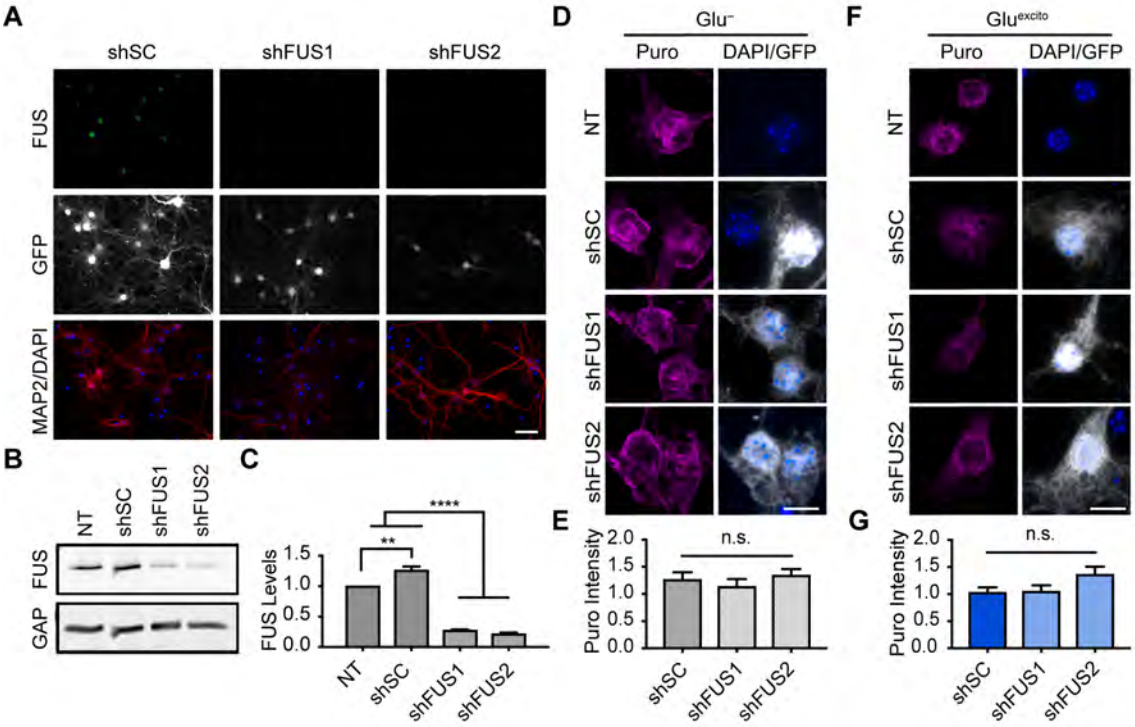

Figure II-6. Reduced protein translation following excitotoxic stress is independent of stress granule formation and FUS levels. (A) Neurons were transduced with shRNAs against mouse FUS (shFUS1, shFUS1) to induce FUS knockdown or a scrambled control (shSC). Transduced cells were identified by expression of a GFP reporter (white). Immunofluorescence staining of FUS (green) reveals FUS knockdown in transduced PCNs. Neurons were identified using a MAP2 antibody (red) and nuclei with DAPI (blue). Scale bar = 50μm. **(B, C)** Western and densitometry analysis confirms FUS knockdown relative to non-transduced (NT) and shSC conditions. A modest increase in FUS levels was observed upon expression of shSC relative the loading standard, GAPDH (GAP; n=3; one-Way ANOVA and Tukey's Post Hoc test, ****p<0.0001, **p<0.01; n=3 biological replicates). **(D, E)** Neurons were pulse-chase labelled with puromycin (Puro; magenta) to assess nascent protein translation in transduced cells (as in Fig. II-5B-D). Puromycin intensity normalized to non-transduced (NT) control. Scale bar = 10μm. **(F, G)** Quantification of puromycin (Puro) staining from (D,E) reveals no statistical difference in the somatic levels of translation following FUS knockdown (shFUS1, shFUS2) relative to shSC (One-way ANOVA and Dunnett's post-hoc test, n.s. = not significant, n = 3 biological replicates). Error bars = SEM.

Excitotoxic FUS Egress is Calcium Mediated

Knowing that calcium is a critical component of excitotoxicity (Bano et al. 2010, Dong et al. 2009, Vaarmann et al. 2013), we sought to determine whether this signaling molecule is necessary and/or sufficient for the response of FUS to Glu^{excito}. The calcium chelator, ethylene glycol tetraacetic acid (EGTA), was added to the cortical neuron media during both the addition of Glu^{excito} and the washout period (**Fig. II-1A**). Remarkably, the presence of EGTA completely prevented excitotoxic FUS egress (**Fig. II-7A,B**). Further, EGTA prevented excitotoxic neuron death, thus confirming the importance of calcium in mediating excitotoxic stress (**Fig. II-7C**).

To test if calcium is sufficient to induce FUS egress I added Ionomycin, an ionophore that increases intracellular calcium, to the neuronal media for one hour. Following treatment, FUS translocation was observed in the vast majority of neurons (89.0±5.6%; **Fig. II-7D,E**). In the context of glutamate-induced excitotoxity, we next investigated upstream mechanisms capable of inducing calcium influx. Depolarizing stimuli, such as potassium, is capable of activating both voltage and ligand gated ion channels. Treatment of neuronal cultures with potassium chloride (KCl) for 10 minutes followed by a 30-minute washout period also induced FUS egress in 76.1±6.1% of cells (**Fig. II-7F,G**). As the glutamate receptors, NMDA and AMPA, are among the primary receptors by which calcium enters the cell following glutamate stimulation, we next tested their involvement in

FUS egress. Strikingly, while the AMPA-inhibitor (NBQX) had no effect on FUS egress, NMDA-inhibition (APV) prevented translocation (**Fig. II-7H,I**).

In addition to excitotoxicity, we previously identified hyperosmolar stress as a trigger of nuclear FUS egress (Sama et al. 2013) and wondered whether calcium also mediates this response. In contrast to Glu^{excito}, there was no effect of EGTA on FUS egress in neurons treated with hyperosmotic levels of sorbitol (**Fig. II-7J,K**). To further assess this distinct relationship between FUS egress caused by Glu^{excito} and hyperosmolar stress, we measured the osmolality of media containing glutamate or sorbitol using an osmometer. Media containing 0.4M sorbitol (a dose capable of inducing FUS egress; **Fig. II-7J,K**) increased media osmolarity by ~130%, while 0.2mM Glutamate (a concentration 20x higher than Glu^{excito}) caused only a 2.5% increase in osmolarity relative to the base media alone. Together these data imply that the mechanisms triggering FUS during excitotoxic and hyperosmotic stress are distinct.

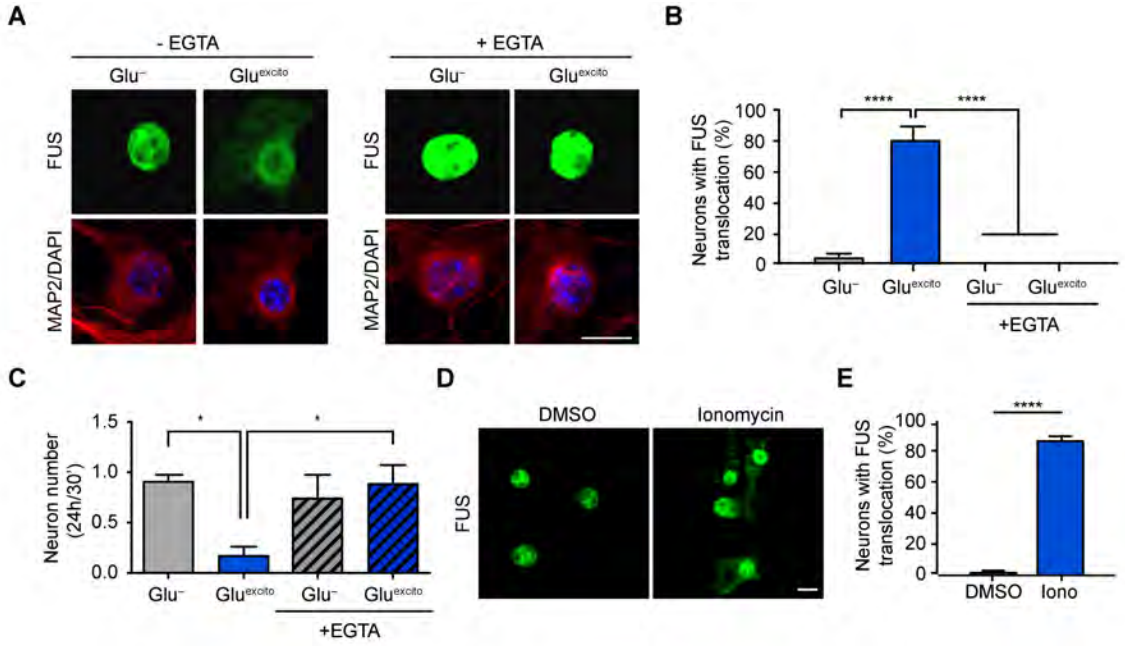

Figure II-7. Calcium is necessary and sufficient for FUS egress in primary cortical neurons. (A) Reducing levels of extracellular calcium with 2mM EGTA attenuates excitotoxic FUS egress (green) in MAP2-postive neurons (red) following excitotoxic insult. Nuclei stained with DAPI (blue). **(B)** Quantification of confocal microscopy in (A) confirms the effect of EGTA treatment (Two-way ANOVA and Tukey's post-hoc test; ****p<0.0001; n=4 biological replicates). **(C)** EGTA applied as in (A,B) further prevents neuron death. **(D)** Application of 10μM Ionomycin for one hour is sufficient to induce FUS egress relative to the DMSO control. **(E)** Quantification of (D); Ionomycin significantly increases the number of neurons exhibiting FUS translocation (Student's T-test; ****p<0.0001; n=3 biological replicates).

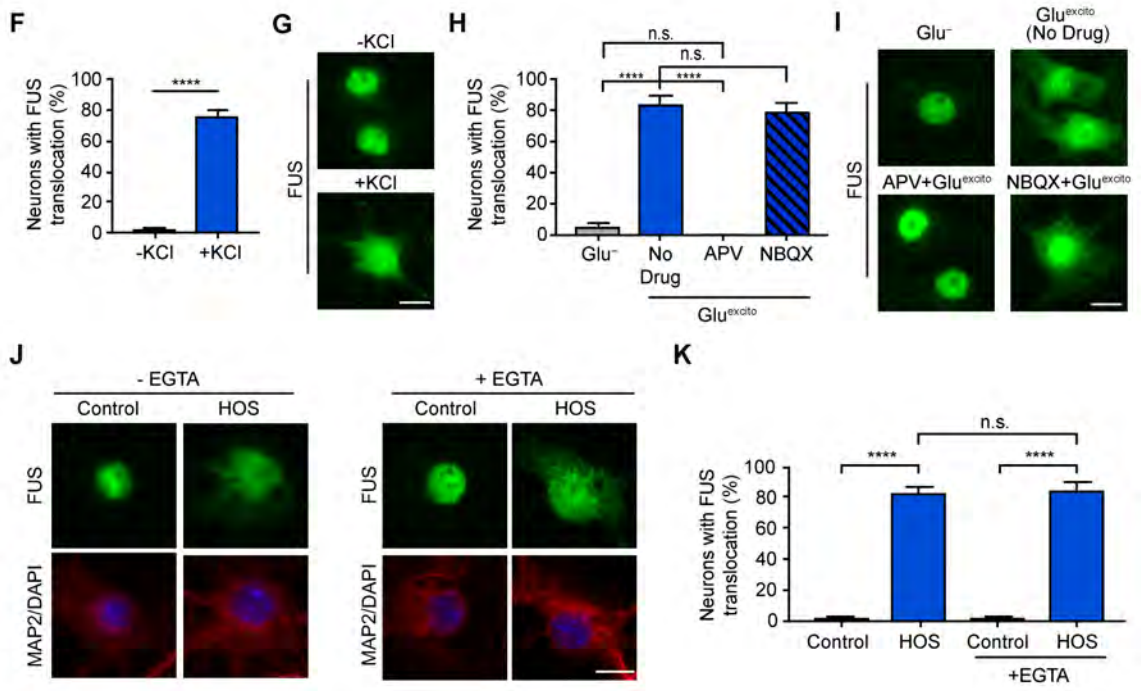

Figure II-7 continued. (F,G) Depolarization of neuronal membranes with 100mM KCl for 10 minutes followed by a 30-minute washout also induces FUS egress (Student's T-test; ****p<0.0001; n=3 biological replicates). **(G,H)** PCNs were treated with NMDA (APV) and AMPA (NBQX) inhibitors 20 minutes prior to as well as during Glu^{excito} treatment and the washout period. Relative to Glu^{excito} alone (No Drug), FUS egress is unaltered by NBQX. APV however significantly reduced the number of PCNs exhibiting egress to levels comparable to Glu^{-} (One-way ANOVA and Tukey's post-hoc test; ****p<0.0001, n.s. = non-significant; n=3 biological replicates). **(J,K)** FUS translocation induced by hyperosmolar stress (HOS) was not significantly reduced by EGTA treatment (two-way ANOVA and Tukey's post-hoc test; ****p<0.0001, n.s. = non-significant; n=3 biological replicates). For all panels, error bars represent SEM and scale bars = 10μm.

Assessment of Protein Modifications and Domains in FUS Egress

Calcium-signaling pathways often involve phosphorylation events to rapidly transmit signals throughout the cell (Berridge et al. 2003). Moreover, multiple studies demonstrate that FUS localization is influenced by posttranslational modifications, including phosphorylation (Darovic et al. 2015, Deng et al. 2014b, Klint et al. 2004, Rhoads et al. 2018b). To determine if excitotoxic FUS egress involved phosphorylation, we evaluated endogenous FUS from neurons using liquid chromatography tandem mass spectrometry (LC-MS/MS). Following the washout period (**Fig II-1A**), lysates were collected from stressed and unstressed neurons for the immunoprecipitation of FUS (**Fig. II-8A**). Immunoprecipitated FUS protein was visualized by silver stain (**Fig. II-8B**) and isolated for downstream analysis by LC-MS/MS. Within a biological replicate, the intensity of FUS peptides detected (MS1) prior to fragmentation (MS2) appeared similar in intensity (**Fig. II-8C**). Although the sequence of individual peptides is not revealed by MS1, these data indicate that FUS is detected to a similar degree in the presence and absence of stress by this analysis. Upon normalizing the intensity of FUS phosphopeptides to total FUS peptides, there was no significant change between Glu^{-} and Glu^{excito} (**Fig. II-8D**), suggesting no difference in the total amount of FUS phosphorylation at this experimental timepoint. This observation is supported by western and silver stain analyses in which no molecular weight shift for FUS was detected following Glu^{excito} (**Fig. II8A,B**).

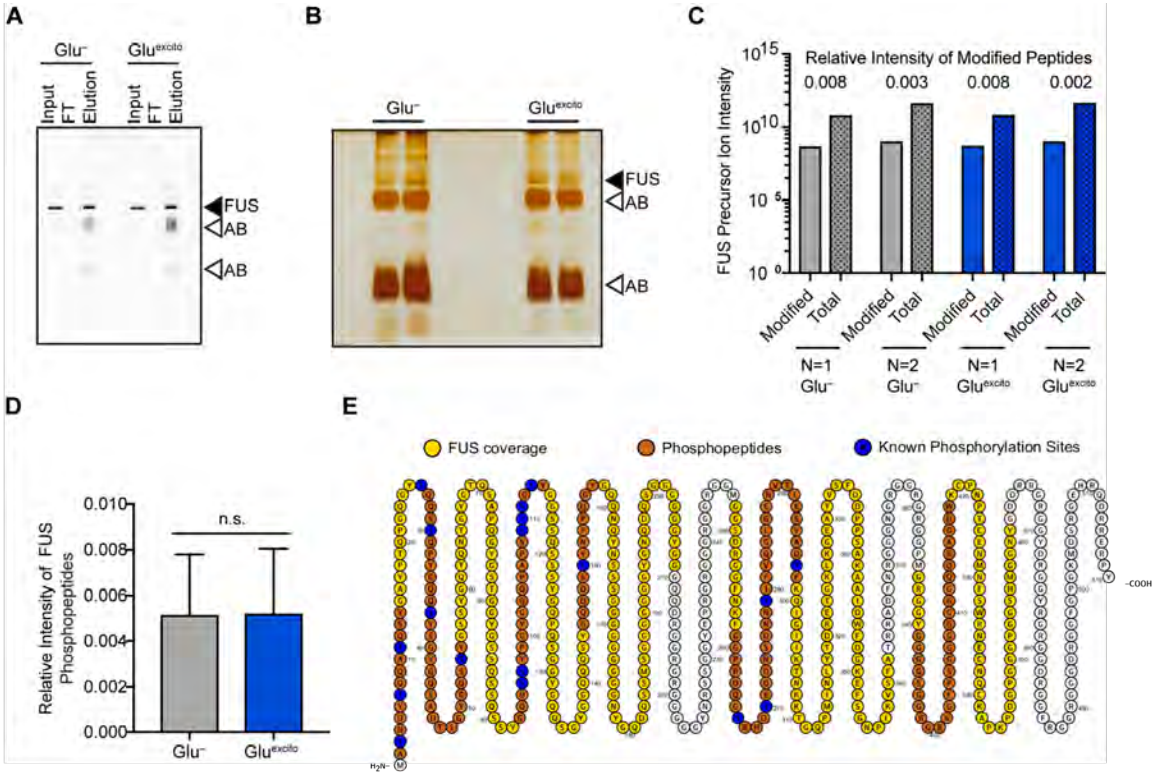

Figure II-8. Differential phosphorylation of FUS was not detected following Glu^{excito}. (A) Western blotting confirms the immunoprecipitation of endogenous FUS from cortical neurons (FT = flow-though) using the Genscript antibody (Fig. II-3). **(B)** Eluates from (A) were visualized by silver stain; FUS bands were removed and digested with chymotrypsin for analysis by LC-MS/MS. For (A,B), black triangles indicate FUS protein bands and white triangles denote heavy and light chain antibody bands (AB = antibody bands). **(C)** Intensity of phospho-modified and unmodified FUS precursor ions detected by the MS1 scan for each condition and replicate. **(D)** Normalization of the intensity of FUS phosphopeptides to total FUS peptides from (C) revealed no change in relative intensity (Student's T-test, n.s. = non-significant, n=2 biological replicates). Error bars = SEM. **(E)** Visualization of the murine FUS sequence and coverage by LC-MS/MS (yellow/orange residues) from n=2 biological replicates (Glu^{-}: n=1 56%, n=2 59% coverage and Glu^{excito}: n=1 77, n=2 78% coverage). A subset of FUS peptides (orange) contained a phosphorylated residue. Although modifications could not be assigned to an exact AA, all but one identified peptide contained 1 or more previously reported phosphorylation event(s) (blue) (Rhoads et al. 2018b).

Although we did not detect differences in the total level of phosphorylation, to determine if individual FUS residues are differentially modified by stress we next assessed the amino acid (AA) sequences of both modified and unmodified FUS peptides generated by MS2 (**Table II-1**). Because of the intrinsically high number of potential phosphorylatable residues in FUS, each identified peptide contained >1 residue able to undergo phosphorylation (**Table II-1**) and thus, the exact AA modified could not be assigned at this time.

In all but one of the phosphopeptides detected (AA 391-419) we noted the presence of residues previously identified as sites of FUS phosphorylation (Rhoads et al. 2018b) (**Fig. II-8E,** blue residues). Thus, our observations are consistent with previous reports of FUS phosphorylation. Interestingly, no previously reported phosphorylation events were found within AA 391-419 (Rhoads et al. 2018). Thus, our data suggest the presence of a murine specific or potentially novel modification (**Fig. II-8E, Table II-1**). Of note, AA 26-38 contained a phosphorylation event only detected upon Glu^{excito}. However, this peptide was only present in one of two Glu^{excito} biological replicates and was therefore not a reproducible event (**Table II-1**).

Although AA 26-38 may represent a potential possibility, based upon a binary presence alone (i.e., present versus not present), we were unable to detect the existence of unique FUS phosphorylation events following Glu^{excito} for any of the peptides in this analysis (**Table II-1**). Differences in the relative intensity of individual peptide species between stress and no stress conditions

Table II-1. FUS peptides identified by LC-MS/MS. Peptides obtained from the MS2 scan and their corresponding amino acid (AA) sequence within mouse FUS. The fraction of phospho-modified over total FUS peptides are detailed for each biological replicate as well as combined (sum). N/A represents peptides not observed within the given mass spectrometry experiment. While not quantitative, these data indicate that no single phosphopeptide was consistently differential between Glu^{-} and Glu^{excito} conditions.

		Fraction of phospho-modified/unmodified FUS peptides					
		Glu^{-}			Glu^{excito}		
FUS AA sequence	**FUS Peptide Sequence from MS2**	**N=1**	**N=2**	**Sum**	**N=1**	**N=2**	**Sum**
2-14	(M)ASNDYTQQATQSY(G)	N/A	2/6	**2/6**	N/A	1/3	**1/3**
26-38	(Y)SQQSSQPYGQQSY(S)	N/A	0/2	**0/2**	1/1	0/1	**1/2**
38-55	(Y)SGYGQSADTSGYGQSSY(G)	1/6	0/7	**1/14**	3/13	0/8	**3/21**
93-114	(Y)GQQSSYPGYGQQPAPSSTSGSY(G)	0/5	1/6	**1/11**	1/7	1/7	**2/14**
145-157	(Y)GQQQSSYNPPQGY(G)	2/11	1/8	**3/19**	1/11	0/6	**1/17**
259-281	(F)GGPRDQGSRHDSEQDNSDNNtIF(V)	1/3	7/82	**8/85**	0/3	5/29	**5/34**
282-298	(F)VQGLGENVTIESVADYF(K)	3/6	1/27	**4/33**	1/1	2/24	**3/25**
391-419	(Y)GGGGSGGGGRGGFPSGGGGGGGQQRAGDW(K)	4/11	0/34	**4/45**	3/13	0/19	**3/32**

may still exist. However, to draw confident conclusions, phosphorylation events would need to be reproducibly detected in multiple replicates and was thus not quantified. Finally, our coverage FUS coverage was not complete (**Fig. II-8E**) and it is possible that an undetected and/or differential phosphorylation event may exist in these unanalyzed regions, such as the NLS (Darovic et al. 2015).

The previous mass spectrometry experiment revealed the experimental complexity behind identifying a single type of potential translation modification in a protein as large as FUS. Thus, to refine our knowledge as to which regions of FUS might 'sense' excitotoxic stress, we next evaluated the contribution of individual domains to FUS egress. FLAG-HA-tagged FUS domain deletion constructs were generated and their basal localization under unstressed conditions validated HEK cells (**Fig. II-9A,B**). In the absence of stress, ΔRGG2-FUS and ΔRGG1/ΔRGG2-FUS localized to the cytoplasm (**Fig. II-9B**), possibly as RGG2 methylation can influence the function of the FUS NLS (Dormann et al. 2012). Moreover, pan-FUS staining (capturing both endogenous as well as exogenous FUS) suggests that ΔRGG2-FUS and ΔRGG1/ΔRGG2-FUS also disrupt the localization of endogenous FUS (**Fig. II-9B**). For this reason, ΔRGG2-FUS and ΔRGG1/ΔRGG2-FUS were not used for further analysis.

The remaining constructs, (full-length, ΔQGSY/partial GLY, ΔGLY, ΔRRM and ΔRRM-FUS) were transiently transfected into cortical neurons to evaluate FUS localization following excitotoxic insult. Under unstressed conditions, all

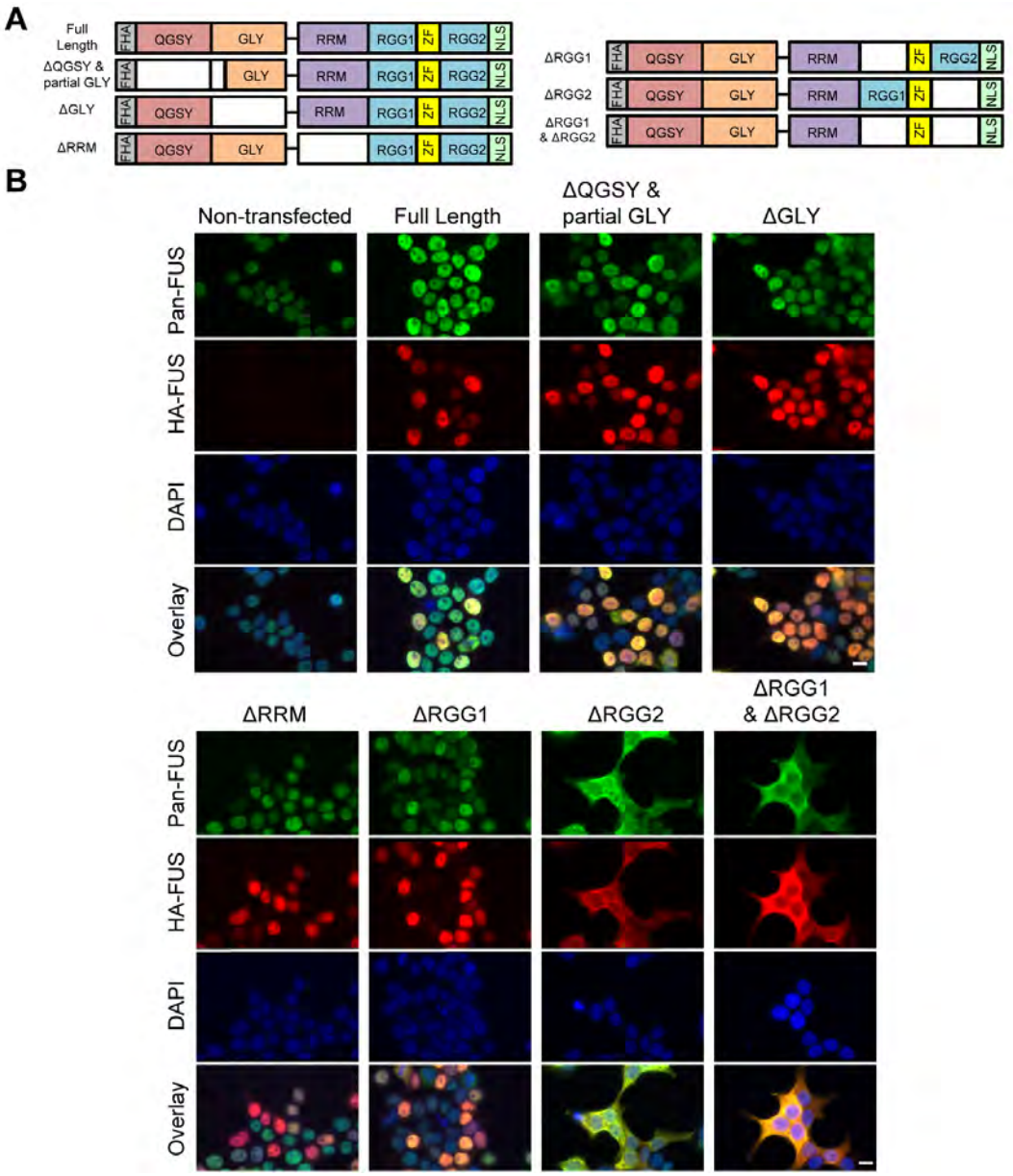

Figure II-9. Contribution of FUS domains to excitotoxic FUS egress. (A) FLAG-HA-FUS domain deletion constructs (FHA = FLAG-HA, QGSY = glycine-serine-tyrosine rich region, GLY = glycine-rich region, RRM = RNA recognition motif, RGG = arginine-glycine-glycine-rich region, ZF = zinc-finger domain and NLS = nuclear localization sequence). **(B)** Constructs were expressed in HEK cells and anti-HA staining (red) demonstrates all FLAG-HA-tagged constructs (except ΔRGG2 and ΔRGG1 & ΔRGG2) exhibited a nuclear localized. Pan-FUS staining (green) indirectly indicates that ΔRGG2 and ΔRGG1/ΔRGG2 further alter the localization of endogenous FUS (n=1 biological replicate).

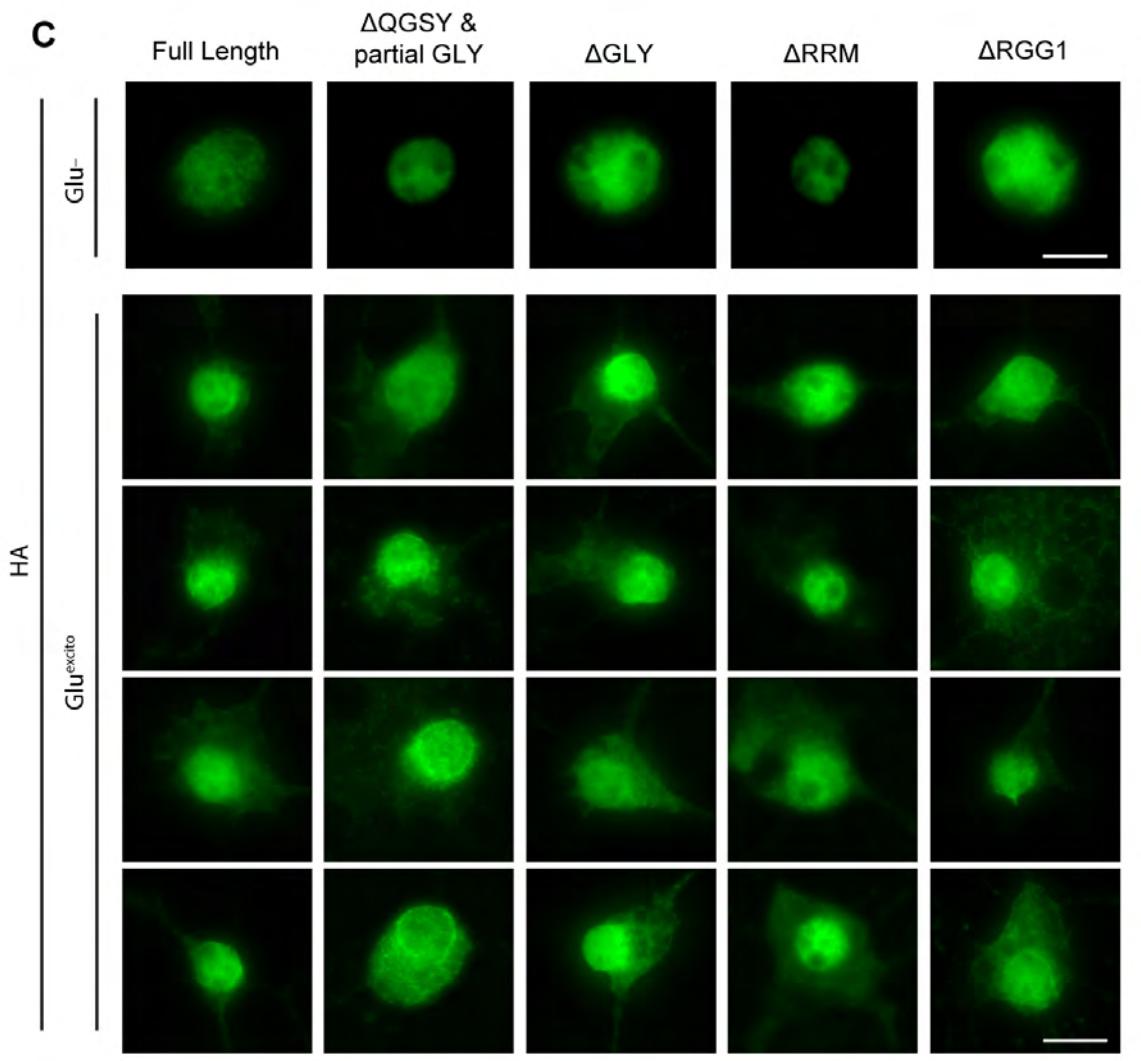

Figure II-9 continued. (C) Nuclear-localizing FLAG-HA-FUS constructs from (B) were expressed in cortical neurons and exposed to Glu^{excito} (n=2 biological replicates for all constructs except ΔRRM which was n=1). Following treatment with Glu^{excito}, HA staining (green) revealed that FUS egress is not inhibited by the deletion of any of the domains tested. To capture the variability of HA-FUS egress following excitotoxic egress, four representative neurons for each construct are shown here. Scale bars = 10μm.

constructs localized to the nucleus under unstressed conditions, as expected (**Fig. II-9B,C**). In the presence of Glu^{excito} however, no single deletion construct appeared to prohibit or impede FUS egress relative to full-length FUS (not quantified; **Fig. II-9C**). These data suggest that as individual domains, these regions of FUS do not contribute to FUS egress although it is possible that multiple domains may be required for FUS translocation (e.g. as FUS contains two RGG1 domains important for RNA interactions, removal of only one domain may not be sufficient to prevent egress). Further, only a subset of FUS domains were tested here. We were unable able to evaluate ΔRGG2-FUS and ΔRGG1/ΔRGG2-FUS due to their intrinsic cytoplasmic localization (**Fig. II-9B**). Further, we did not evaluate the zinc finger domain (**Fig. II-9A**) or NLS, the latter based on the rationale that it would also have resulted in the cytoplasmic localization of FUS under unstressed conditions.

Regulation of Gria2 by FUS Following Excitotoxic Insult

Based upon our puromycin studies, FUS expression does not affect global translation in neurons (**Fig. II-6**). This analysis however may not detect subtle differences in the translation of specific transcripts, especially those targeted to dendrites for local translation (Holt & Schuman 2013). RBPs, such as FUS, play crucial roles in mRNA handling, including splicing, transport, stability and local translation (Sama et al. 2014). With this in mind, I investigated whether an mRNA processing role for FUS is relevant under conditions of Glu^{excito}. To evaluate select

mRNA processing events, I focused on transcripts that directly interact with FUS and are implicated in calcium and/or synapse homeostasis (Lagier-Tourenne et al. 2012). Fluorescence *in situ* hybridization (FISH) was used to investigate the localization and abundance of our candidates (**Table II-2**) in response to stress. If a change in the localization or abundance of candidate were observed, it would suggest a potential functional response of this gene product to stress that could be subject to regulation by FUS.

During this process, we observed that addition of Cytosine β-D-arabinofuranoside (AraC; routinely used to prevent the proliferation of non-neuronal cells by inhibiting DNA replication) diminished the magnitude of probe response to stress in our FISH experiments compared to untreated cells (not shown). For this reason, we did not pursue FISH experiments in AraC-treated neuronal cultures. Upon completing a pilot screen of our selected candidates, we observed an appreciable change in the somatic density of several candidates relative to the unstressed condition: Nd1-L, Ubqln2, Camk2a, BDNF and Gria2 (**Table II-2**). Moreover, of these candidates, a further alteration in dendritic density was only observed for Camk2a and Gria2 (**Table II-2**). Given that we observed a robust increase in FUS levels in dendrites (**Fig. II-3F,G**), FUS is implicated in dendritic gene expression and maintenance of synapses (Ling 2018) structures particularly vulnerable to stress and age-linked defects (Bezprozvanny & Hiesinger 2013, Mattson & Magnus 2006) and thus, we selected these

Table II-2. Candidate mRNAs evaluated by FISH. Based upon a literature search comparing transcripts bound by FUS with transcripts whose expression is altered by neuronal stimulation, we identified seven transcripts for further analysis. Candidate transcripts were analyzed by FISH to assess their distribution and density following excitotoxic insult. Results from non-AraC treated FISH experiments are summarized below.

			Response of Candidate Probe to Excitotoxicity	
Candidate Gene	**Protein Function**	**Biological Replicates***	**Soma**	**Dendrites**
Nd1-L	Actin stabilizing protein	n=1	++ Decrease in density	No change
Ubqln2	Regulates protein degradation; genetically linked to ALS	n=1	+ Increase in density	No change
Camk2a	Prominent kinase in CNS; regulates synaptic function	Consistent increase in probe density following excitotoxic insult (n=2). Stress-induced phenotype was not reproduced upon concurrent expression of shSC (n=1)	++ Increase in density	+ Increase in density
BDNF	CNS growth factor; regulates synaptic function	n=1	+ Increase in density	No change
Homer 1	Post-synaptic scaffolding protein	n=1	~/+ Possible modest increase in number†	No change
Gria1	AMPA subunit; associated with ALS pathogenesis	n=1	~/+ Possible modest increase in number†	No change
Gria2	AMPA subunit; regulates AMPA calcium permeability; associated with ALS pathogenesis	Consistent increase in probe density following excitotoxic insult (n=2). Increase dendritic density is sensitive to FUS knockdown (n=3, **Fig. II-10**)	++ Increase in density	++ Increase in density

* = Following n=1 screen of candidates, only Camk2a and Gria2 were pursued for FUS knockdown studies.

† = A change in puncta was only observed when area was not accounted for. Upon normalization to area (e.g. density), any potential differences previously observed in the non-normalized data were nullified.

two candidates for further analysis to see if the alterations in their density following and contribution to dendritic and synapse biology. To determine if the response of these candidates to stress (**Table II-2**) were FUS dependent. Prior to excitotoxic treatment, endogenous FUS was knocked down using two shRNAs targeting distinct sequences within FUS (Ward et al. 2014); results were compared to neurons expressing a scrambled control shRNA (shSC) (**Fig. II-6A-C**). Unexpectedly, upon expression of the shSC construct, Camk2a no longer exhibited a response to excitotoxicity as previously observed in naïve cells and was thus, not further pursued (**Table II-2B**). Unlike Camk2a, a significant increase in Gria2 transcript density was detected in both the soma and dendrites of cortical neurons expressing shSC (**Fig. II-10A-E**).

Gria2 encodes the GluR2 protein subunit of the AMPA receptor, which plays an important role in synaptic signaling, and is translated following forms of neuronal excitation, including depolarization by KCl (Ju et al. 2004, Wright & Vissel 2012). Consistent with previous findings, reduced expression of FUS did not have a significant effect on the total levels of Gria2 under basal conditions (Lagier-Tourenne et al. 2012) (**Fig. II-10A-E**). In contrast, excitotoxicity-induced changes to Gria2 were significantly attenuated upon FUS knockdown. Dendritic expression of Gria2 was particularly sensitive to FUS levels under Glu^{excito}, as knockdown of FUS restored dendritic Gria2 levels to baseline (**Fig. II-10A-E)**. These data are further supported by confirmation that the Gria2 FISH signal quantified corresponds to RNA and is specific to the Gria2 probe (**Fig. II-10F**). Within the

time course of the analysis, we were unable to detect significant changes in GluR2 protein levels by Western blot analysis of whole cell lysates (Fig. S4D,E). Taken together, these data show that FUS expression is required for excitotoxicity-induced changes to Gria2 processing in neurons.

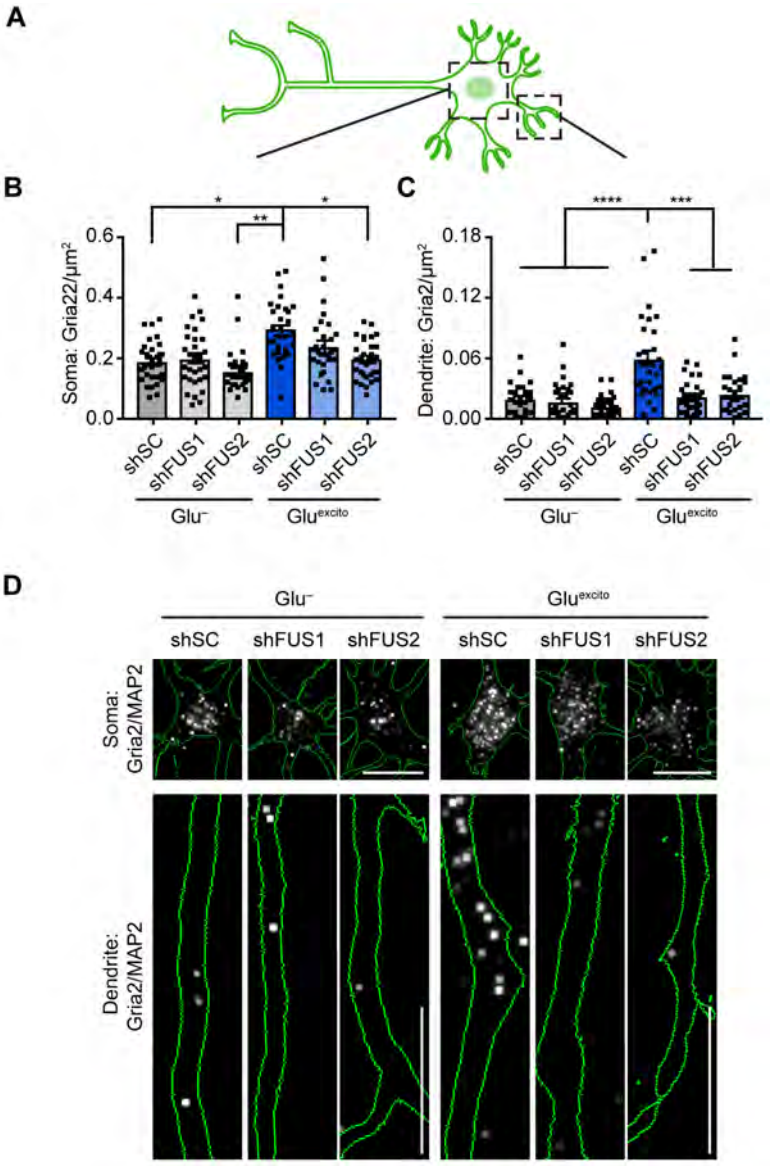

Figure II-10. Elevation of Gria2 mRNA in dendrites following Glu^{excito} requires FUS expression. (A) To evaluate Gria2 mRNA in soma and dendrites, FUS levels were reduced using lentivirus expressing a scrambled control shRNA (shSC) or shRNA against FUS (shFUS1, shFUS2) **(B, C)** Gria2 increased in both **(B)** soma and **(C)** dendrites of shSC transduced neurons following Glu^{excito}. Upon FUS knockdown, dendritic Gria2 did not increase with Glu^{excito} treatment (two-way ANOVA and Dunnett's post-hoc test, ****p<0.0001, ***p<0.001, **p<0.01, *p<0.05, n = 3 biological replicates). Error bars = SEM and black squares indicate single cell measurements, **(D)** Visual representation of (B,C); Gria2 mRNA was detected by FISH (white) in PCNs outlined in green. Scale bars = 10µm.

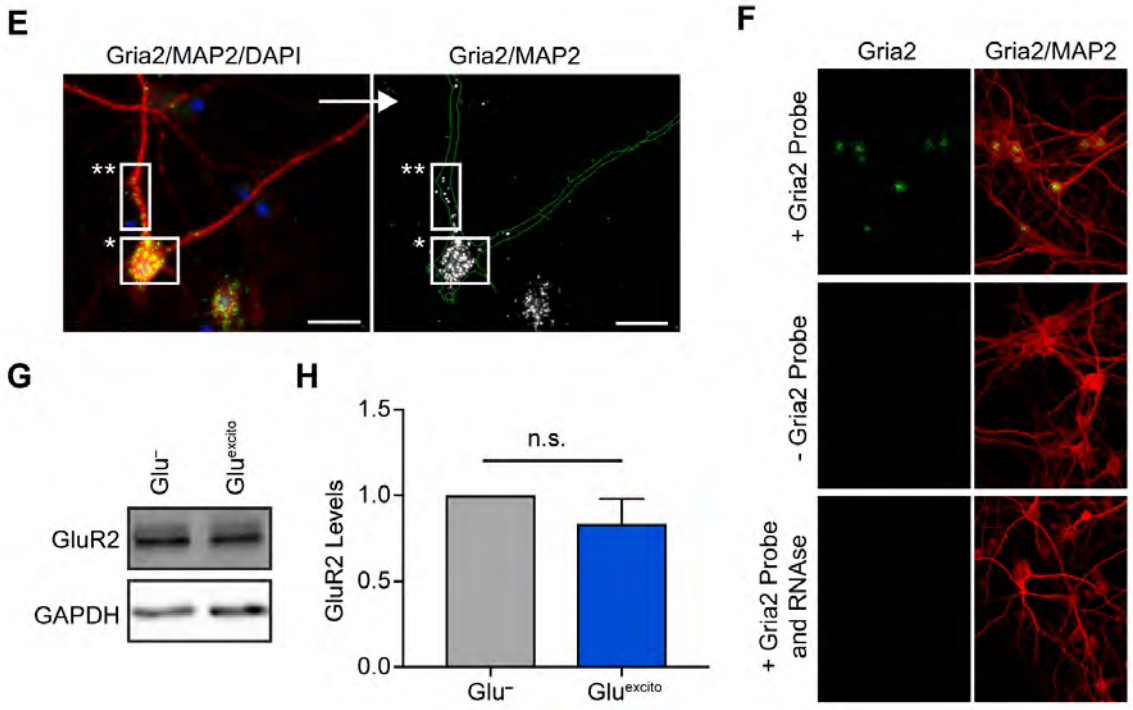

Figure II-10 continued. (E) To generate the images used in (D), Gria2 puncta (green) were digitally dilated and converted to white. Images of MAP2 staining used to denote neurons and dendrites (red) were converted to binary and used to make a MAP2 mask subsequently outlined in green. White boxes exemplify approximate somatic (*) and dendritic (**) regions used for analysis. Scale bars = 25μm. **(F)** Detection of the Gria2 transcript by FISH (green) was confirmed by the absence of signal in 'no probe' and 'RNAse' controls in MAP2-postive neurons (red). **(G, H)** Western and densitometry analysis of steady-state GluR2 protein levels reveal no statistical difference following Glu^{excito} relative to Glu^{-} at 30'. For quantification, GluR2 protein levels were normalized to the loading standard, GAPDH (Student's T-test, n.s. = not significant, n = 5 biological replicates). Error bars = SEM.

Upon identifying a functional consequence of FUS egress, I sought to assess the effect of FUS on neuron survival following excitotoxic insult. To this end, endogenous FUS was reduced by lentiviral transduction of the shFUS1 construct previously described (**Fig II-6, II-11A**) and the number of GFP-positive neurons were quantified 0-4 hours following excitotoxic insult. From this analysis, a modest susceptibility of neurons to FUS knockdown (shFUS1) was observed relative to the control (shSC) in absence of stress (**Fig. II-11B**). Following excitotoxic insult however, both constructs exhibited a sharp decrease in the number of GFP-positive neurons at 1.5 hours, after which the neuron number did not appreciably decline further. (**Fig. II-11B**). Although it was expected that PCNs would be more susceptible to Glu^{excito} following FUS knockdown given the vital roles FUS is known to play in maintaining cellular homeostasis (Sama et al. 2014), this preliminary experiment suggests there is no difference in neuronal susceptibility following FUS knockdown. While we cannot exclude the possibility that the acute effect of excitotoxic stress on cultured primary neurons masked a potential contribution of FUS, it is also possible that FUS does not play an essential role in the cellular response to excitotoxicity (i.e. if there are compensatory mechanisms at play) or even that neurons fare better without FUS (suggesting that FUS may function to promote pro-death pathways).

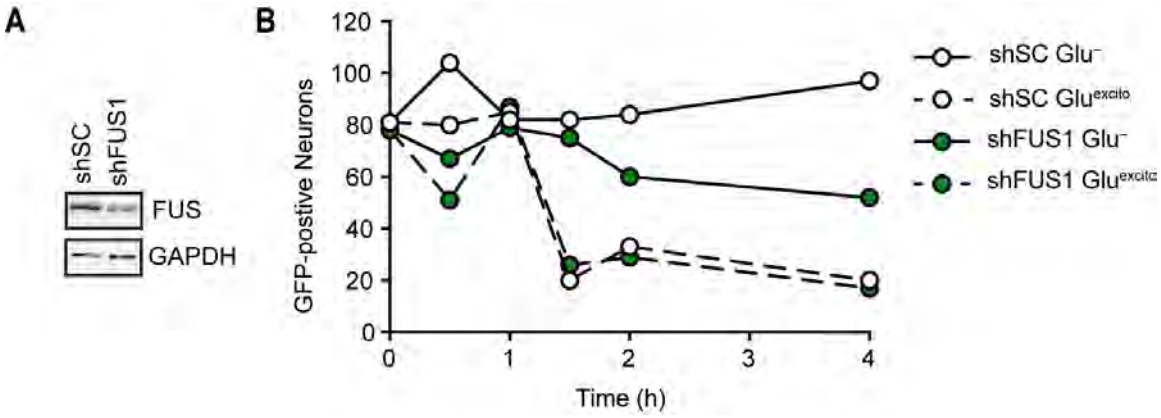

Figure II-11. No apparent effect of FUS knockdown on neuron survival following acute excitotoxic insult. (A) Endogenous FUS was reduced using a lentivirus expressing shRNA against FUS (shFUS1) and a GFP reporter as described in **Fig. II-6**. A scrambled control shRNA (shSC) was used for a negative control. **(B)** The number of GFP-positive neurons was quantified at different timepoints during the washout period following treatment with Glu^{excito}. Following treatment, neuron number rapidly declined by 1.5h for both constructs; no difference between shFUS and shSC was observed (n =1 biological replicate).

Calcium Mediated FUS Egress Occurs in Motor Neurons

Primary motor neurons represent the neuronal cell type that is predominately affected in ALS. Given the effect of calcium on FUS localization in cortical neurons, we sought to extend this finding to motor neuron systems that are more relevant to the study of ALS. Consistent with previous observations in cortical neurons (**Fig II-7D,E**), treatment of DIV 6-8 primary murine motor neurons with Ionomycin was sufficient to shift the C:N ratio of FUS to the cytoplasm **(Fig. II-12A,B)**. Further, application of the glutamatergic agonist, kainic acid, to motor neurons also induced an increase in the C:N ratio of FUS. **(Fig. II-12C,D**). Kainic acid is known to induce motor neuron excitotoxicity (Fryer et al. 1999), and was used here to avoid confounding effects of glutamate uptake by astroglia present in the mixed MN cultures (Rose et al. 2017). We noted a relatively wide range in the C:N ratio of FUS in kainic acid treated neurons; a sub-population of cells exhibited near complete egress of nuclear FUS **(Fig. II-12C,D)**, which was not observed in cortical neurons treated with glutamate.

We additionally sought to examine the response of FUS in human induced pluripotent stem cell (iPSC)-derived motor neurons in control (i.e. 'non-diseased') lines (see Methods and Materials). Treatment of DIV15 iPSC motor neurons with 5-10μM Ionomycin for 1 hour induced FUS egress as well as altered staining patterns of the neuron marker Tubulin β 3 and motor neuron marker Islet 1/2 (**Fig II-12E**). While the change in staining for the cytoskeletal marker, Tubulin β 3, may be similar to previous observations in cortical neurons (**Fig II-7D,E** and **Fig II-**

12A,B), the significance of the reduced and/or redistribution of Islet 1/2, a transcription factor, is less clear. Following oxidative stress, the transcription factor, Pancreatic and Duodenal Homeobox 1, also redistributes to the cytoplasm (Kawamori et al. 2003). Thus, cell stress may additionally induce the egress of transcription factors as well as RBPs and transport machinery.

DIV 40-45 iPSC-derived motor neuron survival has been previously reported following the application of 30-100 glutamate when applied for 2-8 hours (Donnelly et al. 2013). However, treatment of iPSC neurons with excitatory agonists such glutamate (≤200μM for up to 8h at DIV15 or 55) and kainic acid (300μM for 3h at DIV15) failed to induce FUS egress or alter neuronal morphology (as in **Fig II-12E**, untreated). One possibility is that relative to murine neurons, the hiPSC-derived motor neurons may not be comparatively 'mature', and thus unable to undergo glutamatergic excitation. Although we attempted to overcome this by treating iPSC motor neurons with excessive amounts of glutamate (≤ 200μM) at DIV55, we still did not observe a response of FUS or morphological alterations. For future studies it will be important to verify if iPSC neurons are electrophysiologically active in order to assess the response of FUS to excitotoxic stress in this model. Together these data demonstrate that calcium-mediated FUS egress is conserved across multiple neuronal models, implying the existence of a shared cellular phenomenon. That the response of neurons to glutamatergic agonists varied however, likely indicates differences in cellular biology not further explored by this work.

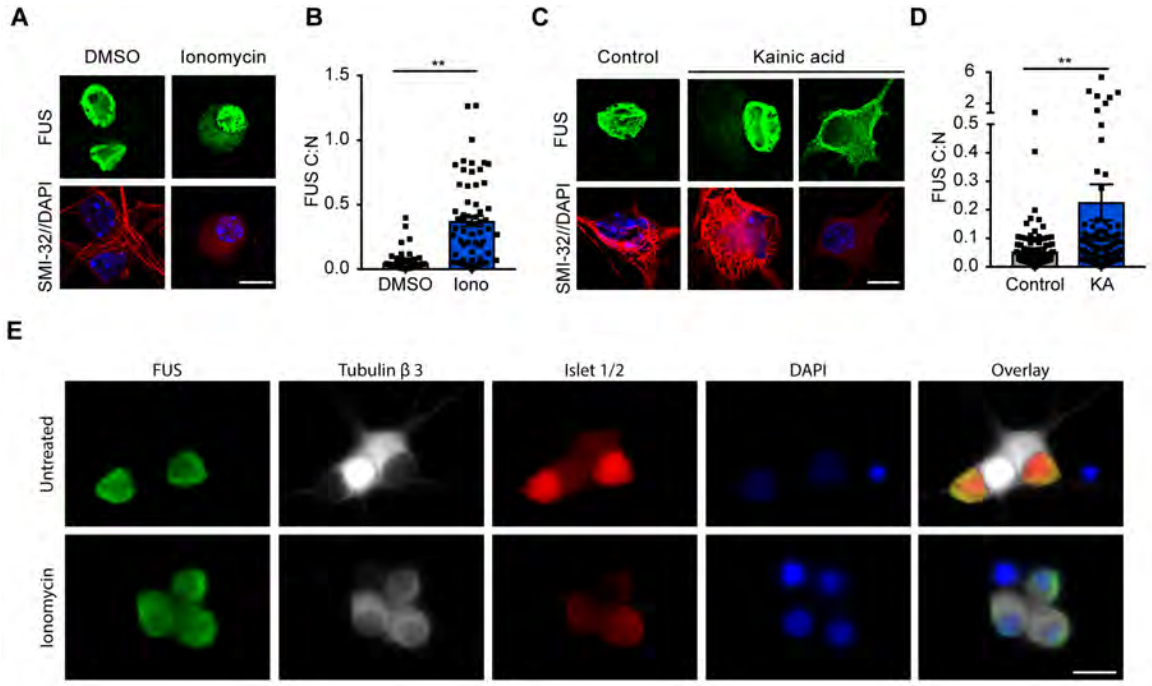

Fig II-12. Calcium-induced FUS egress is observed in primary motor neurons. (A, B) DIV 6-8 murine primary motor neurons treated with Ionomycin (Iono) as in (Fig. II-7). Following treatment, primary motor neurons also exhibit FUS egress as indicated by immunofluorescence and a significant increase in the FUS C:N ratio (Student's T-test, **p<0.01, n=3 biological replicates). Motor neurons were identified using the motor neuron marker, neurofilament H non-phosphorylated (SMI-32; red) and nuclei were stained with DAPI (blue). **(C)** A 10 min treatment of 300μM Kainic acid followed by a 1-hour recovery induced FUS egress in motor neurons. A near depletion of FUS from the nucleus was observed for a subset of cells (Kainic acid, *left)*. **(D)** Kainic acid (KA)-induced FUS egress was statistically significant relative to the washout control (Student's T-test, **p<0.01, n=3 biological replicates). **(B, D)** Black squares indicate individual cell measurements normalized to the average of the replicate control. Accordingly, means represent the normalized average of n = 3 biological replicates. Error bars represent SEM. Scale bars = 10μm. **(E)** Detection of FUS egress (green) in DIV15 hiPSC-derived motor neurons were treated with 5-10μM Ionomycin (n=2 biological replicates). hiPSC-derived motor neurons were identified using the neuronal marker, Tubulin β 3 (white), and the motor neuron marker, Islet 1/2 (red). Nuclei are stained with DAPI (blue). Scale bar = 10μm.

Response of ALS-Mutant FUS to Excitotoxicity

We show a response of endogenous FUS in neuronal models using stressors relevant to ALS (**Fig. II-2,12**). As mutations in FUS cause ALS (Kwiatkowski et al. 2009, Vance et al. 2009), we next sought to examine the response of ALS-mutant FUS to excitotoxicity. The majority of ALS-linked mutations are present within the nuclear localization sequence (NLS) and, as such, these variants exhibit varying degrees of cytoplasmic mislocalization and accumulation (Bosco et al. 2010). Given that both ALS-mutations and Glu^{excito} influence the subcellular localization of FUS, we investigated the relationship between these two factors. A series of FLAG-HA-tagged FUS variants were transiently expressed in primary cortical neurons and the C:N ratio of exogenous FUS was determined in the absence and presence of Glu^{excito} (**Fig. II-13A,B**). In addition to wildtype (WT) FUS, we examined: H517Q, the only autosomal recessive FUS mutation associated with ALS(Kwiatkowski et al. 2009); R521G, representing a mutational 'hot spot' for ALS-FUS (Lattante et al. 2013); and R495X, a particularly aggressive ALS-linked mutation(Sama et al. 2014). The degree of FUS mislocalization has been reported as H517Q≤R521G<<R495X under basal conditions (Bosco et al. 2010), consistent with what was observed here (**Fig. II-13A,B**). As expected, WT FUS exhibited significant nuclear egress in response to Glu^{excito}. Similarly, the C:N ratio for the H517Q and R521G variants also significantly increased following excitotoxic insult (**Fig. II-13A,B)** (Bosco et al. 2010, Kwiatkowski et al. 2009). These data suggest that ALS-linked point mutations within the NLS do not interfere with the response

of FUS to Glu^{excito}. Interestingly, the C:N ratio of R495X, exhibiting a high degree of cytoplasmic expression under basal conditions (Bosco et al. 2010), did not change in response to stress (**Fig. II-13A,B**). We note that following excitotoxic insult, the distribution of all constructs (regardless of their localization under basal conditions) did not significantly differ (**Fig. II-13A,B**). Although we cannot exclude the possibility that truncation of the entire NLS interferes with FUS egress, these data are consistent with an NLS 'celling effect', in that the normal nucleocytoplasmic distribution of R495X-FUS is equivalent to that of 'maximally' redistributed endogenous FUS following excitotoxic insult. The behavior of these variants in our assay has important implications for ALS pathogenesis, in that disease-relevant stressors such as Glu^{excito} could trigger an initial nuclear egress of mutant FUS that ultimately leads to pathological aggregation.

Given the severe cytoplasmic localization of R4595X, we next sought to assess if R495X expression might alter the density of Gria2 under non-stress conditions and/or enhance the stress- and FUS-linked dendritic increase earlier observed (**Fig. II-10**). Analysis of Gria2 in the soma and dendrites of neurons transfected with WT or R495X FUS revealed no appreciable change to transcript density in the presence or absence of stress (**Fig. II-14C,D**). This result was unexpected given that we previously observed a significant increase in the dendritic density of Gria2 in both neuronal soma and dendrites in untransfected cells (**Fig. II-10**). That there was no difference in Gria2 density following expression of WT FUS suggests that the expression of human, WT FUS in a murine system

may exert a dominant negative effect with respect to Gria2 processing. Further, as a mock transfection condition was not included, we cannot exclude the possibility that the act of transfection somehow confounds the previously observed response of Gria2 to excitotoxic insult (**Fig. II-10**).

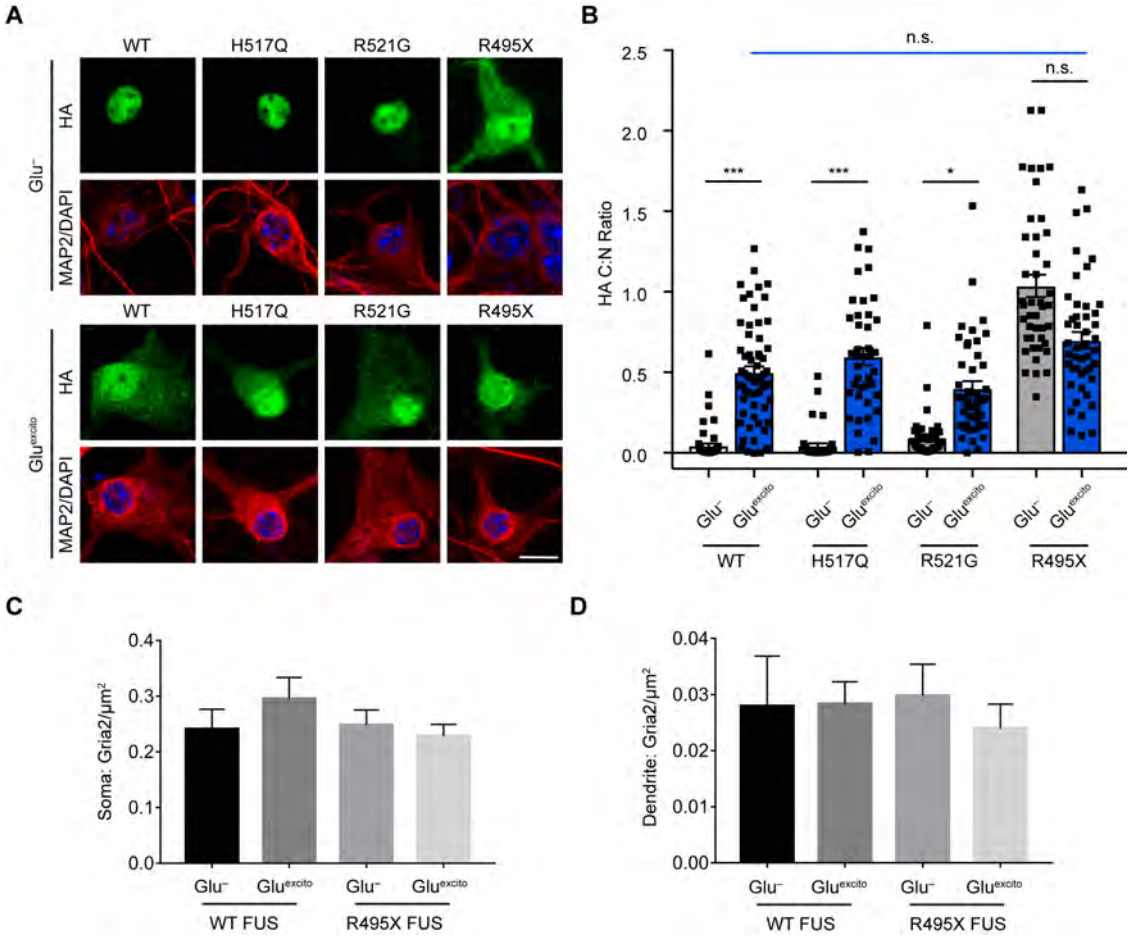

Figure II-13. Excitotoxic stress induces egress of predominately nuclear ALS-linked FUS variants. (A) Neurons transfected with FLAGHA-tagged FUS variants were exposed to Glu^{excito}. Nuclear egress of exogenous FUS was assessed by HA staining (green) in MAP2-positive neurons (red). Nuclei were stained with DAPI (blue). Scale bar = 10µm. **(B)** Quantification variant egress revealed a significant stress-induced increase in the C:N ratio of FUS WT, H517Q and R521G, but not R495X (Student's T-test; ***p<0.001, *p<0.05, n.s. = not significant, n=3-5 biological experiments). Black lines denote individual statistical comparisons made between Glu^{excito} and Glu^{-} for each construct. Following excitotoxic insult, there was no significant difference in the average of C:N ratios of all constructs (one-way ANOVA; n.s. = not significant; blue line). Black squares represent individual, cellular C:N measurements. **(C,D)** The density of Gria2 was evaluated in both **(C)** soma and **(D)** dendrites of neurons transfected with FLAG-HA WT or R495X FUS. Gria2 density did not change following treatment with Glu^{excito} for either construct (n = 1 biological replicates). Error bars represent SEM.

Discussion

This study uncovered an association between disease-linked RBPs and excitotoxicity, a stress that has particularly profound effects on the nucleocytoplasmic distribution of FUS in both cortical (**Fig. II-2B,F**) and motor neurons (**Fig. II-12A-D**). There is a compelling body of evidence linking glutamate-induced excitotoxicity to neurodegenerative diseases, including ALS (Fogarty 2018, Starr & Sattler 2018, Van Den Bosch et al. 2006). For instance, elevated levels of glutamate were detected in biological samples from ALS patients(Plaitakis & Constantakakis 1993, Rothstein et al. 1990, Spreux-Varoquaux et al. 2002). Cell death caused by glutamate and calcium dysregulation has also been documented in multiple animal and cellular models (Hideyama et al. 2012, Kawahara et al. 2004, Kia et al. 2018, Spreux-Varoquaux et al. 2002, Starr & Sattler 2018, Van Den Bosch et al. 2006). The outcomes of this study shed new light on the excitotoxicity cascade and implicate, for the first time, a role for the ALS/FTD-linked protein FUS in this process.

Our results are consistent with a functional role for FUS in response to glutamatergic signaling (Fujii et al. 2005) rather than a non-specific effect of cell death. First, FUS egress precedes cell death (**Fig. II-1**). Second, there is selectivity with respect to proteins that undergo a change in cellular localization; the response of FUS is particularly robust compared to the other proteins assessed in this study (**Fig. II-2, II-4B, II-5G).** Third, the effects of excitotoxicity on Gria2 depend on FUS expression (**Fig. II-10**). FUS binds Gria2 mRNA within introns and

the 3' untranslated region, and Gria2 splicing is effected by FUS expression under basal conditons (Lagier-Tourenne et al. 2012). Under Glu^{excito}, Gria2 density was enhanced in neuronal dendrites in a FUS-dependent manner (**Fig. II-10**). Gria2 encodes the GluR2 protein subunit of the AMPA receptor. Normally, GluR2 is post-transcriptionally edited and GluR2-containing AMPA receptors are calcium impermeable. As such, the calcium permeability of AMPA receptors and the susceptibility of neurons to excitotoxicity is dependent on GluR2 (Van Damme et al. 2007, Van Den Bosch et al. 2006). We speculate that the enhanced dendritic density of Gria2 may serve to increase the number of calcium impermeable (GluR2-containing) AMPA receptors and thereby offset calcium influx caused by existing calcium permeable (GluR2-lacking) receptors. In ALS, this process could be compromised as a result of dysregulated Gria2 editing and/or GluR2 expression (Takuma et al. 1999, Van Damme et al. 2007), particularly in motor neurons that rely heavily on AMPA receptor signaling(Starr & Sattler 2018, Van Den Bosch et al. 2006). The effect of FUS on dendritic Gria2 density following Glu^{excito} (**Fig. II-10**) is novel and consistent with a role of FUS in modulating Gria2 processing. The exact nature of this role however remains to be fully elucidated, and could involve a function of FUS in Gria2 splicing (Lagier-Tourenne et al. 2012), transport (Ling 2018), and/or or stabilization (Udagawa et al. 2015, Yokoi et al. 2017).

While investigating the mechanism(s) underlying excitotoxic FUS egress, we uncovered striking changes to the CRM1 nuclear export pathway (**Fig. II-4**). Inhibition of CRM1-mediated export by KPT-330 failed to restrict both NLS-

tdTomato-NES and FUS within the nucleus under Glu^{excito} (**Fig II-4**). Further, CRM1 localization was significantly shifted towards the cytoplasm (**Fig. II-H,I**). Despite these changes, nucleocytoplasmic transport was not completely dysregulated, as a partial inhibitory effect of KPT-330 on the shuttling reporter was observed (**Fig. II-4**). Our KPT-330 studies suggest that Glu^{excito}-induced FUS egress occurs through a mechanism other than active CRM1 export, and could entail passive diffusion (Ederle et al. 2018) or alternative transport factors (Archbold et al. 2018). Selectivity of RBP egress following Glu^{excito} may stem from differences in nucleocytoplasmic shuttling dynamics, which are influenced by multiple factors including binding interactions and post-translational modifications (Rhoads et al. 2018b). An interesting area of future study could be to elucidate these factors and determine whether they are modulated by stress.

Alterations to CRM1 and Ran (**Fig. II-4**) under Glu^{excito} may represent early signs of nucleocytoplasmic transport decline. Indeed, previous studies show that various forms of stress (e.g., excessive calcium influx, oxidative, and hyperosmotic stress) cause damage to nuclear pores and impair nucleocytoplasmic transport (Bano et al. 2010, Kelley & Paschal 2007, Kodiha et al. 2004, Yasuda et al. 2006, Zhang et al. 2018a). Mice deficient in key astroglial glutamate transporters exhibited both nuclear pore degradation and motor neuron degeneration (Sugiyama et al. 2017). Moreover, the nucleocytoplasmic transport pathway has been implicated in age-related neurodegeneration, particularly in the context of ALS and FTD (Li & Lagier-Tourenne 2018). While most ALS/FTD-associated

studies have focused on the role of mutant proteins in dysregulating nucleocytoplasmic transport (Kim & Taylor 2017, Li & Lagier-Tourenne 2018), ALS/FTD-associated forms of cellular stress (e.g., excitotoxicity) may also contribute to nucleocytoplasmic transport defects in both inherited and sporadic forms of disease. In fact, nucleocytoplasmic transport is an emerging area of therapeutic development and the CRM1 inhibitor KPT-350 is advancing towards ALS clinical trials. Partial inhibition of CRM1 is expected to offset defects in nuclear import. CRM1 inhibitors have had a therapeutic effect in some (Haines et al. 2015, Li & Lagier-Tourenne 2018), but not all (Archbold et al. 2018, Sugiyama et al. 2017), models of neurodegeneration. Collectively, the available data, including our own (**Fig. II-4**), support CRM1-mediated nucleocytoplasmic transport as a viable therapeutic target for neurodegenerative disorders. However, a combination therapy addressing additional effects of stress-induced nuclear pore degradation (i.e., calpain inhibitors (Sugiyama et al. 2017) may be required for a significant therapeutic outcome.

The calcium-mediated response of FUS to Glu^{excito} has additional implications for neurodegeneration, including cases of FUS-mediated ALS. For instance, motor neurons derived from human ALS-FUS induced pluripotent stem cells are intrinsically hyperexcitable (Wainger et al. 2014). Further, the effects of ALS-linked FUS on calcium-mediated motor neuron toxicity is exacerbated by expression of the mutant protein in astrocytes (Kia et al. 2018, Van Damme et al. 2007). Most ALS-linked FUS mutations are located within the NLS (Lattante et al.

2013) and induce a shift in the nucleocytoplasmic equilibrium of the protein toward the cytoplasm, where it is believed to exert a gain of toxic function (Bosco et al. 2010, Sama et al. 2017) (**Fig. II-13**). As ALS-linked variants R521G and H517Q translocate further into the cytoplasm under Glu^{excito} (**Fig. II-13**), we predict these and other variants with impaired binding to nuclear import factors will accumulate in the cytoplasm under conditions of chronic stress *in vivo* (Dormann et al. 2010, Kodiha et al. 2004). Moreover, chronic stress may result in nuclear depletion and cytoplasmic aggregation of wild-type FUS and TDP-43 in sporadic cases as well (Deng et al. 2010, Keller et al. 2012). We propose a model whereby FUS and related RBPs play a functional role in response to normal stimulation and moderate degrees of stress, but that excessive or chronic stress severely disrupts their nucleocytoplasmic equilibrium and contributes to disease pathology.

Acknowledgments

We are thankful to Drs. Kensuke Futai (University of Massachusetts Medical School; UMMS) and Miguel Sena-Esteves (UMMS) for sharing reagents and advice, Dr. Martin Hetzer (Salk Institute) for providing the NLS-tdTomato-NES construct, and to all the members of the Bosco and Landers labs for their valuable input. We are grateful to the following funding sources: US National Institutes of Health (NIH) / National Institute on Neurological Disorders and Stroke R21 NS091860 (DAB) and R01NS078145 (DAB); ALS Association 18-IIA-418 (CF); Zelda Haidek Memorial Scholarship from UMMS (MT).

Methods and Materials

Cell Culture

HEK293-T cells were cultured as described(Sama et al. 2013) in Dulbecco's minimal essential medium (DMEM, Invitrogen 11965118) supplemented with 10% fetal bovine serum (FBS; MilliporeSigma F4135) and 1% penicillin and streptomycin (P/S; Invitrogen 15140122) under standard culture conditions (37°C, 5% CO2/95% air).

Dissociated primary cortical neuron cultures were prepared using cortices from C57BL/6 embryonic day (E)14-15 mice. Embryos were isolated in ice-cold Hanks Buffered Saline Solution (HBSS; MediaTech, 21-023-CV)s and the meninges removed. Cells were dissociated for 12 minutes in 0.05% Trypsin (Invitrogen 25300-054) at 37˚C, diluted in DMEM (Invitrogen 11965118) containing 10% FBS (MilliporeSigma F4135) and strained with a cell strainer before gently pelleting. Cells were then resuspended in Neurobasal media (Invitrogen, 21103049), supplemented with 1% Glutamax (Invitrogen cat#35050-061), 1% P/S (Invitrogen 15140122) and 2% B27 (Invitrogen 0080085-SA), and plated at 1.8-2x10^5 cells/mL on poly-ornithine (final concentration of 1.5 µg/mL; MilliporeSigma, P4957) coated plates or coverslips. Neuronal cultures were grown under standard culture conditions fed every 3-4 days by adding half volumes of supplemented neurobasal media to each well/dish, with additional half changes of media occurring every other feeding. Unless indicated, during the first feeding (DIV 2 or 3) neuron cultures were also treated with a final concentration of 0.5-1µM Cytosine

β-D-arabinofuranoside hydrochloride (AraC; MilliporeSigma C6645) to inhibit non-neuronal cell growth. Experiments were performed on DIV 14-16.

Primary murine astrocytes were isolated from embryonic cortices as described for primary cortical neurons. Following trypsinization (as above), cells were plated ~7-8 $x10^5$ cells/mL in flasks and cultured under standard culture conditions. Media was changed every 3 days. When confluent, cells were resuspended by scraping and re-plated on coverslips at ~6 $x10^4$ cells/mL. Cells were grown for ~2 weeks prior to harvesting for downstream analyses.

Primary motor neurons were isolated from E12.5 embryonic spinal cords as described (Sama et al. 2017). Briefly, after dissociation in 0.1% trypsin (Worthington LS003707) at 37°C for 12 minutes, primary motor neurons were purified using a 6% Optiprep (MilliporeSigma D1556) density gradient and plated on glass coverslips coated with 0.5g/L poly-ornithine (MilliporeSigma, P4957) and natural mouse laminin (Thermo Fisher 23017015). Cells were grown in glia-conditioned Neurobasal medium (Invitrogen, 21103049) and supplemented with 2% B27 (Invitrogen 0080085-SA), 2% horse serum (MilliporeSigma H1270), and 10ng/ml BDNF (PeproTech 450-02), GDNF (PeproTech 450-44), and CNTF (PeproTech 450-50). Primary motor neurons were treated on DIV 6-8 with Ionomycin (MilliporeSigma I9657) or dimethyl sulfoxide (DMSO; Corning, 25-950-CQC) and DIV 8 with kainic acid (Abcam ab144490).

Induced pluripotent stem cells (iPSC) (**Table II-3**) were cultured in Matrigel (Corning CB-40230) coated, 6-well plates in complete mTeSR1 media (StemCell

Technologies 85850) with daily media changes. Lines were clump passaged every 4-6 days following gentle dissociation with Accutase (Corning MT25058CI). To generate motor neurons from iPSCs, an embryoid body (EB) based protocol that mimics embryonic motor neuron development using small molecules and growth factors was adapted from (Ng et al. 2015). Briefly, confluent iPSCs were dissociated to single cells following incubation with 0.5mM (Ethylene diamine tetraacetic acid) EDTA (Millpore Sigma E9884) and transferred to suspension flasks at 150,000 cells/cm^2 in basal differentiation medium in the presence of Y-27632 ROCK inhibitor (10 μM; BD Biosciences, BDB562822) and the dual Smad inhibitors: SB431542 (10 μM; Tocris, 1614), CHIR99021 (3 μM; MilliporeSigma, SML1046), and LDN193189 (100 nM; MilliporeSigma, SML0559). The basal differentiation medium consisted of a 1:1 combination of Neurobasal medium (Invitrogen, 21103049) and DMEM/F12 medium (Corning, MT-15-090-CV) supplemented with N2 (Invitrogen, 17502-048), B27 (Invitrogen, 17504044), Glutamax (Invitrogen, 35050-061) and ascorbic acid (20 μM; MilliporeSigma, A4403). At day 2, EBs were transferred to basal differentiation medium containing dual Smad inhibitors and retinoic acid (RA) (1 μM; MilliporeSigma, R2625). At day 4, the media was changed to the same media as day 2 except that it also included Smoothened agonist (SAG) (1 μM; MilliporeSigma, 566661). At day 7, dual Smad inhibition was discontinued, and media was switched to basal differentiation media supplemented only with RA and SAG (patterning media). At day 9, patterning media was changed to also include DAPT (10 μM; Tocris, 2634). Brain derived

neurotrophic factor (BDNF) (10 ng/mL; Peprotech, 450-02) was included with DAPT with the day 11 media change. At day 13, glial derived neurotrophic factor (GDNF) (10 ng/mL; Peprotech, 450-10) was also included along with DAPT and BDNF.

On day 15, EBs were dissociated with activated papain (5 u/mL; Worthington, LS003126) and DNase I (10 µg/mL; Worthington, LS006355) in papain activation buffer (1.1 mM EDTA, 0.067 mM mercaptoethanol, and 5.5mM cysteine-HCl in EBSS). Cells were resuspended in plating media consisting of Neurobasal media supplemented with B27, Glutamax, 10 ng/mL each BDNF, GDNF, ciliary neurotrophic factor (CNTF; Peprotech, 450-13), insulin-like growth factor 1 (IGF-I; Peprotech, 100-11), and laminin (1 µg/mL; Invitrogen, 23017-015). Neurons were plated at 150,000/cm^2 onto culture dishes or cover slips pre-treated with 25 µg/mL poly-D-Lysine (MilliporeSigma, P7405), 25 µg/mL poly-ornithine (MilliporeSigma, P3655), 3-5 µg/mL laminin and 5 µg/mL fibronectin (MilliporeSigma, F1141). Cells were fed by half-media changes every 2-3 days and harvested for use DIV15-55. Cultures comprised of ~40-50% motor neurons, as indicated by staining with the motor neuron marker, Islet 1/2.

Table II-3. 'Non-diseased' Control iPSC Lines. iPSC line information in regards to those used for those differentiated and analyzed in this work.

Line Name	Genotype	Donor Sex	Age at Biopsy	Reference
18a	Control	F	48	(Boulting et al. 2011)
FTD35#11	Control	M	45	(Freibaum et al. 2015)
TALSCTRL15.12	Control	F	49	Purchased from Target ALS (Target ALS ID: TALSCTRL15.12)

Drug and Stress Application

For glutamate experiments, 100mM glutamate (MilliporeSigma G5889) was freshly prepared in Neurobasal media and diluted using primary conditioned media (PCM) to achieve the desired solution concentration. To apply stress, neuronal media was replaced with glutamate-containing PCM or PCM alone (glutamate-free control) for 10 minutes. After 10 minutes, treatment media was replaced with PCM for 30 minutes or longer depending on the experiment, prior to fixation or lysate collection. Kainic acid (Abcam ab144490) was diluted from 10 mM/ml to 300μM/ml in PCM and added to motor neurons for 10 minutes followed by a replacement with PCM for one hour. Stock solutions of 5mM Ionomycin (MilliporeSigma I9657) prepared in DMSO (Corning, 25-950-CQC) or 1M or sodium arsenite (MilliporeSigma 71287) prepared in water were diluted to 10μM or 1 mM in PCM, respectively, and added to neurons for 1 hour. Sorbitol (MilliporeSigma S6021) was directly dissolved in PCM to obtain a final concentration of 0.4M and applied to cells for 1 hour. For excitotoxicity experiments in which EGTA (MilliporeSigma E3889) was added, a 100mM stock was prepared in water, diluted to 2mM in PCM, and allowed to incubate for 30 minutes prior to use during the experimental time course. To inhibit CRM1, neurons were treated with 500nm KPT-330 (KPT; Cayman Chemical, 18127) dissolved in water on DIV13 for 48 hours prior to treatment with Glu^{excito} as well as during the experimental time course. Stock solutions of 100mM APV (Ascent Scientific) or 50mM NBQX (Ascent Scientific) were prepared in water and diluted in PCM to a final concentration of 50 or 3μM,

respectively. APV and NBQX were added to the neuronal media 20 minutes prior to glutamate exposure as well as during the Glu^{excito} treatment and washout period. A 5M a stock solution of KCl (MilliporeSigma P9541) prepared water and diluted to 100mM in PCM. Neurons were treated with KCl for 10 minutes followed by a 30-minute washout period in PCM alone. Translation was inhibited with 2μM cycloheximide (MilliporeSigma C7698). To stain nuclei of dead and dying cells, fresh propidium iodide (Invitrogen P1304MP) were prepared at a concertation of 2mg/mL (3mM) in Dulbecco's Phosphate-Buffered Salt Solution (DPBS; Corning 21031CV) and added to neurons at a final concentration of 10μM for 15 minutes. Cells were washed twice with DPBS prior to fixation and downstream analysis.

Plasmids and Cloning

Human cDNA for FLAG-HA-tagged WT, H517Q, R521G or R495X FUS were cloned into the lentiviral vector, pLenti-CMV-TO-Puro-DEST (Addgene 670-1) using the In-Fusion HD Cloning Plus kit (Clontech (EMD) 638909). FLAG-HA-FUS domain deletion constructs were generated and cloned into the pLenti-CMV-TO-Puro-DEST backbone by site directed mutagenesis and Gateway LR Clonase reactions (11791020), respectively. To achieve FUS knockdown, shRNA sequences(Ward et al. 2014) were packaged using In-Fusion HD cloning into the lentiviral backbone, CSCGW2 (a generous gift courtesy of Miguel Esteves), which contains a GFP-reporter expressed under a separate CMV promoter. The shRNA targeting sequences were: 5’-GCAACAAAGCTACGGACAA-3’ (shFUS1) and 5’-

GAGTGGAGGTTATGGTCAA-3' (shFUS2) as well as the scrambled control sequence, 5'-AATTCTCCGAACGTGTCACGT-3' (shSC). The shuttling reporter, NLS-tdTomato-NES (a generous gift courtesy of Martin Hetzer(Hatch et al. 2013)) was cloned into the pLenti-CMV-TO-Puro-DEST vector backbone (Addgene 670-1) using Gateway BP and LR Clonase reactions (Invitrogen 11789020 and 11791020, respectively). The shuttling reporter contained an NLS sequence (PPKKKRKVQ) and NES sequence (LQLPPLERLTL) attached to tdTomato by a GGGG linker at the N and C termini, respectively.

Transient Expression of ALS-mutant FUS

For transient transfection experiments, neurons were fed DIV6 and transfected with FLAG-HA-FUS constructs on DIV7 using NeuroMag (Oz Biosciences, NM51000) transfection reagents. 1.0µg DNA and 1.75µL NeuroMag (for one 24-well well; 500uL volume) were combined in an eppendorf tube and brought up to a 50µL volume using Neurobasal media. The DNA mixture was allowed to incubate for 20 minutes before addition to neurons. Upon addition, neuron cultures were placed on a NeuroMag magnet plate (Oz Biosciences MF10096) within the tissue culture incubator for 15 minutes to complete transfection. Transfected neurons were collected for experimental analyses on DIV14-16. For transient transfection of FLAG-HA-FUS into HEK cells, the same protocol was followed except that transfection reagents were diluted in and cell media was changed to Opti-MEM (Invitrogen, 31985070).

Lentiviral Production and Application

High titer lentivirus was prepared as described (Sena-Esteves et al. 2004).Briefly, HEK-293T cells were individually transfected using calcium phosphate with the shRNA or NLS-tdTomato-NES constructs described along with the packing plasmids: CMVdR8.91 plasmid and VSV-G. DNA constructs were prepared using by EndoFree Maxi Prep (Qiagen, 12362). Three hours after transfection, cell media was replaced with Opti-MEM (Invitrogen, 31985070) and virus was collected in open-top Beckman tubes (Beckman Coulter, 344058) by ultracentrifugation at 28,000 rpm in SW32Ti rotor 72 hours following transfection. Lentivirus titer was obtained by the transduction of HEK cells with serially diluted lentivirus. Upon titer determination, virus was added to DIV6 non-AraC treated neurons at an approximate titer of $1.2\text{-}1.8^{10}$ tu/ml. For all transduction experiments except fluorescence *in situ* hybridization, PCNs were AraC treated on DIV7. Transduced neurons were collected 9 days post-transduction (DIV15) for analysis.

Immunofluorescence Analysis

Primary cortical and motor neurons were fixed with 4% paraformaldehyde (PFA; Fisher Scientific AAA1131336) at room temperature for 15 minutes and permeabilized with 0.1-0.2% Triton X-100. Immunofluorescence experiments for conducted as described (Bosco et al. 2010, Sama et al. 2013) with the exception of primary motor neuron samples which were processed according (Sama et al. 2017). Primary antibodies used for all experiments are listed in **Table II-4**.

Table II-4. Primary Antibodies Used for Immunofluorescence and Western Analyses.

Antibody	Species*	Company	Dilution/Incubation**
FUS	R	Bethyl Laboratories A300-293A	IF: 1/1000 1h or 1/500 O/N
FUS	M	Santa Cruz (4H11) sc-47711	IF: 1/200 1h; WB: 1/1000 4˚C O/N
FUS	R	Genscript (in-house)	IF: 1/200; WB: 1/1000 4˚C O/N
FUS	M	Santa Cruz (H-6) sc-373698	IF: 1/200 1h; WB: 1/1000 4˚C O/N
FUS	R	Bethyl Laboratories A300-302A	IF: 1/1000 1h or 1/500 O/N
MAP2	M	MilliporeSigma M9942 (clone HM-2)	IF: 1/1000 1h
MAP2-CY3	M	EMD Millipore MAB3418C3	IF: 1/1000 1h
NeuN	M	EMD Millipore MAB377	IF: 1/200 1h
SMI-32	M	Thermo Fisher	IF: 1/500 O/N
GAPDH	R	MilliporeSigma G9545	WB: 1/20,000 4˚C O/N
GAPDH	M	MilliporeSigma G8795	WB: 1/2,000 4˚C O/N
TAF15	R	Abcam ab134916	IF: 1/250 1h, WB: 1/1000 4˚C O/N
hnRNPA1	M	MilliporeSigma R4528	IF: 1/1000 1h, WB: 1/2000 4˚C O/N
TDP-43	M	EnCor Biotechnology Inc. MCA-3H8	IF: 1/250 1h, WB: 1/500 4˚C O/N
Lamin A/C	M	MilliporeSigma SAB4200236	IF: 1/500 1h
HA	R	Cell Signaling C29F4	IF: 1/500 1h
Eif2a	R	Cell Signaling 9722S	WB: 1/2000 4˚C O/N
Eif2a-P	R	Cell Signaling 9721S	WB: 1/200 4˚C O/N
RAN	R	Bethyl Laboratories A304-297A	IF: 1/250 1h
CRM1	R	Bethyl Laboratories A300-469A	IF: 1/250 1h
Puromycin	R	Fisher Scientific, MABE343MI (clone 12D10)	IF: 1/250 1h, WB: 1/1000 4˚C O/N
G3BP1	R	Proteintech 13057-2-AP	IF: 1/2000 1h
GFP	R	Invitrogen A-21311	IF: 1/1000 1h
ANK-G	M	Santa Cruz (463) sc-12719	IF: 1/100 1h
GluR2	M	MilliporeSigma MAB397	WB: 1/1000 4˚C O/N
GFAP	M	MilliporeSigma G3893	IF: 1/200 1h

*R = rabbit host; M = mouse host

**IF = immunofluorescence; WB = western blot; O/N = overnight

Image Acquisition, Processing and Quantification

Primary motor neuron images were imaged using a widefield fluorescence microscope (Nikon TiE) equipped with a cooled CMOS camera (Andor Zyla). Images were acquired as Z-stacks (0.2μm step size) using a 60x lens. As indicated, primary cortical neurons were imaged using a Lecia TCS SP5 II laser scanning confocal (Leica Microsystems) or Leica DMI6000B microscope as described(Sama et al. 2013). For confocal images of whole cells, 12-bit stacks (Δz = 0.25μM steps, zoom = 3x, n = 23-30 planes) were acquired at 40x with a pixel size of 126nm (1024x1024 pixels; 1000Hz). For dendrites, 12-bit stacks (Δz = 0.08μM steps, zoom = 3x, n = 40-50 planes) were acquired at 63x using a pixel size of 80nm (1024x1024 pixels; 1000Hz). For FISH, mFUS and somatic puromycin analyses, widefield stacks of the entire cell were acquired (z=0.2-.25μm) and deconvolved using the LAS AF One Software Blind algorithm (10 iterations). All neuron images were analyzed using MetaMorph software (Molecular Devices Inc.) or Image J. The background and shading of stacks were corrected as described(Bosco et al. 2010). Sum or maximum projections were created from corrected stacks for downstream analyses.

For the quantification of C:N ratios, a 20x20 pixel region was applied to the nucleus and perinuclear area in the soma for each cell (visualized by DAPI and MAP2, NeuN or SMI-32 respectively) as well as an area within each image that contained no cells (representing background fluorescence). The integrated intensity for the signal of interest was obtained for each region and a ratio of the

cytoplasmic:nuclear (C:N) signal was then generated following subtraction of background signal. For each experiment, statistical comparisons of C:N ratios with or without excitotoxic stress were completed using average C:N ratios collected from ≥three independent biological experiments. For the analysis of dendritic FUS levels, MAP2 was used visualize dendrites and create a mask with MetaMorph. Using the MAP2-defined mask, the integrated intensity of FUS staining was obtained and used to quantify the relative amount of FUS staining in dendrites.

For the quantification of neuron number and neurons exhibiting FUS translocation, ≥10 fields of view were imaged at 40x for each condition tested. As indicated by MAP2 or NeuN staining, neurons were quantified from images with computer assistance from the 'Cell Count' feature in MetaMorph. To assess the percent neurons with protein translocation (FUS, tdTomato, CRM1, RAN), cells were scored for the presence of translocation and divided by the total PCN number to generate the percent population exhibiting a response. Neurons were similarly quantified for cell survival. For KPT-330 experiments, cells were scored for the presence of FUS and/or nuclear PI staining at each time point indicated. To assess neuron survival following FUS knockdown, the number of GFP-positive cells were scored at the indicated timepoint for shSC and shFUS1 conditions.

Puromycin Analysis

Based on previously described experiments (Murakami et al. 2015), 4mM stocks of puromycin (Invitrogen A11138-03) were prepared in water. Neurons were

treated with glutamate as described, except that a final concentration of 2μM puromycin was added to the PCM media during the last 15 minutes of the 'washout' period. As a positive control of translational inhibition, 100 μg/ml cycloheximide (MilliporeSigma C7698) throughout the experimental time course. Neurons were then analyzed by Western or immunofluorescence using an anti-puromycin antibody (**Table II-4**). For the analysis of puromycin immunostaining upon FUS knockdown, a 20x20 pixel region was placed in the soma of GFP-positive cells. Using MetaMorph, the integrated intensity of this region was obtained and used to quantify relative puromycin levels as described above.

Fluorescence in situ *Hybridization (FISH) analysis*

Non-AraC treated neurons were plated on coverslips and transduced with shFUS or shSC-expressing lentivirus on DIV6 and harvested on DIV15. Following stress application, neurons were fixed with fresh 4% paraformaldehyde (Fisher Scientific, F79-500) diluted in RNAse free water (Corning, 46-000-CM) for 30 min at ambient temperature. FISH labeling was completed using a QuantiGene ViewRNA ISH Cell Assay Kit (Affymetrix, QVC0001) according to the manufacturer's instructions. One exception to the protocol was that samples were dehydrated after fixation with two min incubations in 50%, 70%, and 100% ethanol at ambient temperature followed by a second addition of 100% ethanol and stored at -20°C for five days before processing. Probes were designed and tested by Affymetrix. For post-FISH immunofluorescence, after probe labeling coverslips were washed in PBS for five

minutes and then blocked and processed for immunofluorescence as described (Baron et al. 2013). Coverslips were probed with MAP2 and GFP to visualize neurons and transduced cells, respectively. For analysis, neurons with at least two dendrites of 50+ μm lengths that did not excessively overlap with other cells were selected. Max projections of the imaged z-stacks were analyzed using MetaMorph software. For each neuron analyzed, 2-3 dendrites and the soma were assessed for their area and the number of FISH puncta present. Average dendrite data were reported for each cell and 10 cells were analyzed per construct and condition. Images were prepared for visualization as described (Cajigas et al. 2012). Gria2 puncta were digitally dilated. Neuron outlines were created by converting MAP2-images to binary and subsequently outline in green, in MetaMorph.

LDH Analysis

Neuron toxicity to glutamate was analyzed by the LDH assay using the CytoToxx 96 Non-Radioactive Cytotoxicity Assay kit (Promega, G1782).

Western Analysis

Neurons were treated, washed twice with PBS and lysed using RIPA buffer (Boston BioProducts, BP-115-500) supplemented with protease (Roche, 11836170001) and phosphotase inhibitors (Roche, 4906837001). Lysates were centrifuged at 13,500 rpm for 15 minutes, after which the supernatant was collected and its protein concentration determined using a BCA (Thermo Scientific

Pierce, 23227). Lysates were subsequently used for western and densitometry analysis as described(Ward et al. 2014). Protein gels for sodium dodecyl sulphate-polyacrylamide gel electrophoresis were loaded with 8-20µg lysate and GAPDH was used as a loading standard to determine relative protein levels. Primary antibodies used for analysis are described in **Table II-4**; LI-COR secondary antibodies were used as described(Ward et al. 2014).

Osmolarity Measurements

Measurements of media osmolarity (mOsm) were obtained using a Precision Systems Osmette II according to the manufacturer's instructions.

FUS Immunoprecipitation and Analysis by Liquid chromatography–tandem Mass Spectrometry

Neuron cultures from two 10-cm plates (each containing a coverslip to confirm FUS localization by immunofluorescence) were used for LC-MS/MS experiments. Neurons were treated with or without Glu^{excito}, washed twice with DPBS (Corning 21031CV) and resuspended in 750 µL immunoprecipitation (IP) lysis buffer (1% Triton-X 100, 50mM Tris-HCl, 150mM NaCl, 5mM EDTA, 10% glycerol; filter sterilized) containing protease (Roche, 11836170001) and phosphotase inhibitors (Roche, 4906837001). Lysates were incubated at 4˚C for 30 minutes and spun at 13,500 rpm. The concentration of the supernatant was saved and protein concentration measured by bicinchoninic acid assay (BCA; Thermo Scientific

Pierce, 23227); ~2500µg protein lysate was used for the following IP. A 1:4 volume of Protein G Dynabeads beads (Invitrogen 10003D): µg neuron lysate was acquired. Beads were washed with IP lysis buffer, mixed with the Genscript FUS antibody (**Fig. II-3**) in a 1:5 antibody:bead volume ratio in 1 mL of IP lysis buffer and incubated on a tube rotator for 2 hours at 4˚C. After 2 hours, lysis buffer/unbound antibody was removed and beads were mixed with the neuronal lysate overnight on a tube rotator at 4˚C. Beads were washed 3x with 1 mL IP lysis buffer before resuspending in 80µL Laemmli (SDS-Sample) Buffer (Westnet BP-111R) and boiling for 5 minutes to elute FUS protein. Western analysis of a 0.5% IP volume was run to confirm FUS immunoprecipitation. The remainder of the IP volume was run on a 12% SDS-PAGE gel (prepared in a sterile tissue culture hood to minimize contaminants) and gels were stained with a mass spec compatible silver stain (Pierce #24600) according to the manufacture's instructions. FUS bands were cut out using a razor into ~1mM size (~6-8 pieces/band).

Reduction and alkylation of gel bands was completed as described (Shevchenko et al. 2007). Briefly, samples were mixed with 500uL acetonitrile (Fisher Scientific A998-1) with vortexing until white and shrunken in size (~5-10 minutes). Liquid was removed and replaced with freshly prepared ~30-50µL 10 mM dithiothreitol (DTT; MilliporeSigma D0632) in 100 mM ammonium bicarbonate (MilliporeSigma A6141). Samples were incubated for 30 minutes at 56˚C and then cooled to room temperature before removing liquid and washing samples with acetonitrile as described above. Acetonitrile was removed and replaced with ~30-

50µL of freshly prepared 55 mM Iodoacetamide in 100 mM ammonium bicarbonate. Samples were incubated in the dark at room temperature for one hour. Iodoacetamide solution was removed and samples were washed twice with autoclaved water and once with acetonitrile. Acetonitrile was removed and samples were stored at -20˚C until digestion with chymotrypisin (Promega V1062).

To digest samples, chymotrypisin was resolubulized in 50uL 1mM HCl for 500ng/uL to make a working digestion buffer of 10ng/uL chymotrypisin (digestion buffer: 30uL 100mM Ammonium Bicarbonate, 30uL Acetonitrile, 240uL autoclaved water and 6uL of 500ng/uL chymotrypsin). ~50µL digestion buffer was added to samples on ice. After 90 minutes of incubation, 10-20uL of 100mM ammonium bicarbonate buffer was added to cover gel pieces and samples were incubated overnight at 25˚C in a convection incubator to prevent condensation. Peptides were extracted in 1:2 (vol/vol) digestion buffer:extraction buffer (5% formic acid (MilliporeSigma 06473)/acetonitrile) for 15 minutes at 37˚C with gentle shaking (350 rpm). Supernatant was removed and stored at -80˚C prior to analysis by LC-MS/MS. Extracted peptides were run on a Thermo Scientific Q-Exactive with assistance from the UMass Spectrometry Core. A semi-chymotryptic search including phosphorylation was performed on the data. Data were viewed for downstream analysis using Scaffold Viewer.

CHAPTER III: DISCUSSION AND CONCLUSIONS

Excitotoxicity as a Model of Neuronal Stress and Disease

Glutamate is the major neurotransmitter in the central nervous system. With respect to neurons, glutamate causes hormesis, a biphasic phenomenon wherein low glutamate exposure is favorable, but high doses can overstimulate neurons and induce excitotoxicity (Marini et al. 2008, Olney 1989). Thus, the amount of glutamate to which neurons are exposed must be carefully regulated.

Defects in glutamate signaling may arise from the abnormal release or uptake of glutamate from the extracellular space and/or function of postsynaptic glutamate receptors, as observed in trauma or ischemia (Olney 1989, Szydlowska & Tymianski 2010, Van Den Bosch et al. 2006). In regards to neurodegenerative disorders, glutamate-linked dysregulation has likewise been observed in patients with ALS (Gascon et al. 2014, Hideyama et al. 2012, Kawahara et al. 2004, Mitchell et al. 2010, Plaitakis & Constantakakis 1993, Rothstein et al. 1995, Selvaraj et al. 2018), leading to the hypothesis that excitotoxicity contributes to neuronal death (Rothstein 1996). The downstream effects of excitotoxicity include oxidative damage, mitochondrial and ER dysfunction (Fricker et al. 2018) and are all characteristics of cell stress. Intriguingly, multiple ALS-linked proteins, including FUS, participate in the cellular response to stress and/or alter this process when mutated (Sama et al. 2014). Although the mechanisms of glutamate regulation are fairly established, the immediate consequences of dysregulation and potential contribution of cellular mechanisms to disease pathogenicity are less understood.

Here we establish a cellular model (**Fig. II-1A**) to investigate neurodegenerative disease-linked proteins and pathways following excitotoxic insult and their relevance to disease (**Fig. III-1**). Extracellular levels of glutamate are elevated in ALS patients (Fiszman et al. 2010, Spreux-Varoquaux et al. 2002), however, the recorded upper limits of physiological glutamate concentrations vary and are somewhat controversial, in part a reflection of evolving techniques and assay sensitivity (Chiu & Jahr 2017, Le Verche et al. 2011, Moussawi et al. 2011). We selected 10μM glutamate (Glu^{excito}) for our excitotoxic model as this concentration is consistent with relatively recent *in vivo* observations from ALS patients (Fiszman et al. 2010) and is known to cause excitotoxicity in cultured neurons (Schubert & Piasecki 2001). Intriguingly, apart from observations of calcium influx causing ultimate neuronal cell death, there are few reliable markers or assays with which to differentiate excitotoxicity and resultant downstream processes (e.g. apoptosis, autophagy, production of radical oxygen species etc.) (Fricker et al. 2018)3 from alternative cellular insults. Thus, several lines of supporting evidence are presented to verify our induction of excitotoxic stress in primary cortical neurons by 10μM glutamate.

As the term excito*toxicity* implies, neurons treated with 10μM glutamate ultimately die (**Fig. II-1D-E, II-4G, II-11B**) (Schubert & Piasecki 2001). Further, FUS egress, previously observed to promote cell viability following hyperosmotic

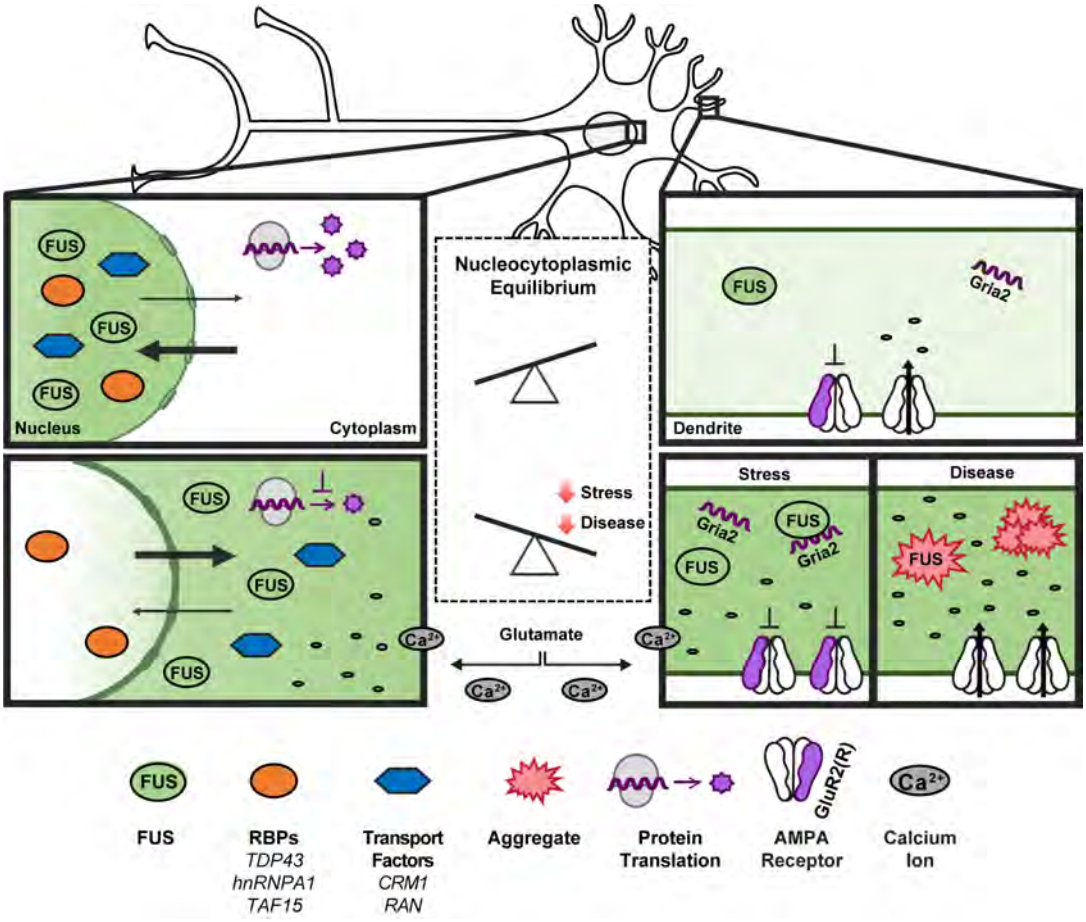

Figure III-1. A model depicting the impact of excitotoxic stress on neuronal homeostasis and disease pathogenesis. Under homeostatic conditions, shuttling RBPs such as FUS are predominately localized within the nucleus (top). Excitotoxic levels of glutamate (bottom) induce a massive influx of calcium and induce nuclear egress of FUS into neuronal soma and dendrites. Excitotoxic stress also leads to translational repression, a re-distribution of nucleocytoplasmic transport factors, and increased levels of Gria2 transcript within dendrites. The expression of FUS is required for enhanced levels of dendritic Gria2 in response to excitotoxic stress, implicating an RNA-processing role for FUS under these conditions. Enhanced levels of edited Gria2 transcript may represent a mechanism to offset the toxic effects of calcium influx. Prolonged or severe stress could manifest in the pathological aggregation of RBPs, including FUS, in neurodegenerative diseases such as ALS and FTD. Aberrant processing of Gria2 and/or GluR2 can occur through several mechanisms (e.g., expression of mutant FUS in astrocytes, loss of FUS function due to aggregation, and other means as described in the text), and contributes to calcium dyshomeostasis during disease.

stress in mammalian cells (Sama et al. 2013), correlates with the glutamate dose applied (**Fig. II-3E**) and suggests neuronal stress has been induced by physiologically elevated glutamate levels (Fiszman et al. 2010, Spreux-Varoquaux et al. 2002). Other phenotypes observed that are consistent with cell stress include: changes to neuronal structure (such as dendritic fragmentation; **Fig. II-1B**), attenuated global translation (**Fig. II-5**) and altered nuclear transport (**Fig. II-4**) (Holcik & Sonenberg 2005, Kelley & Paschal 2007, Yasuda et al. 2006). Thus, these observations further support excitotoxic FUS egress as stress-mediated and are relevant to our understanding of cellular stress and ALS.

As our current understanding of the factors that define the neuronal transition between favorable and unfavorable glutamate exposure are unclear. Our findings, in light of previous reports (Sama et al. 2013), indicate that FUS egress could potentially serve as a sensor of 'stress-induced' stimulation. In line with this hypothesis, FUS egress was not observed in Glu^{excito}-treated primary astrocytes (**Fig. II-3C**), a non-neuronal cell type that is not expected to experience excitotoxity. Moreover, Glu^{excito}-induced FUS egress is attenuated by NMDA inhibition (**Fig. II-7G**) as well as a reduction in extracellular calcium levels (**Fig. II-7A-C**). NMDA is strongly implicated in cortical neuron excitotoxicity and the influx of calcium a primary and ultimately fatal event in this process. (Schubert & Piasecki 2001, Stanika et al. 2009, 2012). Similarly, FUS translocation was observed following treatment with KCl (**Fig. II-7F**). Potassium application is a well-studied means with which to induce neuron depolarization and ion influx (Stanika et al.

2012), thus our results with KCl are consistent with the notion that FUS egress following glutamate-induced stimulation is a neuron specific process. Together, these data confirm that Glu^{excito} specifically induces excitotoxic stress in primary cortical neurons.

Although 10μM glutamate induces neuronal excitotoxicity and ultimate cell death, the time point at which we observe FUS egress has biological relevance (**Fig. III-1**). FUS egress precedes cell death (**Fig. II-1D-E, II-4G, II-11B**) and we observed stress-specific changes to the compartmental density of multiple transcripts (**Table II-2**) as well as FUS-dependent expression of Gria2 (**Fig. II-10C-E**). In further support of a response of FUS to glutamate (vs. a non-specific consequence of cell death), nuclear membrane integrity appears intact (**Fig. II4A**). Moreover, we observed a varied and selective redistribution of multiple proteins (FUS, TDP-43, hnRNPA1, CMR1 and RAN; **Fig. II-2, II-4H-K**), while other proteins associated with RNA and DNA activities were unaffected (TAF15, FMRP and G3BP; **Fig. II-2D,H, II-4B, II-5G**).

That we observe a rapid decline in neuron viability following acute excitotoxic insult may have precluded our ability to assess the effect of factors such as KPT-330 (**Fig. II-4G**) or FUS (**Fig. II-11B**), on cell survival, especially if the effects are subtle. Such acute neuronal demise is a shortcoming of this study and, to this end, chronic and/or *in vivo* models may yield further or more nuanced insight. Nevertheless, this model provides a tractable system with which to probe neuron-specific effects of glutamate stress. We demonstrate a novel nexus of

features widely associated with both stress and disease (**Fig. I-2, III-1**) that is relevant to studies currently ongoing in the neurodegenerative field. Furthermore, our model aids in defining the cellular effects of excitotoxicity and neuronal demise associated with neurodegenerative disorders, including ALS.

Altered Nucleocytoplasmic Compartmentalization in Stress and Disease

RNA Binding Protein Egress and Nucleocytoplasmic Transport

RBPs redistribute throughout the cell in response to stimuli as well as stress and disease. However, how or why this response occurs is not well understood. To understand the nature of RBP distribution, we investigated the localization of a panel of proteins linked to neurodegenerative disease during excitotoxicity, a neurodegenerative disease-linked stress. In doing so we observed RBP egress. However, the degree in redistribution varied (**Fig. III-1, II-2, II-3**) and this implies some form of selectivity. Interestingly, we did not observe a significant change in the localization of the shuttling protein TAF15 following excitotoxic insult at this experimental time point (**Fig. II-2D,H**). It would be interesting to examine the rate of TAF15 egress and/or import change with stress, as such dynamics may be reduced relative to proteins exhibiting a relatively robust response to stress.

In attempt to understand RBP redistribution following excitotoxic stress, we considered what might mechanistically drive the nucleocytoplasmic distribution of these proteins. In light of the robust cytoplasmic accumulation of FUS and predicted nuclear export sequence (NES) in the RRM domain, we first investigated

the involvement of potential export pathways. We found that inhibition of CRM1-mediated export by KPT-330 failed to completely prevent FUS egress (**Fig. II-4C-E**) as well as the positive control (NES-tdTomato-NLS, **Fig. II-4C-E**), indicating global transport is altered. However, unlike FUS, we still observed a partial effect of KPT on NES-tdTomato-NLS localization that suggests Glu^{excito}-induced FUS egress occurs independently of CRM1. This conclusion is consistent with a recent report examining FUS export mechanisms under steady state conditions (Ederle et al. 2018).

To widen our view on the state of global transport during excitotoxic stress, we also evaluated the localization of the shuttling protein RAN, which facilitates both import and export (Kim & Taylor 2017). We found nucleocytoplasmic equilibrium of RAN was also shifted to the cytoplasm (**Fig. II-4J,K**), further confirming that nucleocytoplasmic transport is globally altered by excitotoxic stress. Our observations reflect a growing body of literature implicating stress in impaired nucleocytoplasmic transport (Bano et al. 2010, Kelley & Paschal 2007, Kodiha et al. 2004, Yasuda & Mili 2016, Zhang et al. 2018a). For example, severe oxidative stress was shown to inhibit nuclear import and cause a collapse of the Ran gradient (Kodiha et al. 2004). Similar observations for Ran were reported for cells under hyperosmotic stress (Kelley & Paschal 2007), a stress that, like excitotoxicity, induces FUS egress (Sama et al. 2013). Intriguingly, It was recently observed that specific surface residues can directly promote or impede the association of proteins with nuclear pore components and thus, respectively

increase or decrease their rate of passage independent of transport adaptor proteins (Frey et al. 2018). This phenomenon blurs the line between the traditional binary classification of 'diffuse/passive' and 'adaptor-assisted/active' nuclear transport (Frey et al. 2018) and may have profound implications for our understanding of the nucleocytoplasmic equilibrium of RBPs during stress and disease. For instance, if processes reliant on the RAN gradient, such as transportin-1 (also karyopherin β2) which mediates FUS import (Dormann et al. 2010, 2012), are sufficiently disrupted, such a scenario could result in the accumulation of cytoplasmic FUS independent of CRM1 or other export factors (Ederle et al. 2018). Thus, it would be interesting to directly test the relationship between inhibition of RAN-mediated transport processes and FUS egress.

Unlike excitotoxic-FUS egress (**Fig. 7II-A,B**), the redistribution of FUS to hyperosmotic stress is not calcium-mediated (**Fig. 7II-H,I**) and suggests a difference in upstream mechanism. We do not know how direct the response of FUS to calcium is and thus, it is possible that the molecular underpinnings of excitotoxic and hyperosmotic stress egress may converge downstream through pathways or cellular states resulting from increased molecular crowding or ionic strength (Neuhofer et al. n.d.; Bounedjah et al. 2012; Rødgaard et al. 2008; Dong et al. 2009; Burg et al. 2007). Intriguingly, recent *in vitro* experiments have shown that RNA (Maharana et al. 2018) or other proteins linked to liquid-liquid phase separation (LLPS) (Hofweber et al. 2018) as well as ionic concentration (Qamar et al. 2018) can influence the LLPS dynamics of FUS. Although the extrapolation of

such experiments in cells is currently ongoing, it is intriguing that such conditions can influence the behavior of FUS and may be relevant to the altered dynamics of FUS observed in cells following specific forms of stress, such as calcium-mediated excitotoxity.

In regards to FUS itself, additional *in vitro* experiments indicate that the modification of residues important in creating electrostatic interactions within FUS as well as between RNA and proteins (Hofweber et al. 2018, Qamar et al. 2018, Wang et al. 2018) could have relevance to aspects of cellular FUS function. For instance, under basal conditions, such a biophysical regulation of FUS may manifest as the addition of phospho- or methyl-groups previously shown to influence FUS interactions and transport (Darovic et al. 2015, Dormann et al. 2012, Hofweber et al. 2018). To this end, we hypothesized that FUS phosphorylation might contribute to FUS localization but were unable to conclude a difference in phosphorylation (**Fig. II-8, Table II-1**). Consistent with recent reports of FUS following hyperosmotic stress (Rhoads et al. 2018a), we did not observe a shift in the molecular weight of FUS following excitotoxic insult as observed for known phosphorylated FUS species (Rhoads et al. 2018a). Thus, these correlative observations suggest FUS may not be differentially phosphorylated following excitotoxic stress. However, FUS phosphorylation in the NLS has been shown to impede FUS import (Darovic et al. 2015). Both our mass spectrometry (**Fig. II-8**) as well as domain deletion experiments (**Fig. II-9**) did not address potential modifications to the NLS or neighboring residues that influence FUS transport

(Darovic et al. 2015, Dormann et al. 2012) and thus regulation of FUS egress through this C-terminal domain remains a possibility. While FUS may be modified in response to stress and result in the cytoplasmic accumulation of this protein, it is intriguing to speculate that under conditions of stress in which the cellular environment is vastly altered (e.g. extreme increase in intracellular ions), such changes could potentially be sufficient to disrupt and/or 'override' the normal activities and associations of FUS, consistent with notions derived from *in vitro* reports in which ionic concentration impedes FUS LLPS (Qamar et al. 2018). However, this hypothesis remains untested. Regardless of mechanism, the change in localization may activate differential FUS functions as observed for other RBPs (Cammas et al. 2007, Lin et al. 2007) and, if unregulated, could potentially become pathogenic.

Functional Response of FUS to Excitotoxicity

Within neurons, mRNA localization is key to localized protein expression; nearly half the neurite-enriched proteome is encoded by neurite-localized mRNAs (Zappulo et al. 2017). Neuron excitation induces local mRNA translation in dendrites (Buxbaum et al. 2014, Ju et al. 2004) and the accompanying increase in RBPs is likewise viewed as essential for synaptic mRNA metabolism (Zhang et al. 2012). Although FUS predominantly localizes to the nucleus under basal conditions, a low-level, basal presence of this RBP in dendrites under is well-established (Fujii et al. 2005, Ling 2018) and consistent with our observations (**Fig**

II-F,G). Further, following neuronal excitation by chemically-induced, long term potentiation (LTP) or activation of mGluR5 receptors, FUS specifically increases within dendritic synapses (Fujii et al. 2005, Sephton et al. 2014, Zhang et al. 2012). In the case of mGluR5 stimulation, GFP-tagged FUS was observed to move from the dendritic shaft to spines, although no increase in the total levels of FUS were reported (Fujii et al. 2005). While the localization of FUS to spines was not examined in this study, using the physiological neurotransmitter glutamate, we observed a previously unreported and robust accumulation of FUS in dendritic shafts (**Fig. II-3F,G**) and somatic cytoplasm (**Fig. II-2A,E**).

Beyond a physical increase of FUS in dendrites, we further uncovered a FUS-dependent enrichment of dendritic Gria2 upon exposure to Glu^{excito} (**Fig. II-3F,G, II-10C-F**), although we do not yet know if dendritic FUS is specifically responsible for this effect. Gria2 encodes the GluR2 protein subunit of the AMPA receptor and incorporation of post-transcriptionally edited GluR2 subunit renders AMPA receptors calcium impermeable (Wright & Vissel 2012) (**Fig III-2**). Following neuronal stimulation with mGluR5 or potassium (**Fig II-7F**), Gria2 is locally translated in dendrites (Ju et al. 2004) (**Fig III-2**). Thus, stress-specific Gria2 expression in response to excitotoxic stress is conceivable. Given the acute strength of Glu^{excito}, our observations possibly reflect a homeostatic response to strengthen synapses (Liu & Cull-Candy 2005, Liu & Zukin 2007). During this time, an increase in GluR2-containing AMPA receptors has been observed (Liu & Cull-Candy 2005). While this immediate increase may result from the migration of

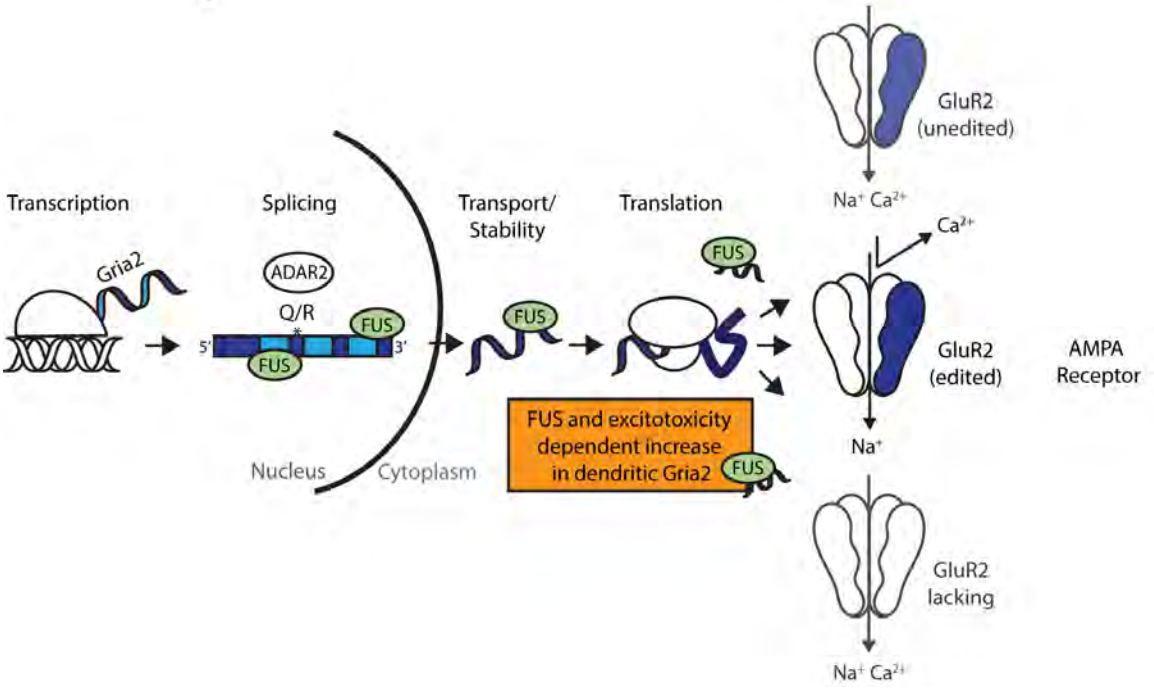

Figure III-2. Normal Gria2/GluR2 biology and association with FUS. Gria2 is transcribed, spliced and edited in the nucleus. Glutamine to arginine (Q/R) post-transcriptional editing is mediated by the enzyme ADAR2, and this editing event confers calcium impermeability to the assembled AMPA receptor and is highly efficient in cortical and spinal neurons (Kawahara et al. 2003, 2004; Nutt & Kamboj 1994). Gria2 is transported to neuronal dendrites for local translation, which can be specifically induced by response stimulation. The Gria2-encoded AMPA subunit, GluR2, is present in the majority of AMPA receptors, although there is a noted biological contribution of GluR2-lacking (calcium permeable) AMPA receptors (Cull-Candy et al. 2006, Gascon et al. 2014). In regards to FUS, FUS does not appear directly linked to Gria2 transcription (Lagier-Tourenne et al. 2012) or GluR2 expression under basal conditions ((Udagawa et al. 2015) and (**Fig. II-10**)). FUS binds both Gria2 introns and 3'UTR and influences the splicing of this transcript, as observed in changes in Gria2 splicing following FUS knockdown (Lagier-Tourenne et al. 2012). Including the findings presented here, we observe a novel FUS-dependent increase of Gria2 in dendrites following excitotoxic insult (**Fig. II-10**).

receptors from an extra-synaptic pool, there may be a potential role for Gria2 translation in the replacement of this pool or the specific need to express of GluR2-containing receptors. Such a hypothesis is consistent with reports of FUS enrichment in post synaptic densities by mass spectrometry following chemical LTP (Zhang et al. 2012) and separate observations of GluR2 translation following application of a potassium-based LTP-linked protocol (Ju et al. 2004). However, whether the effect of FUS on Gria2 stems from acute stimulation or the explicit activation of cell stress pathways is currently unclear and requires further investigation. Regardless, increased expression of Gria2 could serve a protective role following excitotoxic insult by increasing the overall number of calcium-impermeable (GluR2 containing) AMPA receptors by reducing net calcium influx caused by calcium-permeable (GluR2 lacking) receptors (Gascon et al. 2014, Liu & Zukin 2007).

A model in which there is a select increase in Gria2/GluR2 expression is consistent with our preliminary observations that response of Gria1 to excitotoxicity is relatively modest and/or unchanged (**Table II-2**). Although we presume Gria2 is translated in response to excitotoxicity (Ju et al. 2004), we did not detect an increase in total protein (**Fig. II-10G,H**). It is probable that our examination of steady-state, whole-cell lysates lacks the sensitivity to detect subtle changes in rapid protein expression 30 minutes post-insult. The Bosco lab has previously found that labelling nascent peptides was required to detect the translation of select proteins during stress (Baron *et al.* unpublished results).

While we have yet to determine the biological significance of increased Gria2 in dendrites following excitotoxic insult. However, that increased dendric Gria2 expression occurs in a FUS and stress specific manner is novel (**Fig. II-10**) and increases our understanding of FUS function and glutamate signaling. Although FUS has been shown to bind and influence the splicing of Gria2 (**Fig. III-2**) (Lagier-Tourenne et al. 2012), a selective effect of FUS on the levels of endogenous AMPA transcripts has only been observed for Gria1 under non-stimulated conditions (Lagier-Tourenne et al. 2012, Udagawa et al. 2015). Given the involvement of FUS in dendritic RNA transport (Kanai et al. 2004) and 3'UTR-mediated stabilization of synaptic transcripts Gria1 and SynGAPα2 (Udagawa et al. 2015, Yokoi et al. 2017) for expression, it is possible that FUS may function similarly in regards to Gria2 following excitotoxic stimulation. However, we cannot rule out that Gria2 regulation by FUS may also involve splicing (Lagier-Tourenne et al. 2012), transport (Kanai et al. 2004) and/or mRNP remodeling for translation (Buxbaum et al. 2014).

In addition to Gria1 or Gria2, we had also selected Nd1-L as a candidate transcript for assessment of FUS function during excitotoxicity based upon a previously reported relationship between FUS (**Table II-2**). The Nd1-L transcript encodes an actin-stabilizing protein whose transcript levels increase in a FUS-dependent manner following activation of mGluR5 in hippocampal dendrites (Fujii & Takumi 2005, Fujii et al. 2005). As glutamate can also activate mGluR5, we had expected a similar result. However, we observed no change in dendritic Nd1-L and

our preliminary data further suggest the number of somatic Nd1-L transcripts decreases following excitotoxicity (**Table II-2**). As glutamate activates multiple receptors in addition to mGluR5 and there is much crosstalk between the downstream, receptor-activated pathways (Reiner & Levitz 2018) this could represent one reason for this observational conflict. Thus, if not a consequence of cell type differences (hippocampal vs. cortical), understanding the significance of these observations would require further investigation.

Together, our data demonstrate the involvement of FUS in the regulation of the synaptic transcript, Gria2, during excitotoxic stress. These observations provide mechanistic insight into the RNA-processing activities of FUS in neurons. Indeed as FUS knockout and knockdown studies demonstrate FUS as an essential player in shaping dendritic spines (Fujii & Takumi 2005, Fujii et al. 2005, Udagawa et al. 2015, Yokoi et al. 2017), our findings further the importance of FUS in dendritic spine and post-synaptic biology.

Glutamate Signaling and Cellular Stress in ALS

Calcium Defines a New Link Between FUS and ALS

Here we identified a novel redistribution of FUS to the cytoplasm following glutamate-induced excitotoxicity in primary neurons (**Fig III-1**) and together these data uncover a new role for FUS in glutamate signaling pathways. Calcium is a key player in the neuronal response to glutamate and we find that the calcium ionophore, Ionomycin, is sufficient to incite a response of FUS in murine cortical

and motor neurons (**Fig. II-2A,E and II-12A-D**) as well as human iPSC-derived motor neurons (**Fig. II-12E**). Although we do not know how direct the response of FUS to calcium is, these data reveal that increased intracellular calcium consistently induces FUS egress in multiple neuronal models.

The work presented here was predominantly conducted in cortical neurons. Although not the primary affected cell type in ALS, cortical neurons share many properties with motor neurons and are associated with the neurodegenerative disease FTD, which lies on a 'disease-spectrum' with ALS (Ling et al. 2013). Thus, the tractability and amenability to biochemical assays make cortical neurons useful in establishing neuronal precedent. To extend key findings from our cortical neuron system, we used kainic acid to induce excitotoxicity in primary murine motor neurons and observed changes to SMI-32 that are consistent with the notion that kainic acid induces cellular stress (**Fig. II-12A-D**). Intriguingly, unlike cortical neurons, the distribution of FUS C:N ratios in murine spinal cord motor neurons FUS appeared bimodal. This may suggest that a sub-population of neurons exhibit enhanced vulnerability to stress and could, potentially, trigger transneuronal or secondary neuronal degeneration within neighboring cells with time (Fricker et al. 2018) and would be an interesting direction for future research. Although we attempted to induce excitotoxicity with glutamate and kainic acid in iPSC-derived motor neurons using conditions previously described (Donnelly et al. 2013), we were unable to elicit FUS egress or alterations to neuronal morphology, as expected based on our observations in cortical neurons and excitotoxicity

literature. These data suggest that the application of excitotoxic agonists in iPSC did not induce stress in these cells. However, that we consistently observe Ionomycin-induced FUS egress, even in iPSC (**Fig. II-12E**) supports the notion that while different neuron types and/or models may differ in their potential susceptibility to excitation (e.g. due to inherent differences in receptor expression, neuron maturity etc.), once a calcium-mediated 'threshold' is achieved, FUS egress is commonly shared.

The connection we have made between FUS and calcium has implications for FUS in ALS. Although acute, transient expression of ALS-mutant R521 FUS or the severely cytoplasmic variant, P525L FUS, for 72 hours was not sufficient to increase intracellular calcium levels (Tran et al. 2014), hyperexcitability has been observed in ALS-FUS iPSC-derived motor neurons (Wainger et al. 2014). Hyperexcitability describes a state in which neurons are excessively excitable (i.e. an increased propensity for neurons to fire in response to a given stimulus) and is a notable feature of ALS that has been recapitulated in multiple ALS animal and iPSC models (Fogarty 2018). As such, increased synaptic transmission due to hyperexcitability could increase intracellular calcium transients with time and, when compounded by age-related defects in synaptic homeostasis (Bezprozvanny & Hiesinger 2013), could potentially culminate in excitotoxicity to trigger disease-linked FUS pathology (Keller et al. 2012, Vance et al. 2009). Support for this possibility comes from models of ischemia, an event strongly linked to excitotoxicity (Szydlowska & Tymianski 2010), in which RBP translocation (Liu et

al. 2010) as well as the partitioning of RBPs (including FUS and TDP-43) to triton-insoluble aggregates (Kahl et al. 2018) has been observed. Intriguingly, data from ALS-models suggests that hyperexcitability precedes and gives way to hypoexcitability. Hypoexcitability is a state in which neuronal excitation in response to a given stimulus is reduced (Devlin et al. 2015) and has been observed in adult ALS-FUS rodent models (de Lourdes Martínez-Silva et al. 2018) as well as ALS-FUS iPSC models (Naujock et al. 2016). Although the relationship of hypoexcitability to ALS pathology is less clear than hyperexcitability, altered pre-synaptic firing patterns of inhibitory and/or excitatory neurons as well as 'unfavorable' imbalances in calcium-permeable AMPA receptors in post-synaptic hypoexcitable neurons could similarly increase intracellular calcium levels *in vivo* (Delestrée et al. 2014).

ALS-causing FUS mutations result in the mislocalization of mutant FUS to the cytoplasm, the varying degree of which correlates with a reduced age in disease onset (Dormann et al. 2010). ALS-FUS mutations show impaired binding of mutant FUS with the nuclear import protein, Transportin 1 (also called karyopherin β2) (Dormann et al. 2010). Further, recently developed murine models suggest the increased cytoplasmic presence of FUS promotes the formation of ALS-linked phenotypes (Scekic-Zahirovic et al. 2017, Sharma et al. 2016, Zahirovic & Sendscheid 2016). Despite these observations, how FUS forms end-stage disease aggregates and how these mutations functionally contribute to pathogenesis is unclear. We observe the robust redistribution of nuclear ALS-FUS

mutants in response to excitotoxic stress (**Fig. II-13A,B**). Thus, these data support excitotoxicity as a potential mechanism by which nuclear mutant FUS ultimately accumulates in the cytoplasm in end stage tissue.

Unlike the nuclear ALS-FUS mutants tested, we observe that nucleocytoplasmic equilibrium of the severely mislocalized, ALS-mutant, R495X, was not further enhanced by excitotoxic stress (**Fig. II-13A,B)**. Given that mutations cause an increase in cytoplasmic FUS, providing a basis for gain of function mechanism in disease, (Scekic-Zahirovic et al. 2017, Sharma et al. 2016, Zahirovic & Sendscheid 2016), we tested if R495X FUS could alter Gria2 expression in neurons under basal or excitotoxic stress conditions. Our results were inconclusive however as transient expression of human, FLAG-HA-WT FUS (**Fig. II-13C,D**) prevents the dendritic Gria2 phenotype previously uncovered in naïve murine neurons (**Fig. II-10**). Precluding an effect of the transfection itself, these data suggest human FUS may exert a dominant negative effect in our murine system. Although we were unable to determine the effect of R594X FUS on Gria2, others have recently observed that P517L (the murine equivalent of human P525L, a severely mislocalized cytoplasmic ALS-FUS variant) can reduce Gria2 levels through the upregulation of miRNAs targeting this transcript (Capauto et al. 2018). Further, through a non-cell autonomous mechanism, astroglial expression of ALS-FUS mutant, R521G, can reduce AMPA expression in motor neurons and cause calcium-mediated toxicity (Kia et al. 2018). Thus, there is a precedence for the altered regulation of AMPA subunits, including Gria2/GluR2, by mutant FUS in

disease. Over a lifetime mutant FUS may promote conditions of calcium dysregulation and lead to conditions cumulating in excitotoxicity that ultimately cause motor neuron death and FUS egress.

Excitotoxicity, Cellular Stress and Disease

While the potential for a pathogenic relationship between mutant FUS and calcium may apply to FUS-mediated ALS, glutamate-linked calcium dysregulation is also associated with phenotypes common to both familial and sporadic ALS as well as FTD (Gascon et al. 2014, Hideyama et al. 2012, Kawahara et al. 2004, Mitchell et al. 2010, Plaitakis & Constantakakis 1993, Rothstein et al. 1995, Selvaraj et al. 2018). Specific to AMPA receptors, an ALS iPSC model of C9orf72 reports increased vulnerability to calcium through abnormal expression of the AMPA subunit, GluR1 (encoded by Gria1) leading to neuronal susceptibility to calcium (Selvaraj et al. 2018). Calcium-permeable AMPA dysfunction is implicated in iPSC models of FTD (Gascon et al. 2014, Imamura et al. 2016) as well as toxicity in SOD1 ALS motor neuron models (Van Damme et al. 2007). Thus, this investigation provides insight and further supports the potential of glutamate and/or calcium dysregulation in ALS and FTD (Deng et al. 2010, Keller et al. 2012-b).

Aside from the glutamate receptors themselves, nucleocytoplasmic transport has recently emerged as another common theme amongst age-related neurodegenerative diseases, particularly in the context of sporadic and familial ALS as well as FTD (Li & Lagier-Tourenne 2018). While certain pathogenic

mutations are sufficient to induce pore disruption in culture (Zhang et al. 2015), it is possible that stressors, such as excitotoxicity, could also contribute to the development of or exacerbate observed defects. For instance, excitotoxicity-linked depletion of adenosine triphosphate (ATP) (Szydlowska & Tymianski 2010, Yasuda et al. 2006) and/or calcium activation of calpains that degrade nuclear pore proteins (Bano et al. 2010, Sugiyama et al. 2017) could potentially disrupt transport or nuclear pore permeability. In support of this notion, guanosine triphosphate (GTP) can improve reduced import caused by excessive intracellular calcium (Sweitzer & Hanover 1996). Further, mice deficient in the astroglial glutamate transporters, GLAST and GLT1 (also known as EAAT1 and EAAT2; the latter implicated in ALS (Rothstein et al. 1995)), exhibit motor neuron degeneration accompanied by nuclear pore degradation (Sugiyama et al. 2017). Interestingly, motor neuron death was delayed in these mice treated with the CRM1 inhibitor KPT-350 (Sugiyama et al. 2017), an analogue of KPT-330 that is currently being pursued as potential therapy in ALS clinical trials. Although we only observe a partial effect of KPT-330 in our model (**Fig. II-4C-E**), that KPT-330 can modulate the effects of excitotoxicity supports further investigation into this line of therapy, however increased benefit may be observed when used as part of combination therapy.

Akin to transport, excitotoxicity also reduces translation (**Fig. II-5**), another stress-linked phenotype (Aulas et al. 2017) associated with ALS models (Green et al. 2017, Murakami et al. 2015). Surprisingly, global translational repression 30

minutes following excitotoxic insult was not mediated by EIF2α phosphorylation as commonly observed for cellular stress (Holcik & Sonenberg 2005) as well as reported in ALS patients and models (Ilieva et al. 2007, Sharma et al. 2016). Although not examined here, alternative forms of calcium-linked, translational repression such as eukaryotic elongation factor 2 (eEF2)-phosphorylation (Heise et al. 2014, Marin et al. 1997) might be responsible for immediate inhibition (**Fig. II-5)** followed by EIF2α phosphorylation later in the excitotoxic time course (Fan et al. 2013). Together this work reveals hallmarks of cell stress associated with neurodegeneration in a model of excitotoxicity: RBP egress, nucleocytoplasmic transport defects and possibly translational repression. These findings are consistent observations in patients and animal models, and thus further our understanding of cell stress phenotypes and their relevance to disease pathogenesis.

Conclusions

Glutamate is a neurotransmitter that is essential for the function of neurons in the CNS. Dysregulation of this essential molecule can cause neuron toxicity and there is evidence for this outcome in neurodegenerative diseases including ALS and FTD. That the nuclear egress of FUS and additional disease-linked RBPs identified following excitotoxicity is similarly observed in additional contexts (i.e. HOS) supports the dynamic redistribution of these proteins as part of a general response of RBPs to cell stress. While the RBP redistribution may serve as a switch or signal

in cellular state, the functional meaning remains to be uncovered. Interestingly, we identified a potential functional role for FUS following excitotoxic insult that increases our understanding of the cellular response to excitotoxicity as well as current hypothesized mechanisms of neurodegenerative disease. As with many biological processes, low or temporary exposure to stimuli can induce favorable and/or protective mechanisms within a cell, system or organ. However, too much of a “good” thing can be detrimental. In the context of disease, excessive or chronic glutamate stress may permanently disrupt the nucleocytoplasmic equilibrium to the point where RBPs are dysfunctional and promote neuronal demise. Defining this balance is thus an essential part of understanding the consequences of cellular disruptions that ultimately manifest as human disease.

PREFACE TO APPENDIX I

All of the work presented in this appendix was performed by Maeve Tischbein with the following exceptions:

Murine primary motor neuron experiments were performed and analyzed by Dr. Claudia Fallini. Astrocyte cultured media used for osmolarity measurements was a generous gift from Dr. Brigitte Van Zundert (Fritz et al. 2013).

APPENDIX I: Investigation of Hyperosmotic Stress in the CNS

Mutations in FUS cause the neurodegenerative motor neuron disease, amyotrophic lateral sclerosis (ALS) (Kwiatkowski et al. 2009, Vance et al. 2009). In patient tissue, fused in sarcoma (FUS) aggregates in the cytoplasm of motor neurons. Currently >40 ALS-mutations have been identified in FUS and they can be found throughout the protein (Kapeli et al. 2017). Intriguingly, the highest number of single mutations and those mutations occurring at the highest frequency are found in or neighboring the NLS (Lattante et al. 2013), a domain important in maintaining FUS localization. Intriguingly the degree of mislocalization conferred by ALS mutation correlates with a reduced age in disease onset (Dormann et al. 2010) and implies that the FUS mislocalization contributes to disease.

Upon investigation of the normal, cytoplasmic roles of FUS, it was discovered that hyperosmotic stress (HOS) can induce the nuclear egress of FUS and FUS accumulation within cytoplasmic stress granules (Sama et al. 2014). Stress granules are transient presumably protective, mRNA-protein complexes (Buchan & Parker 2009) that can form in response to environmental stressors including hyperosmotic, oxidative and ER stress. To date, much of the research examining the response of FUS to hyperosmotic stress has been conducted in immortalized cells. As ALS affects the central nervous system (CNS), the response of CNS-linked cell types to hyperosmotic stress as well as the physiological relevance of hyperosmotic stress to the CNS remains to be determined. There are reports that hypernatremia, a condition where sodium serum levels are excessively

increased, increases the levels of brain osmolytes (Lien et al. 1990) and hyperosmolar therapy has been suggested as a treatment to reduce brain swelling (i.e. following trauma) (Ropper 2012). More relevant to ALS, solutes such as glutamate are increased in patient CSF and there are reports of non-neuronal cells contributing to ALS through the release of factors that cause non-cell autonomous neuron toxicity in cell cultures models (Fritz et al. 2013, Nagai et al. 2007). Further, inflammation is widely observed in ALS and there is evidence suggesting hyperosmotic stress is linked to and may event serve as a inflammatory stimulus (Brocker et al. 2012). Given the relevance of FUS localization to disease and that FUS egress is observed following HOS suggests HOS as an intriguing, potential pathomechanism. The physiological relevance of hyperosmotic stress to neurodegeneration however is less clear and explored here.

FUS Egress Following Hyperosmotic Stress (HOS) in Primary Motor Neurons

To understand the HOS response of FUS and its potential relevance to ALS, FUS localization was evaluated in response to HOS in primary motor neurons, the primary affected cell type. Extracellular osmolarity was increased with the osmolyte sorbitol, using the same paradigm (0.4M sorbitol for one hour) shown to induce FUS egress in immortalized cells (Sama et al. 2013) and primary cortical neurons (**Fig. II-7**). Following treatment, FUS egress was observed in primary motor neurons and the cytoplasmic:nuclear (C:N) equilibrium of FUS significantly increased (**Fig. AI-1**). While FUS egress seems a common feature of the HOS

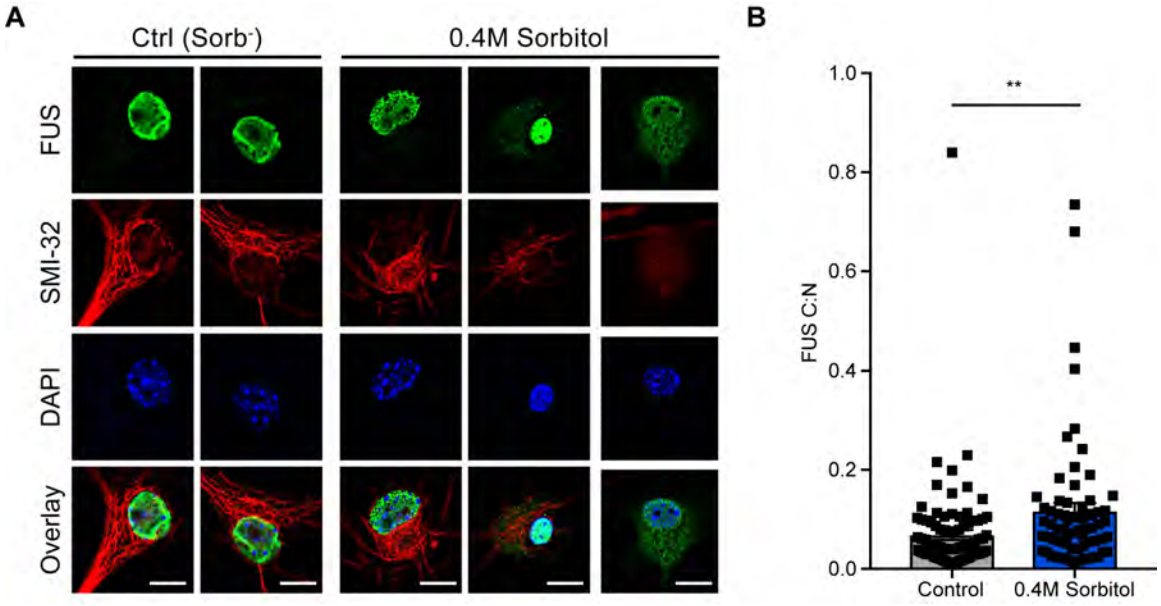

Figure AI-1. FUS egress is observed in primary motor neurons following hyperosmotic stress. (A,B) DIV6-8 primary motor neurons treated with 0.4M sorbitol for one hour exhibit FUS egress (green) and a significant increase in FUS C:N ratio (Student's T-test, **p<0.01, n=3 biological replicates). Motor neurons were identified using the motor neuron marker, SMI-32 (red) and nuclei were stained with DAPI (blue). The extent of cytoplasmic FUS varied to a greater extent between sorbitol treated cells but not controls. In (B), black squares indicate individual cell measurements and experimental means were calculated from the average C:N ratio across the individual biological replicates. Error bars represent SEM. Scale bars = 10μm.

response, the absolute extent of egress appears reduced relative to immortalized cells (Sama et al. 2013) and may reflect biological differences in cell type.

Evaluating Potential Links Between ALS, Non-Cell Autonomous Mechanisms of Disease and Cellular Stress

In ALS motor neurons represent the primary affected cell type, however, pathological aggregates are also observed in non-neuronal, glial cells (Peters et al. 2015). These observations imply that neurons are not the only cell type affected by disease. Thus, understanding the response and/or contribution of glia to CNS stress may provide insight as to the cellular mechanisms underlying ALS pathology and selective degeneration of motor neurons. In considering HOS as a physiological source of stress, we hypothesized that the release of factors from non-neuronal glial cells could potentially increase media osmolarity, thereby serving as possible mechanism by which HOS might be induce or contribute to disease *in vivo*. Given reports of the release of unknown astrocytic factors capable of causing motor neurons toxicity (Fritz et al. 2013, Nagai et al. 2007), we tested if the osmolarity of cultured astrocyte media (ACM) from cells expressing wildtype (WT) or ALS-mutant SOD1 species (G93A, G85R) was increased. Upon measurement of ACM osmolarity (ACM previously described (Fritz et al. 2013)), no correlation with genotype or SOD1 overexpression were observed from this, albeit limited, analysis (**Fig. AI-2A**). While not conclusive, these data suggest that there are no robust changes in ALS-mutant SOD1 ACM osmolarity.

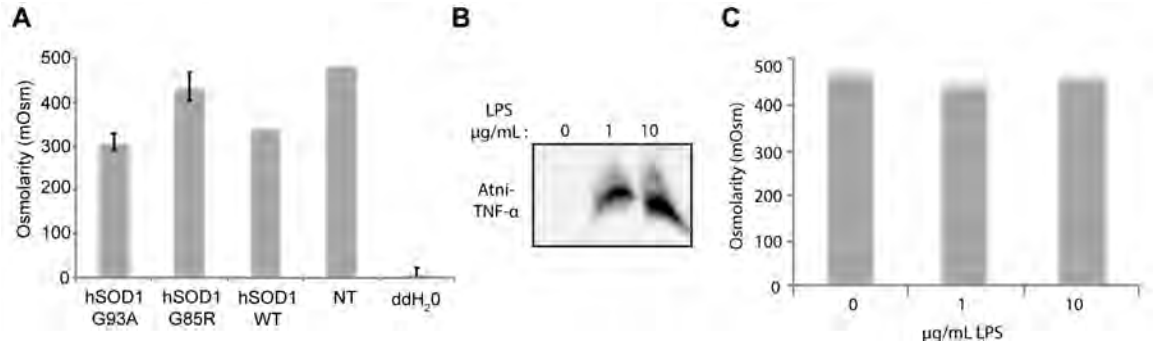

Figure AI-2. Factors secreted by ALS-mutant astrocytes and microglial activation do not appear to robustly influence osmolarity. (A) Media osmolarity astrocyte cultured media (ACM) from murine astrocytes expressing WT or mutant (G93A, G85R) SOD1 species was assessed relative to the non-transgenic control (NT) or water (ddH_2O) alone. N=1 biological replicate; mutant SOD1 ACM was tested in technical duplicates. No appreciable and/or correlative trend could be determined from osmolarity measurements. Error bars represent SEM. **(B)** Primary microglia activation is confirmed by the production of TNF-α following stimulation with LPS. **(C)** The osmolarity of media from microglial cultures did not appreciably change following primary microglial activation using LPS. **(B,C)** n=1 biological replicate; results are consistent with n=2 biological replicate similarly conducted in BV2 cells.

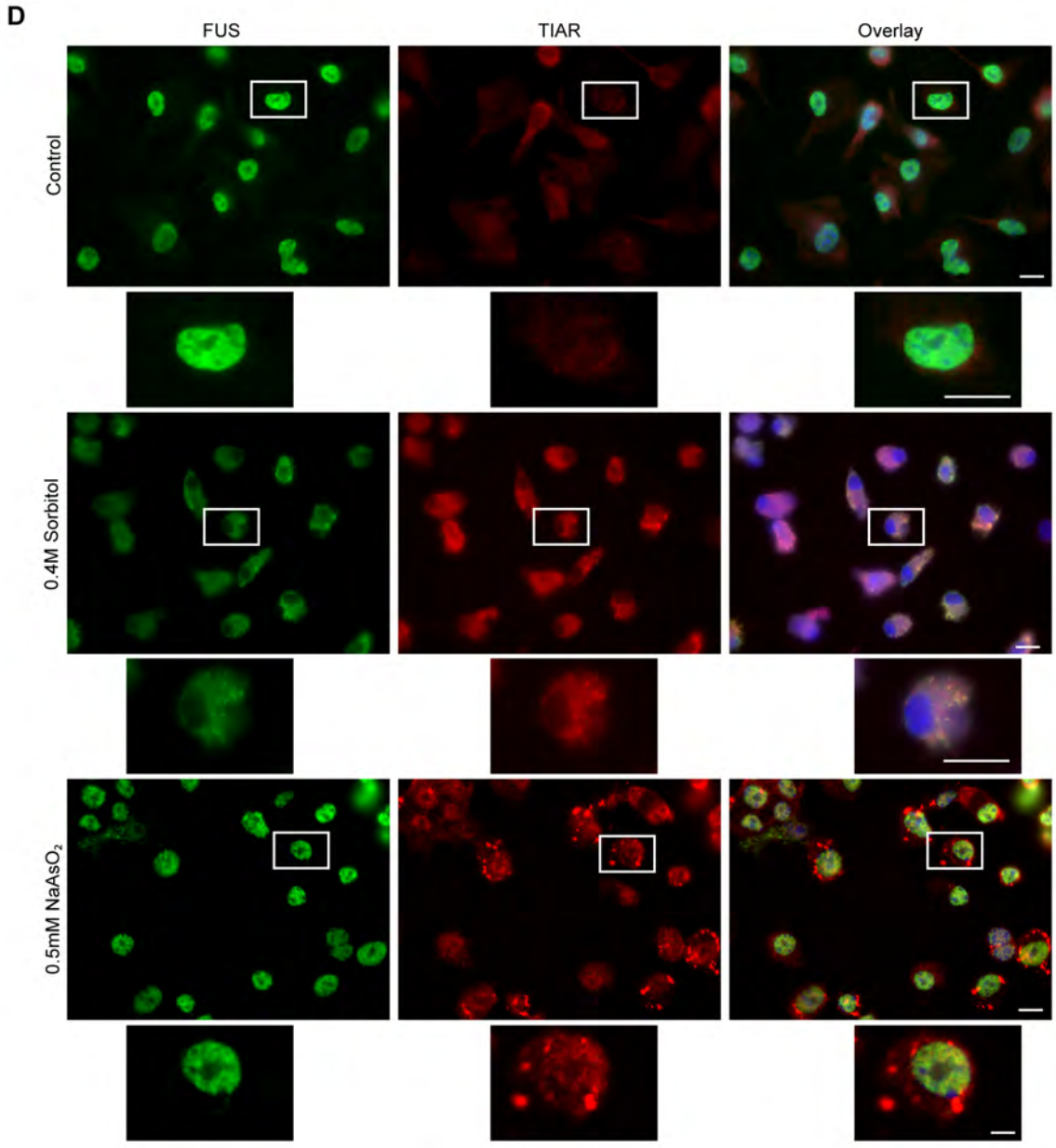

Figure AI-2 continued. (D) Microglia treated with sorbitol or sodium arsenite form stress granules (TIAR, red), however nuclear egress of FUS (green) and subsequent colocalization with stress granules was only observed following sorbitol treatment. White boxes denote areas used for high magnification details. N=2 biological replicates. Scale bars = 10μm.

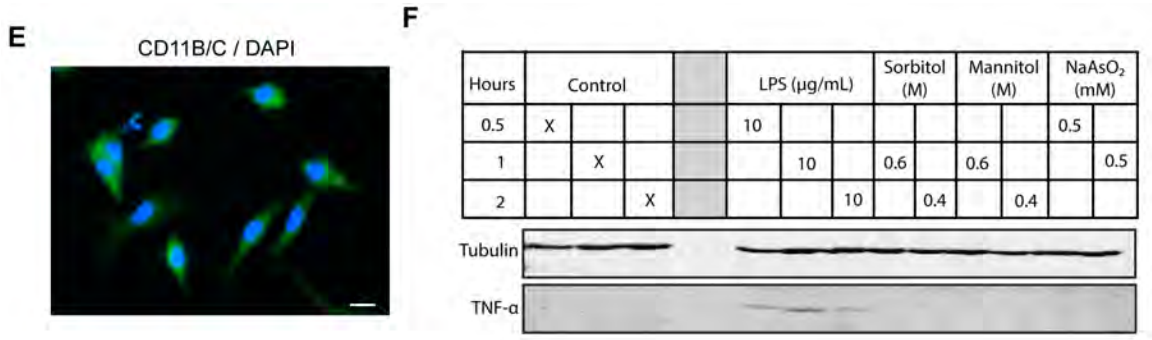

Figure AI-2 continued. (E) Primary microglia used for experiments expressed the expected cell marker CD11B/C (green). Scale bar = 10µm. **(F)** TNF-α production was similarly assessed by western analysis of BV2 cells treated with LPS, HOS (induced by Sorbitol or Mannitol) or oxidative (sodium-arsenite; $NaAsO_2$) stress (n=1 biological replicate). However, TNF-α was only detected following treatment with the positive control, LPS.

Although we did not observe gross alterations to media osmolarity from this primary astrocyte model, activation of primary microglia can release factors (i.e. pro-inflammatory cytokines) into the extracellular space and such activated states are observed in ALS (Saberi et al. 2015) and could potentially trigger HOS. Conversely, HOS has been suggested as potential stimulus of an inflammatory response (Brocker et al. 2012) and thus, understanding the immune cell response to stress could have implications for disease.

To this end, cultures of primary murine microglia were treated with lipopolysaccharide (LPS) to induce activation, the result of which was indicated by the production of TNF-α and observed by western (**Fig. AI-2B**). Next, the osmolarity of the media from these activated cultures was measured, however no robust differences were observed (**Fig. AI-2C**). We next assessed if stress granules and FUS localization paralleled observation from immortalized cells (Sama et al. 2013) and/or cause immune cell activation. Primary microglia were treated with HOS and oxidative stress and stress granules (as indicated by the stress granule marker, TIAR) were observed following both forms of stress (**Fig. AI-2D,E**). Intriguingly, stress granules caused by HOS were smaller and less 'robust' than sodium arsenite granules (**Fig. AI-2D**). Moreover, FUS egress was only observed for HOS treatment and co-localization with cytoplasmic stress granules was qualitatively observed (**Fig. AI-2D**). Both observations are akin to previous reports from immortalized cells (Sama et al. 2013). Upon observing that immune cells exhibit a biological response to stress, we next assessed if such

forms of stress could directly induce their activation. To do so, the production of TNF-α, a marker of immune cell activation was assessed in immortalized, microglial-derived BV2 cells following stress. BV2 cells were treated with LPS as a positive control for cell activation (**Fig. AI-2F**). Although we qualitatively observed BV2 cell activation, TNF-α production was not observed by western following various forms of HOS or oxidative stress (**Fig. AI-2F**).

Conclusions

The relevance of HOS to ALS is currently unclear. From these pilot studies it appears that FUS egress following hyperosmotic stress is common to motor neurons as well as microglia (**Fig. AI-1,2D**). In conjunction with additional observations (**Fig. II-7**, (Sama et al. 2013)) these data confirm FUS egress is part of a common cellular response to HOS. Despite evidence for a connection between HOS and the inflammatory response (Brocker et al. 2012), we did not observe a direct induction of immune cell activation following HOS and *vice versa* from our limited pilot studies (**Fig. AI-2C,F**). Further, the osmolarity of media from astrocytes known to be toxic to motor neurons did not appreciably differ from controls (**Fig. AI-2A**). Although no positive phenotypes were observed here, we cannot rule out potential differences *in vivo,* larger and/or chronic studies using more sensitive techniques and/or relevant models. Thus, HOS could potentially occur though alternative means (i.e. increase in CSF solute concentrations

following trauma or chronic disease) to trigger and/or exacerbate disease and disease-linked phenotypes.

Methods and Materials

Cell Culture and Treatment

Dissociated neuron cultures were prepared as described (see Chapter III Methods and Materials) and primary microglial cultures as previously reported (Rotunno et al. 2014). BV-2 cells were cultured in DMEM F12 50/50 (Corning 10-090-CV) supplemented with 10% fetal bovine serum (FBS; MilliporeSigma F4135) and grown under standard culture conditions (37°C, 5% CO2/95% air). Frozen, 8-fold diluted astrocyte cultured media (ACM) samples were a generous gift from Dr. Brigitte Van Zundert (Fritz et al. 2013). To induce stress, 1M sodium arsenite (MilliporeSigma 71287) prepared in water was diluted 0.5 mM in media and added to cells for 0.5-2 hours. The osmolytes sorbitol (MilliporeSigma S6021) or mannitol (MilliporeSigma M9546) were directly dissolved in media to obtain a final concentration of 0.4-0.6M and applied to cells for 0.5-2 hours. Stocks of 1 mg/ml Lipopolysaccharide (LPS; MilliporeSigma L7770) were prepared and water and diluted in cell media for a final concentration of 1 or 10μM and added to cells.

Immunofluorescence, Image Acquisition and Analysis

Immunofluorescence was completed as described (Bosco et al. 2010, Sama et al. 2017) (see Chapter III Methods and Materials). Primary antibodies and dilutions

used include: 1:1000 FUS (Bethyl Laboratories A300-293A), 1:500 SMI-32 (Thermo Fisher), 1:2500 TIAR (Fisher Scientific BDB610352) and 1:200 CD11B/C (Pierce PA1-46162). Motor neuron images were acquired and processed as described for similar experiments in **Fig. III-12A-D** (see Chapter III Methods and Materials). Single plane microglia images were obtained using a Leica DMI6000B microscope as described (Sama et al. 2013).

Western Analysis

Whole cell lysates from microglia or BV2 cultures were used for Western analysis to detect TNF-α production. Western analysis was conducted as described (Ward et al. 2014) (see Chapter III Methods and Materials). Primary antibodies used include: 1/1000 Tubulin (Lab Made – Dox) and 1:200 TNF-α (Santa Cruz, sc-1351).

Osmolarity Measurements

Measurements of media osmolarity (mOsm) were obtained using a Precision Systems Osmette II according to the manufacturer's instructions.

APPENDIX II: Increased Turnover of ALS-mutant Profilin 1 in Neuronal Cells

The following chapter is a manuscript published in *Proceedings of the National Academy of Sciences.*

My contributions to this manuscript included developing, performing and analyzing experiments examining the turnover of V5-tagged wildtype and ALS- mutant profilin 1 in neuronal cell line, SKNAS (Figure 2 and Supplementary Figure 3).

PNAS

Structural basis for mutation-induced destabilization of profilin 1 in ALS

Sivakumar Boopathy[a,1], Tania V. Silvas[b,1], Maeve Tischbein[a], Silvia Jansen[c], Shivender M. Shandilya[b], Jill A. Zitzewitz[b], John E. Landers[a], Bruce L. Goode[c], Celia A. Schiffer[b], and Daryl A. Bosco[a,b,2]

[a]Department of Neurology, University of Massachusetts Medical School, Worcester, MA 01605; [b]Department of Biochemistry and Molecular Pharmacology, University of Massachusetts Medical School, Worcester, MA 01605; and [c]Department of Biology, Brandeis University, Waltham, MA 02453

Edited by Gregory A. Petsko, Weill Cornell Medical College, New York, NY, and approved May 14, 2015 (received for review December 16, 2014)

Mutations in profilin 1 (PFN1) are associated with amyotrophic lateral sclerosis (ALS); however, the pathological mechanism of PFN1 in this fatal disease is unknown. We demonstrate that ALS-linked mutations severely destabilize the native conformation of PFN1 in vitro and cause accelerated turnover of the PFN1 protein in cells. This mutation-induced destabilization can account for the high propensity of ALS-linked variants to aggregate and also provides rationale for their reported loss-of-function phenotypes in cell-based assays. The source of this destabilization is illuminated by the X-ray crystal structures of several PFN1 proteins, revealing an expanded cavity near the protein core of the destabilized M114T variant. In contrast, the E117G mutation only modestly perturbs the structure and stability of PFN1, an observation that reconciles the occurrence of this mutation in the control population. These findings suggest that a destabilized form of PFN1 underlies PFN1-mediated ALS pathogenesis.

amyotrophic lateral sclerosis | profilin 1 | protein stability | X-ray crystallography | protein misfolding

Mutations in the profilin 1 gene (*PFN1*) were recently associated with both familial and sporadic forms of amyotrophic lateral sclerosis (ALS) (1, 2), an incurable and fatal neurodegenerative disease that primarily targets motor neurons (3). The etiology of sporadic ALS is poorly understood, whereas familial ALS is caused by inheritable genetic defects in defined genes such as *PFN1* (3). PFN1 is a 15-kDa protein that is best known for its role in actin dynamics in the context of endocytosis, membrane trafficking, cell motility, and neuronal growth and differentiation (4). In addition to binding monomeric or G-actin, PFN1 also binds to a host of different proteins through their poly-L-proline motifs and to lipids such as phosphatidylinositol 4,5-bisphosphate (4, 5). However, little is known about the mechanism(s) associated with PFN1-mediated ALS pathogenesis. The observation that most ALS-linked PFN1 variants are highly prone to aggregation in mammalian cultured cells suggests that disease-causing mutations induce an altered, or misfolded, conformation within PFN1 (2). Protein misfolding is a hallmark feature of most neurodegenerative diseases, including ALS (3), and can contribute to disease through both gain-of-toxic-function and loss-of-normal-function mechanisms (6). Although mutations in *PFN1* cause ALS through a dominant inheritance mode (2), there is some evidence supporting a loss-of-function mechanism for mutant PFN1. For example, ALS-linked mutations were shown to abrogate the binding of PFN1 to actin (2) and to impair the incorporation of PFN1 into cytoplasmic stress granules during arsenite-induced stress (7) in cultured cells. Moreover, ectopic expression of these variants in murine motor neurons led to a reduction in both axon outgrowth and growth cone size, consistent with a loss of function through a dominant-negative mechanism (2).

Although ALS-linked mutations were shown to induce PFN1 aggregation, the effect of these mutations on protein stability and structure has not been studied. Because the impact of disease-causing mutations on protein stability varies from protein to protein (8–10), these parameters must be determined empirically. Here, we demonstrate that certain familial ALS-linked mutations severely destabilize PFN1 in vitro and cause faster turnover of the protein in neuronal cells. To gain insight into the source of this mutation-induced instability, the 3D crystal structures for three PFN1 proteins, including the WT protein, were solved by X-ray crystallography. We discovered that the M114T mutation created a cleft that extended into the interior of PFN1. Further, we predict that the most severely destabilizing C71G mutation also creates a cavity near the core of the PFN1 protein, proximal to the cleft formed by M114T. Experimental mutations that create enlarged pockets or cavities are known to exert a destabilizing effect on the protein's native conformation (11), and there are several examples of mutation-induced cavity formation occurring in nature and disease (12, 13). Interestingly, the variant predicted to be the least pathogenic according to recent genetics studies, E117G, was relatively stable and closely resembled the WT protein in every assessment performed herein (2, 14). These data implicate a destabilized form of PFN1 in ALS pathogenesis and call for therapeutic strategies that can stabilize mutant PFN1.

Results

ALS-Linked Mutations Destabilize PFN1 in Vitro. To investigate the effect of ALS-linked mutations on the stability of PFN1, PFN1 proteins were expressed and purified from *Escherichia coli* and subjected to chemical and thermal denaturation analyses. A novel purification protocol that includes sequential cation-exchange and gel filtration chromatography steps was developed

Significance

Mutations in profilin 1 (PFN1) were recently shown to cause amyotrophic lateral sclerosis (ALS); however, little is known about the pathological mechanism of PFN1 in disease. We demonstrate that ALS-linked mutations cause PFN1 to become destabilized in vitro and in cells, likely through a mechanism that involves mutation-induced cavities within the protein core. Changes in protein stability due to disease-causing mutations can play a pivotal role across different disease mechanisms. The destabilized mutant-PFN1 species identified here can serve as an upstream trigger for either loss-of-function or gain-of-toxic-function mechanisms and thus emerges from these studies as a pertinent therapeutic target for the incurable disease ALS.

Author contributions: S.B., T.V.S., M.T., S.J., S.M.S., J.A.Z., J.E.L., B.L.G., C.A.S., and D.A.B. designed research; S.B., T.V.S., M.T., and S.J. performed research; S.B., T.V.S., M.T., S.J., S.M.S., J.A.Z., J.E.L., B.L.G., C.A.S., and D.A.B. analyzed data; and S.B. and D.A.B. wrote the paper.

The authors declare no conflict of interest.

This article is a PNAS Direct Submission.

Data deposition: The crystallography, atomic coordinates, and structure factors have been deposited in the Protein Data Bank, www.pdb.org (PDB ID codes 4X1L, 4X1M, and 4X25).

[1]S.B. and T.V.S. contributed equally to this work.

[2]To whom correspondence should be addressed. Email: Daryl.Bosco@umassmed.edu.

This article contains supporting information online at www.pnas.org/lookup/suppl/doi:10.1073/pnas.1424108112/-/DCSupplemental.

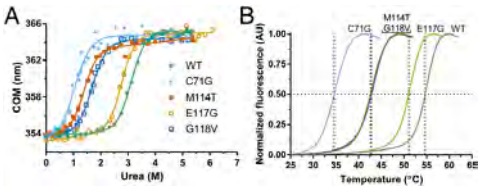

Fig. 1. ALS-linked mutations destabilize PFN1. Chemical and thermal denaturation studies reveal that ALS-linked variants C71G, M114T, and G118V, but not E117G, are severely destabilized relative to PFN1 WT. (*A*) Equilibrium unfolding curves for PFN1 WT and ALS-linked variants generated by measuring the intrinsic tryptophan fluorescence of the indicated protein equilibrated in increasing concentrations of urea. Data were processed to obtain the center of mass (COM) of the emission spectrum and then fit to a two-state model for protein folding. The resulting fits are displayed as solid lines. The corresponding thermodynamic parameters obtained from the fitted data are shown in Table 1. (*B*) Thermal denaturation profiles of PFN1 proteins measured by SYPRO Orange fluorescence as a function of increasing temperature were used to determine the apparent T_m, which is the temperature corresponding to 0.50 fluorescence signal as denoted by the intersection of the dashed lines for each curve.

here and applied to all PFN1 variants (*Materials and Methods*). PFN1 C71G was found to be highly prone to aggregation in *E. coli*, consistent with observations that this variant exhibited particularly low solubility in mammalian cells (2), and therefore was isolated from inclusion bodies (*Materials and Methods*). The biochemical properties of PFN1 C71G purified from inclusion bodies are indistinguishable from PFN1 C71G purified from the soluble lysate of *E. coli* as determined by several assays (Fig. S1), providing confidence that PFN1 proteins purified by these two methods can be directly compared.

To examine the stability of PFN1 proteins, fluorescence from tryptophans (W4 and W32) in PFN1 WT and ALS-linked variants was measured as a function of increasing urea concentration (Fig. 1*A*). To ensure reversibility, the reciprocal analysis was also performed, where denatured PFN1 proteins in urea were refolded upon dilution with buffer (Fig. S2 *A–E*). Only one transition was observed between the folded or native (N) and unfolded (U) states for all PFN1 proteins, indicative of a two-state ($N \leftrightarrows U$) unfolding mechanism. This two-state unfolding model was further substantiated with an unfolding study of two PFN1 proteins (WT and M114T) using CD spectroscopy (Fig. S2*F*). The following thermodynamic parameters were determined by fitting the fluorescence data to a two-state folding model: apparent $\Delta G°$, the free energy of folding; m, the denaturant dependence of $\Delta G°$; and C_m, the midpoint of the unfolding transition (Table 1). Both $\Delta G°$ and C_m were reduced for ALS-linked variants relative to PFN1 WT, particularly for the PFN1 variants C71G, M114T, and G118V, indicating these variants are severely destabilized compared with PFN1 WT (Fig. 1*A* and Table 1). Differential scanning fluorimetry (DSF) with SYPRO Orange, a fluorescent indicator of hydrophobic regions exposed upon protein unfolding, was used next to determine the apparent melting temperature, T_m, for all PFN1 proteins used in this study (15). Consistent with the chemical denaturation results, all ALS-linked variants except E117G exhibited a T_m that was at least 10 °C lower than WT (Fig. 1*B* and Table 1). Based on the denaturation studies, C71G emerges as the most destabilizing mutation in the context of PFN1, whereas the E117G mutation has a relatively modest impact on PFN1 stability.

ALS-Linked PFN1 Exhibits Faster Turnover in a Neuronal Cell Line. The turnover rate for proteins with destabilizing mutations is often faster relative to their WT counterparts, generally because destabilized proteins are misfolded and targeted for degradation by the cellular quality control machinery (16). To determine whether the results of our in vitro denaturation studies extend to a cellular environment, V5-tagged PFN1 variants were transiently transfected into human neuronal SKNAS cells, and PFN1 turnover was assessed by tracking V5-PFN1 protein expression over a 12.5-h time course in the presence of cycloheximide. At the start of the experiment (t = 0 of the cycloheximide time course), all V5-tagged PFN1 variants were expressed at similar levels except that V5-PFN1 C71G, M114T, and G118V partitioned into the insoluble fraction (Fig. 2 *A* and *B*) as reported previously (2). The turnover of both PFN1 C71G and M114T occurred significantly faster than that of PFN1 WT. As early as 2.5 h, the majority of PFN1 C71G and M114T within the soluble fraction had already degraded (Fig. 2 *A* and *C*). This decrease in soluble PFN1 content was not simply due to further PFN1 aggregation, which could confound our analysis, as evidenced by the concomitant clearance of PFN1 from the insoluble fraction at the early time points of cycloheximide exposure (Fig. 2*B*). The faster turnover of PFN1 C71G and M114T in cells closely correlates with their reduced stabilities in vitro, confirming the destabilizing effect of the C71G and M114T mutations. We note that the turnover of PFN1 C71G was faster in the soluble fraction compared with the insoluble fraction (Fig. S3), likely because clearance of insoluble cellular aggregates by the quality control machinery is less efficient compared with the turnover of smaller, soluble species (17). Although PFN1 G118V was destabilized to a similar degree as M114T in vitro, the turnover of this variant within the soluble fraction seemed slower in cells (Fig. 2*C*), which may reflect a stabilizing effect of other proteins and/or factors that interact with PFN1 in the cellular milieu (4), or that this variant is not properly handled by the quality control machinery in the cell. In fact, we detected a low level of insoluble PFN1 G118V that persisted throughout the 12.5-h time course (Fig. 2*B* and Fig. S3).

ALS-Linked Mutations Induce a Misfolded Conformation Within PFN1. We reasoned that ALS-linked variants must undergo some degree of structural or conformational change to account for their destabilization. However, ALS-causing mutations did not perturb

Table 1. Summary of experimental stability and binding measurements for PFN1 variants

	Equilibrium unfolding (N⇆U)*			T_m,† °C		Binding to poly-L-proline†,‡
Variant	$\Delta G°$, kcal·mol^{-1}	m, kcal·mol^{-1}·M^{-1}	C_m, M	Protein alone	+ 4 mM proline	K_d, μM
WT	7.04 ± 0.49	2.25 ± 0.16	3.13 ± 0.31	54.68 ± 0.04	57.25 ± 0.03	463 ± 26
C71G	1.89 ± 0.70	1.95 ± 0.40	0.97 ± 0.41	34.60 ± 0.03	39.96 ± 0.03	687 ± 77
M114T	3.51 ± 0.40	2.51 ± 0.24	1.40 ± 0.21	42.62 ± 0.03	46.52 ± 0.02	572 ± 23
E117G	6.90 ± 0.74	2.49 ± 0.26	2.77 ± 0.42	51.05 ± 0.04	53.78 ± 0.03	407 ± 27
G118V	3.70 ± 0.44	2.20 ± 0.23	1.68 ± 0.26	42.84 ± 0.04	46.92 ± 0.04	397 ± 40

*Errors are shown as SD.
†Errors are shown as SE.
‡K_d values are reported in terms of proline residues.

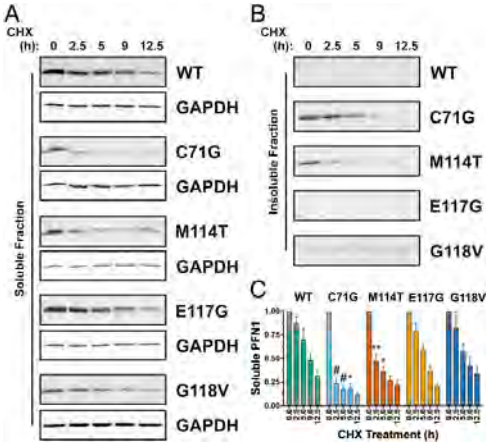

Fig. 2. ALS-linked PFN1 variants exhibit faster turnover in a neuronal cell line. SKNAS cells transiently transfected with V5-PFN1 constructs were treated with cycloheximide (CHX) for up to 12.5 h, during which time lysates were collected and probed by Western analysis with a V5-specific antibody to assess the rate of PFN1 turnover in cells. (*A* and *B*) A representative Western blot analysis of soluble and insoluble fractions from cell lysates demonstrates a decrease in V5-PFN1 protein with time. GAPDH serves a loading control for the soluble fraction. (C) Densitometry analysis of *A* reveals that the turnover of PFN1 C71G and M114T is significantly faster than that of PFN1 WT. Statistical significance was determined using a two-way ANOVA followed by a Tukey's post hoc analysis (*$P < 0.05$, **$P < 0.01$, #$P < 0.0001$). Error bars represent SEM. WT and E117G, $n = 3$; G118V, M114T and C71G, $n = 4$ independent experiments.

the secondary structural elements of PFN1 as determined by CD spectroscopy (Fig. S4), and the fact that similar m values were determined for all PFN1 variants by the urea denaturation analysis suggested these proteins adopt similar tertiary structures as well (Table 1) (18). To probe further for potential structural differences between PFN1 WT and ALS-linked variants, these proteins were subjected to native gel electrophoresis, a biochemical technique capable of detecting conformational differences between misfolded variants and their WT counterparts (19). PFN1 WT and E117G migrated predominately as single, distinct bands with similar mobility, whereas multiple bands of slower mobility were observed for PFN1 variants C71G, M114T, and G118V (Fig. S5*A*). The slower mobility bands likely reflect the larger hydrodynamic volume due to partial unfolding of these variants. In addition, PFN1 C71G, M114T, and G118V produced relatively large-molecular-weight species that were retained in the stacking gel and unable to electrophorese through the separating native gel but were resolublized under conditions used for the denaturing gel (Fig. S5*A*). Analytical size-exclusion chromatography revealed that all PFN1 proteins eluted as expected for soluble, monomeric PFN1 (Fig. S5 *B*–*G*). However, despite equal loading of PFN1 proteins onto the analytical size-exclusion column, the peak area corresponding to soluble monomer PFN1 is reduced for ALS-linked variants, particularly for the most aggregation-prone variant, C71G. These data are consistent with a loss of soluble monomer PFN1 in the form of insoluble species that cannot pass through the analytical size-exclusion column filter.

A Source of Mutation-Induced Destabilization Revealed by X-Ray Crystallography of PFN1. Crystal structures of PFN1 proteins were determined to identify regions within mutant PFN1 that are conformationally distinct from PFN1 WT at atomic resolution. PFN1 WT, E117G, and M114T produced crystals that diffracted at relatively high resolution (~2.2 Å; Table S1). The 3D structure of human PFN1 WT agrees well with previously determined structures (20–22). PFN1 WT and E117G crystallized in the same space group, C121, whereas M114T crystallized in the P6 space group, with two molecules (designated as chains A and B) in the asymmetric unit (Table S1).

Residues 22–36, 46–52, 101–105, 112–120, and 125–128 within PFN1 were used for Cα superimposition of the four molecules (PFN1 WT, M114T chains A and B, and E117G). In agreement with the biochemical analyses described above (Table 1 and Fig. S4), the secondary and tertiary structures of all three PFN1 proteins, including chains A and B of M114T, are highly similar (Fig. 3). Although the space groups for PFN1 WT and M114T crystals were different, we calculated the double difference plots between these and the other PFN1 structures to get a sense for structural perturbations potentially induced by the ALS-linked mutations. Double difference plots were constructed by calculating the distances between all of the Cα atoms in PFN1 WT and an ALS-linked variant separately, and then plotting the difference of the difference between PFN1 structures as described previously (23). Virtually no structural deviations were observed between PFN1 WT and E117G, whereas moderate differences were detected between WT and M114T (Fig. S6).

Next we sought to determine whether these moderate structural changes between PFN1 WT and M114T mapped to regions involved in PFN1 function, namely to residues that make contact with actin (24–31) or poly-L-proline (21, 22, 24, 32, 33). The ternary complex comprised of PFN1 WT, actin, and the poly-L-proline peptide derived from vasodilator-stimulated phosphoprotein (VASP) (21) (PDB ID code 2PAV) is shown in Fig. 4. Residues with the highest (0.3 Å or greater) average of absolute double difference (Avg-Abs-DD) values between PFN1 WT and M114T chain B (Fig. S6*C*) were mapped onto PFN1 WT (Fig. S7). PFN1 M114T chain B was used for this and all subsequent structural comparisons because chain B had lower B factors compared with chain A (Fig. S8). Indeed, several PFN1 residues that reportedly make contacts with actin (V119, H120, G122, and K126) and poly-L-proline (W4, Y7, H134, and S138) also have relatively high Avg-Abs-DD values (Fig. S7).

To assess whether these mutation-induced structural changes are sufficient to alter the normal binding interactions of PFN1,

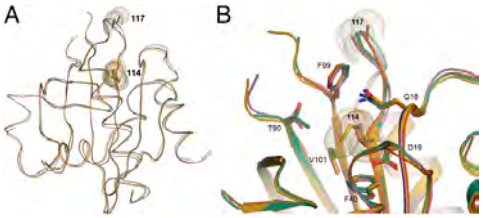

Fig. 3. Superimposition of the crystal structures for PFN1 WT, E117G, and M114T. (*A* and *B*) The secondary and tertiary structures for PFN1 WT (green), E117G (mustard), M114T chain A (pink), and B (red) are highly superimposable. For each structure, sticks and spheres denote the side chains and van der Waals radii, respectively, for residues at position 114 and 117. Residue 117 is located within a solvent-exposed flexible loop that has no discernible secondary structure, whereas Met114 is located within a β-sheet toward the interior of the protein. (*B*) A zoomed cartoon representation showing residues within 4 Å of residue 114. The side chains of these residues are indicated as sticks with nitrogen, oxygen, and sulfur atoms indicated in blue, red, and yellow, respectively. The van der Waals radii of the atoms comprising residue 114 are reduced upon mutation of methionine (green and mustard structures) to threonine (red and pink structures).

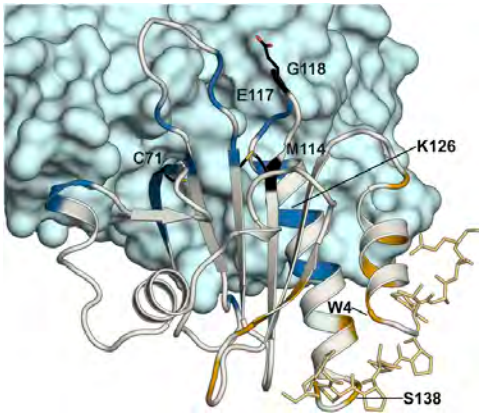

Fig. 4. Structure of actin–PFN1–VASP peptide ternary complex with the actin and poly-L-proline binding residues mapped on PFN1. The X-ray structure of the PFN1 WT (gray)–actin (blue)–poly-L-proline peptide (gold) complex (PDB ID code 2PAV) is shown. Residues reportedly involved in actin binding (V61, K70, S72, V73, I74, R75, E83, R89, K91, P97, T98, N100, V119, H120, G122, N125, K126, Y129, and E130) and poly-L-proline binding (W4, Y7, N10, A13, S28, S30, W32, H134, S138, and Y140) are highlighted in blue and gold, respectively. The sites of ALS-linked mutations investigated in this study are highlighted and labeled in black with side chains displayed as black sticks. Residues involved in actin or poly-L-proline binding that also exhibit Avg-Abs-DD values of 0.3 Å or greater between PFN1 WT and M114T chain B (W4, K126, and S138) are labeled in black (the remaining residues that fulfill this criteria are shown in Fig. S7).

we first monitored changes in the intrinsic tryptophan fluorescence of PFN1 as a function of poly-L-proline peptide concentration (Fig. 5*A*). Our results revealed that the effect of ALS-linked mutations on the PFN1-poly-L-proline interaction was modest, because the apparent dissociation constants (K_d) were within twofold for all PFN1 proteins in this study (Table 1). In fact, excess concentrations of poly-L-proline effectively stabilized all PFN1 proteins as determined by DSF, with the largest increase in T_m observed upon poly-L-proline peptide binding to C71G (Fig. 5*B* and Table 1). Next, we measured the binding capacity of our PFN1 proteins for G-actin by comparing their concentration-dependent abilities to suppress spontaneous polymerization of pyrenyliodoacetamide-labeled actin monomers (34). This assay is based on the fact that PFN1 binds G-actin and inhibits actin nucleation in the absence of formins (34). As expected, increasing concentrations of recombinant PFN1 WT reduced the rate of actin polymerization, whereas the H120E variant that exhibits impaired binding to actin failed to suppress actin polymerization to the same extent (Fig. 6). Of the four ALS-linked variants, only G118V was defective in suppressing actin polymerization, which was most apparent at the highest concentration of PFN1 used in this assay, although this effect did not reach statistical significance (Fig. 6). These data argue against a general mechanism for PFN1-mediated ALS pathogenesis that involves impaired direct binding between PFN1 and either poly-L-proline or actin.

Importantly, the X-ray crystal structures reveal a possible mechanism by which ALS-linked mutations destabilize PFN1. Residues Thr90, Met114, and Gln18 contribute to the formation of a surface exposed pocket that was detected using SiteMap (Fig. 7). Mutation of methionine to threonine at position 114 increased the size of this pocket, thereby forming a cleft, because the residues nearby failed to rearrange and compensate for the loss of van der Waals contacts (Fig. 7*B*). This cleft is expected to exert a destabilizing effect on the native conformation of PFN1 owing to this loss of van der Waals contacts and the reduced hydrophobicity of the threonine side chain relative to that of methionine (11). Moreover, hydrophobic residues that are otherwise buried in the PFN1 WT structure were exposed by the cleft in the PFN1 M114T structure (Fig. 7 and Fig. S9). To investigate the potential impact of the C71G mutation on PFN1 structure, the cysteine side chain of residue 71 was removed to mimic a glycine amino acid in the PFN1 WT structure using PyMOL. Interestingly, this mutation is predicted to form a void in the core of the protein that partially overlaps with the cleft observed in the PFN1 M114T crystal structure (Fig. 7*B*). Analysis using PyMOL and SiteMap suggest that, unlike the solvent-accessible WT and the M114T pocket, the proposed C71G void is buried within the core of the protein. Solvent-inaccessible voids have a more destabilizing effect than solvent-exposed cavities (11, 35), providing an explanation for why the C71G mutation is more destabilizing than M114T (Fig. 1).

Discussion

Here we show that ALS-linked mutations severely destabilize (Fig. 1) and alter the native protein conformation (Fig. 3) of PFN1. Changes in protein stability owing to disease-causing mutations, whether these mutations stabilize or destabilize the protein, are thought to play a pivotal role in various disease mechanisms (13). In the context of ALS, disease-linked mutations destabilize Cu, Zn-superoxide dismutase (SOD1) (9), but instead hyperstabilize TAR DNA-binding protein 43 (TDP-43) (8, 10, 36). These findings underscore the importance of defining the toxic properties of disease-linked proteins, thereby directing the rational design of therapeutic strategies against those offending proteins (3).

Our X-ray crystal structures of PFN1 proteins illuminate a probable source of mutation-induced destabilization. An enlarged surface pocket, or void, forms as a result of the M114T mutation (Fig. 7). The destabilizing effect of similar voids has been demonstrated using a systematic site-directed mutagenesis approach with lysozyme and is thought to arise from a loss of hydrophobic interactions (11, 35). Examples of mutation-induced cavity formation and destabilization have also been observed in nature (13). Interestingly, modeling the removal of the cysteine side chain at position 71 creates an internal cavity that is predicted to partially overlap the cleft formed by M114T, raising the intriguing possibility that both mutations destabilize PFN1 through a common mechanism that involves the loss of hydrophobic and van der Waals contacts within the same region of PFN1 (Fig. 7). Because

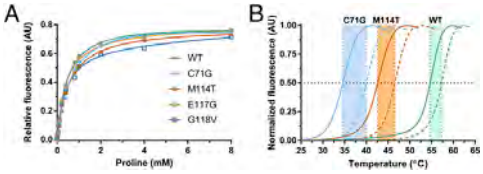

Fig. 5. ALS-linked PFN1 variants retain the ability to bind poly-L-proline. (*A*) Binding of PFN1 to the poly-L-proline peptide was monitored by measuring the intrinsic tryptophan fluorescence of the indicated PFN1 protein as a function of increasing peptide concentration. The data points were fit using a one-site total binding model in GraphPad Prism and the apparent dissociation constants (K_d) obtained from the fit are shown in Table 1. Note that the concentration of the peptide is reported in terms of [proline] because the peptide stock is supplied as a mixture of poly-L-proline species (*Materials and Methods*). (*B*) DSF was performed as described in Fig. 1*B* in the presence (dashed lines) and absence (solid lines) of 4 mM proline. The presence of proline increases the T_m for all PFN1 proteins used in this study (Table 1), as illustrated here for WT, C71G, and M114T.

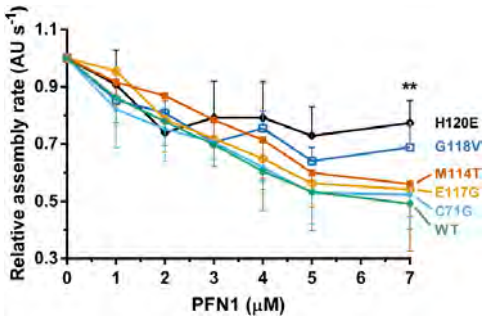

Fig. 6. The binding of PFN1 proteins to G-actin. Polymerization of monomeric rabbit muscle actin (3 μM, 5% pyrene-labeled) was monitored in the presence of increasing concentrations of WT or ALS-linked PFN1 variants and used to derive relative rates of polymerization (n = 3). The variant H120E, which is impaired in binding to actin, fails to suppress spontaneous actin polymerization as effectively as WT PFN1. Although G118V is relatively weak in suppressing actin polymerization, the data did not reach statistical significance. Statistical significance was determined using a two-way ANOVA followed by a Tukey's post hoc analysis. $^{**}P \leq 0.01$ for WT vs. H120E at 7 μM concentration. No other significant comparisons with WT were obtained. Other significant comparisons included C71G vs. H120E and E117G vs. H120E ($P \leq 0.05$) at 7 μM concentration. Error bars represent SD.

G118V is located within a solvent-exposed flexible loop, it is difficult to predict whether this mutation propagates structural changes to the same region affected by M114T. We note that the phi and psi angles for Gly118 are in a region of the Ramachandran plot that are generally disallowed for a valine residue, and therefore we speculate that the G118V mutation also induces a conformational change within PFN1 that allows valine to adapt dihedral angles that are energetically more favorable.

Our study also provides insight into the relative pathogenicity of ALS-linked PFN1 variants. The pathogenicity of the E117G variant was called into question after it had been detected in the control population (2, 14, 37, 38). Moreover, this variant exhibited mild phenotypes compared with other ALS-linked PFN1 variants in cell-based functional experiments (2, 7). Here, the E117G mutation had only a modest effect on the stability and structure of PFN1 (Table 1 and Fig. S6), supporting the view that E117G is a risk factor for disease rather than overtly pathogenic (1, 14). Further, the E117G mutation was detected in sporadic ALS and frontotemporal lobar degeneration cases (14, 37–40), consistent with the idea that environmental factors and/or genetic modifiers contribute to PFN1 E117G toxicity. In fact, proteasome inhibition triggered the aggregation of PFN1 E117G (2), suggesting that cellular stress may exacerbate PFN1 misfolding and dysfunction in vivo.

Although the mechanism of PFN1 in ALS has yet to be fully elucidated, the destabilized mutant-PFN1 species identified here can serve as an upstream trigger for either loss-of-function or gain-of-toxic-function mechanisms. Several investigations from cell-based experiments support a loss-of-function mechanism for ALS-linked PFN1 variants with respect to actin binding (2), actin dynamics (2), and stress granule assembly (7). For example, PFN1 variants immunoprecipitated less actin from mammalian cells compared with PFN1 WT (2). Our in vitro results suggest this is unlikely due to a general defect in the inherent ability of mutant PFN1 to directly bind actin (Fig. 6) but may be the consequence of mutant PFN1 being sequestered away from actin and/or engaged in other aberrant interactions within the cell. Moreover, ALS-linked mutations do not simply abrogate the direct-binding interaction between PFN1 and the poly-L-proline motif (Fig. 5*A*) that is present in many biological PFN1 ligands. These data, however, do not rule out the possibility that mutation-induced misfolding and destabilization culminate in defective actin homeostasis in vivo. PFN1 plays a complex role in actin homeostasis, requiring coordinated interactions between PFN1 and many other cellular factors that ultimately dictate the fate of different actin networks within the cell (41).

The misfolding of PFN1 variants may also induce gain of toxic functions and interactions, the latter via aberrant protein–protein interactions through exposed hydrophobic patches, such as those detected for PFN1 M114T (Fig. S9). Further, the aggregation of PFN1 variants can potentially sequester other vital proteins, including those with poly-L-proline binding motifs (4), culminating in compromised actin and/or cellular homeostasis (6).

Although the downstream effect of ALS-linked PFN1 on actin dynamics and other cellular processes have not been elucidated, our data identify misfolded and destabilized PFN1 as a potential upstream trigger of the adverse events that culminate in ALS, opening new avenues for therapeutic advancement in ALS. One potential direction is the development of pharmacological chaperones (16). For example, small molecules that fill the void formed by the M114T mutation are expected to stabilize the protein (35). Our data with poly-L-proline (Fig. 5*B*) suggest that small-molecules binding to other regions of PFN1 could also stabilize the protein. We posit that stabilizing mutant PFN1 will restore the normal structure and function of the protein, thereby preventing the pathogenic cascade leading to ALS.

Materials and Methods

A pET vector containing human PFN1 flanked by NdeI and EcoRI restriction sites was kindly provided by Bruce Goode, Brandeis University, Waltham, MA. The mutant PFN1 DNA (2) was amplified using primers 5′- GGACCATATGGCCGGGTGGAAC -3′ and 5′- GCCTGAATTCTCAGTACTGGGAACGC -3′ and ligated into the pET vector using NdeI and EcoRI restriction sites. BL21 (DE3) pLysS cells (200132; Agilent Technologies) transformed with PFN1 constructs were cultured in LB containing 100 $\mu g \cdot mL^{-1}$ ampicillin and 34 $\mu g \cdot mL^{-1}$ chloramphenicol at 37 °C until an OD_{600} of 0.7, at which point PFN1 expression was induced by addition of 1 mM isopropyl β-D-thiogalactopyranoside (0487; Amresco) for either 3 h at 37 °C (for WT and E117G) or 24 h at 18 °C (for C71G, M114T, and G118V). Cells were harvested by centrifugation and stored until purification. Refer to *Supporting Information* for complete details on methods.

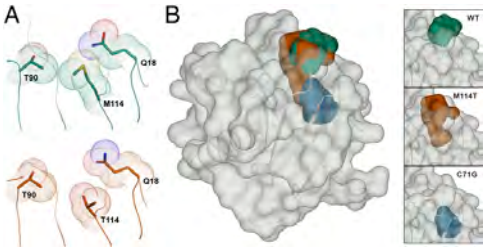

Fig. 7. The M114T mutation causes a surface-exposed pocket to expand into the core of the PFN1 protein. (*A*) Residues are depicted as described in Fig. 3. The van der Waals radii of residues 90, 114, and 18 are in contact in the PFN1 WT structure (*Top*). These contacts are reduced by the M114T mutation (*Bottom*) owing to the smaller size of threonine, leading to an enlargement of the surface-exposed pocket. (*B*) PFN1 WT is shown with a transparent surface and the secondary structure is shown in cartoon representation. The surface pocket volume for PFN1 WT (green) and the cleft volume for PFN1 M114T chain B (red) are depicted as opaque surfaces and were generated using SiteMap. The predicted cavity (blue) for PFN1 C71G (generated using PyMOL) overlays with the M114T void, and unlike the WT and M114T volumes, is not surface-exposed. The insets (*Right*) show the aforementioned voids for WT (*Top*), M114T chain B (*Middle*), and C71G (*Bottom*).

ACKNOWLEDGMENTS. We thank K. Boggio and the Proteomics and Mass Spectrometry Facility [University of Massachusetts Medical School (UMMS)] for analysis of recombinant PFN1 proteins; C. R. Matthews (UMMS) for the use of his circular dichroism spectrophotometers and fluorimeter; and O. Bilsel, C.-H. Wu, C. Fallini, N. Cohen, and B. Mackness for helpful advice with experiments and the manuscript. We acknowledge funding from National Institutes of Health Grants R01 NS090352, R01 NS078145, and R01 NS067206 (to D.A.B.); R01 NS073873 (to J.E.L.); P01 GM091743 (to C.A.S. and S.M.S.); P01 GM091743-03S1 (to T.V.S.); R01 GM063691 (to B.L.G.); and R01 GM54836 (to J.A.Z.); and from Target ALS (to J.E.L., D.A.B., and B.L.G.).

1. Smith BN, et al. (2015) Novel mutations support a role for Profilin 1 in the pathogenesis of ALS. *Neurobiol Aging* 36(3):1602.e17–1602.e27.
2. Wu CH, et al. (2012) Mutations in the profilin 1 gene cause familial amyotrophic lateral sclerosis. *Nature* 488(7412):499–503.
3. Bosco DA, LaVoie MJ, Petsko GA, Ringe D (2011) Proteostasis and movement disorders: Parkinson's disease and amyotrophic lateral sclerosis. *Cold Spring Harb Perspect Biol* 3(10):a007500.
4. Witke W (2004) The role of profilin complexes in cell motility and other cellular processes. *Trends Cell Biol* 14(8):461–469.
5. Lambrechts A, et al. (1997) The mammalian profilin isoforms display complementary affinities for PIP2 and proline-rich sequences. *EMBO J* 16(3):484–494.
6. Winklhofer KF, Tatzelt J, Haass C (2008) The two faces of protein misfolding: Gain- and loss-of-function in neurodegenerative diseases. *EMBO J* 27(2):336–349.
7. Figley MD, Bieri G, Kolaitis RM, Taylor JP, Gitler AD (2014) Profilin 1 associates with stress granules and ALS-linked mutations alter stress granule dynamics. *J Neurosci* 34(24):8083–8097.
8. Austin JA, et al. (2014) Disease causing mutants of TDP-43 nucleic acid binding domains are resistant to aggregation and have increased stability and half-life. *Proc Natl Acad Sci USA* 111(11):4309–4314.
9. Rotunno MS, Bosco DA (2013) An emerging role for misfolded wild-type SOD1 in sporadic ALS pathogenesis. *Front Cell Neurosci* 7:253.
10. Watanabe S, Kaneko K, Yamanaka K (2013) Accelerated disease onset with stabilized familial amyotrophic lateral sclerosis (ALS)-linked mutant TDP-43 proteins. *J Biol Chem* 288(5):3641–3654.
11. Eriksson AE, et al. (1992) Response of a protein structure to cavity-creating mutations and its relation to the hydrophobic effect. *Science* 255(5041):178–183.
12. Joerger AC, Ang HC, Fersht AR (2006) Structural basis for understanding oncogenic p53 mutations and designing rescue drugs. *Proc Natl Acad Sci USA* 103(41): 15056–15061.
13. Yue P, Li Z, Moult J (2005) Loss of protein structure stability as a major causative factor in monogenic disease. *J Mol Biol* 353(2):459–473.
14. Fratta P, et al. (2014) Profilin1 E117G is a moderate risk factor for amyotrophic lateral sclerosis. *J Neurol Neurosurg Psychiatry* 85(5):506–508.
15. Vedadi M, et al. (2006) Chemical screening methods to identify ligands that promote protein stability, protein crystallization, and structure determination. *Proc Natl Acad Sci USA* 103(43):15835–15840.
16. Ringe D, Petsko GA (2009) What are pharmacological chaperones and why are they interesting? *J Biol* 8(9):80.
17. Verhoef LG, Lindsten K, Masucci MG, Dantuma NP (2002) Aggregate formation inhibits proteasomal degradation of polyglutamine proteins. *Hum Mol Genet* 11(22): 2689–2700.
18. Myers JK, Pace CN, Scholtz JM (1995) Denaturant m values and heat capacity changes: relation to changes in accessible surface areas of protein unfolding. *Protein Sci* 4(10): 2138–2148.
19. Rotunno MS, et al. (2014) Identification of a misfolded region in superoxide dismutase 1 that is exposed in amyotrophic lateral sclerosis. *J Biol Chem* 289(41): 28527–28538.
20. Fedorov AA, Pollard TD, Almo SC (1994) Purification, characterization and crystallization of human platelet profilin expressed in Escherichia coli. *J Mol Biol* 241(3): 480–482.
21. Ferron F, Rebowski G, Lee SH, Dominguez R (2007) Structural basis for the recruitment of profilin-actin complexes during filament elongation by Ena/VASP. *EMBO J* 26(21): 4597–4606.
22. Mahoney NM, Rozwarski DA, Fedorov E, Fedorov AA, Almo SC (1999) Profilin binds proline-rich ligands in two distinct amide backbone orientations. *Nat Struct Biol* 6(7): 666–671.
23. Prabu-Jeyabalan M, Nalivaika EA, Romano K, Schiffer CA (2006) Mechanism of substrate recognition by drug-resistant human immunodeficiency virus type 1 protease variants revealed by a novel structural intermediate. *J Virol* 80(7):3607–3616.
24. Cedergren-Zeppezauer ES, et al. (1994) Crystallization and structure determination of bovine profilin at 2.0 A resolution. *J Mol Biol* 240(5):459–475.
25. Chik JK, Lindberg U, Schutt CE (1996) The structure of an open state of beta-actin at 2.65 A resolution. *J Mol Biol* 263(4):607–623.
26. Hájková L, Björkegren Sjögren C, Korenbaum E, Nordberg P, Karlsson R (1997) Characterization of a mutant profilin with reduced actin-binding capacity: Effects in vitro and in vivo. *Exp Cell Res* 234(1):66–77.
27. Korenbaum E, et al. (1998) The role of profilin in actin polymerization and nucleotide exchange. *Biochemistry* 37(26):9274–9283.
28. Porta JC, Borgstahl GE (2012) Structural basis for profilin-mediated actin nucleotide exchange. *J Mol Biol* 418(1-2):103–116.
29. Schutt CE, Myslik JC, Rozycki MD, Goonesekere NC, Lindberg U (1993) The structure of crystalline profilin-beta-actin. *Nature* 365(6449):810–816.
30. Sohn RH, Chen J, Koblan KS, Bray PF, Goldschmidt-Clermont PJ (1995) Localization of a binding site for phosphatidylinositol 4,5-bisphosphate on human profilin. *J Biol Chem* 270(36):21114–21120.
31. Suetsugu S, Miki H, Takenawa T (1998) The essential role of profilin in the assembly of actin for microspike formation. *EMBO J* 17(22):6516–6526.
32. Björkegren C, Rozycki M, Schutt CE, Lindberg U, Karlsson R (1993) Mutagenesis of human profilin locates its poly(L-proline)-binding site to a hydrophobic patch of aromatic amino acids. *FEBS Lett* 333(1-2):123–126.
33. Ostrander DB, Ernst EG, Lavoie TB, Gorman JA (1999) Polyproline binding is an essential function of human profilin in yeast. *Eur J Biochem* 262(1):26–35.
34. Pollard TD, Cooper JA (1984) Quantitative analysis of the effect of Acanthamoeba profilin on actin filament nucleation and elongation. *Biochemistry* 23(26):6631–6641.
35. Eriksson AE, Baase WA, Wozniak JA, Matthews BW (1992) A cavity-containing mutant of T4 lysozyme is stabilized by buried benzene. *Nature* 355(6358):371–373.
36. Ling SC, et al. (2010) ALS-associated mutations in TDP-43 increase its stability and promote TDP-43 complexes with FUS/TLS. *Proc Natl Acad Sci USA* 107(30): 13318–13323.
37. Dillen L, et al. (2013) Explorative genetic study of UBQLN2 and PFN1 in an extended Flanders-Belgian cohort of frontotemporal lobar degeneration patients. *Neurobiol Aging* 34(6):1711.e1–1711.e5.
38. van Blitterswijk M, et al. (2013) Profilin-1 mutations are rare in patients with amyotrophic lateral sclerosis and frontotemporal dementia. *Amyotroph Lateral Scler Frontotemporal Degener* 14(5-6):463–469.
39. Tiloca C, et al. (2013) Screening of the PFN1 gene in sporadic amyotrophic lateral sclerosis and in frontotemporal dementia. *Neurobiol Aging* 34(5):1517.e9–1517.e10.
40. Yang S, et al. (2013) Mutation analysis and immunopathological studies of PFN1 in familial and sporadic amyotrophic lateral sclerosis. *Neurobiol Aging* 34(9): 2235.e7–2235.e10.
41. Rotty JD, et al. (2015) Profilin-1 serves as a gatekeeper for actin assembly by Arp2/3-dependent and -independent pathways. *Dev Cell* 32(1):54–67.
42. Palmer I, Wingfield PT (2012) Preparation and extraction of insoluble (inclusion-body) proteins from Escherichia coli. *Curr Protoc Protein Sci* Chap 6, Unit 6.3.
43. Bilsel O, Yang L, Zitzewitz JA, Beechem JM, Matthews CR (1999) Time-resolved fluorescence anisotropy study of the refolding reaction of the alpha-subunit of tryptophan synthase reveals nonmonotonic behavior of the rotational correlation time. *Biochemistry* 38(13):4177–4187.
44. Greene RF, Jr, Pace CN (1974) Urea and guanidine hydrochloride denaturation of ribonuclease, lysozyme, alpha-chymotrypsin, and beta-lactoglobulin. *J Biol Chem* 249(17):5388–5393.
45. Mackness BC, Tran MT, McClain SP, Matthews CR, Zitzewitz JA (2014) Folding of the RNA recognition motif (RRM) domains of the amyotrophic lateral sclerosis (ALS)-linked protein TDP-43 reveals an intermediate state. *J Biol Chem* 289(12):8264–8276.
46. Winter G (2010) xia2: An expert system for macromolecular crystallography data reduction. *J Appl Cryst* 43:186–190.
47. Kabsch W (2010) Xds. *Acta Crystallogr D Biol Crystallogr* 66(Pt 2):125–132.
48. McCoy AJ, et al. (2007) Phaser crystallographic software. *J Appl Cryst* 40(Pt 4):658–674.
49. Emsley P, Cowtan K (2004) Coot: Model-building tools for molecular graphics. *Acta Crystallogr D Biol Crystallogr* 60(Pt 12 Pt 1):2126–2132.
50. Adams PD, et al. (2010) PHENIX: A comprehensive Python-based system for macromolecular structure solution. *Acta Crystallogr D Biol Crystallogr* 66(Pt 2):213–221.
51. Murshudov GN, Vagin AA, Dodson EJ (1997) Refinement of macromolecular structures by the maximum-likelihood method. *Acta Crystallogr D Biol Crystallogr* 53(Pt 3): 240–255.
52. Lu J, Pollard TD (2001) Profilin binding to poly-L-proline and actin monomers along with ability to catalyze actin nucleotide exchange is required for viability of fission yeast. *Mol Biol Cell* 12(4):1161–1175.

Supporting Information

Boopathy et al. 10.1073/pnas.1424108112

SI Materials and Methods

Purification of Recombinant PFN1. Cells containing recombinant PFN1 were lysed by sonication in 10 mM citrate and 10 mM NaCl, pH 5.0 (buffer A) containing protease inhibitor (11873580001; Roche). The lysate was cleared by centrifugation and applied to a Nuvia cPrime hydrophobic cation exchange column (35-mL column volume) (156-3402; Bio-Rad) preequilibrated with buffer A using an ÄKTAPurifier FPLC system (GE Healthcare). Bound impurities were eluted with 200 mL linear gradient of 10 mM citrate and 1 M NaCl, pH 5.0 (buffer B). PFN1-containing fractions eluted at 100% buffer B at ∼300 mL from the start of the gradient. SDS/PAGE was used to identify PFN1-containing fractions, which were pooled and dialyzed into buffer A with 6,000–8,000 molecular weight cut-off dialysis tubing (8015-40; Membrane Filtration Products, Inc.) before being applied to an anion (Q-resin) exchange column (17-0510-01; GE Healthcare). PFN1 eluted in the flow-through and was concentrated to 1–2 mL using stirred ultrafiltration cells (5123 and 5121; Millipore) and then applied to a Sephacryl S-100 HR (17-1194-01; GE Healthcare) size-exclusion column preequilibrated with PBS. PFN1 proteins eluted at ∼200 mL and were >95% pure as assessed by SDS/PAGE analysis with Coomassie Brilliant Blue stain. The identity and purity of the PFN1 proteins were verified by intact mass analysis at the Proteomics and Mass Spectrometry Facility (University of Massachusetts Medical School). The concentration of PFN1 was determined spectrophotometrically at an absorbance of 280 nm using a molar extinction coefficient of 18,450 $M^{-1}{\cdot}cm^{-1}$. Aliquots of PFN1 proteins were stored at –80 °C, typically at concentrations between 60–600 μM.

When PFN1 C71G was purified from inclusion bodies, BL21 (DE3) pLysS cells expressing C71G were cultured as described for PFN1 WT and C71G-containing inclusion bodies were extracted as previously described (42). Inclusion bodies were solubilized in 50 mM Tris·HCl, pH 7.0, containing 5 mM EDTA, 5 mM DTT, and 3 M guanidinium hydrochloride (buffer C) at ambient temperature. The solubilized inclusion bodies were diluted in buffer C to a PFN1 C71G concentration of ∼5 $mg{\cdot}mL^{-1}$. PFN1 C71G was refolded in buffer A containing 0.5 M L-arginine at ambient temperature under conditions where the final concentrations of guanidinium hydrochloride and C71G were below 0.1 M and 0.2 $mg{\cdot}mL^{-1}$, respectively. The refolded protein was dialyzed in buffer A at 4 °C and purified using a Sephacryl S-100 HR column as described for PFN1 WT.

Equilibrium Unfolding Experiments. For equilibrium unfolding experiments using tryptophan fluorescence, solutions of increasing urea concentration were prepared from a concentrated stock solution of 10.546 M urea in PBS using a Hamilton Microlab 500 titrator. PFN1 was mixed into the urea solutions to a final concentration of 2 μM with 1 mM Tris(2-carboxyethyl)phosphine) (TCEP) and the samples were equilibrated for 15–30 min. The intrinsic tryptophan fluorescence of PFN1 was measured at 25 °C with a T-format Horiba Fluorolog fluorimeter using an excitation wavelength of 295 nm. Three emission spectra (310 nm to 450 nm) were collected for each sample and averaged. The concentration of the urea in each sample was measured using an Abbe refractometer after data acquisition. Data were processed to obtain the center of mass (COM) of the emission spectrum. The COM was fit to a two-state transition model as previously described and the thermodynamic parameters, apparent ΔG° (the free energy of folding), m (the denaturant dependence of ΔG°), and C_m (the midpoint of the unfolding transition) were determined with the program Savuka (43, 44). Because the quantum yield of the native and unfolded states was within a factor of 2, the use of COM analysis is justified. We explicitly checked this by a rigorous global analysis using singular value decomposition and showed that the fit of the urea dependence basis vector gave thermodynamic parameters that were within the error of the COM and CD spectroscopy analyses, and no indications of non-two-state behavior. For equilibrium unfolding experiments using CD spectroscopy, PFN1 (10 μM) was equilibrated in various concentrations of urea as described above and CD spectra were acquired from 215 nm to 260 nm using a Jasco J-810 spectropolarimeter. Three spectra were averaged and the mean residual ellipticity (MRE) at 220 nm was plotted as a function of urea concentration and fit to a two-state equilibrium unfolding model.

For protein refolding experiments, a concentrated stock of PFN1 (100–250 μM) denatured in urea (4–8.5 M) was diluted in urea/PBS to obtain a series of samples with decreasing concentrations of urea, 10 μM PFN1 and 1 mM TCEP. Samples were equilibrated for 30 min before acquisition of fluorescence emission spectra as described above.

DSF. Samples containing WT or mutant PFN1 (20 μM) in PBS with 20× SYPRO Orange (S6651; Invitrogen) were pipetted in quadruplicate into a 384-well plate and subjected to heat denaturation using a Bio-RadCFX384 Touch Real-Time PCR Detection System. The temperature was increased from 25 °C to 100 °C in 0.3 °C increments and at each increment fluorescent intensities were acquired using HEX detector (excitation 515–535 nm, emission 560–580 nm). PFN1 proteins were analyzed alone and in the presence of the poly-L-proline peptide (molecular weight 1,000–10,000, P2254; Sigma). Because this peptide was supplied from the manufacturer as a mixture of poly-L-proline species, the concentration is reported here in units of proline (molecular weight 115.13 $g{\cdot}mol^{-1}$). For experiments with the poly-L-proline peptide, PFN1 was prepared with 4 mM proline. The fluorescence intensities for the four replicates were averaged, normalized to the maximum fluorescence intensity, and plotted as a function of temperature to obtain melting curves, which were fit with a sigmoidal function in GraphPad Prism to determine the midpoint of transition or the apparent T_m.

Measuring PFN1 Turnover in Cells. Human SKNAS cells were cultured in DMEM (11965; Gibco) containing 10% (vol/vol) FBS (F4135; Sigma-Aldrich) and 1% (wt/vol) penicillin and streptomycin (10378; Gibco) under standard culture conditions (37 °C, 5% CO_2/95% air). SKNAS cells were transiently transfected with 0.5 μg of V5-PFN1 plasmids (2) in 24-well plates using 1.75 μL NeuroMag (NM50500; OZ Biosciences) diluted in Opti-MEM (38915; Invitrogen). After 12 h of V5-PFN1 expression, translation was inhibited with 30 $\mu g{\cdot}mL^{-1}$ cycloheximide (C7698; Sigma-Aldrich). Cells were lysed at specific time points during a 12.5-h time course following cycloheximide addition using RIPA buffer (BP-115-500; Boston BioProducts) supplemented with protease inhibitors (11836170001; Roche) and centrifuged at 19,357 × *g* for 15 min, after which the supernatant (containing soluble PFN1) was collected. The remaining pellet (containing insoluble PFN1) was washed once with RIPA lysis buffer, centrifuged again, and resolubilized with 8 M urea in volumes equal to their soluble counterparts. The protein concentration of the soluble fractions was determined using a bicinchoninic acid assay (23227; Thermo Scientific Pierce). Samples were processed

and subjected to Western blot and densitometry analyses essentially as described (19). Western blots were probed using V5-specific (1:1,000, R96025; Invitrogen) and GAPDH-specific (1:20,000, G9545; Sigma) antibodies. Bands corresponding to soluble V5-PFN1 were normalized to the loading control, GAPDH, and then to the band corresponding to cycloheximide treatment for "0 h" for each protein. For each biological replicate, visible bands corresponding to insoluble V5-PFN1 were normalized to their respective 0 h PFN1 C71G band. Statistical significance was determined using a two-way ANOVA followed by Tukey's post hoc analysis.

CD Spectroscopy. CD spectra of WT PFN1 or mutants (10 μM in PBS) were acquired from 190 nm to 260 nm at a scan speed of 2 s per wavelength with a 1-mm cuvette at 25 °C using a AVIV Biomedical CD spectrometer model 400. Data reflect an average of five scans that were blank subtracted. The resulting ellipticity curves were transformed to mean residue ellipticity as described (45).

Acidic Native PAGE. The method for acidic native PAGE analysis of basic proteins described by the Mario Lebendiker laboratory (wolfson.huji.ac.il/purification/) was used. Briefly, 29:1 acrylamide-bisacrylamide (BP1408-1; Fisher Scientific) native gels were cast with 7.5% (wt/vol) polyacrylamide in the resolving gel, pH 4.3, and 3% (wt/vol) polyacrylamide in the stacking gel, pH 6.8. The gel sample containing WT or mutant PFN1 (0.8 $\mu g \cdot \mu L^{-1}$) was prepared under native conditions using ice-cold acetate–KOH, pH 6.8 and 10% (vol/vol) glycerol with 0.025% (wt/vol) of methylene blue. PFN1 proteins (10 μg) were loaded onto the gel and subjected to reversed polarity electrophoresis under ice-cold conditions for 2 h at 100 V. The protein bands were visualized with Coomassie Brilliant Blue as described above for denaturing gels.

Analytical Size-Exclusion Chromatography. WT or mutant PFN1 (50 μL of PFN1 at 0.8 $\mu g \cdot \mu L^{-1}$) were subjected to analytical size-exclusion chromatography at 4 °C using a Superdex 75 column (17-5174-01; GE Healthcare) equilibrated with PBS and a flow rate of 0.5 $mL \cdot min^{-1}$. For each trial ($n = 2$), elution profiles were acquired using absorbance at 280 nm and normalized to the peak value of WT PFN1. The area under peak was calculated using GraphPad Prism.

Protein Crystallization and X-Ray Structural Determination. PFN1 crystals were grown by hanging drop vapor diffusion after mixing the PFN1 protein with a 1:1 ratio of reservoir solution at 25 °C for WT and E117G and at 18 °C for M114T. Reservoir solution for WT contained 50 mM KH_2PO_4, 36% (wt/vol) PEG 8,000 and 100 mM MES, pH 6.0. Reservoir solution for E117G contained 50 mM KH_2PO_4, 41% (wt/vol) PEG 8,000 and 100 mM MES, pH 6.0. Reservoir solution for M114T contained 750 mM sodium citrate, 200 mM NaCl, and 100 mM Tris, pH 7.5.

E117G crystals where soaked in cryoprotectant composed of 25% (vol/vol) ethylene glycol and 75% (vol/vol) reservoir solution and M114T crystals were passed through mineral oil before mounting for data collection. Diffraction data were collected using a Rigaku 007 MicroMax HF rotating anode X-ray generator, under a nitrogen cryostream at 100 K (Oxford Cryosystems), on a Saturn944+ CCD detector.

The data were processed using Xia2 (46) [running XDS (47)] for WT and M114T and HKL2000 (HKL Research) for E117G. All three structures were solved via molecular replacement with Phaser (48) using the profilin structure PDB ID code 1FIK (20) as the starting model followed by multiple rounds of manual model building performed with Coot (49). WT was refined with PHENIX (50) and E117G with REFMAC5 (51) using standard refinement protocols. M114T was refined with PHENIX using twin refinement with the twin law {h,-h-k,l} applied through refinement, because the data were highly twinned with a twin fraction estimated to be 0.48.

Structural Analysis. SiteMap (Schrödinger, LLC) was used to identify and evaluate the mutation-site cavity volumes. Figures were generated using PyMOL (Schrödinger, LLC).

Poly-L-Proline Peptide Binding Experiments. The intrinsic tryptophan fluorescence of WT or ALS-PFN1 (2 μM) as a function of increasing concentrations of the poly-L-proline peptide described above at 25 °C was used to measure binding of PFN1 to poly-L-proline as previously described (52). The samples were excited at 295 nm and three emission spectra between 310 nm and 450 nm were collected for each sample and averaged. The fluorescence emission intensity at 323 nm was baseline-corrected, normalized, plotted as a function of poly-L-proline and fit to a one-site total binding model in GraphPad Prism to yield apparent K_d values.

Inhibition of Spontaneous Actin Assembly. Gel-filtered monomeric rabbit muscle actin (3 μM, 5% pyrene-labeled) was converted to Mg–ATP–actin immediately before use in each reaction and mixed with 7 μL of different concentrations of PFN1 WT, and PFN1 mutants or control buffer and 3 μL of 20× initiation mix (40 mM $MgCl_2$, 10 mM ATP, and 1 M KCl) in 60-μL reactions. Actin polymerization was monitored over time at 365 nm excitation and 407 nm emission in a PTI fluorometer at 25 °C. Average relative rates of actin polymerization ($n = 3$) were determined based on the slopes of the assembly curves during the first 500 s of each reaction and plotted against increasing concentrations of PFN1 (mutants). Statistical significance was determined using a two-way ANOVA followed by Tukey's post hoc analysis.

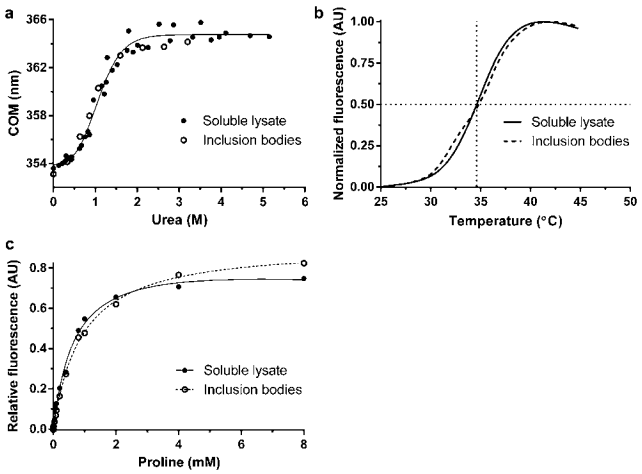

Fig. S1. A comparison of PFN1 C71G purified from the soluble lysate of *Escherichia coli* vs. from inclusion bodies. (*A*) Equilibrium unfolding and (*B*) thermal denaturation curves (described in Fig. 1) for PFN1 C71G purified from the soluble lysate and inclusion bodies. The apparent melting temperature of PFN1 C71G purified from inclusion bodies (34.62 ± 0.05 °C) is the same as that purified from soluble lysate (34.60 ± 0.03 °C). (*C*) PFN1 C71G has similar affinities to poly-L-proline as determined by the binding assay described in Fig. 6 irrespective of whether this variant was purified from the soluble lysate or inclusion bodies.

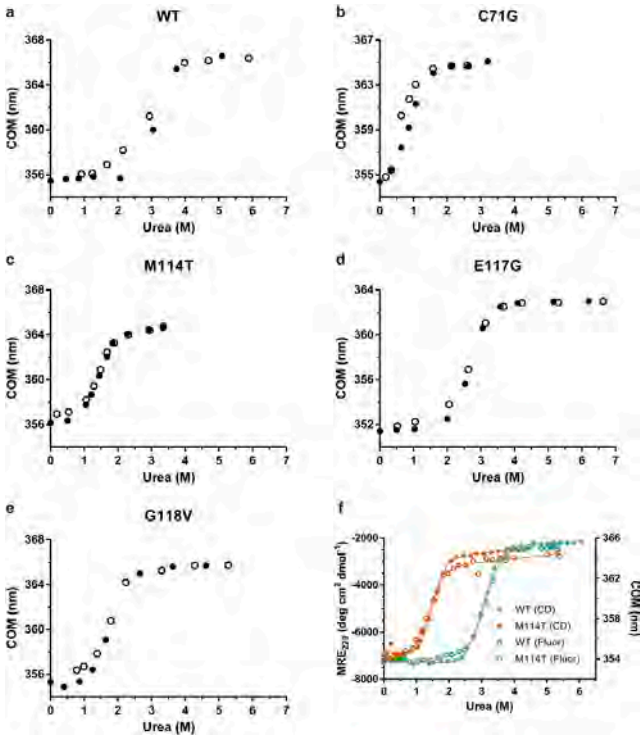

Fig. S2. All PFN1 variants unfold by a two-state process. (*A–E*) PFN1 variants denatured in urea were refolded by diluting the urea. The final concentration of PFN1 in each sample was 10 μM and tryptophan fluorescence was used to monitor folding. The equilibrium transition regions overlay closely for the unfolding and refolding curves, indicating that the unfolding reaction is reversible. Filled and open circles represent unfolding and refolding, respectively. (*F*) The two-state unfolding of PFN1 observed by intrinsic fluorescence (data from Fig. 1*A*; Fluor) was verified by CD measurements for PFN1 WT and M114T. The concentration of protein used was 2 μM and 10 μM for tryptophan fluorescence and CD measurements, respectively. The *y* axis on the left is the mean residue ellipticity at 220 nm (MRE_{220}) obtained from CD experiments, whereas the *y* axis on the right reflects the change in the COM (as shown in Fig. 1). The thermodynamic parameters obtained by fitting the CD data agree well with those obtained from the fluorescence data (Table 1) and are as follows: for WT $\Delta G° = 7.16 \pm 0.11$ kcal·mol^{-1}, $m = 2.36 \pm 0.04$ kcal·mol^{-1}·M^{-1}, $C_m = 3.03 \pm 0.07$ M; for M114T $\Delta G° = 4.35 \pm 0.10$ kcal·mol^{-1}, $m = 2.95 \pm 0.06$ kcal·mol^{-1}·M^{-1}, $C_m = 1.47 \pm 0.05$ M.

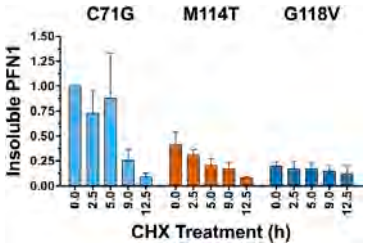

Fig. S3. The turnover of insoluble PFN1 in SKNAS cells. The experiment was carried out as described in Fig. 2, and a representative Western blot analysis of the insoluble fraction is shown in Fig. 2*B*. The data above reflect the densitometry results from an average of $n = 2$ (M114T) or $n = 3$ (C71G and G118V) independent experiments and error bars represent SEM. Each sample was normalized to the PFN1 C71G band corresponding to "time 0." The turnover of C71G within the insoluble fraction was slower relative to C71G within the soluble fraction (compare this graph to that in Fig. 2*C*). There was relatively less M114T and G118V in the insoluble fraction compared with C71G, and the small fraction of insoluble G118V persisted throughout the experimental time course.

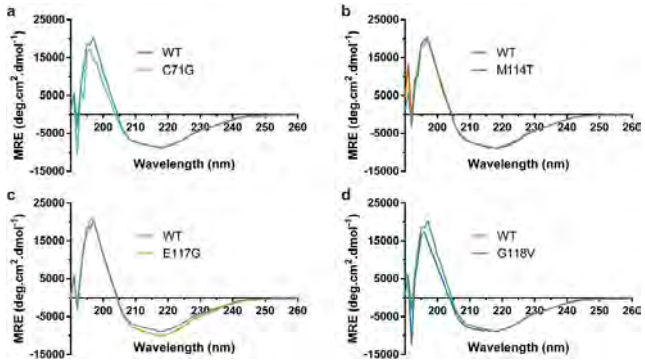

Fig. S4. ALS-linked PFN1 variants retain the same secondary structure as PFN1 WT. (*A–D*) Far UV CD spectra for the indicated PFN1 variant (10 μM) overlaid with CD spectrum for PFN1 WT (10 μM).

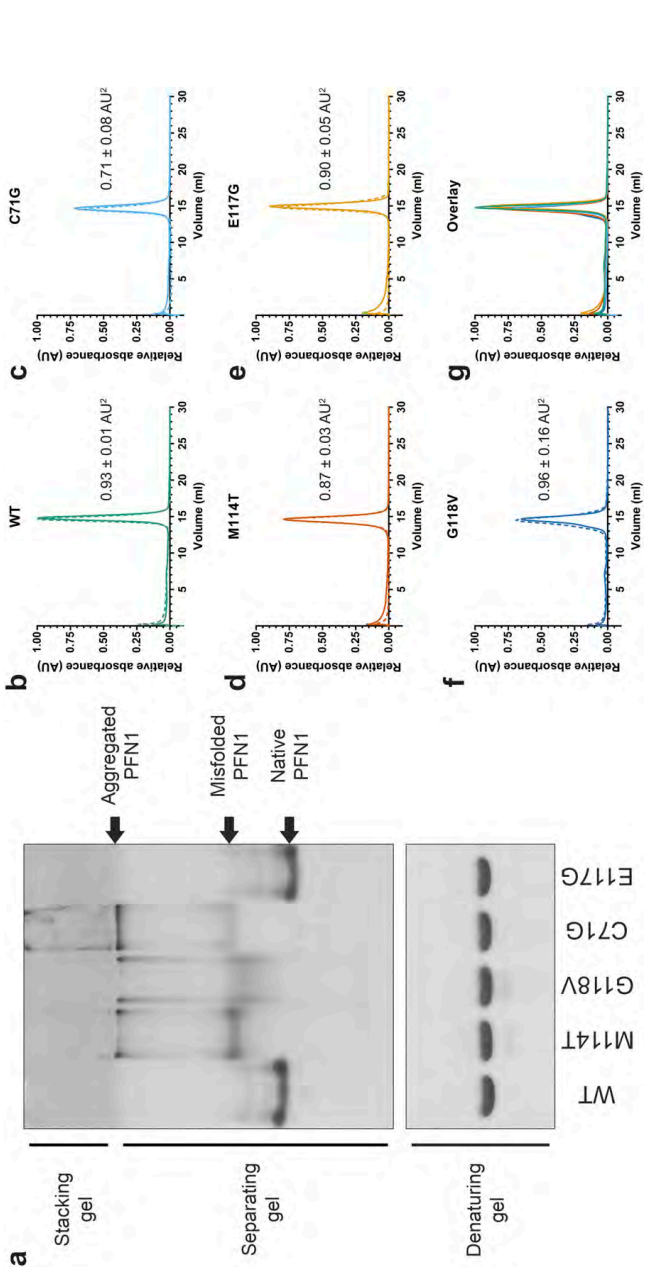

Fig. S5. Analysis of PFN1 proteins by native page and analytical size-exclusion chromatography. (*A*) PFN1 proteins (10 μg) were subjected to native (*Top*) or denaturing (*Bottom*) gel electrophoresis and detected with Coomassie Brilliant Blue stain. The mobility of native PFN1 WT is indicated. PFN1 E117G migrates with a slightly faster mobility than PFN1 WT owing to the addition of a negatively charged amino acid. Misfolded ALS-linked PFN1 variants migrate with slower mobility and form aggregated species that are retained in the stacking gel. This gel is representative of $n = 2$ experiments using proteins from different purification preparations. (*B–F*) The indicated PFN1 protein (40 μg) was subjected to analytical size-exclusion chromatography using a Superdex 75 column. A single peak corresponding to the expected elution volume (~15 mL) for monomeric PFN1 was detected for all PFN1 proteins. The experiments were carried out in duplicate for each variant, indicated by solid ($n = 1$ experiment) and dashed ($n = 2$ experiment) lines. The average relative peak area ± the SD is indicated to the right of each curve. Despite equal sample loading, the peak area of PFN1 C71G and M114T is lower than that of WT (within error), consistent with a reduced level of soluble protein for these ALS-linked variants. (*G*) An overlay of *B–F* for the $n = 1$ experiment demonstrates a similar elution profile for all PFN1 proteins.

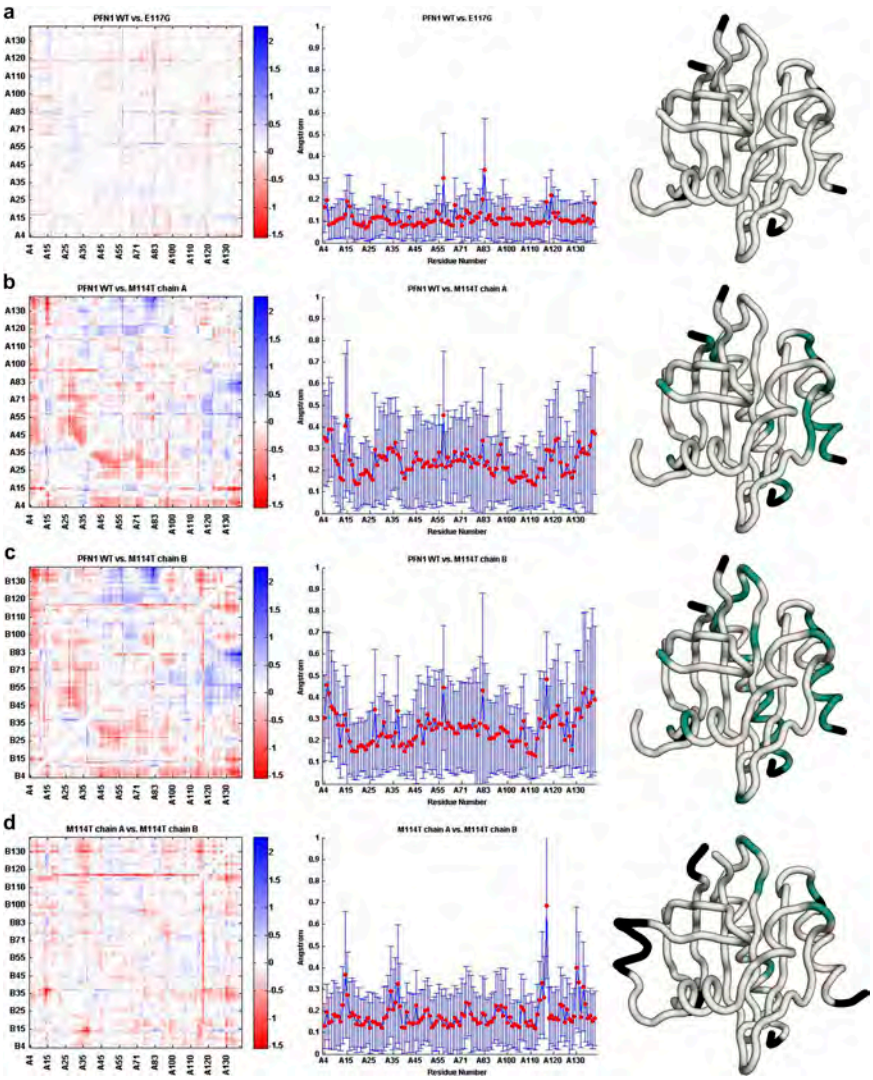

Fig. S6. Structural changes induced by the M114T mutation revealed in double difference plots. Double different plots (*Left*) of WT vs. E117G (*A*), WT vs. M114T chain A (*B*), WT vs. M114T chain B (*C*), and M114T chains A vs. B (*D*). The Avg-Abs-DD values are plotted as a function of residue number for each structural comparison (*Middle*); these plots provide an indication for residues that undergo a structural change between the proteins that are being compared. Residues with Avg-Abs-DD values of 0.3 Å or greater are plotted onto the structure (*Right*) of PFN1 WT (*A–C*) and PFN1 M114T chain A (*D*) in green. Residues not used in this analysis are colored black.

Fig. S7. Actin and poly-L-proline binding residues exhibit relatively high double difference values. Residues that have Avg-Abs-DD values of 0.3 Å or greater that are also engaged in actin binding (V119, H120, G122, and K126) or poly-Pro binding (W4, Y7, H134, and S138) are mapped onto the structure of PFN1 WT in magenta. All other residues with Avg-Abs-DD values of 0.3 Å or greater are highlighted in green. Residues with Avg-Abs-DD values between chain A and chain B of M114T 0.3 Å or greater (Fig. S6*D*) were excluded from this analysis. Residues not used in this analysis are colored black.

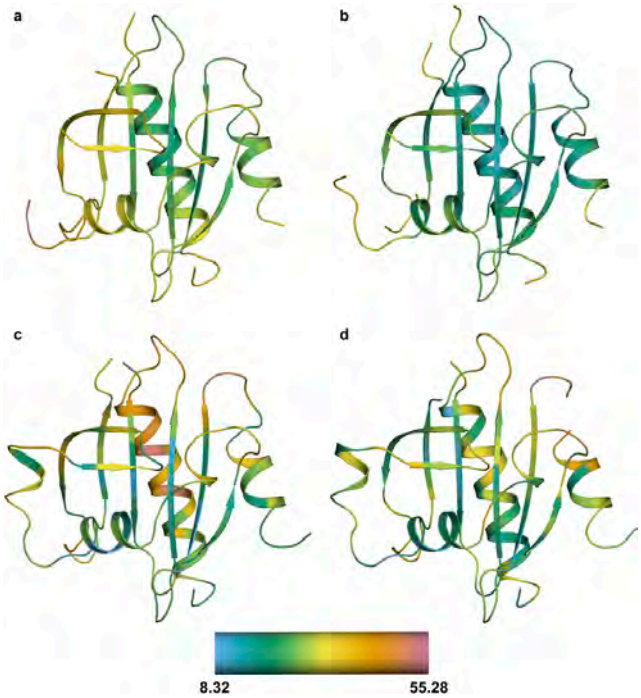

Fig. S8. The calculated α-carbon B factors for all PFN1 structures. Cartoon representations of WT (*A*), E117G (*B*), and M114T chains A (*C*) and B (*D*). Residues are colored according to the α-carbon B factors using the scale shown at the bottom. The average α-carbon B factor for WT, E117G, and M114T chains A and B structures are 30.52, 22.94, 29.47, and 27.33, respectively. Because the average B factor is higher for M114T chain A, M114T chain B was used for structural analyses unless otherwise noted.

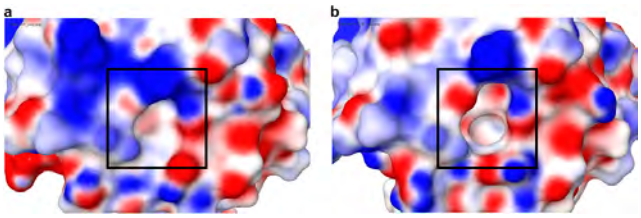

Fig. S9. Electrostatic surface potential (ESP) of PFN1 WT and PFN1 M114T. A comparison of the ESP for PFN1 WT (*A*) and M114T (*B*) around the surface pocket (for WT) and cleft (for M114T) shown in Fig. 7. Comparison of the ESP was calculated using Maestro (Schrödinger, LLC). The Red_White_Blue color scheme was used to depict the ESP of both surfaces, where red denotes negative, blue denotes positive, and white denotes neutral ESP. The minimum and maximum values are −0.12 and 0.12, respectively. The cleft (boxed region in *B*) formed by M114T exposes a deeper pocket comprised of hydrophobic residues that would otherwise be buried beneath the surface-exposed pocket (boxed region in *A*) in PFN1 WT.

Table S1. Crystallographic and refinement statistics of human PFN1 structures

Statistics	WT	E117G	M114T
Resolution, Å	2.160	2.170	2.230
Space group	C121	C121	P6
a, Å	74.26	73.65	81.69
b, Å	31.84	31.71	81.69
c, Å	61.02	60.54	65.35
A, °	90	90	90
B, °	122.66	122.03	90
Γ, °	90	90	120
Z	1	1	2
R_{merge}, % linear	0.075	0.036	0.147
I/sigma	13.3	12.2	12.4
Completeness, %	99.28	99.49	99.58
Total no. of reflections	20,783	16,453	76,801
No. of unique reflections	6,416	6,422	12,156
R_{factor}, %	0.2159	0.1965	0.1952
R_{free}, %	0.2469	0.2139	0.2383
RMSD in bond lengths, Å	0.002	0.003	0.003
RMS angle, °	0.62	0.67	0.61
Temperature, °C	−80	−80	−80
Residues missing	1, 2, 57–62, 92–96	1, 2, 59–62, 81,82, 93–95, 140	
Chain A			1, 93–97
Chain B			1, 13, 91–97
PDB ID code	4X1L	4X1M	4X25

PREFACE TO APPENDIX III

All of the work presented in this appendix was performed by Maeve Tischbein.

Fibroblast line Control (3)/AG16409 was a generous gift from the Budnik lab. I am thankful to Drs. Vivian Budnik, Baojin Ding and Ashely James for their conversations, insight and advice.

APPENDIX III: Investigating a Relationship Between FUS, MegaRNPs and Disease

Disruptions in nucleocytoplasmic transport have recently emerged as a widespread theme amongst neurological disorders (Li & Lagier-Tourenne 2018). In the field neurodegeneration, particularly the motor neuron disease amyotrophic lateral sclerosis (ALS), there has been much attention regarding the mislocalization of transport factors and cargo, however alterations to the structure and composition of the nuclear envelope may also contribute to the observed defects. One critical feature of the nuclear envelope is lamin. Lamins are intermediate filaments that form mesh-like matrix along the inner nuclear membrane of the nuclear envelope. There are two types of Lamins. First, B-type lamins (Lamin B), which are expressed are expressed early in development and, second, A-type lamin (Lamin A), expressed in differentiated cells and can be alternatively spliced to form Lamin C, (Fradkin & Budnik 2016). Together, they form the laminar matrix, which provides structure and integrity to the nuclear envelope by anchoring components of cytosolic cytoskeletal network. More than structural support, lamins can also influences nuclear function by binding chromosomes and nuclear transcription factors. Disruption of nuclear matrix can lead to the inappropriate clustering of nuclear pores and disruption in chromatin organization, resulting in alterations to gene expression (Coutinho et al. 2009, Wiggan et al. 2017).

Notably, disease resulting from lamin mutations are referred to as laminopathies, the most well-known of which is Hutchinson-Gilford progeria syndrome (HGPS) (Coutinho et al. 2009). HGPS is a rare genetic disease which manifests as ‘pre-mature aging’ in children. This disease affects 1 per 4–8 million live births and the life expectancy is primarily 13 years. HGPS is caused by autosomal dominant mutations in Lamin A and while there are multiple associated mutations, >90% of cases are caused by the mutation G608G which results in the mis-splicing of prelamin (McClintock et al. 2007). Immature Lamin A (prelamin) undergoes several round of C-terminal processing: first, C-terminal farnesylation, followed the cleavage of three terminal amino acids, methylation and second round of C-terminal cleavage in which 15 amino acids and the farnesyl modification are removed to form mature Lamin A. The G608G mutation prevents the second round of C-terminal cleavage resulting in an improperly farnesylated protein, referred to as progerin, that forms abnormally strong association with the nuclear envelope (Coutinho et al. 2009, McClintock et al. 2007). As a result, the nuclear envelope becomes notably misshapen, often described as ‘blebbing’ (Coutinho et al. 2009).

Nuclear export primarily occurs though nuclear pores, however recent studies have suggested the presence of an alternative export pathway (nuclear budding) that may be relevant to HGPS and general nucleocytoplasmic transport. This emerging pathway was first observed in the nuclei of *Drosophila* skeletal muscle in response to neuromuscular Wingless/DFz2 (in humans: Wnt-1/DFrizzled2) signaling (Speese et al. 2012). In this pathway, large nuclear RNP

granules (megaRNPs) containing synaptic and mitochondrial mRNAs are brought to the nuclear envelope where they induce rearrangements of the laminar matrix, bud from the inner nuclear membrane (C-terminal fragment of DFz2 (DFz2C)-positive granules appearing enveloped by Lamin A) and then fuse with the outer nuclear membrane for release into the cytoplasm(Jokhi et al. 2013, Li et al. 2016, Speese et al. 2012). Mutations in *Drosophila* Lamin A, equivalent to human HGPS-causing mutations, results a decrease of DFz2C-postive Lamin A foci and increased blebbing (Li et al. 2016). Upon expression of HGPS-linked *Drosophila* Lamin A mutations, mitochondria degeneration and neuromuscular junction defects were observed (Li et al. 2016). It is hypothesized that improper export of mRNA through this pathway contributes to the development of these phenotypes resulting in detrimental cellular effects, including accelerated aging (Li et al. 2016).

The connection between age-linked neurodegenerative disease and laminopathy pathologies is not well studied. However, defects in nucleocytoplasmic transport and partitioning are emerging as relevant to neurodegenerative disease as well as the normal gaining process. Lamin specifically has gained attention in Tauopathy models (Frost et al. 2016), Parkinson's (Miller et al. 2013) as well as the normal aging process (McClintock et al. 2007, Scaffidi et al.). Mutations in multiple RNA binding proteins (RBPs), including fused in sarcoma (FUS) and TAR DNA-binding protein 43 (TDP-43), cause ALS, an adult onset neurodegenerative disease that affects motor neurons (Brown & Al-Chalabi 2017). Further nuclear envelope abnormalities and nuclear

mRNA accumulation are observed in *Drosophila* models of ALS (Freibaum et al. 2015) and mislocalization of transport factors has been observed both the patient tissue of inherited (familial) as well as sporadic ALS (Freibaum et al. 2015, Kinoshita et al. 2009, Zhang et al. 2015). Thus, RNA processing and nucleocytoplasmic transport appear important to the pathomechanism of ALS. To investigate the potential relevance of Lamin-mediated disruptions to the development of ALS-linked, nucleocytoplasmic transport phenotypes, we evaluated the expression of ALS-linked RBPs in models of HGPS as well as HGPS/Lamin-linked processes in neuronal modes of ALS.

Progerin-Induced Nuclear Misfolding Alters Expression of ALS-linked RBPs

To probe for a connection between disruptions in the laminar matrix and neurodegenerative-disease linked phenotypes, we evaluated the expression and localization of ALS-linked RBPs in primary fibroblasts expressing HGPS-linked, Lamin A mutations known to alter nuclear morphology (**Table AIII-1**). Fibroblast lines were grown until they reached ~50-70% confluency and were collected for western analysis (**Fig. AIII-1A-E**). TDP-43 levels were significantly decreased in only the G608G lines, relative to the pooled control (**Fig. AIII-1B,C**). Although not significant, FUS protein also levels appeared reduced in both these lines as well (**Fig. AIII-1B,D**). Interestingly, both FUS and TDP43 levels did not appear reduced in the R644C line (**Fig. AIII-1B,C**) suggesting the effects of the G608G mutation are more severe than R644C. This is supported by the observation that both

Table AIII-1. Primary fibroblast lines. Characteristics of HGPS and non-diseased controls used for experimental analysis.

Fibroblast Line Name	Coriell ID	Affected Status	Source	Mutation	Sex	Age at Sampling (Year)	Passage*
G608G (1)	AG11513	Yes; HGPS	Skin, leg	GLY608GLY	Female	8	5
G608G (2)	AG06297	Yes; HGPS	Skin, thigh	GLY608GLY	Male	8	18
R644C	GM00989	Yes; HGPS	Skin	ARG644CYS	Male	20	15
Control (1)	GM02036	No	Skin	--	Female	11	13
Control (2)	GM03440	No	Skin, leg	--	Male	20	4
Control (3)	AG16409**	No	Skin	--	Male	12	4

*From time of purchase from Coriell.

**With the exception of AG16409, all lines were purchased from Coriell. AG16409 was a generous gift from the Budnik lab.

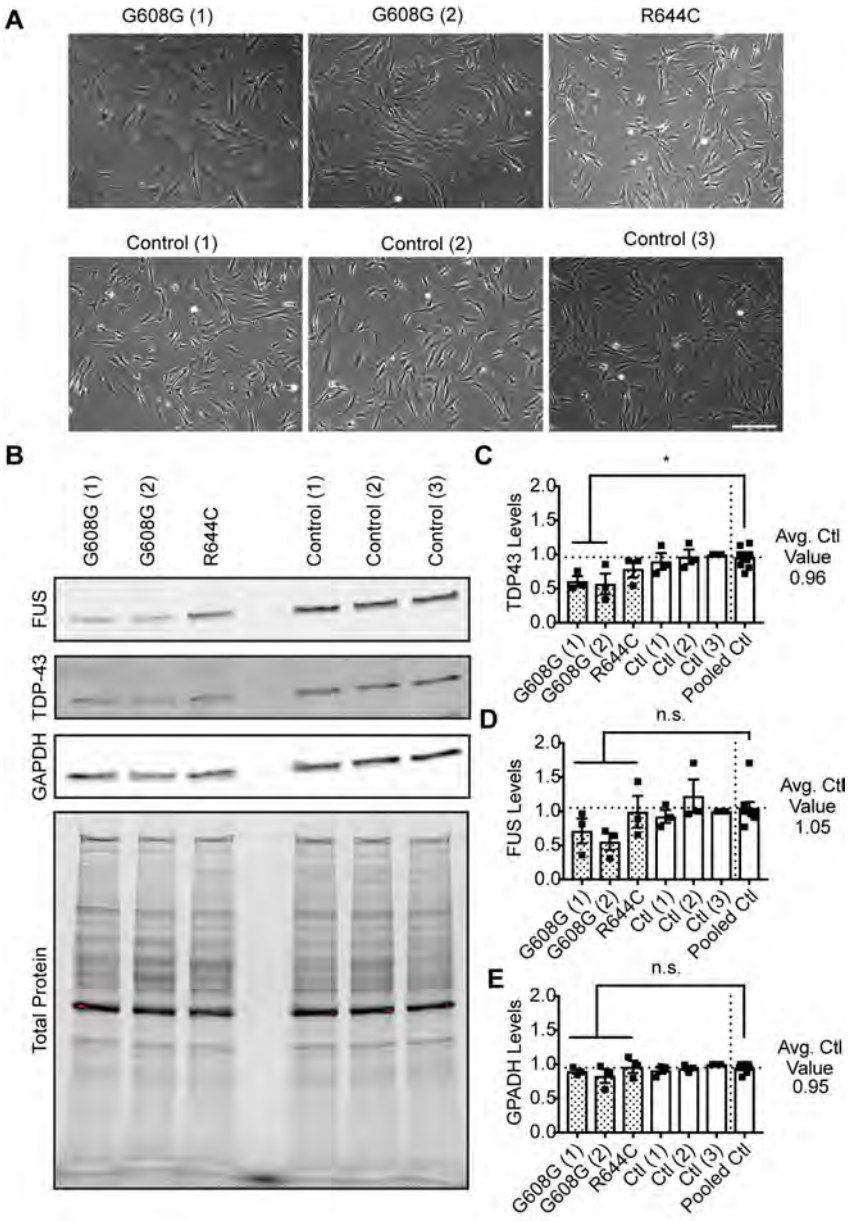

Figure AIII-1. TDP-43 protein expression is altered in G608G-HGPS expressing fibroblasts. **(A)** Phase images of fibroblast lines used for analysis of ALS-linked RBP expression. Scale bar = 50μm. **(B)** Western and **(C-E)** densitometry analysis of fibroblast protein lysates revealed that TDP-43 protein levels, unlike FUS or GAPDH, are significantly decreased in both G608G lines compared to the pooled control (one-way ANOVA; *p<0.05, n.s. = non-significant, n = 3 experimental replicates). For quantification, RBP levels from all six lines were normalized to total protein levels and then the pooled control. Error bars = SEM.

G608G lines also grew at a slower rate in culture. There was no significant or trending decrease in GAPDH levels for any fibroblast line indicating that not all proteins are affected by the presence of the G608G mutations (**Fig. AIII-1B,E**).

We next sought to observe the distribution of these RBPs *in situ*. To denote the nucleus and nuclear envelope immunofluorescence of Lamin A/C was performed. As expected, misshapen nuclei were observed in HGPS-mutant expressing fibroblasts (**Fig. AIII-2A**). Akin to the trend observed by western (**Fig. AIII-1**), a decrease in the number of cells with robust nuclear FUS staining was observed in both G608G fibroblast lines (**Fig. AIII-2A**). This observation was confirmed following quantification of qualitative FUS levels and nuclear envelope morphology; the number of cells with essentially no FUS staining was increased in these lines (**Fig. AIII-2B-H**; as indicated by both green and magenta bars for 'None'). It was also observed that this phenotype could be observed in both normal and misshapen nuclei (**Fig. AIII-2B-H**). This suggests that the observed reduction in FUS immunoreactivity phenotype does not correlate with nuclear envelope distortion. Upon staining for TDP-43 all but one line, G608G (2), exhibited robust nuclear staining (**Fig. AIII-2B-I**). Interestingly, this loss of nuclear signal detected by immunofluorescence does not appear to faithfully match the Western analysis in which TDP-43 levels were reduced in both G608G lines. Together, these experiments together indicate that HGPS-causing Lamin mutations influence the expression of the ALS-linked proteins, FUS and TDP-43 (**Fig. AIII-1,2**), although the significance of our immunofluorescence observations is unclear at this time.

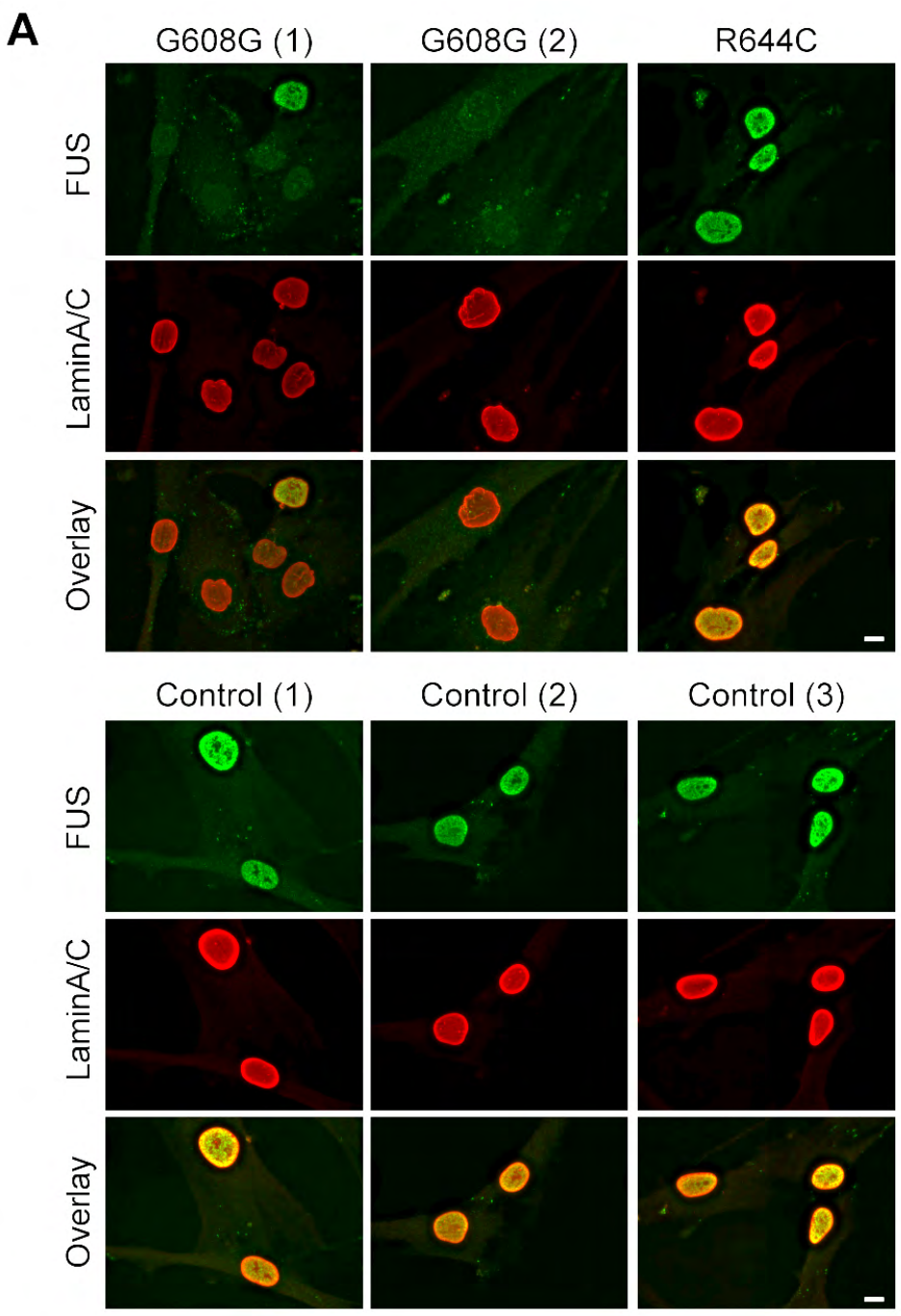

Figure AIII-2. Decreased detection of endogenous FUS and increased nuclear envelope misshapenness in G608G fibroblast lines. (A) Immunofluorescence of FUS (green) reveal a decreased detection of this protein in fibroblast lines containing the G608G mutation. Nuclear envelope distortion, as indicated by Lamin A/C staining (red), was also observed in G608G fibroblast lines. Scale bar = 10μm.

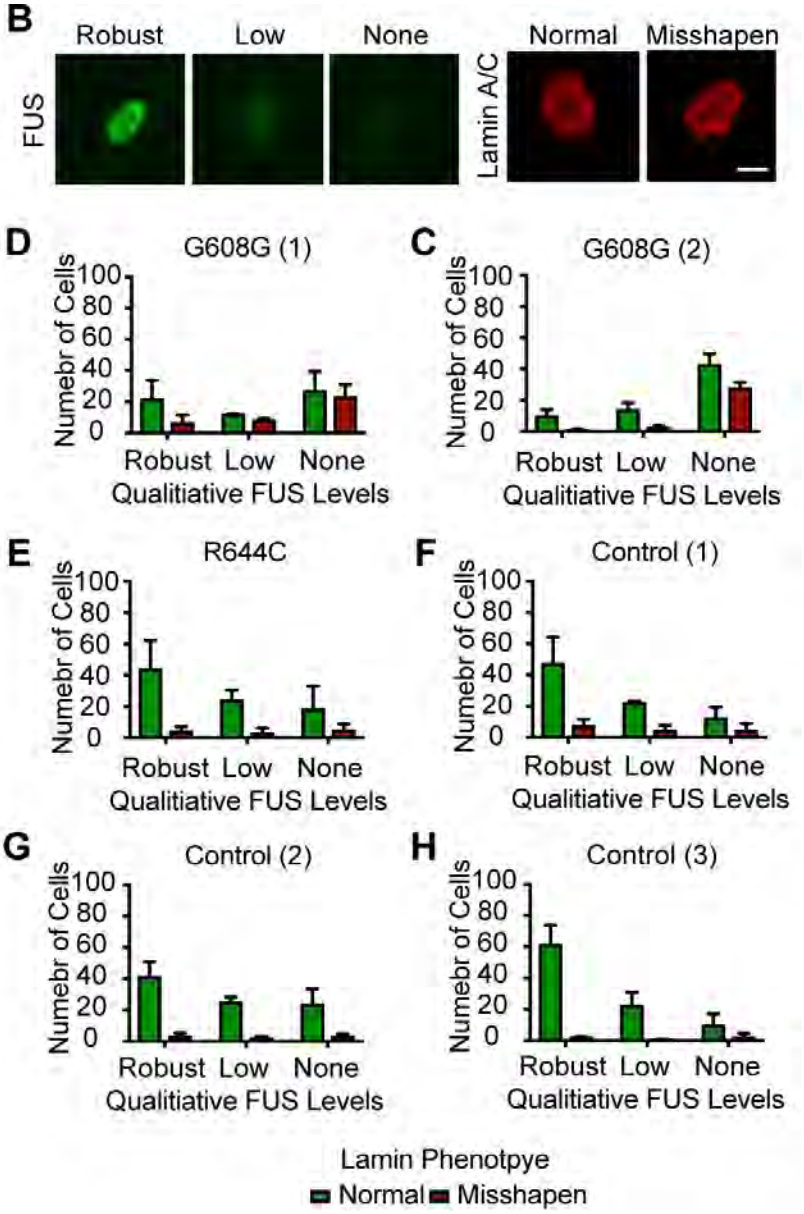

Figure AIII-2 continued. (B) Qualitative scoring of FUS staining levels and nuclear envelope shape was conducted. FUS levels were evaluated as Robust, Low or None and nuclear envelop shape (as indicated by Lamin A/C staining) as normal or misshapen. Scale bar = 10µm. **(C-H)** In G608G lines there was an increased number of cells with reduced FUS staining as well as misshapen nuclear envelopes. However, reduced FUS staining was observed in fibroblasts with normal as well as misshapen nuclear envelope morphology (n = 3 experimental replicates, 100 cells per line and replicate were quantified).

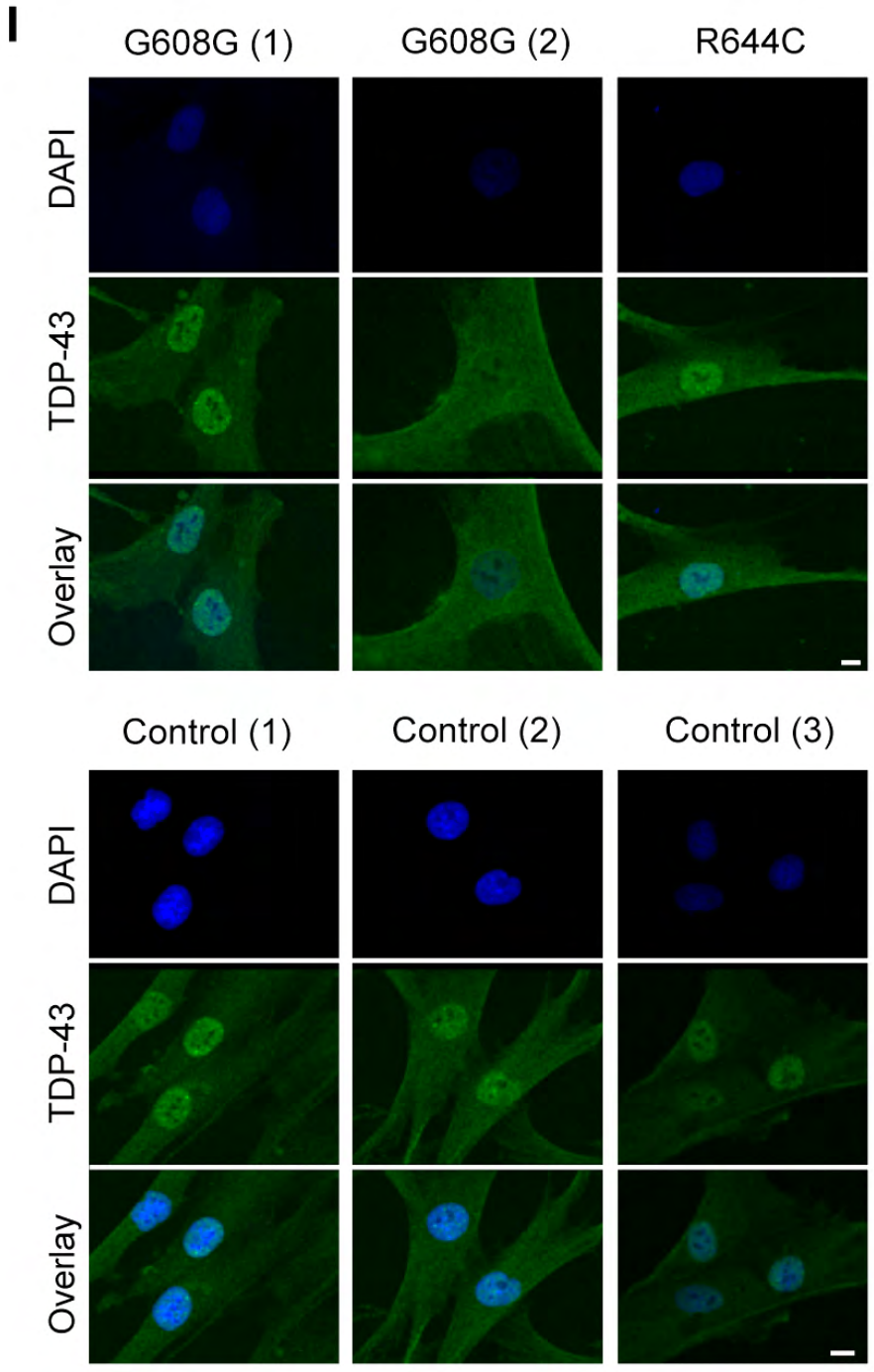

Figure AIII-2 continued. (I) TDP-43 staining in HGPS and control fibroblast lines. For all lines expect G608G (2), TDP-43 staining (green) was strongest in the nucleus (indicated by DAPI, blue). For G608G (2), there were notably more cells with reduced nuclear TDP43 staining than other conditions (observations were not quantified or scored; n = 1 experimental replicate). Scale bar = 10μm.

Increased Lamin puncta observed in PCNs after excitotoxic treatment

The previous experiments suggest that ALS-linked RBPs are affected by HGPS-causing mutations in the nuclear matrix protein, Lamin A. Both FUS and TDP-43 regulate various aspects of RNA regulation, including the expression of synaptic transcripts, and alterations in RNA processing by ALS-mutations in these proteins is hypothesized to contribute to disease(Ling 2018). Further, both FUS and TDP-43 have been shown to associate with a variety of RNA-protein complexes including transport granules, stress granules as well as nuclear transcriptional and splicing complexes(Ratti & Buratti 2016). Similarly, megaRNPs are thought to contain transcripts essential for the formation of neuromuscular synapses (Li et al. 2016, Speese et al. 2012) and their nuclear export is disrupted in a Lamin-A *Drosophila* model of HGPS (Li et al. 2016). Thus, RBP and megaRNP biology both appear affected by disruptions to the laminar matrix.

In light of such parallels, we considered if megaRNP biology could also be affected in models of ALS, in which RBP localization and nucleocytoplasmic transport are likewise disrupted. Nuclear envelope-adjacent Lamin A foci have previously been used to indicate the presence of megaRNPs as these complexes remodel and become surrounded Lamin as they pass through the nuclear envelope. Thus, to test this hypothesis, the presence of Lamin A foci was evaluated in a cellular model of excitotoxity, a neuronal form of stress associated ALS and capable of causing FUS and TDP-43 egress (**Fig. II-2**) as well as disrupt nuclear export (**Fig. II-4**). Following excitotoxic treatment of primary cortical

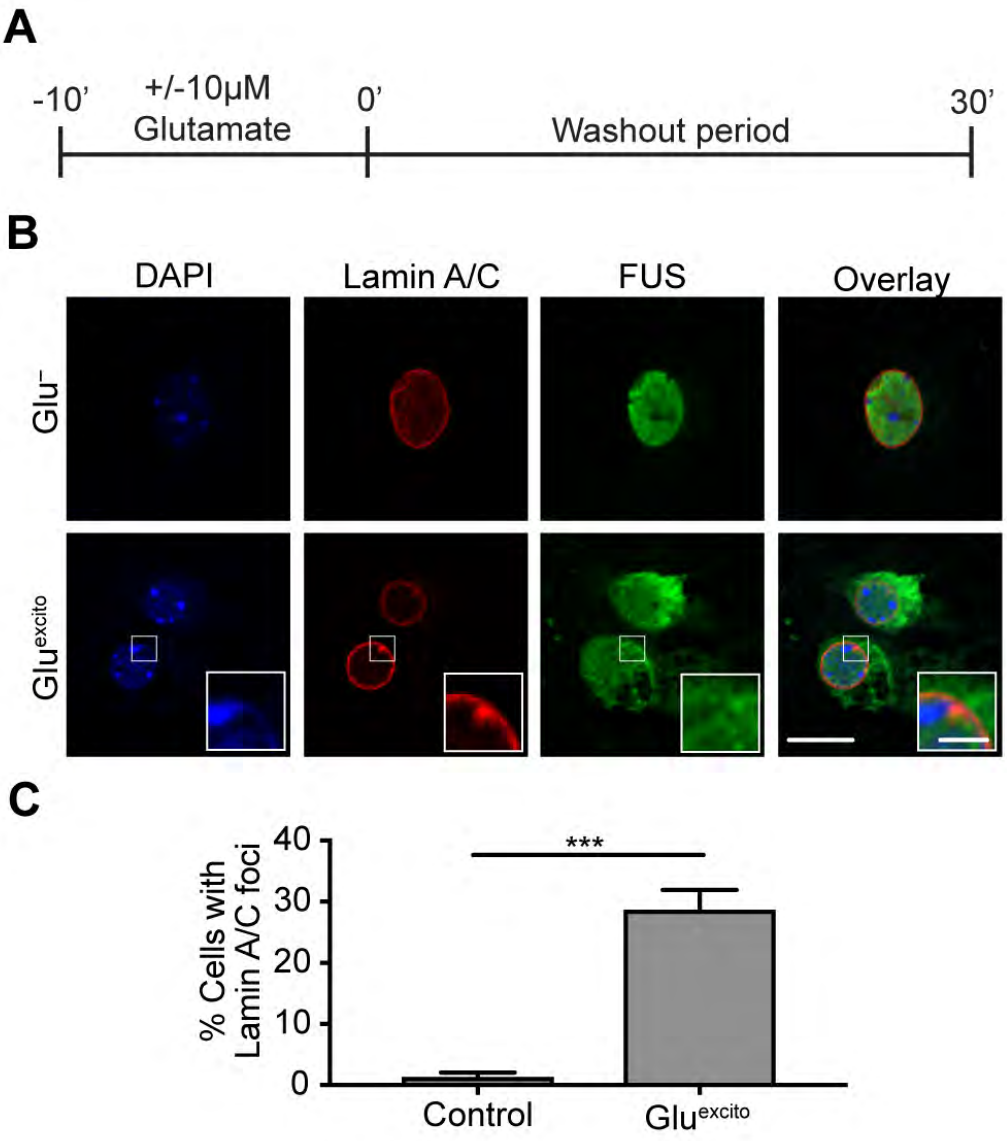

Figure AIII-3. Increased Lamin A/C foci following excitotoxic stress. (A) Excitotoxic stress induced primary cortical neurons using 10μM glutamate for 10 minutes followed by a 30-minute washout period. **(B)** Lamin A/C staining (red) revealed the nuclear envelope as well as the foci exhibiting excitotoxic FUS egress (green). Scale bars = 10μm. High magnification insets of white boxes show FUS staining is not enhanced within Lamin A/C foci. Nuclei were stained with DAPI (blue). High magnification scale bars = 2.5μm. **(C)** The number of neurons with Lamin A/C foci from (B) were significantly increased following excitonic insult (Student's T-test, ***$p<0.001$, n= 4 biological replicates, 46-200 neurons per condition were quantified). Scale bars represent SEM.

neurons, we observed a significant increase in the number of Lamin A/C foci (**Fig. AIII-3A,B**). Moreover, it was qualitatively observed that these granules were not enriched for FUS, an RBP that robustly translocate to the cytoplasmic following excitotoxic insult (**Fig. AIII-3 A**). The observed increase in Lamin A/C-positive distortions observed in a model of ALS are consistent with similar previous finding made in a *Drosophila* model of HGPS. Although the validation of neuronal foci and their functional significance remains to be determined, these data support the potential relevance of Lamin-linked nuclear envelope processes and neurodegenerative disease.

Conclusions

The mislocalization of normally nuclear, disease-linked RBPs is well-documented in models of cellular stress and disease. Moreover, defects in nucleocytoplasmic transport have recently emerged as a common theme in neurodegenerative disease as well. As a result, these observations have sparked an interest in understanding the relationship between these two disease-linked pathologies. Here we consider the relevance of the nuclear envelope and nuclear envelop-linked processes to pathological ALS phenotypes and disease models.

First using a model of the laminopathy, HGPS, we uncovered alterations in the physical expression of the ALS-linked RBPs, FUS and TDP-43. In two separate fibroblasts line expressing the common HGPS mutation, G608G, we observed a significant decrease in TDP-43 protein levels and a trending, but not significant,

decrease in FUS level by western (**Fig. AIII-1**). Interestingly, upon evaluation of these proteins by immunofluorescence, we observed an increased number of G608G-expressing fibroblasts with apparently decreased FUS staining (**Fig. AIII-2A-H**). However, we cannot rule out that FUS may be somehow modified in these mutant cells in a manner that precludes their detection by the antibody used, thus reducing immunoreactivity and appearing decreased. Intriguingly, a pilot immunofluorescence experiment of TDP-43 revealed that, unlike FUS, a loss of TDP-43 staining from a subset of cells was only observed in the G608G (2) line (**Fig. AIII-2I**). Given that a significant decrease in TDP-43 protein levels was observed by western (**Fig. AIII-1**), if reproducible, our immunofluorescence observations suggest that the decrease in TDP-43 levels may possibly reflect a reduction across the population of cells vs. an effect from a subpopulation of cells devoid of TDP-43. Intriguingly, although G608G is known to cause alterations in nuclear morphology (Coutinho et al. 2009), reduced FUS staining was not restricted to cells with notably disturbed nuclear envelopes (**Fig. AIII-2D,C**). This observation suggests that the effect of G608G on FUS is not linked the presence of this phenotype and may result from alternative consequences not evaluated here (i.e. altered chromosomal rearrangement, nuclear pore function etc.).

Together, although the significance of our western and immunofluorescence observations are not clear, it appears that disruptions to the nuclear lamina can alter RBP dynamics. It was surprising that a redistribution of these proteins was not observed, as seen in models of stress and disease (Sama

et al. 2013). To confirm this possibility, a quantitative analysis of FUS staining intensity could be completed; biochemical fractionation might not capture this observed effect, given it occurs in a subset of cells. Intriguingly, sporadic spinal motor neurons with TDP-43, pathology have hnRNPA1 reactivity (another ALS-linked protein) and thus, a similar mechanism could be at play (Honda et al. 2014).

In contrast to the evaluation of phenotypes in a model of disrupted lamin biology, we also assessed if HGPS and lamin-linked processes (megaRNP export) were disrupted in a cellular model of ALS (excitotoxicity), thereby providing insight as to the relevance of nuclear envelope disruptions to ALS. Interestingly, we observed an increase in the number of Lamin A/C-puncta following excitotoxic stress (**Fig. III-3**), consistent with a possibly change to megaRNP export (e.g. increased export or impaired export, resulting in overall increase in number). Given that excitotoxity causes FUS and TDP-43 egress (**Fig. II-2**), influences the processing of synaptic transcripts (**Table II-2, Fig. II-10**) and induces mitochondria dysfunction (the latter two downstream effects linked to megaRNP-contained transcripts (Jokhi et al. 2013, Li et al. 2016)), it is intriguing to think that the functional response of FUS and/or TDP-43 might contribute to the regulation transcripts present within megaRNPs and/or megaRNP complex formation/export itself. However, confirmation of these foci as megaRNP through co-localization of additional markers and visualization by electron microscopy (Speese et al. 2012) would be first required. Upon validation it would be interesting to reduce FUS or TDP-43 levels and/or express ALS-linked mutant proteins and observe their effect

on this phenotype. Although not investigated at this time, the observations described here support a possible connection between lamin-mediated disruptions the nuclear envelope and phenotypes associated with neurodegenerative disease. Thus, they may have relevance to our understanding of the development or consequences of altered nucleocytoplasmic shuttling observed in ALS.

Methods and Materials

Cell Culture and Treatment

Fibroblasts lines were obtained from Coriell (**Table AIII-1**). AG11513 cells were plated on gelatin coated plates (MilliporeSigma G1890); the remaining lines were plated on uncoated dishes. All lines were grown under standard culture conditions (37°C, 5% CO2/95% air). AG11513 was grown in 50:50 Dulbecco's minimal essential medium with glucose (DMEM, Invitrogen 11965118):MEM with Earle's salts (Invitrogen 11095080) supplemented with 2mM L-Glutamine (Gln; 25030081), 1% penicillin and streptomycin (P/S; Invitrogen 15140122) and 15% fetal bovine serum (FBS; not inactivated; MilliporeSigma F2442). Lines: GM00989, AG0697, GM02036 and GM03440 were grown in Eagle's MEM with Earle's Salts supplemented with non-essential amino acids (Invitrogen 11140050), 2mM Gln, 1% P/S and 15% FBS (not inactivated). AG16409 was grown in DMEM with glucose supplemented with 2mM Gln, Sodium Pyruvate (Invitrogen 11360070) and 1% P/S and 10% heat inactivated FBS (MilliporeSigma F4135). All cultures were passed at 1:2-1:5 dilutions. Dissociated neuron cultures were prepared as described (see Chapter III Methods and Materials)

To induce stress, 100mM glutamate (MilliporeSigma G5889) was freshly prepared in Neurobasal media and diluted using primary conditioned media (PCM) to the desired concentration. To apply stress, neuronal media was replaced with glutamate-containing PCM or PCM alone (glutamate-free control) for 10 minutes. After 10 minutes, treatment media was replaced with PCM for 30 minutes or longer depending on the experiment, prior to fixation or lysate collection.

Immunofluorescence, Image Acquisition and Analysis

Immunofluorescence was completed as described (Bosco et al. 2010, Sama et al. 2017) (see Chapter III Methods and Materials). Primary antibodies and dilutions used include: 1:1000 FUS (Bethyl Laboratories A300-293A), 1:500 Lamin A/C (MilliporeSigma SAB4200236) and 1/1000 TDP-43 (EnCor Biotechnology Inc. MCA-3H8). Single plane microglia images were obtained using a Leica DMI6000B microscope as described (Sama et al. 2013). The number of cells with peri-nuclear envelope Lamin A/C foci were quantified and expressed as a percent.

Western Analysis

Whole cell lysates from fibroblasts were obtained and processed for Western as described (Ward et al. 2014) (see Chapter III Methods and Materials). Primary antibodies used include: 1/1000 TDP-43 (EnCor Biotechnology Inc. MCA-3H8), 1/200 FUS (Santa Cruz 4H11 sc-47711) and 1:2000 GAPDH (MilliporeSigma G8795).

Bibliography

Alberti S, Hyman AA. 2016. Are aberrant phase transitions a driver of cellular aging? *Bioessays. 38(10):*959-68

Andersson MK, Ståhlberg A, Arvidsson Y, Olofsson A, Semb H, et al. 2008. The multifunctional FUS, EWS and TAF15 proto-oncoproteins show cell type-specific expression patterns and involvement in cell spreading and stress response. *BMC Cell Biol.* 9(1):37

Antonescu CR, Elahi A, Humphrey M, Lui MY, Healey JH, et al. 2000. Specificity of TLS-CHOP rearrangement for classic myxoid/round cell liposarcoma: absence in predominantly myxoid well-differentiated liposarcomas. *J Mol Diagn*. 2(3):132–38

Archbold HC, Jackson KL, Arora A, Weskamp K, Tank EMH, et al. 2018. TDP43 nuclear export and neurodegeneration in models of amyotrophic lateral sclerosis and frontotemporal dementia. *Sci Rep*. 8(1):4606

Armstrong RA. 2012. On the “classification” of neurodegenerative disorders: discrete entities, overlap or continuum? *Folia Neuropathol*. 50(3):201–8

Aulas A, Fay MM, Lyons SM, Achorn CA, Kedersha N, et al. 2017. Stress-specific differences in assembly and composition of stress granules and related foci. *J Cell Sci.* 130(5):927–37

Bae JS, Simon NG, Menon P, Vucic S, Kiernan MC. 2013. The puzzling case of hyperexcitability in amyotrophic lateral sclerosis. *J Clin Neurol*. 9(2):65–74

Bano D, Dinsdale D, Cabrera-Socorro A, Maida S, Lambacher N, et al. 2010. Alteration of the nuclear pore complex in Ca(2+)-mediated cell death. *Cell Death Differ.* 17(1):119–33

Baron DM, Kaushansky LJ, Ward CL, Sama RRK, Chian R-J, et al. 2013. Amyotrophic lateral sclerosis-linked FUS/TLS alters stress granule assembly and dynamics. *Molecular Neurodegeneration*. 8(1):30

Bensimon G, Lacomblez L, Meininger V. 1994. A controlled trial of riluzole in amyotrophic lateral sclerosis. ALS/Riluzole Study Group. *N Engl J Med.* 330(9):585–91

Bentmann E, Neumann M, Tahirovic S, Rodde R, Dormann D, Haass C. 2012. Requirements for stress granule recruitment of fused in sarcoma (FUS) and TAR DNA-binding protein of 43 kDa (TDP-43). *J. Biol. Chem.* 287(27):23079–94

Berridge MJ, Bootman MD, Roderick HL. 2003. Calcium signalling: dynamics, homeostasis and remodelling. *Nat. Rev. Mol. Cell Biol.* 4(7):517–29

Bertram L, Tanzi RE. 2005. The genetic epidemiology of neurodegenerative disease. *J. Clin. Invest.* 115(6):1449–57

Bezprozvanny I, Hiesinger PR. 2013. The synaptic maintenance problem: membrane recycling, Ca2+ homeostasis and late onset degeneration. *Molecular Neurodegeneration*. 8(1):23

Blokhuis AM, Groen E, Koppers M. 2013. Protein aggregation in amyotrophic lateral sclerosis. *Acta Neuropathol.* 125(6):777-94

Bosco DA, Lemay N, Ko HK, Zhou H, Burke C, et al. 2010. Mutant FUS proteins that cause amyotrophic lateral sclerosis incorporate into stress granules. *Hum. Mol. Gen.* 19(21):4160–75

Boulting GL, Kiskinis E, Croft GF, Amoroso MW, Oakley DH, et al. 2011. A functionally characterized test set of human induced pluripotent stem cells. *Nat. Biotechnol.* 29(3):279–86

Bounedjah O, Hamon L, Savarin P, Desforges B, Curmi PA, Pastré D. 2012. Macromolecular crowding regulates assembly of mRNA stress granules after osmotic stress: new role for compatible osmolytes. *J. Biol. Chem.* 287(4):2446–58

Boyd JD, Lee P, Feiler MS, Zauur N, Liu M, et al. 2014. A high-content screen identifies novel compounds that inhibit stress-induced TDP-43 cellular aggregation and associated cytotoxicity. *J Biomol Screen*. 19(1):44–56

Brocker C, Thompson DC, Vasiliou V. 2012. The role of hyperosmotic stress in inflammation and disease

Brown RH, Al-Chalabi A. 2017. Amyotrophic Lateral Sclerosis. *N Engl J Med.* 377(2):162–72

Buchan JR, Parker R. 2009. Eukaryotic stress granules: the ins and outs of translation. *Mol. Cell*. 36(6):932–41

Burg MB, Ferraris JD, Dmitrieva NI. 2007. Cellular response to hyperosmotic stresses. *Physiological Reviews*

Burke KA, Janke AM, Rhine CL, Fawzi NL. 2015. Residue-by-Residue View of In Vitro FUS Granules that Bind the C-Terminal Domain of RNA Polymerase II. *Mol. Cell*. 60(2):231–41

Buxbaum AR, Wu B, Singer RH. 2014. Single β-actin mRNA detection in neurons reveals a mechanism for regulating its translatability. *Science*. 343(6169):419–22

Cajigas IJ, Tushev G, Will TJ, tom Dieck S, Fuerst N, Schuman EM. 2012. The local transcriptome in the synaptic neuropil revealed by deep sequencing and high-resolution imaging. *Neuron*. 74(3):453–66

Calvio C, Neubauer G, Mann M, Lamond AI. 1995. Identification of hnRNP P2 as TLS/FUS using electrospray mass spectrometry. *RNA*

Cammas A, Pileur F, Bonnal S, Lewis SM, Lévêque N, et al. 2007. Cytoplasmic relocalization of heterogeneous nuclear ribonucleoprotein A1 controls translation initiation of specific mRNAs. *Mol. Biol. Cell*. 18(12):5048–59

Capauto D, Colantoni A, Lu L, Santini T, Peruzzi G, et al. 2018. A Regulatory Circuitry Between Gria2, miR-409, and miR-495 Is Affected by ALS FUS Mutation in ESC-Derived Motor Neurons. *Mol. Neurobiol.* 344(22):1688–17

Cheah BC, Vucic S, Krishnan AV, Kiernan MC. 2010. Riluzole, neuroprotection and amyotrophic lateral sclerosis. *Curr. Med. Chem.* 17(18):1942–1199

Chen H, Richard M, Sandler DP, Umbach DM, Kamel F. 2007. Head injury and amyotrophic lateral sclerosis. *Am. J. Epidemiol.* 166(7):810–16

Chen S, Tran S, Sigler A, Murphy TH. 2011. Automated and quantitative image analysis of ischemic dendritic blebbing using< i> in vivo</i> 2-photon microscopy data. *J. Neurosci. Methods*

Chiu DN, Jahr CE. 2017. Extracellular Glutamate in the Nucleus Accumbens Is Nanomolar in Both Synaptic and Non-synaptic Compartments. *Cell Rep*. 18(11):2576–83

Chou C-C, Zhang Y, Umoh ME, Vaughan SW, Lorenzini I, et al. 2018. TDP-43 pathology disrupts nuclear pore complexes and nucleocytoplasmic transport in ALS/FTD. *Nat Neurosci.* 21(2):228–39

Chovatiya R, Medzhitov R. 2014. Stress, inflammation, and defense of homeostasis. *Mol. Cell*. 54(2):281–88

Ciervo Y, Ning K, Jun X, Shaw PJ, Mead RJ. 2017. Advances, challenges and future directions for stem cell therapy in amyotrophic lateral sclerosis. *Molecular Neurodegeneration*. 12(1):85

Ciryam P, Lambert-Smith IA, Bean DM, Freer R, Cid F, et al. 2017. Spinal motor neuron protein supersaturation patterns are associated with inclusion body formation in ALS. *Proc. Natl. Acad. Sci. U.S.A.* 114(20):E3935–43

Colombrita C, Zennaro E, Fallini C, Weber M, Sommacal A, et al. 2009. TDP-43 is recruited to stress granules in conditions of oxidative insult. *J Neurochem.* 111(4):1051–61

Conicella AE, Zerze GH, Mittal J, Fawzi NL. 2016. ALS Mutations Disrupt Phase Separation Mediated by α-Helical Structure in the TDP-43 Low-Complexity C-Terminal Domain. *Structure*. 24(9):1537–49

Couratier P, Corcia P, Lautrette G, Nicol M, Marin B. 2017. ALS and frontotemporal dementia belong to a common disease spectrum. *Rev. Neurol. (Paris)*. 173(5):273–79

Coutinho HDM, Falcão-Silva VS, Gonçalves GF, da Nóbrega RB. 2009. Molecular ageing in progeroid syndromes: Hutchinson-Gilford progeria syndrome as a model. *Immun Ageing*. 6:4

Crozat A, Aman P, Mandahl N, Ron D. 1993. Fusion of CHOP to a novel RNA-binding protein in human myxoid liposarcoma. *Nature*. 363(6430):640–44

Cull-Candy S, Kelly L, Farrant M. 2006. Regulation of Ca2+-permeable AMPA receptors: synaptic plasticity and beyond. *Curr. Opin. Neurobiol.* 16(3):288–97

Dao TP, Kolaitis R-M, Kim HJ, O'Donovan K, Martyniak B, et al. 2018. Ubiquitin Modulates Liquid-Liquid Phase Separation of UBQLN2 via Disruption of Multivalent Interactions. *Mol. Cell*. 69(6):965–66

Darovic S, Mihevc SP, Župunski V, Gunčar G, Štalekar M, et al. 2015. Phosphorylation of C-terminal tyrosine 526 in FUS impairs its nuclear import. *J Cell Sci.*

Davis GW. 2013. Homeostatic signaling and the stabilization of neural function. *Neuron*. 80(3):718–28

de Lourdes Martínez-Silva M, Imhoff-Manuel RD, Sharma A, Heckman CJ, Shneider NA, et al. 2018. Hypoexcitability precedes denervation in the large

fast-contracting motor units in two unrelated mouse models of ALS. *Elife*. 7:e30955

DeJesus-Hernandez M, Mackenzie IR, Boeve BF, Boxer AL, Baker M, et al. 2011. Expanded GGGGCC hexanucleotide repeat in noncoding region of C9ORF72 causes chromosome 9p-linked FTD and ALS. *Neuron*. 72(2):245–56

Delestrée N, Manuel M, Iglesias C, Elbasiouny SM, Heckman CJ, Zytnicki D. 2014. Adult spinal motoneurones are not hyperexcitable in a mouse model of inherited amyotrophic lateral sclerosis. *J. Physiol. (Lond.)*. 592(7):1687–1703

Deng H, Gao K, Jankovic J. 2014a. The role of FUS gene variants in neurodegenerative diseases. *Nat Rev Neurol.* 10(6):337–48

Deng H-X, Zhai H, Bigio EH, Yan J, Fecto F, et al. 2010. FUS-immunoreactive inclusions are a common feature in sporadic and non-SOD1 familial amyotrophic lateral sclerosis. *Ann Neurol.* 67(6):739–48

Deng Q, Holler CJ, Taylor G, Hudson KF, Watkins W, et al. 2014b. FUS is Phosphorylated by DNA-PK and Accumulates in the Cytoplasm after DNA Damage. *J Neurosci.* 34(23):7802–13

Devlin A-C, Burr K, Borooah S, Foster JD, Cleary EM, et al. 2015. Human iPSC-derived motoneurons harbouring TARDBP or C9ORF72 ALS mutations are dysfunctional despite maintaining viability. *Nat Commun*. 6:5999

Dewey CM, Cenik B, Sephton CF, Dries DR, Mayer P, et al. 2011. TDP-43 is directed to stress granules by sorbitol, a novel physiological osmotic and oxidative stressor. *Mol. Cell. Biol.* 31(5):1098–1108

Di Giorgio FP, Carrasco MA, Siao MC, Maniatis T, Eggan K. 2007. Non-cell autonomous effect of glia on motor neurons in an embryonic stem cell-based ALS model. *Nat Neurosci.* 10(5):608–14

Doi H, Koyano S, Suzuki Y, Nukina N, Kuroiwa Y. 2010. The RNA-binding protein FUS/TLS is a common aggregate-interacting protein in polyglutamine diseases. *Neurosci. Res.* 66(1):131–33

Dong X-X, Wang Y, Qin Z-H. 2009. Molecular mechanisms of excitotoxicity and their relevance to pathogenesis of neurodegenerative diseases. *Acta Pharmacol Sin.* 30(4):379–87

Donnelly CJ, Zhang P-W, Pham JT, Heusler AR, Mistry NA, et al. 2013. RNA toxicity from the ALS/FTD C9ORF72 expansion is mitigated by antisense intervention. *Neuron*. 80(2):415–28

Dormann D, Haass C. 2011. TDP-43 and FUS: a nuclear affair. *Trends Neurosci.* 34(7):339–48

Dormann D, Haass C. 2013. Fused in sarcoma (FUS): an oncogene goes awry in neurodegeneration. *Mol. Cell. Neurosci.* 56:475–86

Dormann D, Madl T, Valori CF, Bentmann E, Tahirovic S, et al. 2012. Arginine methylation next to the PY-NLS modulates Transportin binding and nuclear import of FUS. *EMBO J.* 31(22):4258–75

Dormann D, Rodde R, Edbauer D, Bentmann E, Fischer I, et al. 2010. ALS-associated fused in sarcoma (FUS) mutations disrupt Transportin-mediated nuclear import. *EMBO J.* 29(16):2841–57

Ederle H, Funk C, Abou-Ajram C, Hutten S, Funk EBE, et al. 2018. Nuclear egress of TDP-43 and FUS occurs independently of Exportin-1/CRM1. *Sci Rep*. 8(1):7084

Elobeid A, Libard S, Leino M, Popova SN, Alafuzoff I. 2016. Altered Proteins in the Aging Brain. *Journal of Neuropathology & Experimental Neurology*. 75(4):316–25

Eykens C, Robberecht W. 2015. The Genetic basis of amyotrophic lateral sclerosis: recent breakthroughs. *Advances in Genomics and Genetics.* 5:327-345

Fan J, Long H, Li Y, Liu Y, Zhou W, et al. 2013. Edaravone protects against glutamate-induced PERK/EIF2α/ATF4 integrated stress response and activation of caspase-12. *Brain Research*. 1519:1–8

Fay MM, Anderson PJ, Ivanov P. 2017. ALS/FTD-Associated C9ORF72 Repeat RNA Promotes Phase Transitions In Vitro and in Cells. *Cell Rep*. 21(12):3573–84

Feigin VL, Abajobir AA, Abate KH, et al. 2017. Global, regional, and national burden of neurological disorders during 1990–2015: a systematic analysis for the Global Burden of Disease Study 2015. *Lancet Neurol.* 16(11):877-897

Fiszman ML, Ricart KC, Latini A, Rodríguez G, Sica REP. 2010. In vitro neurotoxic properties and excitatory aminoacids concentration in the cerebrospinal fluid of amyotrophic lateral sclerosis patients. Relationship with the degree of certainty of disease diagnoses. *Acta Neurol. Scand.* 121(2):120–26

Fogarty MJ. 2018. Driven to decay: Excitability and synaptic abnormalities in amyotrophic lateral sclerosis. *Brain Research Bulletin*. 140:318–33

Fradkin LG, Budnik V. 2016. This bud's for you: mechanisms of cellular nucleocytoplasmic trafficking via nuclear envelope budding. *Curr. Opin. Cell Biol.* 41:125–31

Freibaum BD, Lu Y, Lopez-Gonzalez R, Kim NC, Almeida S, et al. 2015. GGGGCC repeat expansion in C9orf72 compromises nucleocytoplasmic transport. *Nature*. 525(7567):129–33

Frey S, Rees R, Schünemann J, Ng SC, Fünfgeld K, et al. 2018. Surface Properties Determining Passage Rates of Proteins through Nuclear Pores. *Cell*. 174(1):202–9

Fricker M, Tolkovsky AM, Borutaite V, Coleman M, Brown GC. 2018. Neuronal Cell Death. *Physiological Reviews*. 98(2):813–80

Fritz E, Izaurieta P, Weiss A, Mir FR, Rojas P, et al. 2013. Mutant SOD1-expressing astrocytes release toxic factors that trigger motoneuron death by inducing hyperexcitability. *J. Neurophysiol.* 109(11):2803–14

Frost B, Bardai FH, Feany MB. 2016. Lamin Dysfunction Mediates Neurodegeneration in Tauopathies. *Curr Biol.* 26(1):129–36

Fryer HJ, Knox RJ, Strittmatter SM, Kalb RG. 1999. Excitotoxic death of a subset of embryonic rat motor neurons in vitro. *J Neurochem.* 72(2):500–513

Fujii R, Okabe S, Urushido T, Inoue K, Yoshimura A, et al. 2005. The RNA binding protein TLS is translocated to dendritic spines by mGluR5 activation and regulates spine morphology. *Curr Biol.* 15(6):587–93

Fujii R, Takumi T. 2005. TLS facilitates transport of mRNA encoding an actin-stabilizing protein to dendritic spines. *J Cell Sci.* 118(Pt 24):5755–65

Gal J, Zhang J, Kwinter DM, Zhai J, Jia H, et al. 2011. Nuclear localization sequence of FUS and induction of stress granules by ALS mutants. *Neurobiol. Aging*. 32(12):2323.e27–.e40

Gandhi S, Abramov AY. 2012. Mechanism of Oxidative Stress in Neurodegeneration. *Oxidative Medicine and Cellular Longevity*. 2012(3):1–11

Gascon E, Lynch K, Ruan H, Almeida S, Verheyden JM, et al. 2014. Alterations in microRNA-124 and AMPA receptors contribute to social behavioral deficits in frontotemporal dementia. *Nature Medicine*. 20(12):1444–51

Geevasinga N, Menon P, Nicholson GA, Ng K, Howells J, et al. 2015. Cortical Function in Asymptomatic Carriers and Patients With C9orf72 Amyotrophic Lateral Sclerosis. *JAMA Neurol*. 72(11):1268–74

Green KM, Glineburg MR, Kearse MG, Flores BN, Linsalata AE, et al. 2017. RAN translation at C9orf72-associated repeat expansions is selectively enhanced by the integrated stress response. *Nat Commun*. 8(1):2005

Grima JC, Daigle JG, Arbez N, Cunningham KC. 2017. Mutant Huntingtin Disrupts the Nuclear Pore Complex. *Neuron*

Guo L, Kim HJ, Wang H, Monaghan J, Freyermuth F, et al. 2018. Nuclear-Import Receptors Reverse Aberrant Phase Transitions of RNA-Binding Proteins with Prion-like Domains. *Cell*. 173(3):677–692.e20

Haines JD, Herbin O, la Hera de B, Vidaurre OG, Moy GA, et al. 2015. Nuclear export inhibitors avert progression in preclinical models of inflammatory demyelination. *Nat Neurosci.* 18(4):511–20

Han TW, Kato M, Xie S, Wu LC, Mirzaei H, et al. 2012. Cell-free Formation of RNA Granules: Bound RNAs Identify Features and Components of Cellular Assemblies. *Cell*. 149(4):768–79

Hatch EM, Fischer AH, Deerinck TJ, Hetzer MW. 2013. Catastrophic nuclear envelope collapse in cancer cell micronuclei. *Cell*. 154(1):47–60

Heise C, Gardoni F, Culotta L, di Luca M, Verpelli C, Sala C. 2014. Elongation factor-2 phosphorylation in dendrites and the regulation of dendritic mRNA translation in neurons. *Front Cell Neurosci*. 8:35

Hicks GG, Singh N, Nashabi A, Mai S, Bozek G, et al. 2000. Fus deficiency in mice results in defective B-lymphocyte development and activation, high levels of chromosomal instability and perinatal death. *Nat Genet.* 24(2):175–79

Hideyama T, Yamashita T, Aizawa H, Tsuji S, Kakita A, et al. 2012. Profound downregulation of the RNA editing enzyme ADAR2 in ALS spinal motor neurons. *Neurobiology of Disease*. 45(3):1121–28

Hirokawa N. 2006. mRNA transport in dendrites: RNA granules, motors, and tracks. *J Neurosci.* 26(27):7139–42

Hofweber M, Hutten S, Bourgeois B, Spreitzer E, Niedner-Boblenz A, et al. 2018. Phase Separation of FUS Is Suppressed by Its Nuclear Import Receptor and Arginine Methylation. *Cell*. 173(3):706–13

Holcik M, Sonenberg N. 2005. Translational control in stress and apoptosis. *Nat. Rev. Mol. Cell Biol.* 6(4):318–27

Holt CE, Schuman EM. 2013. The central dogma decentralized: new perspectives on RNA function and local translation in neurons. *Neuron*. 80(3):648–57

Honda H, Hamasaki H, Wakamiya T, Koyama S, Suzuki SO, et al. 2014. Loss of hnRNPA1 in ALS spinal cord motor neurons with TDP-43-positive inclusions. *Neuropathology*. 35(1):37–43

Ichikawa H, Shimizu K, Hayashi Y, Ohki M. 1994. An RNA-binding protein gene, TLS/FUS, is fused to ERG in human myeloid leukemia with t(16;21) chromosomal translocation. *Cancer Res.* 54(11):2865–68

Iko Y, Kodama TS, Kasai N, Oyama T, Morita EH, et al. 2004. Domain architectures and characterization of an RNA-binding protein, TLS. *Journal of Biological Chemistry*. 279(43):44834–40

Ilieva EV, Ayala V, Jové M, Dalfó E, Cacabelos D, et al. 2007. Oxidative and endoplasmic reticulum stress interplay in sporadic amyotrophic lateral sclerosis. *Brain*. 130(Pt 12):3111–23

Imamura K, Sahara N, Kanaan NM, Tsukita K, Kondo T, et al. 2016. Calcium dysregulation contributes to neurodegeneration in FTLD patient iPSC-derived neurons. *Sci Rep*. 6:34904

Ishigaki S, Masuda A, Fujioka Y, Iguchi Y, Katsuno M, et al. 2012. Position-dependent FUS-RNA interactions regulate alternative splicing events and transcriptions. *Sci Rep*. 2:529

Ito D, Hatano M, Suzuki N. 2017. RNA binding proteins and the pathological cascade in ALS/FTD neurodegeneration. *Sci Transl Med*. 9(415):eaah5436

Johnson JO, Pioro EP, Boehringer A, Chia R, Feit H, et al. 2014. Mutations in the Matrin 3 gene cause familial amyotrophic lateral sclerosis. *Nat Neurosci.* 17(5):664–66

Jokhi V, Ashley J, Nunnari J, Noma A, Ito N, et al. 2013. Torsin mediates primary envelopment of large ribonucleoprotein granules at the nuclear envelope. *Cell Rep*. 3(4):988–95

Ju W, Morishita W, Tsui J, Gaietta G, Deerinck TJ, et al. 2004. Activity-dependent regulation of dendritic synthesis and trafficking of AMPA receptors. *Nat Neurosci.* 7(3):244–53

Kabashi E, Valdmanis PN, Dion P, Spiegelman D, McConkey BJ, et al. 2008. TARDBP mutations in individuals with sporadic and familial amyotrophic lateral sclerosis. *Nat Genet.* 40(5):572–74

Kahl A, Blanco I, Jackman K, Baskar J, Milaganur Mohan H, et al. 2018. Cerebral ischemia induces the aggregation of proteins linked to neurodegenerative diseases. *Sci Rep*. 8(1):2701

Kanai K, Shibuya K, Sato Y, Misawa S, Nasu S, et al. 2012. Motor axonal excitability properties are strong predictors for survival in amyotrophic lateral sclerosis. *J. Neurol. Neurosurg. Psychiatry*. 83(7):734–38

Kanai Y, Dohmae N, Hirokawa N. 2004. Kinesin transports RNA: isolation and characterization of an RNA-transporting granule. *Neuron*. 43(4):513–25

Kapeli K, Martinez FJ, Yeo GW. 2017. Genetic mutations in RNA-binding proteins and their roles in ALS. *Hum. Genet.* 136(9):1193–1214

Kato M, Han TW, Xie S, Shi K, Du X, et al. 2012. Cell-free formation of RNA granules: low complexity sequence domains form dynamic fibers within hydrogels. *Cell*. 149(4):753–67

Kawahara Y, Ito K, Sun H, Aizawa H, Kanazawa I, Kwak S. 2004. Glutamate receptors: RNA editing and death of motor neurons. *Nature*. 427(6977):801–1

Kawahara Y, Ito K, Sun H, Kanazawa I, Kwak S. 2003. Low editing efficiency of GluR2 mRNA is associated with a low relative abundance of ADAR2 mRNA in white matter of normal human brain. *Eur. J. Neurosci.* 18(1):23–33

Kawamori D, Kajimoto Y, Kaneto H, Umayahara Y, Fujitani Y, et al. 2003. Oxidative stress induces nucleo-cytoplasmic translocation of pancreatic transcription factor PDX-1 through activation of c-Jun NH(2)-terminal kinase. *Diabetes*. 52(12):2896–2904

Kedersha N, Anderson P. 2007. Mammalian stress granules and processing bodies. *Meth. Enzymol.* 431:61–81

Kedersha N, Ivanov P, Anderson P. 2013. Stress granules and cell signaling: more than just a passing phase? *Trends Biochem. Sci.* 38(10):494–506

Keller BA, Volkening K, Droppelmann CA, Ang L-C, Rademakers R, Strong MJ. 2012. Co-aggregation of RNA binding proteins in ALS spinal motor neurons: evidence of a common pathogenic mechanism. *Acta Neuropathol.* 124(5):733–47

Kelley JB, Paschal BM. 2007. Hyperosmotic stress signaling to the nucleus disrupts the Ran gradient and the production of RanGTP. *Mol. Biol. Cell*. 18(11):4365–76

Kia A, McAvoy K, Krishnamurthy K, Trotti D, Pasinelli P. 2018. Astrocytes expressing ALS-linked mutant FUS induce motor neuron death through release of tumor necrosis factor-alpha. *Glia*. 66(5):1016–33

Kiernan MC, Vucic S, Cheah BC, Turner MR, Eisen A. 2011. Amyotrophic lateral sclerosis. *The Lancet*

Kim HJ, Taylor JP. 2017. Lost in Transportation: Nucleocytoplasmic Transport Defects in ALS and Other Neurodegenerative Diseases. *Neuron*. 96(2):285–97

Kino Y, Washizu C, Aquilanti E, Okuno M, Kurosawa M, et al. 2011. Intracellular localization and splicing regulation of FUS/TLS are variably affected by

amyotrophic lateral sclerosis-linked mutations. *Nucleic Acids Res.* 39(7):2781–98

Kino Y, Washizu C, Kurosawa M, Yamada M, Miyazaki H, et al. 2015. FUS/TLS deficiency causes behavioral and pathological abnormalities distinct from amyotrophic lateral sclerosis. *Acta Neuropathol Commun*. 3(1):24

Kinoshita Y, Ito H, Hirano A, Fujita K, Wate R, et al. 2009. Nuclear Contour Irregularity and Abnormal Transporter Protein Distribution in Anterior Horn Cells in Amyotrophic Lateral Sclerosis. *Journal of Neuropathology & Experimental Neurology*. 68(11):1184–92

Klint P, Hellman U, Wernstedt C, Aman P, Ron D. 2004. Translocated in liposarcoma (TLS) is a substrate for fibroblast growth factor receptor-1. *Cell Signal.* 16(4):515–20

Kodiha M, Chu A, Matusiewicz N, Stochaj U. 2004. Multiple mechanisms promote the inhibition of classical nuclear import upon exposure to severe oxidative stress. *Cell Death Differ.* 11(8):862–74

Koleske AJ. 2013. Molecular mechanisms of dendrite stability. *Nat. Rev. Neurosci.* 14(8):536–50

Kotas ME, Medzhitov R. 2015. Homeostasis, inflammation, and disease susceptibility. *Cell*. 160(5):816–27

Kuroda M, Sok J, Webb L, Baechtold H, Urano F, et al. 2000. Male sterility and enhanced radiation sensitivity in TLS(-/-) mice. *EMBO J.* 19(3):453–62

Kültz D. 2005. Molecular and evolutionary basis of the cellular stress response. *Annu. Rev. Physiol.* 67:225–57

Kwiatkowski TJ, Bosco DA, LeClerc AL, Tamrazian E, Vanderburg CR, et al. 2009. Mutations in the FUS/TLS gene on chromosome 16 cause familial amyotrophic lateral sclerosis. *Science*. 323(5918):1205–8

Kwon I, Kato M, Xiang S, Wu L, Theodoropoulos P, et al. 2013. Phosphorylation-regulated binding of RNA polymerase II to fibrous polymers of low-complexity domains. *Cell*. 155(5):1049–60

Lagier-Tourenne C, Polymenidou M, Cleveland DW. 2010. TDP-43 and FUS/TLS: emerging roles in RNA processing and neurodegeneration. *Hum. Mol. Gen.* 19(R1):R46–R64

Lagier-Tourenne C, Polymenidou M, Hutt KR, Vu AQ, Baughn M, et al. 2012. Divergent roles of ALS-linked proteins FUS/TLS and TDP-43 intersect in processing long pre-mRNAs. *Nat Neurosci.* 15(11):1488–97

Lanson NA, Pandey UB. 2012. FUS-related proteinopathies: lessons from animal models. *Brain Research*. 1462:44–60

Lattante S, Rouleau GA, Kabashi E. 2013. TARDBP and FUS mutations associated with amyotrophic lateral sclerosis: summary and update. *Hum. Mutat.* 34(6):812–26

Le Verche V, Ikiz B, Jacquier A. 2011. Glutamate pathway implication in amyotrophic lateral sclerosis: what is the signal in the noise. *J Receptor Ligand.* 4:1-22

Lee BJ, Cansizoglu AE, Süel KE, Louis TH, Zhang Z, Chook YM. 2006. Rules for nuclear localization sequence recognition by karyopherin beta 2. *Cell*. 126(3):543–58

Lee K-H, Zhang P, Kim HJ, Mitrea DM, Sarkar M, et al. 2016. C9orf72 Dipeptide Repeats Impair the Assembly, Dynamics, and Function of Membrane-Less Organelles. *Cell*. 167(3):774–788.e17

Lenzi J, De Santis R, de Turris V, Morlando M, Laneve P, et al. 2015. ALS mutant FUS proteins are recruited into stress granules in induced pluripotent stem cell-derived motoneurons. *Dis Model Mech*. 8(7):755–66

Li N, Lagier-Tourenne C. 2018. Nuclear pores: the gate to neurodegeneration. *Nat Neurosci.* 21(2):156–58

Li Y, Hassinger L, Thomson T, Ding B, Ashley J, et al. 2016. Lamin Mutations Accelerate Aging via Defective Export of Mitochondrial mRNAs through Nuclear Envelope Budding. *Curr Biol.* 26(15):2052–59

Lien YH, Shapiro JI, Chan L. 1990. Effects of hypernatremia on organic brain osmoles. *J. Clin. Invest.* 85(5):1427–35

Lim SM, Choi WJ, Oh K-W, Xue Y, Choi JY, et al. 2016. Directly converted patient-specific induced neurons mirror the neuropathology of FUS with disrupted nuclear localization in amyotrophic lateral sclerosis. *Molecular Neurodegeneration*. 1–13

Lin J-C, Hsu M, Tarn W-Y. 2007. Cell stress modulates the function of splicing regulatory protein RBM4 in translation control. *PNAS*. 104(7):2235–40

Ling S-C. 2018. Synaptic Paths to Neurodegeneration: The Emerging Role of TDP-43 and FUS in Synaptic Functions. *Neural Plast.* 2018:8413496

Ling S-C, Polymenidou M, Cleveland DW. 2013. Converging mechanisms in ALS and FTD: disrupted RNA and protein homeostasis. *Neuron*. 79(3):416–38

Liu SJ, Cull-Candy SG. 2005. Subunit interaction with PICK and GRIP controls Ca2+ permeability of AMPARs at cerebellar synapses. *Nat Neurosci.* 8(6):768–75

Liu SJ, Zukin RS. 2007. Ca2+-permeable AMPA receptors in synaptic plasticity and neuronal death. *Trends Neurosci.* 30(3):126–34

Liu X, Niu C, Ren J, Zhang J, Xie X, et al. 2013. The RRM domain of human fused in sarcoma protein reveals a non-canonical nucleic acid binding site. *Biochim Biophys Acta*. 1832(2):375–85

Liu Y, Gao Y, Wu Y, Wang H. 2010. Histochemical Mapping of hnRNP A2/B1 in Rat Brain After Ischemia–Reperfusion Insults. *… of Histochemistry & …*

Lu T, Pan Y, Kao SY, Li C, Kohane I, et al. Gene regulation and DNA damage in the ageing human brain. *Nature.* 429(6994):883-91

Madabhushi R, Pan L, Tsai L-H. 2014. DNA damage and its links to neurodegeneration. *Neuron*. 83(2):266–82

Maharana S, Wang J, Papadopoulos DK, Richter D, Pozniakovsky A, et al. 2018. RNA buffers the phase separation behavior of prion-like RNA binding proteins. *Science*

Marin P, Nastiuk KL, Daniel N, Girault JA, Czernik AJ, et al. 1997. Glutamate-dependent phosphorylation of elongation factor-2 and inhibition of protein synthesis in neurons. *J. Neurosci.* 17(10):3445–54

Marini AM, Jiang H, Pan H, Wu X, Lipsky RH. 2008. Hormesis: a promising strategy to sustain endogenous neuronal survival pathways against neurodegenerative disorders. *Ageing Res. Rev.* 7(1):21–33

Maruyama H, Morino H, Ito H, Izumi Y, Kato H, et al. 2010. Mutations of optineurin in amyotrophic lateral sclerosis. *Nature*. 465(7295):223–26

Mathis S, Le Masson G. 2018. RNA-Targeted Therapies and Amyotrophic Lateral Sclerosis. *Biomedicines*. 6(1):

Mattson MP, Magnus T. 2006. Ageing and neuronal vulnerability. *Nat. Rev. Neurosci.* 7(4):278–94

McClintock D, Ratner D, Lokuge M, Owens DM, Gordon LB, et al. 2007. The mutant form of lamin A that causes Hutchinson-Gilford progeria is a biomarker of cellular aging in human skin. *PLoS ONE*. 2(12):e1269

McConnell MJ, Lindberg MR, Brennand KJ, Piper JC, Voet T, et al. 2013. Mosaic copy number variation in human neurons. *Science*. 342(6158):632–37

McDonald KK, Aulas A, Destroismaisons L, Pickles S, Beleac E, et al. 2011. TAR DNA-binding protein 43 (TDP-43) regulates stress granule dynamics via differential regulation of G3BP and TIA-1. *Hum. Mol. Gen.* 20(7):1400–1410

Mehta P, Kaye W, Raymond J, Wu R, Larson T, et al. 2018. Prevalence of Amyotrophic Lateral Sclerosis - United States, 2014. *MMWR Morb. Mortal. Wkly. Rep.* 67(7):216–18

Merner ND, Girard SL, Catoire H, Bourassa CV, Belzil VV, et al. 2012. Exome sequencing identifies FUS mutations as a cause of essential tremor. *Am. J. Hum. Genet.* 91(2):313–19

Mili S, Moissoglu K, Macara IG. 2008. Genome-wide screen reveals APC-associated RNAs enriched in cell protrusions. *Nature*. 453(7191):115–19

Miller JD, Ganat YM, Kishinevsky S, Bowman RL, Liu B, et al. 2013. Human iPSC-based modeling of late-onset disease via progerin-induced aging. *Cell Stem Cell*. 13(6):691–705

Miller RG, Mitchell JD, Moore DH. 2012. Riluzole for amyotrophic lateral sclerosis (ALS)/motor neuron disease (MND). *Cochrane Database Syst Rev*. (3):CD001447

Mitchell J, Paul P, Chen H-J, Morris A, Payling M, et al. 2010. Familial amyotrophic lateral sclerosis is associated with a mutation in D-amino acid oxidase. *Proc. Natl. Acad. Sci. U.S.A.* 107(16):7556–61

Mitchell JC, Mcgoldrick P, Vance C, Hortobágyi T, Sreedharan J, et al. 2013. Overexpression of human wild-type FUS causes progressive motor neuron degeneration in an age- and dose-dependent fashion. *Acta Neuropathol.* 125(2):273–88

Molliex A, Temirov J, Lee J, Coughlin M, Kanagaraj AP, et al. 2015. Phase separation by low complexity domains promotes stress granule assembly and drives pathological fibrillization. *Cell*. 163(1):123–33

Moussawi K, Riegel A, Nair S, Kalivas PW. 2011. Extracellular glutamate: functional compartments operate in different concentration ranges. *Front Syst Neurosci.* 5:94

Murakami T, Qamar S, Lin JQ, Schierle GSK, Rees E, et al. 2015. ALS/FTD Mutation-Induced Phase Transition of FUS Liquid Droplets and Reversible Hydrogels into Irreversible Hydrogels Impairs RNP Granule Function. *Neuron*. 88(4):678–90

Murphy TH, Li P, Betts K, Liu R. 2008. Two-photon imaging of stroke onset in vivo reveals that NMDA-receptor independent ischemic depolarization is the major cause of rapid reversible damage to dendrites and spines. *J Neurosci.* 28(7):1756–72

Musiek ES, Holtzman DM. 2016. Mechanisms linking circadian clocks, sleep, and neurodegeneration. *Science*. 354(6315):1004–8

Nagai M, Re DB, Nagata T, Chalazonitis A, Jessell TM, et al. 2007. Astrocytes expressing ALS-linked mutated SOD1 release factors selectively toxic to motor neurons. *Nat Neurosci.* 10(5):615–22

Nakaya T, Alexiou P, Maragkakis M, Chang A, Mourelatos Z. 2013. FUS regulates genes coding for RNA-binding proteins in neurons by binding to their highly conserved introns. *RNA*. 19(4):498–509

Naujock M, Stanslowsky N, Bufler S, Naumann M, Reinhardt P, et al. 2016. 4-Aminopyridine Induced Activity Rescues Hypoexcitable Motor Neurons from Amyotrophic Lateral Sclerosis Patient-Derived Induced Pluripotent Stem Cells. *Stem Cells*. 34(6):1563–75

Neumann M, Bentmann E, Dormann D, Jawaid A, DeJesus-Hernandez M, et al. 2011. FET proteins TAF15 and EWS are selective markers that distinguish FTLD with FUS pathology from amyotrophic lateral sclerosis with FUS mutations. *Brain*. 134(9):2595–2609

Neumann M, Rademakers R, Roeber S, Baker M, Kretzschmar HA, Mackenzie IRA. 2009a. A new subtype of frontotemporal lobar degeneration with FUS pathology. *Brain*. 132(Pt 11):2922–31

Neumann M, Roeber S, Kretzschmar HA, Rademakers R, Baker M, Mackenzie IRA. 2009b. Abundant FUS-immunoreactive pathology in neuronal intermediate filament inclusion disease. *Acta Neuropathol.* 118(5):605–16

Ng S-Y, Soh BS, Rodriguez-Muela N, Hendrickson DG, Price F, et al. 2015. Genome-wide RNA-Seq of Human Motor Neurons Implicates Selective ER Stress Activation in Spinal Muscular Atrophy. *Cell Stem Cell*. 17(5):569–84

Nijssen J, Comley LH, Hedlund E. 2017. Motor neuron vulnerability and resistance in amyotrophic lateral sclerosis. *Acta Neuropathol.* 133(6):863–85

Nutt SL, Kamboj RK. 1994. Differential RNA editing efficiency of AMPA receptor subunit GluR-2 in human brain. *Neuroreport*. 5(13):1679–83

Olney JW. 1989. Excitatory amino acids and neuropsychiatric disorders. *Biol. Psychiatry*. 26(5):505–25

Palop JJ, Chin J, Mucke L. 2006. A network dysfunction perspective on neurodegenerative diseases. *Nature*. 443(7113):768–73

Patel A, Lee HO, Jawerth L, Maharana S, Jahnel M, et al. 2015. A Liquid-to-Solid Phase Transition of the ALS Protein FUS Accelerated by Disease Mutation. *Cell*. 162(5):1066–77

Peters OM, Ghasemi M, Brown RH. 2015. Emerging mechanisms of molecular pathology in ALS. *J. Clin. Invest.* 125(5):1767–79

Plaitakis A, Constantakakis E. 1993. Altered metabolism of excitatory amino acids, N-acetyl-aspartate and N-acetyl-aspartylglutamate in amyotrophic lateral sclerosis. *Brain Research Bulletin*

Posey AE, Ruff KM, Harmon TS, Crick SL, Li A, et al. 2018. Profilin reduces aggregation and phase separation of huntingtin N-terminal fragments by preferentially binding to soluble monomers and oligomers. *J. Biol. Chem.* 293(10):3734–46

Qamar S, Wang G, Randle SJ, Ruggeri FS, Varela JA, et al. 2018. FUS Phase Separation Is Modulated by a Molecular Chaperone and Methylation of Arginine Cation-π Interactions. *Cell*. 173(3):720–734.e15

Raddaoui E, Donner LR, Panagopoulos I. 2002. Fusion of the FUS and ATF1 genes in a large, deep-seated angiomatoid fibrous histiocytoma. *Diagn. Mol. Pathol.* 11(3):157–62

Ratti A, Buratti E. 2016. Physiological Functions and Pathobiology of TDP-43 and FUS/TLS proteins. *J Neurochem.*

Reber S, Stettler J, Filosa G, Colombo M, Jutzi D, et al. 2016. Minor intron splicing is regulated by FUS and affected by ALS-associated FUS mutants. *EMBO J.*

Reiner A, Levitz J. 2018. Glutamatergic Signaling in the Central Nervous System: Ionotropic and Metabotropic Receptors in Concert. *Neuron*. 98(6):1080–98

Renton AE, Chiò A, Traynor BJ. 2014. State of play in amyotrophic lateral sclerosis genetics. *Nat Neurosci.* 17(1):17–23

Renton AE, Majounie E, Waite A, Simón-Sánchez J, Rollinson S, et al. 2011. A hexanucleotide repeat expansion in C9ORF72 is the cause of chromosome 9p21-linked ALS-FTD. *Neuron*. 72(2):257–68

Rhoads SN, Monahan ZT, Yee DS, Leung AY, Newcombe CG, et al. 2018a. The prion-like domain of FUS is multiphosphorylated following DNA damage without altering nuclear localization. *Mol. Biol. Cell*. mbcE17120735

Rhoads SN, Monahan ZT, Yee DS, Shewmaker FP. 2018b. The Role of Post-Translational Modifications on Prion-Like Aggregation and Liquid-Phase Separation of FUS. *Int J Mol Sci*. 19(3): pii: E886

Riancho J, Bosque-Varela P, Perez-Pereda S, Povedano M, de Munaín AL, Santurtun A. 2018. The increasing importance of environmental conditions in amyotrophic lateral sclerosis. *Int J Biometeorol*. 78(Suppl 12):450–14

Rogelj B, Easton LE, Bogu GK, Stanton LW, Rot G, et al. 2012. Widespread binding of FUS along nascent RNA regulates alternative splicing in the brain. *Sci Rep*. 2:603

Ropper AH. 2012. Hyperosmolar therapy for raised intracranial pressure. *N Engl J Med.* 367(8):746–52

Rose CR, Felix L, Zeug A, Dietrich D, Reiner A, Henneberger C. 2017. Astroglial Glutamate Signaling and Uptake in the Hippocampus. *Front Mol Neurosci*. 10:451

Rosen DR, Siddique T, Patterson D, Figlewicz DA, Sapp P, et al. 1993. Mutations in Cu/Zn superoxide dismutase gene are associated with familial amyotrophic lateral sclerosis. *Nature*. 362(6415):59–62

Ross CA, Poirier MA. 2004. Protein aggregation and neurodegenerative disease. *Nature Medicine*. 10(7):S10–S17

Rothstein JD. 1996. Excitotoxicity hypothesis. *Neurology*. 47(4 Suppl 2):S19–25–discussionS26

Rothstein JD, Tsai G, Kuncl RW, Clawson L, Cornblath DR, et al. 1990. Abnormal excitatory amino acid metabolism in amyotrophic lateral sclerosis. *Ann Neurol.* 28(1):18–25

Rothstein JD, Van Kammen M, Levey AI, Martin LJ, Kuncl RW. 1995. Selective loss of glial glutamate transporter GLT-1 in amyotrophic lateral sclerosis. *Ann Neurol.* 38(1):73–84

Rotunno MS, Auclair JR, Maniatis S, Shaffer SA, Agar J, Bosco DA. 2014. Identification of a misfolded region in superoxide dismutase 1 that is exposed in amyotrophic lateral sclerosis. *J. Biol. Chem.* 289(41):28527–38

Rowland LP, Shneider NA. 2001. Amyotrophic lateral sclerosis. *N Engl J Med.* 344(22):1688–1700

Saba L, Viscomi MT, Caioli S, Pignataro A, Bisicchia E, et al. 2015. Altered Functionality, Morphology, and Vesicular Glutamate Transporter Expression of Cortical Motor Neurons from a Presymptomatic Mouse Model of Amyotrophic Lateral Sclerosis. *Cereb. Cortex*

Sabatelli M, Moncada A, Conte A, Lattante S, Marangi G, et al. 2013. Mutations in the 3' untranslated region of FUS causing FUS overexpression are associated with amyotrophic lateral sclerosis. *Hum. Mol. Gen.* 22(23):4748–55

Saberi S, Stauffer JE, Schulte DJ, Ravits J. 2015. Neuropathology of Amyotrophic Lateral Sclerosis and Its Variants. *Neurol Clin*. 33(4):855–76

Salameh JS, Brown RH, Berry JD. 2015. Amyotrophic Lateral Sclerosis: Review. *Semin Neurol*. 35(4):469–76

Sama R, Ward CL, Bosco DA. 2014. Functions of FUS/TLS From DNA Repair to Stress Response: Implications for ALS. *ASN Neuro.* 6(4):

Sama RRK, Fallini C, Gatto R, McKeon JE, Song Y, et al. 2017. ALS-linked FUS exerts a gain of toxic function involving aberrant p38 MAPK activation. *Sci Rep*. 7(1):1205

Sama RRK, Ward CL, Kaushansky LJ, Lemay N, Ishigaki S, et al. 2013. FUS/TLS assembles into stress granules and is a prosurvival factor during hyperosmolar stress. *J Cell Physiol.* 228(11):2222–31

Saxena S, Caroni P. 2011. Selective neuronal vulnerability in neurodegenerative diseases: from stressor thresholds to degeneration. *Neuron*. 71(1):35–48

Saxena S, Roselli F, Singh K, Leptien K, Julien J-P, et al. 2013. Neuroprotection through excitability and mTOR required in ALS motoneurons to delay disease and extend survival. *Neuron*. 80(1):80–96

Scaffidi P, Science TM, 2006. Lamin A–Dependent Nuclear Defects in Human Aging. *Science.* 312(5776):1059-63

Scekic-Zahirovic J, Oussini HE, Mersmann S, Drenner K, Wagner M, et al. 2017. Motor neuron intrinsic and extrinsic mechanisms contribute to the pathogenesis of FUS-associated amyotrophic lateral sclerosis. *Acta Neuropathol.* 17(Suppl 1):4662–20

Schmidt EK, Clavarino G, Ceppi M, Pierre P. 2009. SUnSET, a nonradioactive method to monitor protein synthesis. *Nat. Methods*. 6(4):275–77

Schmouth J-F, Dion PA, Rouleau GA. 2014. Genetics of essential tremor: from phenotype to genes, insights from both human and mouse studies. *Prog. Neurobiol.* 119-120:1–19

Schoen M, Reichel JM, Demestre M, Putz S, Deshpande D, et al. 2015. Super-Resolution Microscopy Reveals Presynaptic Localization of the ALS/FTD Related Protein FUS in Hippocampal Neurons. *Front Cell Neurosci*. 9:496

Schubert D, Piasecki D. 2001. Oxidative glutamate toxicity can be a component of the excitotoxicity cascade. *J Neurosci.* 21(19):7455–62

Schulz DJ, Goaillard J-M, Marder EE. 2007. Quantitative expression profiling of identified neurons reveals cell-specific constraints on highly variable levels of gene expression. *PNAS*. 104(32):13187–91

Schwartz JC, Ebmeier CC, Podell ER, Heimiller J, Taatjes DJ, Cech TR. 2012. FUS binds the CTD of RNA polymerase II and regulates its phosphorylation at Ser2. *Genes Dev.* 26(24):2690–95

Schwartz JC, Podell ER, Han SSW, Berry JD, Eggan KC, Cech TR. 2014. FUS is sequestered in nuclear aggregates in ALS patient fibroblasts. *Mol. Biol. Cell*. 25(17):2571–78

Schwartz JC, Wang X, Podell ER, Cech TR. 2013. RNA seeds higher-order assembly of FUS protein. *Cell Rep*. 5(4):918–25

Selvaraj BT, Livesey MR, Zhao C, Gregory JM, James OT, et al. 2018. C9ORF72 repeat expansion causes vulnerability of motor neurons to Ca2+-permeable AMPA receptor-mediated excitotoxicity. *Nat Commun*. 9(1):347

Sena-Esteves M, Tebbets JC, Steffens S, Crombleholme T, Flake AW. 2004. Optimized large-scale production of high titer lentivirus vector pseudotypes. *J. Virol. Methods*. 122(2):131–39

Sephton CF, Tang AA, Kulkarni A, West J, Brooks M, et al. 2014. Activity-dependent FUS dysregulation disrupts synaptic homeostasis. *Proc. Natl. Acad. Sci. U.S.A.*

Sharma A, Lyashchenko AK, Lu L, Nasrabady SE, Elmaleh M, et al. 2016. ALS-associated mutant FUS induces selective motor neuron degeneration through toxic gain of function. *Nat Commun*. 7:10465

Shevchenko A, Tomas H, Havli sbreve J, Olsen JV, Mann M. 2007. In-gel digestion for mass spectrometric characterization of proteins and proteomes. *Nature Protocols*. 1(6):2856–60

Shing DC, McMullan DJ, Roberts P, Smith K, Chin S-F, et al. 2003. FUS/ERG Gene Fusions in Ewing's Tumors. *Cancer Res.* 63(15):4568–76

Speese SD, Ashley J, Jokhi V, Nunnari J, Barria R, et al. 2012. Nuclear envelope budding enables large ribonucleoprotein particle export during synaptic Wnt signaling. *Cell*. 149(4):832–46

Spreux-Varoquaux O, Bensimon G, Lacomblez L, Salachas F, Pradat PF, et al. 2002. Glutamate levels in cerebrospinal fluid in amyotrophic lateral sclerosis: a reappraisal using a new HPLC method with coulometric detection in a large cohort of patients. *J Neurol. Sci.* 193(2):73–78

Sreedharan J, Blair IP, Tripathi VB, Hu X, Vance C, et al. 2008. TDP-43 mutations in familial and sporadic amyotrophic lateral sclerosis. *Science*. 319(5870):1668–72

St George-Hyslop P, Lin JQ, Miyashita A, Phillips EC, Qamar S, et al. 2018. The Physiological and Pathological Biophysics of Phase Separation and Gelation of RNA Binding Proteins in Amyotrophic Lateral Sclerosis and Fronto-Temporal Lobar Degeneration. *Brain Research*

Stanika RI, Pivovarova NB, Brantner CA, Watts CA, Winters CA, Andrews SB. 2009. Coupling diverse routes of calcium entry to mitochondrial dysfunction and glutamate excitotoxicity. *Proc. Natl. Acad. Sci. U.S.A.* 106(24):9854–59

Stanika RI, Villanueva I, Kazanina G, Andrews SB, Pivovarova NB. 2012. Comparative impact of voltage-gated calcium channels and NMDA receptors on mitochondria-mediated neuronal injury. *J Neurosci.* 32(19):6642–50

Starr A, Sattler R. 2018. Synaptic dysfunction and altered excitability in C9ORF72 ALS/FTD. *Brain Research*. 1693(Pt A):98–108

Stoeger T, Battich N, Pelkmans L. 2016. Passive Noise Filtering by Cellular Compartmentalization. *Cell*. 164(6):1151–61

Storlazzi CT. 2003. Fusion of the FUS and BBF2H7 genes in low grade fibromyxoid sarcoma. *Hum. Mol. Gen.* 12(18):2349–58

Sugiyama K, Aida T, Nomura M, Takayanagi R, Zeilhofer HU, Tanaka K. 2017. Calpain-Dependent Degradation of Nucleoporins Contributes to Motor Neuron Death in a Mouse Model of Chronic Excitotoxicity. *J Neurosci.* 37(36):8830–44

Svetoni F, De Paola E, La Rosa P, Mercatelli N, Caporossi D, et al. 2017. Post-transcriptional regulation of FUS and EWS protein expression by miR-141 during neural differentiation. *Hum. Mol. Gen.*

Sweitzer TD, Hanover JA. 1996. Calmodulin activates nuclear protein import: a link between signal transduction and nuclear transport. *PNAS*. 93(25):14574–79

Szydlowska K, Tymianski M. 2010. Calcium, ischemia and excitotoxicity. *Cell Calcium*. 47(2):122–29

Takarada T, Tamaki K, Takumi T, Ogura M, Ito Y, et al. 2009. A protein-protein interaction of stress-responsive myosin VI endowed to inhibit neural progenitor self-replication with RNA binding protein, TLS, in murine hippocampus. *J Neurochem.* 110(5):1457–68

Takuma H, Kwak S, Yoshizawa T, Kanazawa I. 1999. Reduction of GluR2 RNA editing, a molecular change that increases calcium influx through AMPA receptors, selective in the spinal ventral gray of patients with amyotrophic lateral sclerosis. *Ann Neurol.* 46(6):806–15

Tan AY, Manley JL. 2009. The TET family of proteins: functions and roles in disease. *J Mol. Cell. Biol.* 1(2):82–92

Tan AY, Riley TR, Coady T, Bussemaker HJ, Manley JL. 2012. TLS/FUS (translocated in liposarcoma/fused in sarcoma) regulates target gene transcription via single-stranded DNA response elements. *Proc. Natl. Acad. Sci. U.S.A.* 109(16):6030–35

Taylor JP, Brown RH, Cleveland DW. 2016. Decoding ALS: from genes to mechanism. *Nature*. 539(7628):197–206

Tran LT, Gentil BJ, Sullivan KE, Durham HD. 2014. The voltage-gated calcium channel blocker lomerizine is neuroprotective in motor neurons expressing mutant SOD1, but not TDP-43. *J Neurochem.*

Udagawa T, Fujioka Y, Tanaka M, Honda D, Yokoi S, et al. 2015. FUS regulates AMPA receptor function and FTLD/ALS-associated behaviour via GluA1 mRNA stabilization. *Nat Commun*. 6:7098

Uversky VN. 2016. Intrinsically disordered proteins in overcrowded milieu: Membrane-less organelles, phase separation, and intrinsic disorder. *Curr. Opin. Struct. Biol.* 44:18–30

Vaarmann A, Kovac S, Holmström KM, Gandhi S, Abramov AY. 2013. Dopamine protects neurons against glutamate-induced excitotoxicity. *Cell Death Dis*. 4(1):e455–55

Van Damme P, Bogaert E, Dewil M, Hersmus N, Kiraly D, et al. 2007. Astrocytes regulate GluR2 expression in motor neurons and their vulnerability to excitotoxicity. *Proc. Natl. Acad. Sci. U.S.A.* 104(37):14825–30

Van Den Bosch L, Van Damme P, Bogaert E, Robberecht W. 2006. The role of excitotoxicity in the pathogenesis of amyotrophic lateral sclerosis. *Biochim Biophys Acta*. 1762(11-12):1068–82

Van Langenhove T, van der Zee J, Sleegers K, Engelborghs S, Vandenberghe R, et al. 2010. Genetic contribution of FUS to frontotemporal lobar degeneration. *Neurology*. 74(5):366–71

van Oordt WH, Diaz-Meco MT, cell JLTJO, 2000. The MKK3/6-p38–signaling cascade alters the subcellular distribution of hnRNP A1 and modulates alternative splicing regulation. *J Cell Biol*

van Zundert B, Izaurieta P, Fritz E, Alvarez FJ. 2012. Early pathogenesis in the adult-onset neurodegenerative disease amyotrophic lateral sclerosis. *J. Cell. Biochem.* 113(11):3301–12

Vance C, Rogelj B, Hortobágyi T, De Vos KJ, Nishimura AL, et al. 2009. Mutations in FUS, an RNA processing protein, cause familial amyotrophic lateral sclerosis type 6. *Science*. 323(5918):1208–11

Vucic S, Nicholson GA, Kiernan MC. 2008. Cortical hyperexcitability may precede the onset of familial amyotrophic lateral sclerosis. *Brain*. 131(Pt 6):1540–50

Wainger BJ, Kiskinis E, Mellin C, Wiskow O, Han SSW, et al. 2014. Intrinsic Membrane Hyperexcitability of Amyotrophic Lateral Sclerosis Patient-Derived Motor Neurons. *Cell Rep*. 7(1):1–11

Wang J, Choi J-M, Holehouse AS, Lee HO, Zhang X, et al. 2018. A Molecular Grammar Governing the Driving Forces for Phase Separation of Prion-like RNA Binding Proteins. *Cell*

Wang J-W, Brent JR, Tomlinson A, Shneider NA, McCabe BD. 2011. The ALS-associated proteins FUS and TDP-43 function together to affect Drosophila locomotion and life span. *J. Clin. Invest.* 121(10):4118–26

Wang X, Schwartz JC, Cech TR. 2015. Nucleic acid-binding specificity of human FUS protein. *Nucleic Acids Res.*

Ward CL, Boggio KJ, Johnson BN, Boyd JB, Douthwright S, et al. 2014. A loss of FUS/TLS function leads to impaired cellular proliferation. *Cell Death Dis*. 5(12):e1572

Waters BL, Panagopoulos I, Allen EF. 2000. Genetic characterization of angiomatoid fibrous histiocytoma identifies fusion of the FUS and ATF-1 genes induced by a chromosomal translocation involving bands 12q13 and 16p11. *Cancer Genet. Cytogenet.* 121(2):109–16

Wiggan O, Schroder B, Krapf D, Bamburg JR, DeLuca JG. 2017. Cofilin Regulates Nuclear Architecture through a Myosin-II Dependent Mechanotransduction Module. *Sci Rep*. 7:40953

Wright A, Vissel B. 2012. The essential role of AMPA receptor GluR2 subunit RNA editing in the normal and diseased brain. *Front Mol Neurosci*. 5:34

Writing Group, Edaravone (MCI-186) ALS 19 Study Group, Abe K, Aoki M, Tsuji S, Sobue G. 2017. Safety and efficacy of edaravone in well defined patients with amyotrophic lateral sclerosis: a randomised, double-blind, placebo-controlled trial. *Lancet Neurol*. 16(7):505–12

Wyss-Coray T. 2016. Ageing, neurodegeneration and brain rejuvenation. *Nature*. 539(7628):180–86

Xu G, Stevens SM, Kobeissy F, Kobiessy F, Brown H, et al. 2012. Identification of proteins sensitive to thermal stress in human neuroblastoma and glioma cell lines. *PLoS ONE*. 7(11):e49021

Yang L, Gal J, Chen J, Zhu H. 2014. Self-assembled FUS binds active chromatin and regulates gene transcription. *Proc. Natl. Acad. Sci. U.S.A.* 111(50):17809–14

Yasuda K, Mili S. 2016. Dysregulated axonal RNA translation in amyotrophic lateral sclerosis. *WIREs RNA*

Yasuda K, Zhang H, Loiselle D, Haystead T, Macara IG, Mili S. 2013. The RNA-binding protein Fus directs translation of localized mRNAs in APC-RNP granules. *J Cell Biol.* 203(5):737–46

Yasuda Y, Miyamoto Y, Saiwaki T, Yoneda Y. 2006. Mechanism of the stress-induced collapse of the Ran distribution. *Exp. Cell Res.* 312(4):512–20

Yogev S, Shen K. 2017. Establishing Neuronal Polarity with Environmental and Intrinsic Mechanisms. *Neuron*. 96(3):638–50

Yokoi S, Udagawa T, Fujioka Y, Honda D, Okado H, et al. 2017. 3'UTR Length-Dependent Control of SynGAP Isoform α2 mRNA by FUS and ELAV-like Proteins Promotes Dendritic Spine Maturation and Cognitive Function. *Cell Rep*. 20(13):3071–84

Yoshimura A, Fujii R, Watanabe Y, Okabe S, Fukui K, Takumi T. 2006. Myosin-Va facilitates the accumulation of mRNA/protein complex in dendritic spines. *Curr Biol.* 16(23):2345–51

Yoshizawa T, Ali R, Jiou J, Fung HYJ, Burke KA, et al. 2018. Nuclear Import Receptor Inhibits Phase Separation of FUS through Binding to Multiple Sites. *Cell*. 173(3):693–705.e22

Zahirovic JS, Sendscheid O. 2016. Toxic gain of function from mutant FUS protein is crucial to trigger cell autonomous motor neuron loss. *The EMBO …*

Zappulo A, van den Bruck D, Ciolli Mattioli C, Franke V, Imami K, et al. 2017. RNA localization is a key determinant of neurite-enriched proteome. *Nat Commun*. 8(1):583

Zhang G, Neubert TA, Jordan BA. 2012. RNA binding proteins accumulate at the postsynaptic density with synaptic activity. *J Neurosci.* 32(2):599–609

Zhang K, Daigle JG, Cunningham KM, Coyne AN, Ruan K, et al. 2018a. Stress Granule Assembly Disrupts Nucleocytoplasmic Transport. *Cell*

Zhang K, Donnelly CJ, Haeusler AR, Grima JC, Machamer JB, et al. 2015. The C9orf72 repeat expansion disrupts nucleocytoplasmic transport. *Nature*. 525(7567):56–61

Zhang T, Wu Y-C, Mullane P, Ji YJ, Liu H, et al. 2018b. FUS Regulates Activity of MicroRNA-Mediated Gene Silencing. *Mol. Cell*. 69(5):787–88

Zinszner H, Albalat R, Ron D. 1994. A novel effector domain from the RNA-binding protein TLS or EWS is required for oncogenic transformation by CHOP. *Genes Dev.* 8(21):2513–26

Zinszner H, Sok J, Immanuel D, Yin Y, Ron D. 1997. TLS (FUS) binds RNA in vivo and engages in nucleo-cytoplasmic shuttling. *J Cell Sci.* 110 (Pt 15):1741–50